

Aquifer recharge and evapotranspiration from the rivers in western Kansas

by

Sarah Auvenshine

B.S., University of Illinois, 2003
M.S., Kansas State University, 2011

AN ABSTRACT OF A DISSERTATION

submitted in partial fulfillment of the requirements for the degree

DOCTOR OF PHILOSOPHY

Department of Civil Engineering
College of Engineering

KANSAS STATE UNIVERSITY
Manhattan, Kansas

2018

Abstract

Western Kansas has a semi-arid climate where the demand for water resources is greater than the natural supply. To meet the demand for irrigated agriculture, the groundwater has been extracted at a rate greater than the natural recharge rate, resulting in declining water table in the aquifer and reduced streamflow in the rivers and streams in the region. An assessment of the rivers in western Kansas was conducted to determine the fluxes between the river, groundwater, and the atmosphere. Riverbeds were instrumented to determine the conductivity of the riverbed sediments, the transmission losses of the Arkansas River were modeled to determine the interactions between the surface water and groundwater, and the evapotranspiration of the Arkansas River corridor was estimated using satellite remote sensing to quantify of water lost to the atmosphere. The Arkansas River and Cimarron River are shown to have a high hydraulic conductivity and a large infiltration capacity at the surface of the riverbed. However, the large surface infiltration capacity does not translate into large transmission losses, which are a fraction of the rate of the surface infiltration capacity of the riverbed. Thus, surface infiltration is only one factor of what controls the transmission losses. It is shown that transmission losses for a connected river-aquifer system are driven by induced infiltration by riparian vegetation. The interactions between the surface, groundwater and atmosphere were assessed over time, revealing that the flux to the atmosphere can be decoupled from the Arkansas River discharge and the groundwater recharge. While the declining discharge in the Arkansas River can be attributed to the extraction of groundwater resources and the management of surface water resource, the atmospheric fluxes are independent of the surface water and groundwater at an annual scale. When the river ecosystem is water stressed, the trees continue to draw water. This points to both the reliable store of water from the alluvial aquifer and the ability of the tree

community to respond to water stress. While the water in the alluvial deposits are currently being lost from the system through evapotranspiration, this provides a potential store for consideration in future water management decisions.

Aquifer recharge and evapotranspiration from the rivers in western Kansas

by

Sarah Auvenshine

B.S., University of Illinois, 2003
M.S., Kansas State University, 2011

A DISSERTATION

submitted in partial fulfillment of the requirements for the degree

DOCTOR OF PHILOSOPHY

Department of Civil Engineering
College of Engineering

KANSAS STATE UNIVERSITY
Manhattan, Kansas

2018

Approved by:

Major Professor
Dr. David Steward

Copyright

© Sarah Auvenshine 2018.

Abstract

Western Kansas has a semi-arid climate where the demand for water resources is greater than the natural supply. To meet the demand for irrigated agriculture, the groundwater has been extracted at a rate greater than the natural recharge rate, resulting in declining water table in the aquifer and reduced streamflow in the rivers and streams in the region. An assessment of the rivers in western Kansas was conducted to determine the fluxes between the river, groundwater, and the atmosphere. Riverbeds were instrumented to determine the conductivity of the riverbed sediments, the transmission losses of the Arkansas River were modeled to determine the interactions between the surface water and groundwater, and the evapotranspiration of the Arkansas River corridor was estimated using satellite remote sensing to quantify of water lost to the atmosphere. The Arkansas River and Cimarron River are shown to have a high hydraulic conductivity and a large infiltration capacity at the surface of the riverbed. However, the large surface infiltration capacity does not translate into large transmission losses, which are a fraction of the rate of the surface infiltration capacity of the riverbed. Thus, surface infiltration is only one factor of what controls the transmission losses. It is shown that transmission losses for a connected river-aquifer system are driven by infiltration induced by riparian vegetation. The interactions between the surface, groundwater and atmosphere were assessed over time, revealing that the flux to the atmosphere can be decoupled from the Arkansas River discharge and the groundwater recharge. While the declining discharge in the Arkansas River can be attributed to the extraction of groundwater resources and the management of surface water resource, the atmospheric fluxes are independent of the surface water and groundwater at an annual scale. When the river ecosystem is water stressed, the trees continue to draw water. This points to both the reliable store of water from the alluvial aquifer and the ability of the tree

community to respond to water stress. While the water in the alluvial deposits are currently being lost from the system through evapotranspiration, this provides a potential store for consideration in future water management decisions.

Table of Contents

List of Figures	xi
List of Tables	xvi
Acknowledgements	xviii
Chapter 1 - Introduction.....	1
Chapter 2 - Literature Review.....	5
Hydrologic Processes.....	5
Infiltration	5
Groundwater-Surface Water Interactions	8
Evapotranspiration	13
Hydrology of Kansas	16
Chapter 3 - Mapping Infiltration Capacity of a Riverbed.....	18
Introduction.....	18
Methods	20
Mini-disk Tension Infiltrimeters:.....	20
Double-Ring Infiltrimeters:.....	22
Recharge from a River	23
Application at the Field sites	23
Site Selection Plan	23
Instrumentation of the Riverbed	26
Analysis.....	28
Interpolation between sites.....	32
Results.....	34
One-Dimensional Infiltration at Surface Using Hydrus-1D	37
Scenario 1: Free Drainage of a 1-m sand column.....	38
Scenario 2: Impermeable lower layer	39
Scenario 3: Two Layer Constant Pressure Head with Free Drainage.....	41
Discussion.....	43
Conclusions.....	49
Chapter 4 - Transmission Loss Model	50

Introduction.....	50
Methods	54
Case Study	57
Results and Discussion	63
Conclusions.....	72
Chapter 5 - Decoupling Evapotranspiration from River Discharge.....	74
Introduction.....	74
Methods	78
Simplified Surface Energy Balance (SSEB).....	78
Data Processing.....	80
Extraction to the River.....	80
Mean Tree Distance	81
Temporal Interpolation of ET data	82
The Water Balance.....	83
Case Study	84
Results and Discussion	87
Conclusions.....	97
Chapter 6 - Synthesis	99
Chapter 7 - Summary and Conclusions	110
References.....	114
Appendix A - Instructions for Processing Satellite Imagery	123
Instruction on How to Select and Download Landsat Scenes	124
Step 1. Register and Log In to http://earthexplorer.usgs.gov/	124
Step 2. Identify the location by defining points in the map view.	124
Step 3. In the search criteria menu, define the desired date range.....	124
Step 4. Under the Data Sets tab in the search criteria menu, select L4-5 TM under Landsat Archive.....	125
Step 5. Under the Additional Criteria tab, select “Less than 30%” under the Cloud Cover option.	125
Step 6. Click on the results tab to see the results.	126
Step 7. Download individual scenes	129

Step 8. Select the Level 1 Product	129
Step 9. Save the zip file (.tar.gz) to an appropriate location.....	130
Step 10. Unzip the file	130
Evapotranspiration from Weather Data	132
BEAM VISAT	135
Simple Surface Energy Balance (SSEB) application	137
Step 1. Select Working Directory	137
Step 2. Calculate NDVI	138
Step 3. Create Hot and Cold Pixel Table	138
Step 4. Calculate Evaporative Fraction.....	138
Step 5. Calculate ET	138
Creating Composite Bands in ArcGIS.....	140
Appendix B - Site Information and Instrumentation Results.....	145
Site 1: Arkansas River at Syracuse, Kansas	146
Site 2: Arkansas River near the South Ditch Head Gate	149
Site 3: Arkansas River at Lakin, Kansas.....	155
Site 4: Arkansas River at Deerfield, Kansas.....	161
Site 5: Arkansas River at Garden City, Kansas	167
Site 6: Arkansas River at Cimarron, Kansas.....	174
Site 7: South Ditch at Deerfield, Kansas	179
Site 8: Cimarron River at Elkhart, Kansas.....	183
Site 9: Cimarron River in Morton County, Kansas	187
Site 10: Cimarron River at Ulysses, Kansas	190
Site 11: Cimarron River in Haskell County, Kansas	196
Site 12: Cimarron River in Seward County, Kansas	198
Site 13: North Cimarron River near Ulysses, Kansas.....	203

List of Figures

Figure 3-1: Map of Kansas with the Groundwater Management Districts	25
Figure 3-2: Hydrologic Soil Groups in Southwest Kansas	26
Figure 3-3: Map of Southwest Kansas Showing the Site Locations.....	30
Figure 3-4: Double-Ring Infiltrometer in a Dry Riverbed.....	30
Figure 3-5: Analysis of Double-Ring Infiltrometer Data	31
Figure 3-6: Automated Mini-disk Tension Infiltrometers in a Dry Riverbed	31
Figure 3-7: Cumulative Infiltration for Eq. [1].....	31
Figure 3-8: Location of the Bear Creek Fault Line in southwestern Kansas.....	33
Figure 3-9: Hydraulic Conductivity of the Riverbed Using the Double-Ring Infiltrometer	36
Figure 3-10: Map of Southwest Kansas with Interpolated Hydraulic Conductivities	37
Figure 3-11: Free Drainage of Sand - Pressure Heads.....	39
Figure 3-12: Free Drainage of Sand - Fluxes.....	39
Figure 3-13: Impermeable Layer - Pressure Heads	40
Figure 3-14: Impermeable Layer - Fluxes	41
Figure 3-15: Two-Layer Sand-Clay - Pressure Heads.....	42
Figure 3-16: Two-Layer Sand-Clay - Fluxes.....	42
Figure 4-1: Riverbed Conductivity of the Arkansas River and the Cimarron River in Western Kansas.....	57
Figure 4-2: V-shaped Channel.....	59
Figure 4-3. Transmission Loss Model Applied to the Arkansas River on July 4, 2005	62
Figure 4-4. Comparisons between Measured and Modeled Discharge in the Arkansas River....	65
Figure 4-5. Average Transmission Loss Factor by Month	66
Figure 4-6. Transmission Losses between Syracuse and Deerfield, 2000.....	70
Figure 4-7. Transmission Losses between Syracuse and Deerfield, 1999 to 2003.....	71
Figure 5-1. Thermal Band of Western Kansas on 4 July 2005.....	79
Figure 5-2. Selection of Hot and Cold pixels for 4 July 2005	79
Figure 5-3. Water Balance Model of the Arkansas River.....	84
Figure 5-4: Garden City Weather Station	85
Figure 5-5. Logistic Function for the Mean Tree Distance to the Arkansas River.....	86

Figure 5-6: SSEB Daily ET in SW Kansas: 08 September 2000, Reference ET is 8.17 mm	88
Figure 5-7: Evapotranspiration along the Arkansas River on September 8, 2000.....	89
Figure 5-8: Evapotranspiration along the Arkansas River, Moving Average of 4 days in 2000.	90
Figure 5-9. Water Balance of the Arkansas River in 1985	91
Figure 5-10. Annual Water Balance of the Arkansas River	93
Figure A-1. USGS EarthExplorer.....	124
Figure A-2. Data Set Options from USGS EarthExplorer.....	125
Figure A-3. Search Results from USGS EarthExplorer.....	126
Figure A-4. Footprint of Result from USGS EarthExplorer.....	127
Figure A-5. Image of Results from USGS EarthExplorer	128
Figure A-6. Additional Result from USGS EarthExplorer.....	129
Figure A-7. Options for Download.....	129
Figure A-8. Files in typical LANDSAT 5 TM package	130
Figure A-9. Bushland Reference ET Calculator	133
Figure A-10. Inputs for Computation of Daily Referenc ET.....	133
Figure A-11. Excerpt of Data Sheet with Weather Data	134
Figure A-12. Simple Surface Energy Balance (SSEB) Application.....	137
Figure A-13. ArcMap 10 with Landsat Scene	140
Figure A-14. Selection of Images to Include in Composite Bands.....	141
Figure A-15. Resultant Composite Band with Default Settings	142
Figure A-16. Assignment of Colors for the Bands for Natural Color in Layer Properties.....	142
Figure A-17. Composite Band with Natural Color Displayed.....	143
Figure A-18. Assignment of Colors for the Bands for Color Infrared in Layer Properties.....	143
Figure A-19. Composite Band with Color Infrared Displayed.....	144
Figure B-1. Site 1: Arkansas River at Syracuse, Kansas	146
Figure B-2. Single-Ring Infiltrometer results for Site 1	147
Figure B-3: Site 2: Arkansas River near the South Ditch Head Gate	149
Figure B-4. Site 2: Results from Mini-Disk Infiltrometer in Arkansas River near the South Ditch Head Gate.....	150
Figure B-5. Double-Ring Infiltrometer results for Site 2	151
Figure B-6. Mini-Disk Infiltrometer (h = -6 cm) results for Site 2	152

Figure B-7. Mini-Disk Infiltrometer (h = -2 cm) results for Site 2	152
Figure B-8. Site 3: Arkansas River at Lakin, Kansas	155
Figure B-9. Double-Ring Infiltrometer results for Site 3	155
Figure B-10. Mini-Disk Infiltrometer (h = -6 cm) results 1 of 4 for Site 3	156
Figure B-11. Mini-Disk Infiltrometer (h = -6 cm) results 2 of 4 for Site 3	156
Figure B-12. Mini-Disk Infiltrometer (h = -6 cm) results 3 of 4 for Site 3	157
Figure B-13. Mini-Disk Infiltrometer (h = -6 cm) results 4 of 4 for Site 3	157
Figure B-14. Mini-Disk Infiltrometer (h = -2 cm) results 1 of 4 for Site 3	157
Figure B-15. Mini-Disk Infiltrometer (h = -2 cm) results 2 of 4 for Site 3	158
Figure B-16. Mini-Disk Infiltrometer (h = -2 cm) results 3 of 4 for Site 3	158
Figure B-17. Mini-Disk Infiltrometer (h = -2 cm) results 4 of 4 for Site 3	158
Figure B-18. Site 4: Arkansas River at Deerfield, Kansas	161
Figure B-19. Double-Ring Infiltrometer results for Site 4	162
Figure B-20. Mini-Disk Infiltrometer (h = -2 cm) results 1 of 3 for Site 4	163
Figure B-21. Mini-Disk Infiltrometer (h = -2 cm) results 2 of 3 for Site 4	163
Figure B-22. Mini-Disk Infiltrometer (h = -2 cm) results 3 of 3 for Site 4	163
Figure B-23. Site 5: Arkansas River at Garden City, Kansas	167
Figure B-24. Site 5: Results from Mini-Disk Infiltrometer in Arkansas River at Garden City, Kansas	168
Figure B-25. Double-Ring Infiltrometer results for Site 5	169
Figure B-26. Mini-Disk Infiltrometer (h = -6 cm) results for Site 5.....	170
Figure B-27. Mini-Disk Infiltrometer (h = -2 cm) results for Site 5.....	170
Figure B-28. Site 6: Arkansas River at Cimarron, Kansas	174
Figure B-29. Site 6: Results from Mini-Disk Infiltrometer in Arkansas River at Cimarron, Kansas	175
Figure B-30. Double-Ring Infiltrometer results Site 6	176
Figure B-31. Mini-Disk Infiltrometer (h = -6 cm) results for Site 6.....	177
Figure B-32. Mini-Disk Infiltrometer (h = -2 cm) results for Site 6.....	177
Figure B-33. Double-Ring Infiltrometer results for Site 7	179
Figure B-34. Mini-Disk Infiltrometer (h = -6 cm) results 1 of 3 for Site 7	180
Figure B-35. Mini-Disk Infiltrometer (h = -6 cm) results 2 of 3 for Site 7	180

Figure B-36. Mini-Disk Infiltrrometer (h = -6 cm) results 3 of 3 for Site 7	180
Figure B-37. Mini-Disk Infiltrrometer (h = -2 cm) results 1 of 3 for Site 7	181
Figure B-38. Mini-Disk Infiltrrometer (h = -2 cm) results 2 of 3 for Site 7	181
Figure B-39. Mini-Disk Infiltrrometer (h = -2 cm) results 3 of 3 for Site 7	181
Figure B-40. Site 8: Cimarron River at Elkhart, Kansas	183
Figure B-41. Site 8: Results from Mini-Disk Infiltrrometer in Cimarron River at Elkhart, Kansas	184
Figure B-42. Double-Ring Infiltrrometer results for Site 8	185
Figure B-43. Site 12: Cimarron River in Morton County, Kansas	187
Figure B-44. Double-Ring Infiltrrometer results for Site 9	187
Figure B-45. Mini-Disk Infiltrrometer (h = -2 cm) results 1 of 3 for Site 9	188
Figure B-46. Mini-Disk Infiltrrometer (h = -2 cm) results 2 of 3 for Site 9	189
Figure B-47. Mini-Disk Infiltrrometer (h = -2 cm) results 3 of 3 for Site 9	189
Figure B-48. Site 10: Cimarron River at Ulysses, Kansas.....	190
Figure B-49. Site 10: Results from Mini-Disk Infiltrrometer in Cimarron River at Ulysses, Kansas	191
Figure B-50. Double-Ring Infiltrrometer results for Site 10	192
Figure B-51. Mini-Disk Infiltrrometer (h = -6 cm) results for Site 10.....	193
Figure B-52. Mini-Disk Infiltrrometer (h = -2 cm) results for Site 10.....	193
Figure B-84. Site 11: Cimarron River near Haskell, Kansas.....	196
Figure B-85. Double-Ring Infiltrrometer results for Site 11	197
Figure B-86. Site 12: Cimarron River in Seward County, Kansas	198
Figure B-87. Double-Ring Infiltrrometer results for Site 12	199
Figure B-88. Mini-Disk Infiltrrometer (h = -6 cm) results 1 of 3 for Site 12	200
Figure B-89. Mini-Disk Infiltrrometer (h = -6 cm) results 2 of 3 for Site 12	200
Figure B-90. Mini-Disk Infiltrrometer (h = -6 cm) results 3 of 3 for Site 12	200
Figure B-91. Mini-Disk Infiltrrometer (h = -2 cm) results 1 of 3 for Site 12	201
Figure B-92. Mini-Disk Infiltrrometer (h = -2 cm) results 2 of 3 for Site 12	201
Figure B-93. Mini-Disk Infiltrrometer (h = -2 cm) results 3 of 3 for Site 12	201
Figure B-94. Site 13: North Cimarron River near Ulysses, Kansas	203

Figure B-95. Site 13: Results from Mini-Disk Infiltrometer in North Cimarron River near Ulysses, Kansas..... 204

Figure B-96. Double-Ring Infiltrometer results for Site 13 205

Figure B-97. Mini-Disk Infiltrometer (h = -6 cm) results for Site 13..... 206

Figure B-98. Mini-Disk Infiltrometer (h = -2 cm) results for Site 13..... 206

List of Tables

Table 3-1: Gradation Analysis of the Riverbed Sediments	32
Table 3-2: Hydraulic Conductivity of the Riverbed from Double-Ring Infiltrometers.....	34
Table 3-3: Unsaturated Hydraulic Conductivity from Automated Mini-disk Tension Infiltrometers.....	35
Table 3-4: Unsaturated Hydraulic Conductivity from Mini-disk Tension Infiltrometers	35
Table 3-5: Hydrus-1D Water Flow Parameters	38
Table 4-1: USGS Daily Discharge Data Availability for Arkansas River and Ditches.....	58
Table 4-2. USGS Site Locations Downstream from State Line	61
Table 4-3. Hydraulic Conductivity at the Model Stations.	61
Table 4-4. Discharge Values from July 4, 2005	63
Table 4-5. Transmission Loss Factors and Summary Statistics	64
Table 4-6. Comparison of Transmission Loss Models	69
Table 5-1. Evapotranspiration and Discharge along the Arkansas River of 4 days in 2000.	90
Table 5-2: Annual Water Balance Model of the Arkansas River	92
Table 5-3. Descriptive Statistics for Annual Water Balance	93
Table 5-4. Correlation Coefficients between Annual Water Balance Components	94
Table B-1. Soil parameters by texture from Carsel and Parish (1988).....	146
Table B-2. Calculation of Hydraulic Conductivity for Site 1	147
Table B-3. Constant Head Permeability Test for Site 1.....	148
Table B-4. Well log near Site 1	148
Table B-5. Calculation of Hydraulic Conductivity, K, for Site 2	151
Table B-6. Calculation of K(h) for Site 2	152
Table B-7. Results from automated mini-disk tension infiltrometer for Site 2	153
Table B-8. Well log near Site 2	154
Table B-9. Calculation of Hydraulic Conductivity for Site 3	156
Table B-10. Calculation of K(h) for Site 3	159
Table B-11. Constant Head Permeability Test for Site 3.....	159
Table B-12. Well log near Site 3	160
Table B-13. Calculation of Hydraulic Conductivity for Site 4.....	162

Table B-14. Calculation of K(h) for Site 4	164
Table B-15. Constant Head Permeability Test for Site 4.....	164
Table B-16. Well log near site 4	165
Table B-17. Calculation of Hydraulic Conductivity for Site 5.....	169
Table B-18. Calculation of K(h) for Site 5	170
Table B-19. Results from automated mini-disk tension infiltrometer for Site 5	171
Table B-20. Well log near Site 5	173
Table B-21. Calculation of Hydraulic Conductivity for Site 6.....	176
Table B-22. Calculation of K(h) for Site 6	177
Table B-23. Well log for Site 6.....	178
Table B-24. Calculation of Hydraulic Conductivity for Site 7	179
Table B-25. Calculation of K(h) for Site 7	182
Table B-26. Calculation of Hydraulic Conductivity for Site 8.....	185
Table B-27. Results from automated mini-disk tension infiltrometer for Site 8	186
Table B-28. Calculation of Hydraulic Conductivity for Site 9.....	188
Table B-29. Calculation of K(h) for Site 9	189
Table B-30. Calculation of Hydraulic Conductivity for Site 10.....	192
Table B-31. Calculation of K(h) for Site 10	193
Table B-32. Results from automated mini-disk tension infiltrometer for Site 10	194
Table B-33. Calculation of Hydraulic Conductivity for Site 11	197
Table B-34. Calculation of Hydraulic Conductivity for Site 12.....	199
Table B-35. Calculation of K(h) for Site 12	202
Table B-36. Calculation of Hydraulic Conductivity for Site 13.....	205
Table B-37. Calculation of K(h) for Site 13	206
Table B-38. Results from automated mini-disk tension infiltrometer for Site 13	207

Acknowledgements

Acknowledgment is due to my major professor, Dr. David Steward, for the patience and guidance he has provided over the last decade of graduate studies. Thank you to the graduate and undergraduate water resources research team including Hrvoje Magzan, Noura Saadi, Scott Kempin, and Weston “Wes” Koehn. They have provided assistance in the field and in the lab and offered feedback and support over the course of my doctoral studies. Extra special thanks to Andy Allen for the above and being able to trouble shoot and fix anything. Without his expertise, the automated mini-disk infiltrometers would not have been automated. Thank you to Trevor Ahring on providing valuable resources and assistance from GMD 3. I thank my Navy colleagues who have provided their support and encouragement over the last four years: Doug, Judy, Chuck, Jack, Dave and Carey.

I thank Dr. DeAnn Presley for the use and instruction of infiltrometers and Dr. Prasana Gowda and Jerry “Jed” Moorhead. at USDA ARS Bushland for introducing me to the methods and tools of evapotranspiration. Appreciation is due to the members of my committee: Dr. G. Kluitenberg, Dr. S. Datta, Dr. M. Daniels, Dr. N. Mladenov, and Dr. S. Kulesza.

I thank my family. My parents, Maureen and Ron Auvenshine, have provided me a good educational foundation and instilled the self-motivation for success. My brothers and sisters have provided a competitive environment and many lessons learned. My in-laws, Linda and Bill Olson, have provides years of encouragement and support. My husband, Jesse, and two children, Thela and Denver, have provided me with the love, joy, and motivation to accomplish this work.

Chapter 1 - Introduction

An assessment of the rivers in western Kansas was conducted to determine the fluxes between the river, groundwater, and the atmosphere. The two major rivers in western Kansas, the Arkansas River and the Cimarron River, were instrumented with infiltrometers, and the hydraulic conductivity was derived from the infiltration measurements and interpolated along the length of the rivers within the study area. These riverbeds were determined to have a great capacity to transmit water to the lower layers of the river systems. While the hydraulic conductivity of the riverbed indicates that there is a good connection between the Arkansas River and the underlying aquifer, the actual transmission losses are a fraction of what is expected. Applying a simple transmission loss model to the Arkansas River in western Kansas reveals that the hydraulic conductivity of the riverbed is not the controlling factor for the transmission losses, and the results point to evapotranspiration. A seasonal factor of plant development predominantly in the western reach of the Arkansas River induces infiltration and seasonal transmission losses from the river. The transmission losses are controlled, in part, by seasonal vegetation growth, available storage in the river alluvium, and a confining layer under the river alluvium. By exploring the role of evapotranspiration in the Arkansas River corridor with satellite remote sensing, it was discovered that evapotranspiration is controlled by seasonal demands of the vegetation and is independent of the quantity of discharge of the river. The annual evapotranspiration from the Arkansas River corridor is consistent across the period of study, indicating that the trees and other riparian vegetation are drawing from a reliable source of water disconnected from the river. The alluvial aquifer is that reliable source of water in periods of drought when the river discharge is at a minimum. In years of normal or above normal river discharge, the riparian vegetation has a limited capacity to consume water, limiting the amount

of water the river system loses to the atmosphere. The discharge of the Arkansas River is controlled by a reservoir upstream in Colorado and by diversions to irrigation ditches. An increase in the amount of water in the river channel is not expected to increase the amount of water lost to the atmosphere from evapotranspiration. Instead, an increase in the amount of water in the river would result first in the refilling of the alluvial aquifer and then in water conveyed downstream toward Great Bend, Kansas.

The original plan for this dissertation was to learn how the rivers in western Kansas could be used as a conduit between the rivers and the groundwater. This would inform how the rivers could be used to “refill” the Ogallala Aquifer or at least extend the useable life of the aquifer. The Ogallala Aquifer is a large store of underground freshwater that spans eight states including Texas, Wyoming, and Kansas. The development of the Ogallala began around the 1950s with the use of pumps and center pivot irrigation systems to extract and apply the groundwater to the fields. The number of irrigated acres in Kansas increased from 1950 and peaked around 1980, after which the acreage has remained constant (Rogers and Lamm, 2012). The rate of groundwater extraction is greater than the average annual recharge, resulting in a declining water table. Parts of the Ogallala Aquifer in Kansas have declined more than 150 feet resulting in areas of the aquifer with no saturated thickness remaining (McGuire, 2017). As the water levels in the aquifer decreased, so has the streamflow in the Arkansas River, and the extent of perennial flow in streams across western Kansas has also declined (Angelo, 1994; Juracek and Eng, 2017). The rivers and streams are reacting to the decline in groundwater levels by a combination of losing their surface water to the groundwater system through streambed infiltration and losing the groundwater baseflow. The Arkansas River has changed from a gaining river system that is

connected to the groundwater to a losing river (Yang, 2012). This response to groundwater decline indicates that the rivers would be a natural conduit for groundwater recharge.

The focus of this study shifted away from identifying locations along the rivers that are suitable for focused recharge zones and developing a transmission loss model that can predict the quantity of water lost to the aquifer towards a study focused on evapotranspiration. By using remotely sensed imagery, atmospheric fluxes are included in the groundwater-surface water interactions to better understand the river system. The transmission loss model evolved to a simple model that captures the unexplained variability with a transmission loss factor. An assessment of this factor, as it compares with other model inputs, provides insight to the components of river transmission loss that are dependent on temporal variabilities rather than being constant over time. The automated mini-disk tension infiltrometers were reused from the work on my Master's thesis at Konza Prairie and supplement the variable tension mini-disk infiltrometers and the double-ring infiltrometers for streambed instrumentation. This collection of infiltrometers was applied to the riverbeds of western Kansas to determine the infiltration capacity in the riverbed. While the measurements and the map of interpolated hydraulic conductivity provide valuable information about the properties of the riverbed and how it changes over the length of the river reach, those measurements did not inform the remainder of this study to the extent expected. It was expected that the measurements collected at the riverbed scale would be an important factor in the transmission loss model and the hydraulic conductivity mapped within the riverbed would exhibit a pattern that would also inform the transmission loss model. These factors are discussed later.

The chapters of the dissertation are organized to provide a logical flow of the progression of this body of work with this general introduction as Chapter 1. Chapter 2 provides an overview

of what is known with respect to infiltration, the ground water-surface water interactions, remote sensing of evapotranspiration, and the hydrology of western Kansas. Chapter 3 is a study of the infiltration of the riverbed with application to the two large rivers in western Kansas – the Arkansas River and the Cimarron River. Chapter 4 is the development and application of a simple river transmission loss model with the goal of explaining and predicting the amount of river discharge lost to the riverbed. Chapter 5 is the examination of the role of evapotranspiration on the Arkansas River system using satellite remote sensing and models that convert the thermal imagery to daily evapotranspiration estimates along the river. Chapter 6 is a synthesis and discussion that ties together the previous three chapter with the known state of science and seeks to communicate the larger points of discovery of this dissertation and the ramifications. Chapter 7 succinctly summarizes the work in this study. Two Appendixes provide additional information. Appendix A has instructions for collecting and processing data for the Simple Surface Energy Balance (SSEB) method to estimate evapotranspiration. Appendix B has the results from the riverbed instrumentation and additional site information.

Chapter 2 - Literature Review

Hydrologic Processes

The hydrologic cycle, or the water cycle, is a representation of earth's waters - the stores, pathways, and processes. Among the processes are precipitation, infiltration, evapotranspiration, surface runoff, and groundwater flow. This study focuses on the hydrologic processes of infiltration, groundwater- surface water interactions, and evapotranspiration and their interdependence within a river system with considerations to the hydrologic scale of these processes.

Hydrologic processes span a wide range of spatial and temporal scales and occur over about eight orders of magnitude in time and space (Klemes, 1983). Bloschl and Sivapalan (1995) proposed two approaches for addressing scale issues in hydrologic modeling. The first approach is model-oriented and focuses on scaling of state variables, model parameters, inputs and conceptualizations, where scaling is transferring information across scales. Upscaling includes distributing and aggregating values, and downscaling is disaggregating and singling out values. The second approach is dimensional analysis and similarity. Similarity seeks to relate one system to another using a scale factor based on a common characteristic between the two systems. The challenge with studying the interactions between different hydrologic processes is the scale issue and selecting an appropriate approach that will bridge the differing scales across the processes.

Infiltration

Infiltration is the process of water entering a soil. The process of infiltration is important because it applies to a range of topics including irrigation, groundwater recharge, contaminant transport, and ecosystem health. Infiltration is also important because it is a link between the

surface and subsurface processes in the hydrologic cycle. At early times in infiltration processes, the infiltration rate is high as matric forces dominate the process and an initially dry soil becomes saturated. At later times, the infiltration rate approaches a steady-state under gravitational forces. For infiltration into a riverbed, the factors affecting the rate of infiltration are the saturation of the riverbed sediments, the hydraulic properties of the sediments, and the variability of the hydraulic properties.

Infiltration capacity of the streambed is an important parameter in estimating the groundwater-surface water interactions and the transmission losses from rivers to aquifers. River transmission losses are a subset of groundwater-surface water interactions. In an environment with limited water resources, transmission losses from rivers provide a potential source of focused groundwater recharge that naturally collects and conveys large volumes of water to the groundwater aquifers. Hydraulic conductivity is a key variable in determining the river-aquifer connection (Conrad and Beljin, 1996; Calver, 2001) and the rate at which transmission losses would occur. Characterizing the hydraulic conductivity is challenging because the riverbed hydraulic conductivity can be highly variable (Bruen and Osman, 2004) and may evolve over time (Nowinski et al., 2011). Variations in the values of hydraulic conductivity from measurements within the riverbed are expected and result from the type of instrumentation used, the analysis performed, and the spatial variability of hydraulic conductivity both along a river transect and with depth (Landon et al., 2001).

Methods for determining hydraulic conductivity include estimates based on the soil textural class or gradation of the soil, instream measurements, and numerical modeling. Analytical models characterize streambed exchanges (Zlotnik and Huang, 1999) including chemical or thermal tracers (Constantz, 1998; Constantz, 2008; Zellweger, 1994). In-stream

measurements include slug tests, permeameters, tension infiltrometers, and seepage flux with seepage meters. Comparisons of multiple in situ methods reveal no method is superior than others as each has tradeoffs between cost, time, types of results obtained, ease of use, and ease of analysis (Gribb et al., 2004). Measurement methods may focus on vertical or horizontal properties. The permeameters and infiltrometers measure the vertical hydraulic conductivity (Landon et al., 2001), and slug test measure in the horizontal direction (Rus et al., 2001). Combining measurement methods allow for the characterization of anisotropic sediments. In situ measurements have the benefit of limiting disturbance of the soil. The boundary conditions for in situ measurements are difficult to control and may require some disturbance of the sample under interrogation or require making assumptions about the soil and hydraulic properties in lieu of direct measurements.

Laboratory measurements use soil samples that are extracted from the site and analyzed in the controlled environment of the laboratory. While some disturbance of the soil samples is expected, measurements conducted in a laboratory setting have a clear set of boundary conditions. To determine the hydraulic conductivity of a soil, constant head permeability test and a falling head permeability test are direct applications of Darcy's Law. Constant head permeability tests are typically performed on soils with higher permeability, and the falling head test is typically performed on finer soils where the hydraulic conductivity is expected to be low. Gradation tests are used to determine the grain size distribution, allowing classification of the soil. Two types of soil classification are USDA classification system and the Unified Soil Classification System (USCS). Grain size analysis provides another means to estimate for hydraulic conductivity by using established empirical relationships based on grain size distribution (Vukovic and Soro, 1992; Alyamani and Sen, 1993; Lopez et al., 2015), but this

approach has high errors in river environments even after empirical adjustments (Rosas et al., 2014).

Groundwater-Surface Water Interactions

Groundwater-surface water interactions are controlled by the streambed, and they are complex interactions that link the studies of hydrology, biogeochemistry, and ecology (Fleckenstein et al., 2010; Sophocleous, 2002; Brunner et al., 2017). Groundwater and surface water have historically been managed independently with little understanding of the connection between the two. It is important to understand the connection and the exchanges between the surface and groundwater and how human or natural influences to one will impact the other. The water exchanges between the surface water and the groundwater occur in the hyporheic zone and are called hyporheic exchanges, and this mixing of shallow groundwater and surface water are important for biogeochemical processes (Winter et al., 1998). The spatial variability of the riverbed and the type of connection between the stream and aquifer impacts how and where the exchanges occur. The riverbed has high spatial variation in its infiltration capacity with the highest hydraulic conductivity typically found in the center of the channel (Chen, 2005; Kennedy et al., 2009; Murdock and Kelly, 2003). In the Republican River, Nebraska, horizontal hydraulic conductivity is about three to four times larger than vertical hydraulic conductivity due to processes that deposit clay and other fine material in heterogeneous layers (Chen, 2000; Chen, 2004). If a river is a connected-losing or connected-gaining river, then the exchanges would occur at the banks (Genereux and Bandopadhyay, 2001). If a river is a disconnected-losing river, then the flux from the surface water in the river to the groundwater would occur along the bottom width of the river (Brunner et al., 2009). The state of connection between the surface water and the groundwater is critical for infiltration. Transmission losses are one type of

groundwater-surface water exchange. In a river, transmission losses are the losses of the river's flow over the length of river. In this study, transmission losses are associated with infiltration into the riverbed without a corresponding inflow back from the groundwater to the river.

Groundwater-surface water interactions can be characterized by numerous methods. Each method differs in the scale and resolution and, like infiltration measurements, have trade-offs. The selection of methods, including sampling density, depends on the goals of the study (Kalbus et al., 2006). In Kennedy et al. (2008), sampling at 0.05 point per m² reduced the occurrence of error of five streambed attributes including hydraulic conductivity to 10% or less. Several methods are available to estimate recharge from ephemeral and intermittent streambeds. Spatial distribution of relative channel losses can be interpreted from remotely sensed optical images, but the images are not suitable for quantitative measurement unless they are coupled with ground truth data from in-stream measurements or another type of model validation (Walter et al., 2012). Temperature may be used as a tracer for river-aquifer interactions but only when the temperatures are sufficiently different (Schmidt et al., 2006). The challenge with characterizing the exchanges between surface water and groundwater is the spatial scale in which the fluxes are measured. The exchanges are typically measured over a meter or sub-meter scale, but the fluxes occur at a river reach scale. The properties of the connection exhibit high spatial variations along with the temporal variations (Genereux et al., 2008).

Groundwater-surface water interactions are impacted by human activity. Substantial flow decreases have resulted from groundwater extraction (Postel, 2000). The decrease in the groundwater levels reduces the groundwater inflow and shifts the rivers from a gaining stream that received flow from the groundwater to a losing system that loses channel flow to the streambed. A review by Zekster et al. (2005) highlighted four areas of environmental impacts

when groundwater is overdrawn. A decline in surface water and stream flow is expected especially when the surface water is connected to the overdrawn groundwater aquifer. A reduction in vegetation will occur if the vegetation relies on the groundwater source. Land subsidence occurs when the pores in the matrix of the aquifer sediments are dewatered resulting in the loss of pore pressure and compressing the pore space. The final effect of groundwater extraction is sea water or deep groundwater intrusion, which may result in the contamination of a freshwater aquifer.

Transmission losses from a river are a potential source of focused recharge to refill depleted groundwater stores at a greater rate than areal recharge. The areal recharge is limited by the annual precipitation, the soil permeability, and annual evapotranspiration. Although covering a smaller area, the groundwater recharge rates from a river have the potential to infiltrate at a much higher rate than areal recharge. As water tables decline in response to unsustainable groundwater extraction (Konikow and Kendy, 2005), the hydrologic regime of a river changes. Brunner et al. (2009) stated that if the area between a river and a groundwater system is fully saturated, then that flow regime is connected. The connected regime may be losing, where the primary flow direction is from the river to the groundwater, or it may be gaining, where the groundwater discharges into the river. If the area between the river and groundwater system is unsaturated, then that flow regime is considered disconnected. A clogging layer is a necessary criterion for river-aquifer disconnection (Brunner et al., 2009a). The infiltration rate of a connected, losing river-aquifer system is proportional to the head difference between the river and aquifer. In a fully disconnected river-aquifer system, the infiltration rate is at a maximum value and is not dependent on the depth to water table. The riverbed hydraulic conductivity is the primary factor that controls groundwater recharge, and that riverbed property

can be highly variable (Calver, 2001; Bruen and Osman, 2004). Other factors that control transmission losses are the quantity of available water in the river (Jordan, 1977), the properties of the underlying layers (Kalbus et al., 2009), the state of connection between the river and aquifer, and the available storage in the soil and groundwater. Transmission losses and infiltration do not equate to groundwater recharge. Recharge will always be less than infiltration because some fraction of the infiltration will be lost to evapotranspiration (Shanafield and Cook, 2014). The ability of an infiltration event to contribute to recharge is dependent on the duration of flow and initial moisture condition of the stream banks (Batlle-Aguilar and Cook, 2012) as well as the fraction of transmission losses consumed by evapotranspiration.

The transmission losses vary over time and position in the channel. Infiltration is highest at the onset of flow and at each stage increase, where the water level in the channel is rising, resulting in an infiltration rate higher than under a steady-state condition (Batlle-Aguilar and Cook, 2012). When the water level in the channel is constant, infiltration is at a near constant rate. Transmission losses from a river or stream produce groundwater mounds, and the propagation of the infiltrated water and potential contaminants would be limited to the banks of the ditch (Dages et al., 2008). Induced infiltration is the process of water infiltrating from a surface source to the groundwater water as the result of lowering the water level in the aquifer. Groundwater pumping near a stream lowers the water table in the vicinity of the pump and induces infiltration from the stream. As a result, the discharge of the stream is reduced. Areal recharge and its contribution to baseflow is a factor in reducing the impact of stream depletion due to pumping (Chen and Shu, 2002). The reduction of baseflow as a result of a declining groundwater level has a greater impact on the total river discharge lost than the impact of induced river infiltration. The impact of induced infiltration becomes negligible after pumping,

while the impacts of baseflow persist. A high conductance streambed responds to pumping with greater stream depletion. For a low conductance stream, the reduction in baseflow is a significant percent (90%) of the total stream depletion and can have lasting impacts even after pumping concludes (Chen and Shu, 2002).

Transmission loss models are used to quantify and predict the streamflow lost to the aquifer. Quantifying transmission losses are simple when a river is well gaged. Over a large scale, flow gaging can be used to estimate transmission losses if there are no significant tributaries or surface water extractions (Cook, 2015). The difference between the upstream gage and the downstream gage is the amount gained or lost. Transmission loss estimation is challenging when a river is not well gaged or when the cessation of flow occurs between gages. Several transmission loss models have been developed, and they generally are a function of the upstream discharge plus a mechanism for losses along a length of a river. Niswonger et al. (2008) provides a method to estimate streambed hydraulic conductivity by using the changes in the streamflow front velocity as streamflow progresses down an initially dry channel. Costa et al. (2013) takes an event-based approach to determine a transmission loss rate for a Brazilian river system with channel transmission losses correlating to input river flow. Jordan (1977) applies an exponential decay function that uses the upstream and downstream volume to determine the rate of transmission loss per mile. The transmission loss per mile could be applied to less well gaged streams to determine transmission losses on similar types of streams. The United States Department of Agriculture (USDA) Natural Resources Conservation Service (NRCS) National Engineering Handbook (NEH) model for transmission losses is an approach that estimates the volume of runoff and peak discharge for ephemeral streams following a storm event (Woodward, 2007). The NEH model can be used with observed stream flow data, or

model parameters can be predicted. The Lewis-Milne model is used for boarder irrigation systems and has been improved upon by Singh et al. (1990). The Lewis-Milne model is based on mass conservation and assumes a constant water depth and has been used to estimate recharge from overbank flooding from rivers (Doble et al, 2012). Abdulrazzak and Morel-Seytoux (1983) developed an approximate analytical solution for recharge over a water table and identified the transient parameters of stream-aquifer interactions affected by the development of a groundwater mound. Others have attempted to simplify the infiltration and transmission loss models that approximate results of computationally intensive numerical modeling (Crosbie et al., 2014; Reid and Dreiss, 1990).

Evapotranspiration

Evapotranspiration (ET) is the hydrologic flux from the surface to the atmosphere via evaporation from surface water or soil moisture or via transpiration from vegetation. ET is an important component of earth's surface energy balance and an important component to the water balance and hydrologic processes especially in semi-arid and arid environments with limited water resources. ET quantities and rates are used in calculations of soil water storage, runoff to streams and recharge to aquifers, and informs the management of water. Water can be conserved by limiting evapotranspiration (Evans and Sadler, 2008). Efforts to measure ET often focus on a water balance approach or an energy balance approach (Evelt et al., 2012).

In a losing river system, the transmission losses from a river provide a source of available water for plant development. In an arid or semi-arid region, evapotranspiration from riparian vegetation is significant. If transmission losses from a river are cycled into the atmosphere via evapotranspiration, then less water is available. Less water is available for groundwater recharge, less water is conveyed downstream in the river channel, and less water is available for

beneficial use in agriculture or industry. In water-constrained environments, water resources are managed to minimize the losses of unproductive ET allowing rivers and aquifers to be maintained as reliable sources of fresh water for domestic and agricultural use. Knowing the stores and fluxes of water in a river system provides insight into the impact the river flows have on the rates of evapotranspiration and groundwater recharge.

Phreatophytes and other riparian vegetation draw from the available water in the groundwater and alluvial deposits. Phreatophytes are plants with deep roots that tap into the groundwater and are a pathway for evapotranspiration. The change in the location and density of phreatophytes provides insight into changes in the available water (Ahring and Steward 2012). Diurnal water table fluctuations are a method to determine groundwater consumption by phreatophytes (Loheide et al., 2005). Groundwater fluctuations caused by water demands of phreatophytes are controlled by meteorological drivers, characteristics of the vegetation, and the specific yield of the sediments (Butler et al., 2007). Groundwater ET in riparian zones can draw up water from deep in the aquifer to the water table resulting in a seasonal mixing of shallow and deep aquifer waters (Chen, 2007). ET rates from vegetation and the land surface are high when the system has available water and when there are driving factors to move the water from the ground to the atmosphere; those factors include temperature, humidity, and wind speed.

Quantifying ET rates is challenging due to its spatial dependencies and the costs associated with direct measurements. Multiple methods to estimate evapotranspiration exist that have their own assumptions, strengths and weaknesses (Gowda et al., 2008). Generally, the methods fall into one of four categories: water balance, water vapor fluxes, component estimation, and large-scale estimations. Water balance measurement methods include lysimeters or soil evaporation pan that measure the stores and fluxes of water in a defined system. Large

scale lysimeters that directly measure ET are limited to research stations such as USDA ARS-Bushland and are typically used to validate other ET estimation methods (Evetts et al., 2012; Gowda et al., 2012). Water vapor flux measurements include Bowen Ratio or Eddy covariance. Component estimation includes sap-flow measurements or soil evaporation. Large-scale estimation includes scintillometer measurements and remote sensing.

The large-scale estimation methods typically combine remotely sensed imagery from satellite or aerial platforms with ground truth measurements to provide a map of ET over a region. Two large-scale methods are the Surface Energy Balance Algorithm for Land (SEBAL) (Bastiaanssen et al., 2005) and the Mapping Evapotranspiration at High Resolution using Internalized Calibration (METRIC) (Allen et al., 2007) method. These two methods share the assumption that the near-surface temperature difference between the land surface and the air varies linearly with land surface temperature. That assumption is used to estimate the sensible heat flux. The relationship between the near-surface temperature difference and the land surface is derived based on hot and cold anchor pixels from remotely sensed thermal imagery. For these anchor pixels, the hot pixel represents dry and bare agricultural fields, and the cold pixel represents wet and well-vegetated fields. With these anchor pixels and the assumption of the linear relationship, the hot pixel is assumed to experience no latent heat flux ($ET = 0$) and the cold pixel has the maximum ET. The Surface Energy Balance System (SEBS) (Su, 2002) and the Simplified Surface Energy Balance (SSEB) (Senay et al., 2007) take a similar approach. For the SSEB, these assumptions are further simplified to state that the latent heat flux varies linearly between the hot and cold pixels. Application of the SSEB model against large monolith lysimeters showed that the model accounted for 84% of the variations in the observed ET values (Gowda et al., 2009).

Hydrology of Kansas

The study area is western Kansas. The climate of Kansas includes three Köppen climate types: hot-summer humid continental in the northern edge of the state, cold semi-arid in the western quarter of the state, and humid subtropical for the remaining the area (Peel et al., 2007). The average areal recharge from the land surface ranges from less than 0.01 m (0.5 inches) per year in the western reaches of the Ogallala Aquifer in Kansas to 0.1 m (4 inches) over the eastern reaches of the Ogallala Aquifer in Sedgewick and Harvey Counties, Kansas (Hansen, 1991). The average annual precipitation is less than the potential evapotranspiration in western Kansas resulting in a reliance of surface water and groundwater to supplement the atmospheric demand for water. The annual average precipitation ranges from less than 0.46 m (18 inches) in the western edge of Kansas to more than 1.02 m (40 inches) in the east. The mean annual runoff is 2.5×10^{-3} m (0.1 inches) over the study area of western Kansas (Wetter, 1990). Reitz et al., (2017), estimates annual runoff between 0 m and 0.06 m (0 and 2.4 inches), between 0.24 m and 0.68 m (9.4 in and 24 in) of annual evapotranspiration, and between 0 m and 0.06 m (0 and 2.4 inches) of annual recharge. These values show that the study area has an evapotranspiration demand that is greater than the annual precipitation with little runoff and recharge.

The rate of groundwater extraction far exceeds the natural rate of areal recharge resulting in year-to-year declines of the water table. Formations of the High Plains Aquifer have already been depleted, and models show that portions of Ogallala Aquifer in southwestern Kansas are already below a minimum saturated thickness threshold (Buchanan et al., 2015). The declining groundwater levels in the Ogallala Aquifer and declining river discharges have resulted in a change in the hydrologic regime and a shift from a connected river-aquifer system to a disconnected system. In western Kansas, the decline in river discharge has correlated with lower

groundwater levels in the Ogallala Aquifer, resulting in perennial rivers becoming ephemeral with intermittent flow. The volume of water that would have historically been discharged to the rivers in western Kansas has been captured by the aquifer. Because the groundwater is not discharging to the rivers, the capture of the river discharge has lessened the aquifer storage loss by approximately 12% (Liu et al., 2010). Groundwater extraction has reduced the number and extent of perennial streams in western Kansas (Angelo, 1994; Sophocleous et al., 1988). Similar effects have been documented elsewhere in the western United States (Zekster et al., 2005) as well as in Australia (Cook, 2015) and China (Konikow and Kendy, 2005). Other contributors to streamflow reduction are surface water diversion and evapotranspiration within the river. The demands on water resources go beyond the economic or agricultural uses; the riparian ecosystem that depends on the surface water is at risk if the groundwater resources continue to be extracted at an unsustainable rate. Growing demands on water resources require that groundwater and surface water be managed as a single resource. The interactions between the groundwater and surface water as well as the atmospheric flux are critical to understanding a river system to inform water management decisions.

Chapter 3 - Mapping Infiltration Capacity of a Riverbed

Introduction

Infiltration capacity of a streambed is an important parameter in estimating the groundwater-surface water interactions and the transmission losses from rivers to aquifers. River transmission losses are a subset of groundwater-surface water interactions. In an environment with limited water resources, transmission losses from rivers provide a potential source of focused groundwater recharge that naturally collects and conveys high volumes of water to the groundwater aquifers. Hydraulic conductivity is a key variable in determining the river-aquifer connection (Conrad and Beljin, 1996; Calver, 2001) and the rate at which transmission losses would occur. Characterizing the hydraulic conductivity is challenging because the riverbed hydraulic conductivity can be highly variable (Bruen and Osman, 2004) and evolve over time (Nowinski et al., 2011). Variations in the values of hydraulic conductivity from measurements within the riverbed result from the type of instrumentation used, the analysis performed, and the spatial variability of hydraulic conductivity along a river transect and with depth (Landon et al., 2001).

Methods for determining hydraulic conductivity include estimates based on the soil textural class or gradation of the soils, instream measurements, and numerical modeling. Analytical models characterize streambed exchanges (Zlotnik and Huang, 1999) including chemical or thermal tracers (Constantz, 1998; Constantz, 2008; Zellweger, 1994). In-stream measurements include slug tests, permeameters, tension infiltrometers, and seepage flux with seepage meters. Comparisons of multiple in situ methods reveal no method is superior than others as each has tradeoffs between cost, time, types of results obtained, ease of use, and ease of analysis (Gribb et al., 2004). Measurement methods may focus on vertical or horizontal

properties. The permeameters and infiltrometers measure the vertical hydraulic conductivity (Landon et al., 2001), and slug test measure in the horizontal direction (Rus et al., 2001). Combining measurement methods allow for the characterization of anisotropic sediments. In situ measurements have the benefit of limiting disturbance of the soil. The boundary conditions for in situ measurements are difficult to control and may require some disturbance of the sample under interrogation or making assumptions about the soil and hydraulic properties in lieu of direct measurements.

Laboratory measurements use soil samples that are extracted from the site and analyzed in the controlled environment of the laboratory. While some disturbance of the soil samples is expected, measurements conducted in a laboratory setting have a clear set of boundary conditions. To determine the hydraulic conductivity of a soil, constant head permeability test and a falling head permeability test are direct applications of Darcy's Law. Constant head permeability tests are typically performed on higher permeability, and the falling head test is typically performed on finer soils where the hydraulic conductivity is expected to be low. Gradation tests are used to determine the grain size distribution, allowing classification of the soil. Two types of soil classification are USDA classification system and the Unified Soil Classification System (USCS). Grain size analysis provides another means to estimate for hydraulic conductivity by using established empirical relationships based on grain size distribution (Vukovic and Soro, 1992; Alyamani and Sen, 1993; Lopez et al., 2015), but this approach has high errors in river environments even after empirical adjustments (Rosas et al., 2014).

In this study, the Arkansas River and the Cimarron River were instrumented to collect infiltration data of riverbeds. These infiltration values were transformed into hydraulic

conductivity, and the spatial variability of the hydraulic conductivity was analyzed and interpolated across the length of the rivers. From this, the infiltration capacity of the riverbeds can be modeled to predict the transmission loss and potential groundwater recharge. Knowing the spatial variability of the hydraulic conductivity provides insight into how much focused groundwater recharge is possible. Based on the infiltration measurements and the known discharge in the river, the infiltration capacity of the riverbeds is shown to be much greater than the transmission losses observed by river gaging stations.

Methods

Mini-disk Tension Infiltrimeters:

Mini-disk tension infiltrimeters measure the cumulative infiltration of water into an unsaturated soil. For in situ measurements, mini-disk tension infiltrimeters, due to their compact size and modest use of water, are suitable to collect multiple data points with minimal time and effort at field sites with limited accessibility. The models used to translate the measured cumulative infiltration to hydraulic conductivity use the two-term cumulative infiltration equation, Eq. [1], from Philip (1957):

$$I = C_1 t^{1/2} + C_2 t \quad [1]$$

where

I = cumulative infiltration per unit area (m),

t = time (s),

C_1 = sorptivity coefficient ($\text{m s}^{-1/2}$)

C_2 = hydraulic conductivity coefficient (m s^{-1}).

Various studies (Haverkamp et al., 1994; Zhang 1997; Vandervaere et al., 2000) have proposed different interpretations of the coefficients and their relationship to sorptivity and hydraulic conductivity. Zhang (1997) uses the following expression, Eq. [2] to model the unsaturated hydraulic conductivity, $K(h)$, from the second coefficient, C_2 , and the expression for A_2 :

$$K(h_0) = C_2/A_2 \quad [2]$$

where the formula for A_2 is dependent on the value of n :

$$A_2 = \frac{11.65(n^{0.1}-1)\exp[2.92(n-1.9)\alpha h]}{(\alpha r_0)^{0.91}}, \text{ for } n \geq 1.9 \quad [3a]$$

$$A_2 = \frac{11.65(n^{0.1}-1)\exp[7.5(n-1.9)\alpha h]}{(\alpha r_0)^{0.91}}, \text{ for } n < 1.9 \quad [3b]$$

In equations [3a] and [3b], h is the tension (m) which is set by the infiltrometer, r is the radius of the infiltrometer disk (m), α and n are soil parameters defining the shape of $K(h)$.

The parameters in equations [3a] and [3b] used to determine A_2 are dependent on the characteristics of the measurement device or on the properties of the soil. The tension of the infiltrometer can be varied with the use of an adjustable suction control tube in a bubble chamber or the infiltrometer can have a fixed tension with a bubbling capillary tube. The tensions typically range from 0.5 cm to 6 cm. For the automated mini-disk tension infiltrometers, the data is automatically collected and recorded via differential pressure transducers. Madsen and Chandler (2007) provides instruction on how the data from the pressure transducers in the automated mini-disk infiltrometers is processed into cumulative infiltration. The soil parameters of the equations are assumed based on soil texture provided in Carsel and Parrish (1988).

After the unsaturated hydraulic conductivity is computed, the Gardner model (Gardner 1958), as shown in Eq. [4], is applied to determine the saturated hydraulic conductivity.

$$K(h) = K_s e^{-\alpha h} \quad [4]$$

where $K(h)$ is the unsaturated hydraulic conductivity (m s^{-1}) at tension, h (m), and K_s is the saturated hydraulic conductivity (m s^{-1}). The parameter, α is the same soil parameter as above that defines the shape of $K(h)$. With the exponential component of the equation being less than 1, $K(h)$ will always be less than K_s . In addition, as the tension is increased, $K(h)$ will decrease.

If multiple measurements of $K(h)$ are taken at various tensions, then α can be directly calculated instead of assumed.

Double-Ring Infiltrometers:

Like the mini-disk tension infiltrimeters, Double-Ring Infiltrimeters also measure the cumulative infiltration of water, but the Double-Ring Infiltrimeters measure infiltration into a field saturated soil instead of an unsaturated soil. The implementation of the Double-Ring Infiltrimeter follows the instruction in the Methods of Soil Analysis (Reynolds et al., 2002). The two concentric rings are inserted into the soil and water is maintained at a constant depth. The outer ring acts as a buffer to limit lateral flow from the center ring. The volume of water added in the center ring is recorded and used to compute the saturated hydraulic conductivity. If the infiltration from the center ring is assumed to be vertical and the hydraulic gradient is one, then the infiltration rate is equal to the hydraulic conductivity. Often, the outer ring reduces but does not eliminate lateral flow from the center ring, and adjustments to the infiltration rate are applied to adjust for divergent flow.

To account for divergent flow using the Double-Ring Infiltrimeter, the following equation relates the saturated hydraulic conductivity, K_s , to the quazi-steady infiltration rate, q_s .

$$K_s = \frac{q_s}{[H/(C_1d+C_2a)]+\{a/[\alpha^*(C_1d+C_2a)]\}+1} \quad [5]$$

where H is the steady depth of ponded water in the ring (m), a is the ring radius (m), d is the depth of insertion of the ring into the soil (m). Values for the macroscopic capillary length, α^* , is assumed based on the soil texture and structure from Reynolds et al. (2002). When the insertion depth, d , is greater than or equal to 0.03 m (3 cm) and the ponded height of water, H , is greater than or equal to 0.05 m (5 cm), then the values of the quazi-empirical constants, C_1 and C_2 are assumed to be 0.316π and 0.184π , respectively.

Recharge from a River

For a river disconnected from the groundwater, the hydraulic gradient is assumed to be one, and the infiltration capacity is equal to the hydraulic conductivity of the riverbed. This assumes that the riverbed is the controlling factor for transmission losses and that the process is a one-dimensional vertical infiltration. The amount of water lost from the river and available for groundwater recharge would be the product of the width of the river, the length of the river segment and the hydraulic conductivity.

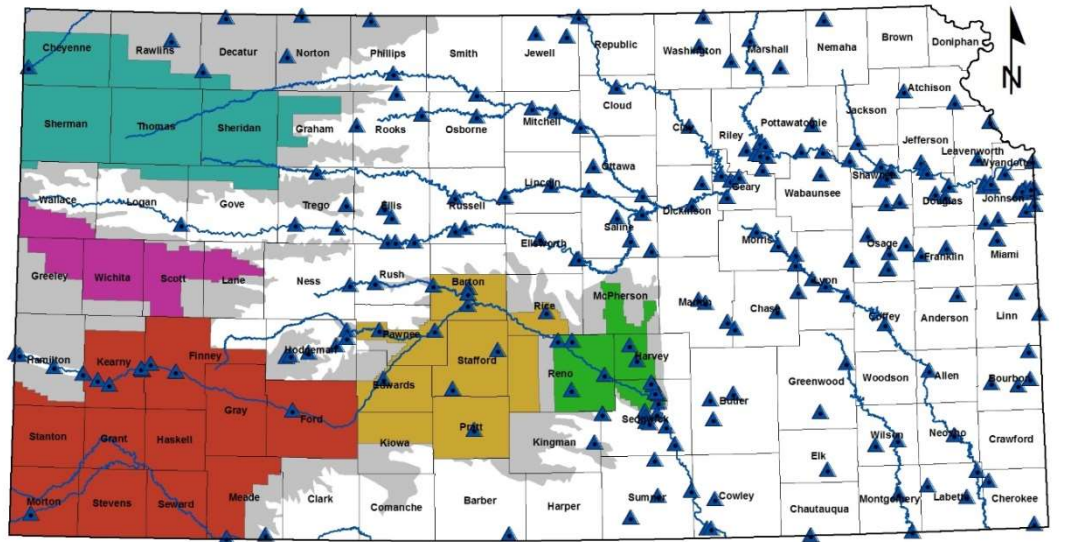
Modeling infiltration processes in a soil profile provides insight into the rates of infiltration and what factors control infiltration capacity. To simulate the one-dimensional infiltration, the riverbed hydraulic properties are modeled in Hyrus-1D. Hydrus-1D is a software package that simulates one-dimensional movement of water, heat and solutes through soil by solving Richards equation using numerical solution. Inputs to Hydrus-1D for infiltration analysis include selections of hydraulic models, soil hydraulic parameters, soil profile, initial conditions and boundary conditions. The time scale and observations points are selected to collect data and to report on the pressure heads and fluxes at the defined time steps and observation points.

Application at the Field sites

Site Selection Plan

The instrumentation of the Arkansas River and Cimarron River is focused on the region within the Kansas Groundwater Management District (GMD) 3. GMD 3 manages the groundwater in the Ogallala Aquifer in the southwest corner of Kansas as shown in Figure 3-1. The region was selected because it contains both major rivers within its boundaries and has operational United States Geological Survey (USGS) gaging stations providing daily discharge

measurements of the rivers. Previous studies of the rivers include Ahring and Steward (2012), which examined the hydraulic properties of the river in this region based on the change in phreatophytes, deep rooted plants that draw water from groundwater sources. The location and density of the phreatophytes along the rivers were mapped using aerial imagery of the region before and after the development of the Ogallala Aquifer, and the changes inform the relationship of the Arkansas River and the Cimarron River to the aquifer. The soils of the region have been characterized by the United States Department of Agriculture (USDA) Natural Resources Conservation Service (NRCS) using the four hydrologic soil groups. The map of the hydrologic soil groups for southwest Kanas is shown in Figure 3-2. Site selection was based off past studies of the Arkansas and Cimarron Rivers, access to the sites, and spacing along the river. The goal the site visits was to have one site from each of the counties in the region. Additional sites would be beneficial to provide more confidence in interpolating the hydraulic properties of the riverbed and to determine the optimal sampling density of the riverbed. However, access to the riverbed limited the instrumentation of additional sites.



Legend

- ▲ USGS gauges
 - Rivers
 - County Boundaries
 - High Plains Aquifer
- GMD**
- | | | | | |
|---|---|---|---|---|
| 1 | 2 | 3 | 4 | 5 |
|---|---|---|---|---|

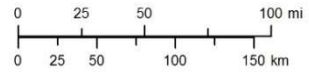


Figure 3-1: Map of Kansas with the Groundwater Management Districts

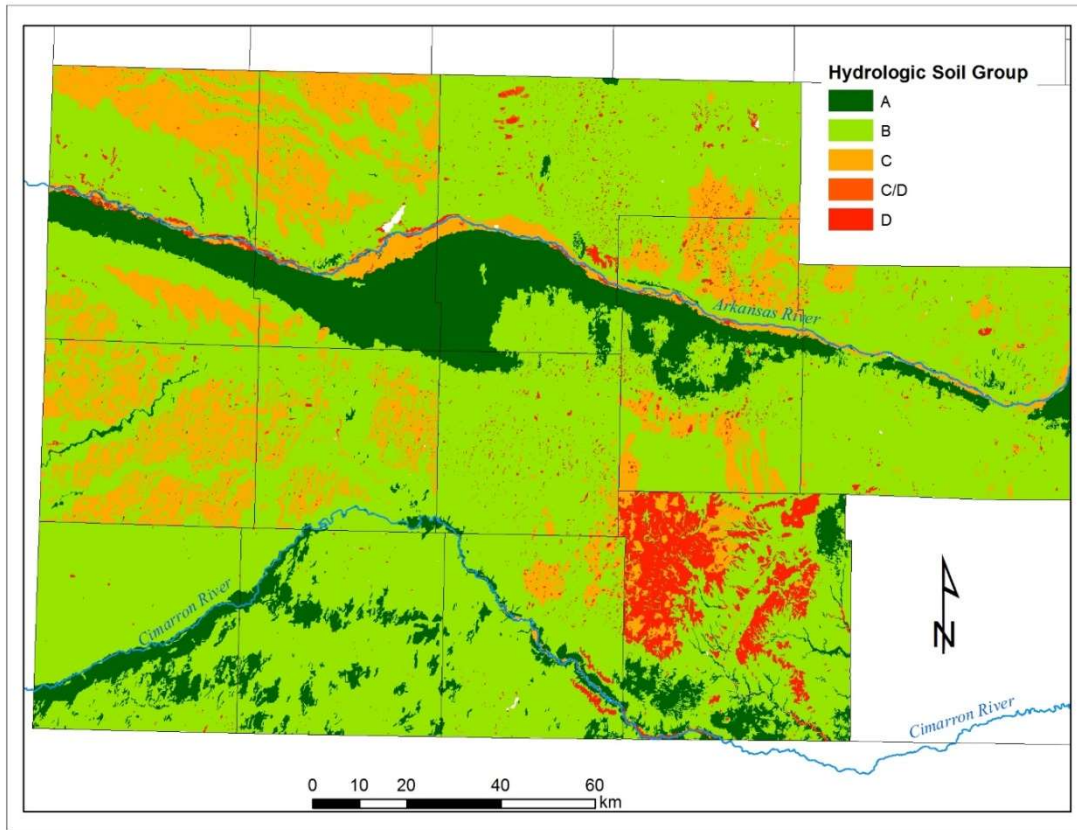


Figure 3-2: Hydrologic Soil Groups in Southwest Kansas

Instrumentation of the Riverbed

The sites were instrumented with the Double-Ring Infiltrimeters and mini-disk tension infiltrimeters over the course of three site visits. The water was sourced from local public water supplies. Minimal site preparation was needed to set up the instrumentation. The riverbed was generally clear of dense vegetation and debris that would inhibit placement of the infiltrimeters. The riverbed sediments did not require any addition of material to enhance the hydraulic contact between the infiltrimeters and the riverbed. The Double-Ring Infiltrimeters were set up in the center of the dry riverbed as seen in Figure 3-4. The diameter of the outer ring, inner ring, the

insertion depth and ponded height varied for each site and is documented in Appendix B. The water levels in the rings were maintained at a constant height. The volume of water added to the inside chamber was measured and recorded as the cumulative infiltration. The mini-disk tension infiltrometers were used in the riverbed next to where the Double-Ring Infiltrometer was set up. The manually operated mini-disk tension infiltrometers were manufactured by Decagon have a disk radius of 2.25 cm and have a bubble chamber to provide an adjustable tension between 0.5 cm and 7 cm. The adjustable tube was set up to collect data at tensions of 2 cm and 6 cm. The water levels in the infiltrometer were recorded at predetermined time steps. The values were recorded on a record sheet and later analyzed to determine the unsaturated hydraulic conductivity.

The automated mini-disk tension infiltrometers were installed in the river bed to characterize the spatial variability of the infiltration capacity at a riverbed scale. The automated mini-disk infiltrometers have the tension controlled by a capillary tube for 3 cm of tension. The diameter of the disks for all automated mini-disk tension infiltrometers are 1.58 cm. Two lines of measurement were set up; the main instrumentation line was across the channel and the secondary instrumentation line was along the length of the channel. The nominal spacing of the measurements was 0.6 m (2 ft), using instrumentation stands as seen in Figure 3-6. The automated mini-disk tension infiltrometers record the water level via pressure transducers and transmits the data through a mote network to the data collection laptop (Madsen and Chandler, 2007). The wireless motes were setup to provide a clear line-of-sight to the data collection laptop. The data tables for the automated mini-disk tension infiltrometers were downloaded from the application and converted to an Excel format for later processing. Due to the

availability of the data collection laptop, the automated mini-disk tension infiltrometers were only operational for the last of the three trips to the site visits.

Soil samples were collected from the sites, and gradation analysis was performed in the lab to determine soil type. Gradation analysis was performed on the soil samples. First, the samples were dried in an oven to remove moisture; samples were periodically weighed during the drying process until a constant weight was achieved. Next, the dry samples were run through a series of sieves. The weight of the sample retained on each of the sieves was measured and recorded. If the sample contains enough fine material (approximately 50 g), a hydrometer analysis was performed to partition the fine soil that passes the #200 sieve into silt and clay. From the gradation analysis, the soil type characterized in the field is confirmed or revised. The soil parameters, n and α , are assumed based on the soil type, and those parameters are used in the infiltration analysis to determine unsaturated hydraulic conductivity. A subset of soil samples was also subjected to a constant head permeameter test in the laboratory to determine hydraulic conductivity. The data and results are captured in Appendix B.

Analysis

Appendix B contains (1) a vicinity map of the sites including aerial imagery, (2) a map of the results of the automated mini-disk tension infiltrometer results, (3) results and computations for the double-ring infiltrometer measurements, (4) results and computations for the mini-disk tension infiltrometers, (5) results of the automated mini-disk tension infiltrometers, (6) constant-head permeability results, and (7) well logs from the Water Well Completion Records (WWC5) Database from the Kansas Geological Survey. Not all of the sites had the same data and results due to the availability of the instrumentation and the inconsistent extraction of soil samples.

The locations of the sites are shown in Figure 3-3. Data collected from the Double-Ring Infiltrometers was processed using equation [5]. Figure 3-4 and Figure 3-5 show the field instrumentation and a sample analysis of the Double-Ring Infiltrometers. From Figure 3-5, the slope the line in the linear regression equation, 2.66×10^{-4} m/s (0.0266 cm/s), is the quazi-steady infiltration rate, q_s , used in equation [5]. The data collected at the sites with the mini-disk tension infiltrometers was analyzed using equation [1] with the Zhang (1997) equations [2], [3a] and [3b]. The parameters n and α were assumed based on soil textural class using Carsel and Parish (1988). Figure 3-6 and Figure 3-7 show the riverbed instrumentation of the mini-disk tension infiltrometers and a sample of the analysis using the one-dimensional infiltration equation [1]. From Figure 3-7, the first coefficient of the polynomial regression equation, 8.66×10^{-5} m/s (0.00866 cm/s), is the C_2 from equation [2]. Additional results are captured in Appendix B.

Gradation analysis and the resulting USDA soil classification are shown in Table 3-1. Not all sites were characterized by gradation due to the inconsistent collection of soil samples. Table 3-1 identifies those sites without gradation information with “N/A”. For available samples without a sufficient mass of fine material to further characterize, the percent clay is negligible and is shown as “NEGL”. The soils in the Arkansas River are consistently sands with a very low percentage of fines that pass through the #200 sieve. The soils in the Cimarron River shift from a sand in the far southwest of Morton County to a loamy sand for the further east site in Haskell County. The North Cimarron River has a sandy loam bottom. From Carsel and Parrish (1988), a typical hydraulic conductivity for a sand is 29.70 cm/hour or 8.25×10^{-5} m/s, and for a loam sand is 14.50 cm/hour or 4.03×10^{-5} m/s.

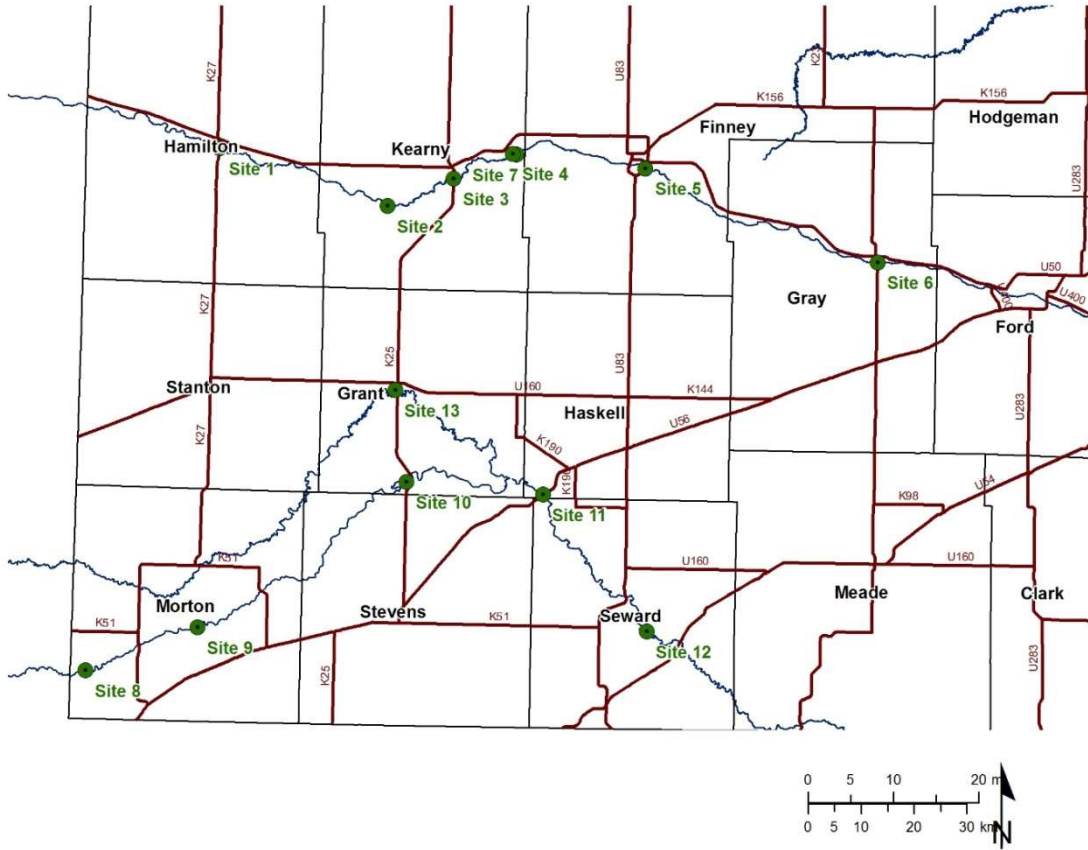


Figure 3-3: Map of Southwest Kansas Showing the Site Locations



Figure 3-4: Double-Ring Infiltrometer in a Dry Riverbed

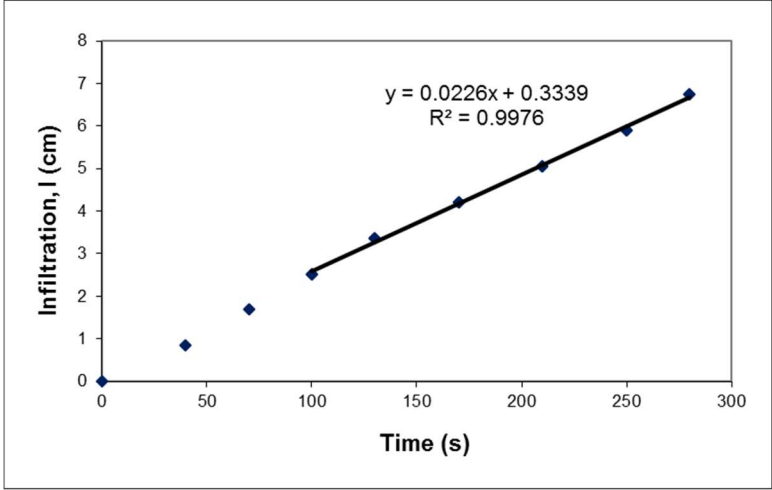


Figure 3-5: Analysis of Double-Ring Infiltrometer Data



Figure 3-6: Automated Mini-disk Tension Infiltrimeters in a Dry Riverbed

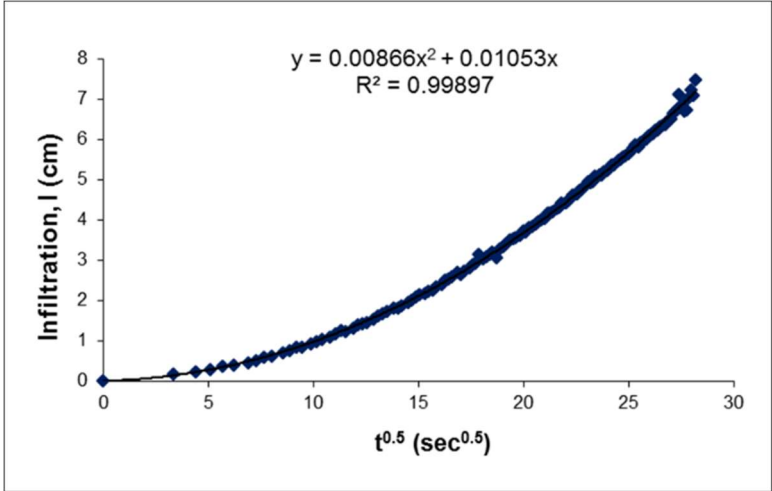


Figure 3-7: Cumulative Infiltration for Eq. [1]

Table 3-1: Gradation Analysis of the Riverbed Sediments

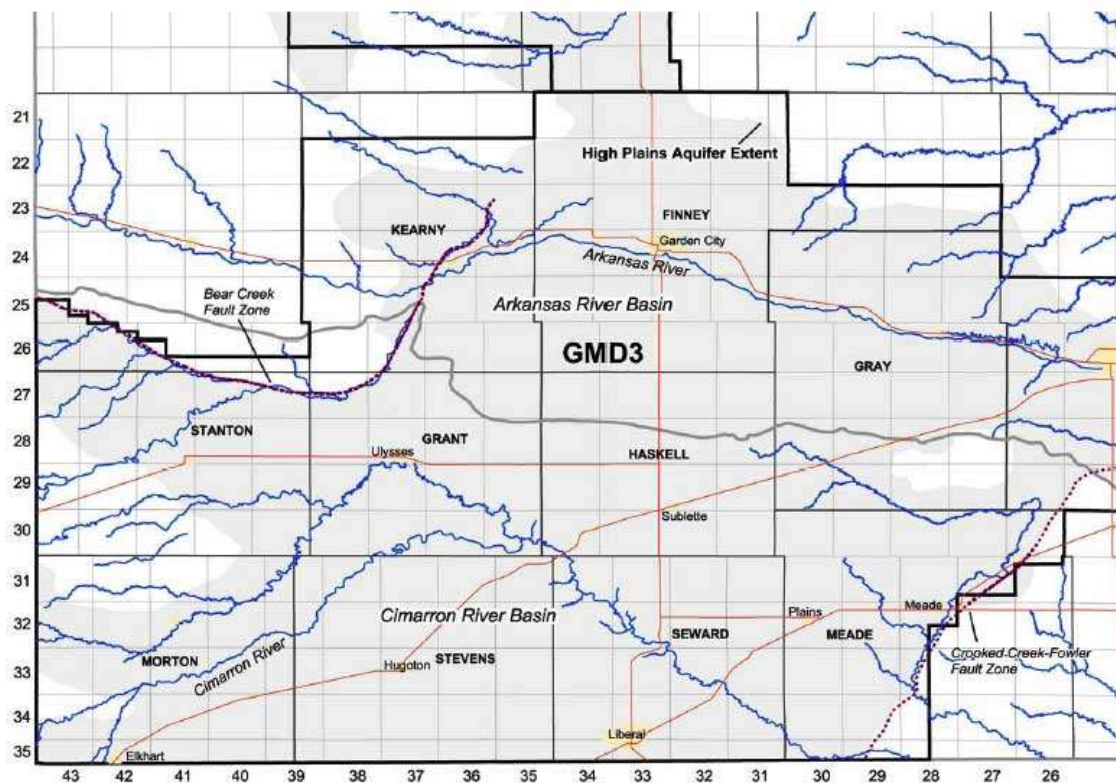
Site	Description	Soil Type	% Sand	% Fines	% Clay
1	Arkansas River at Syracuse	Sand	98.9	1.1	NEGL
2	Arkansas River near South Ditch	Sand	99.7	0.3	NEGL
3	Arkansas River at Lakin	Sand	N/A	N/A	N/A
4	Arkansas River at Deerfield	Sand	N/A	N/A	N/A
5	Arkansas River at Garden City	Sand	98.9	1.1	NEGL
6	Arkansas River at Cimarron	Sand	99.8	0.2	NEGL
7	South Ditch at Deerfield	Sand	N/A	N/A	N/A
8	Cimarron River at Elkhart	Sand	94.1	5.9	NEGL
9	Cimarron River at Morton	Sand	95.0	5.0	NEGL
10	Cimarron River at Ulysses	Loamy Sand	86.4	13.6	2.2
11	Cimarron River at Haskell	Loamy Sand	83.6	16.4	2.3
12	Cimarron River at Seward	N/A	N/A	N/A	N/A
13	North Cimarron River at Ulysses	Sandy Loam	73.6	26.4	6.4

Note: For sites with “NEGL” for percent clay, the sediments contain a negligible amount of clay. For sites with “N/A”, data was not collected.

Interpolation between sites

The instrumentation of the sites in the riverbed characterizes the hydraulic properties at that site, but to ascertain the properties along the length of the river, the point data is interpolated. Since spatial correlation of a geographic variable tends to increase with the decrease in distance between two measurements, a nearest-neighbor interpolation was applied. A nearest-neighbor interpolation informed by geology was used to extend the point measurements of the hydraulic conductivity to the length of the river. Although the results from the mini-disk tension infiltrometers indicated variation within the sites, the results did not indicate a predictable pattern or an expected pattern at the riverbed scale. It is expected that a higher hydraulic conductivity to be located at the center of the channel or where the water is deepest (Chen, 2005). As a result, the values for the saturated hydraulic conductivity from the Double-Ring Infiltrometers

measurements were used in the interpolation. The geology of Kansas informed the interpolation of hydraulic conductivity using the Bear Creek Fault line. The Bear Creek Fault, as shown in Figure 3-8, is the western boundary of the Ogallala Aquifer, and crosses the Arkansas River in Kearny County, KS. The segment of the Arkansas River up-gradient of Bear Creek Fault was assumed to be different from the segment down-gradient of the Bear Creek Fault because of the underlying aquifer. Generally, the hydraulic conductivity of the river segment would have the same value as the nearest instrumented site. The exception is for the segment that straddles the fault. The segment to the east of the fault was assigned the value of the nearest site to the west of the fault (Site 1) instead of the closer station east of the fault (Site 2) at the Bear Creek Fault.



Source: Whittemore et al. (2005)

Figure 3-8: Location of the Bear Creek Fault Line in southwestern Kansas

Results

Infiltration rates into the riverbed along the Arkansas River are consistently high as is expected from a sand. Infiltration rates along the Cimarron River are lowest in Grant and Seward Counties, and highest in Morton County at the far southwest of the state. The resulting hydraulic conductivities and the unsaturated hydraulic conductivities are shown in Table 3-2, Omissions in the following two tables are due either to the varying availability of the measurement devices at the time of instrumentation or to site conditions prohibiting the collection of data. For earlier collection dates, the automated mini-disks were non-functional due to the availability of the data collection laptop, and only the manual mini-disk tension infiltrometers were used.

Table 3-3, and Table 3-4. Appendix B has the saturated hydraulic conductivities obtained from the tension infiltrometers using the Gardner model. Figure 3-9 shows the point values for hydraulic conductivity in the riverbeds of the study area using the Double-Ring Infiltrometer. The hydraulic conductivity is highest in the Arkansas River in Kearny County near the head gate of the South Ditch; this location is also closest to the Bear Creek fault line. The hydraulic conductivity is lowest in the Cimarron River in Seward County. The interpolation of the point measurements of hydraulic conductivity at the sites to the length of the Arkansas River and Cimarron River are shown in Figure 3-10.

Table 3-2: Hydraulic Conductivity of the Riverbed from Double-Ring Infiltrometers

Site	Description	K(sat) (m/s)
1	Arkansas River at Syracuse	1.8E-05
2	Arkansas River near South Ditch	1.4E-03
3	Arkansas River at Lakin	1.4E-05
4	Arkansas River at Deerfield	7.0E-05
5	Arkansas River at Garden City	9.8E-05
6	Arkansas River at Cimarron	3.3E-04
7	South Ditch at Deerfield	1.0E-05

8	Cimarron River at Elkhart	7.7E-05
9	Cimarron River at Morton	3.2E-05
10	Cimarron River at Ulysses	2.0E-06
11	Cimarron River at Haskell	1.2E-05
12	Cimarron River at Seward	3.6E-06
13	North Cimarron River at Ulysses	4.6E-05

Omissions in the following two tables are due either to the varying availability of the measurement devices at the time of instrumentation or to site conditions prohibiting the collection of data. For earlier collection dates, the automated mini-disks were non-functional due to the availability of the data collection laptop, and only the manual mini-disk tension infiltrometers were used.

Table 3-3: Unsaturated Hydraulic Conductivity from Automated Mini-disk Tension Infiltrimeters

Site	Description	K(h = -3) (m/s)		
		Mean	StdDev	n
1	Arkansas River at Syracuse			
2	Arkansas River near South Ditch	1.8E-04	1.5E-04	20
3	Arkansas River at Lakin			
4	Arkansas River at Deerfield			
5	Arkansas River at Garden City	1.7E-04	1.1E-04	49
6	Arkansas River at Cimarron	3.1E-04	2.3E-04	49
7	South Ditch at Deerfield			
8	Cimarron River at Elkhart	5.0E-05	1.5E-05	20
9	Cimarron River at Morton			
10	Cimarron River at Ulysses	2.0E-04	2.9E-04	31
11	Cimarron River at Haskell			
12	Cimarron River at Seward			
13	North Cimarron River at Ulysses	3.7E-05	2.2E-05	15

Table 3-4: Unsaturated Hydraulic Conductivity from Mini-disk Tension Infiltrimeters

Site	Description	K(h=-2 cm) (m/s)			K(h=-6 cm) (m/s)		
		Mean	StdDev	n	Mean	StdDev	n
1	Arkansas River at Syracuse						
2	Arkansas River near South Ditch	3.4E-04		1	1.3E-04		1
3	Arkansas River at Lakin	3.9E-04	8.6E-05	4	2.1E-04	2.4E-04	4
4	Arkansas River at Deerfield	5.3E-04	2.0E-04	3			
5	Arkansas River at Garden City	1.1E-04		1	1.3E-04		1
6	Arkansas River at Cimarron	2.1E-04		1	6.1E-05		1

7	South Ditch at Deerfield	4.9E-04	2.9E-04	3	1.6E-03	1.3E-03	3
8	Cimarron River at Elkhart						
9	Cimarron River at Morton	2.5E-04	1.5E-04	3			
10	Cimarron River at Ulysses						
11	Cimarron River at Haskell						
12	Cimarron River at Seward	4.7E-05	1.9E-05	3	1.9E-05	4.4E-06	3
13	North Cimarron River at Ulysses	6.0E-05		1	5.6E-05		1

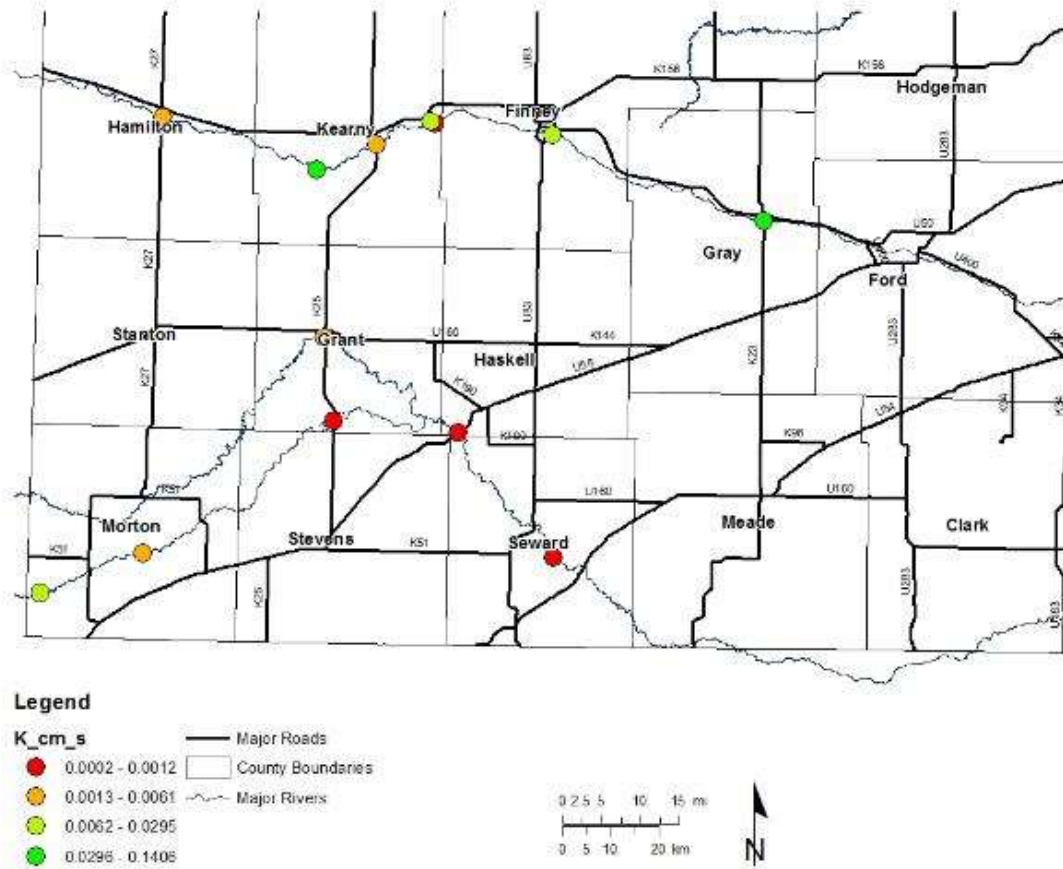


Figure 3-9: Hydraulic Conductivity of the Riverbed Using the Double-Ring Infiltrimeter

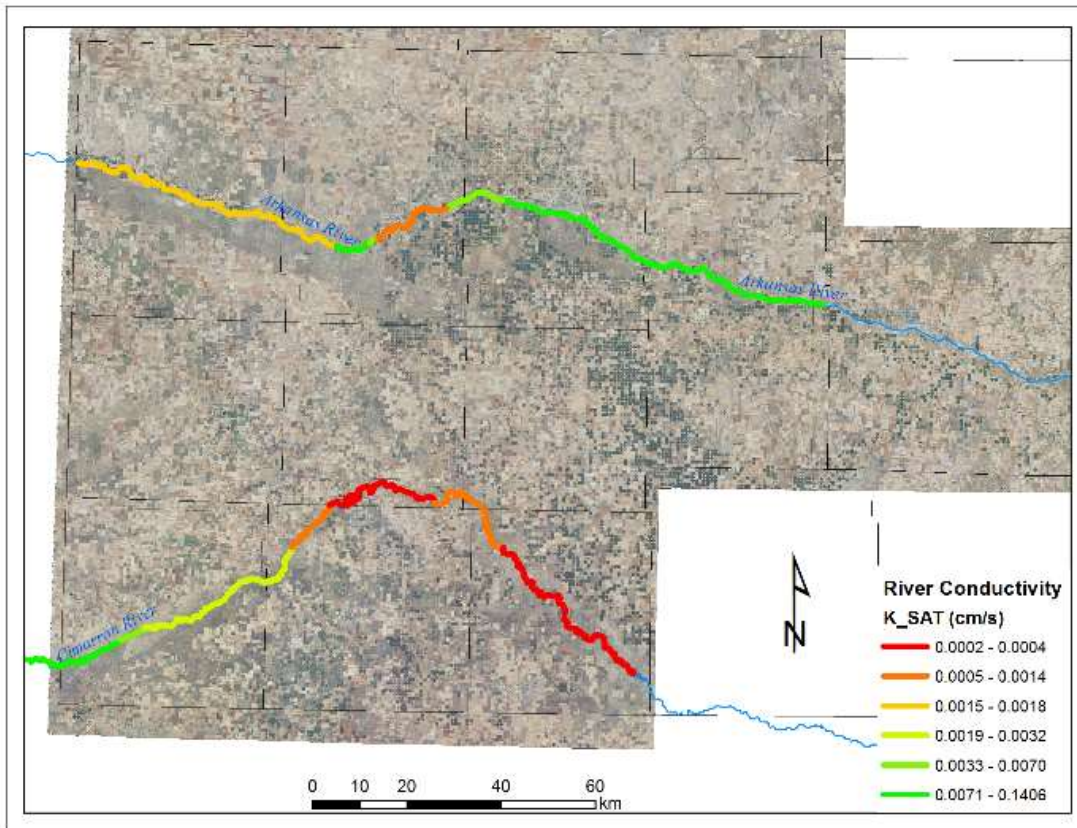


Figure 3-10: Map of Southwest Kansas with Interpolated Hydraulic Conductivities

One-Dimensional Infiltration at Surface Using Hydrus-1D

Gravity driven infiltration into the riverbed was simulated using Hydrus-1D and a model of the Arkansas River at Syracuse. To evaluate the impact of unknown properties of the geology below the surface of the riverbed, three scenarios were modeled: (1) free drainage of a sand, (2) sand with an impermeable lower boundary condition, and (3) sand with an underlying layer of clay with a free-drainage lower boundary condition. For the free drainage of sand, the hydraulic conductivity from the field measurements at Syracuse were used. The saturated hydraulic conductivity at Syracuse was measured to be 1.8×10^{-5} m/s or 6.48 cm/hr. For all other hydraulic properties, values for sand were taken from the soil catalog within Hydrus-1D. The

van Genuchten-Mualem model (van Genuchten, 1980) for single porosity was selected as the hydraulic model.

For model simplicity, the depth of the profile was set at 1 meter. A constant pressure head of 1 cm was established as the upper boundary condition. The lower boundary condition was varied based on the scenario. The parameters for the model are recorded in Table 3-5.

Table 3-5: Hydrus-1D Water Flow Parameters

Water Flow Parameters	Sand	Clay
Residual Water Content, Q_r	0.045	0.068
Saturated Water Content, Q_s	0.43	0.38
Water Retention Parameter, α (1/cm)	0.145	0.008
Water Retention Parameter, N	2.68	1.09
Hydraulic Conductivity, K_s (cm/hour)	6.48	0.2
Tortuosity parameter, l	0.5	0.5

Scenario 1: Free Drainage of a 1-m sand column

For the first scenario, the initial conditions have the pressure head, h , at the surface set to 1 cm and -18.06 cm for the rest of the profile. Observation nodes were set at depths of 19 cm, 39, 59, 79, and 99 cm. Hydrus-1D output graphs of the pressure head and fluxes at the five observation nodes are in Figure 3-11 and Figure 3-12. The results show the pressure head increases as the wetting front arrives at each observation node. The maximum pressure head is equal to the upper boundary condition of 1 cm. The fluxes are constant through the water column after 4.5 hours and the constant flux is equal to the saturated hydraulic conductivity.

Observation Nodes: Pressure Heads

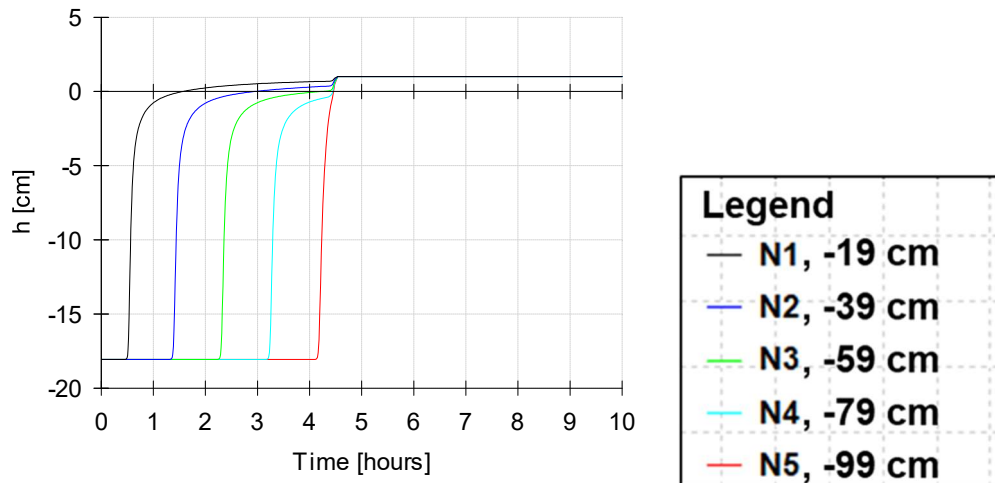


Figure 3-11: Free Drainage of Sand - Pressure Heads

Observation Nodes: Fluxes

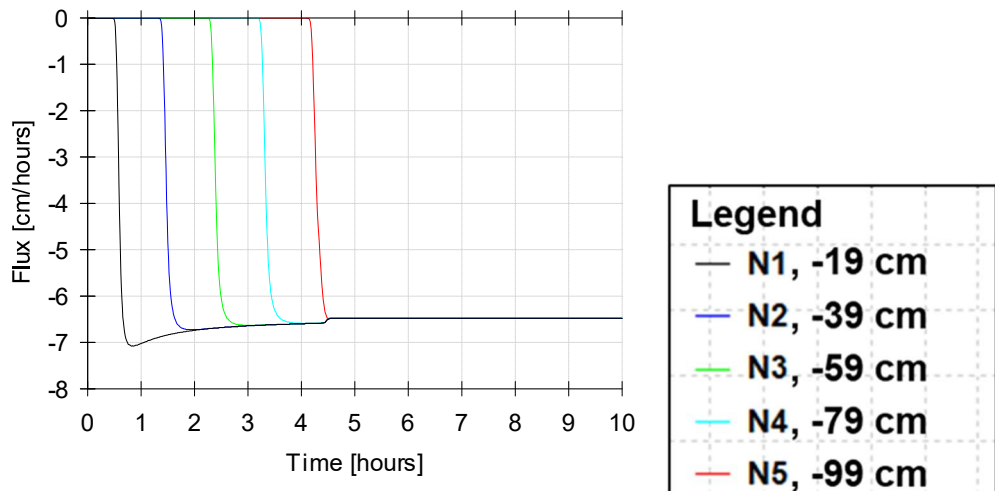


Figure 3-12: Free Drainage of Sand - Fluxes

Scenario 2: Impermeable lower layer

In the second scenario, the lower boundary condition is changed from a free drainage to a zero-flux boundary to represent an impermeable layer. The initial conditions and the material properties of the sand layer are the same from the first scenario. Hydrus-1D output graphs of the pressure head and fluxes at the five observation nodes are in Figure 3-13 and Figure 3-14. The

results show that the first four hours of the simulation are very similar to the first scenario. As water infiltrates the soil column, the pressure heads at the observation nodes increase and approach value of the pressure head at the upper boundary (1 cm) and the fluxes approach the hydraulic conductivity of the material. After four hours, the pressures and fluxes change from what is observed in a free drainage simulation to that of a static profile. The fluxes become zero and the pressure heads are dependent on the depth of the observation node. The soil profile becomes saturated, and since no water can drain, no additional water can infiltrate.

Observation Nodes: Pressure Heads

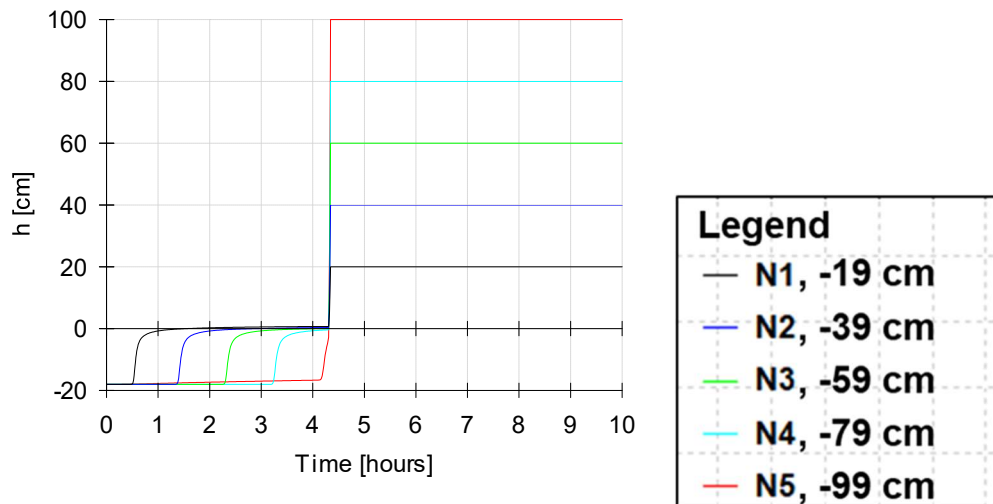


Figure 3-13: Impermeable Layer - Pressure Heads

Observation Nodes: Fluxes

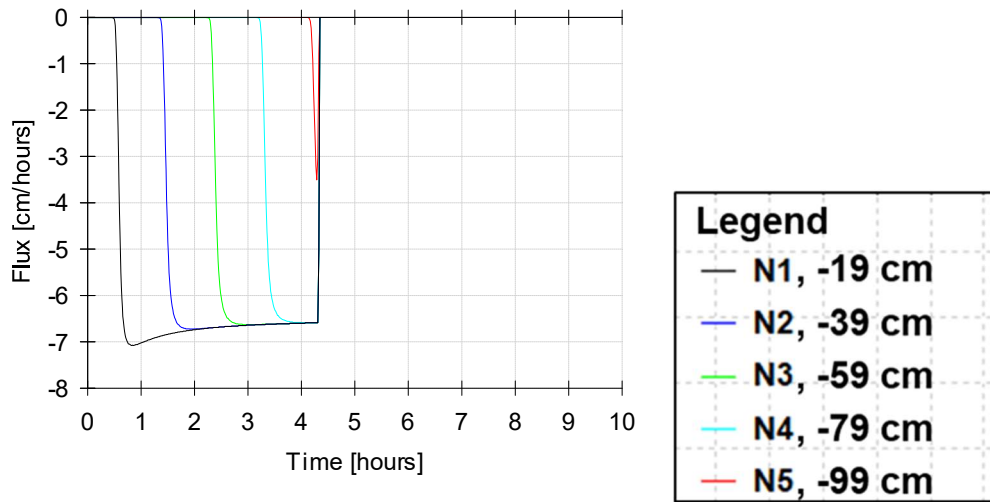


Figure 3-14: Impermeable Layer - Fluxes

Scenario 3: Two Layer Constant Pressure Head with Free Drainage

The third scenario maintains the top 99 cm of the profile as sand, but the bottom 1 cm was changed to a clay. The lower boundary condition is free-drainage. The top 1 cm of the soil profile has the pressure head set to 1 cm. Between the top 1 cm and the bottom 1 cm, the pressure head is -18.06 cm. The bottom 1 cm of profile is the clay with a pressure head set to -154.36 cm. The initial condition for the pressure head is set as the field capacity of the soil. Hydrus-1D output graphs of the pressure head and fluxes at the five observation nodes are in Figure 3-15 and Figure 3-16. As the water infiltrates the water column, the fluxes are high, controlled by the hydraulic conductivity of the sand layer, while the clay layer controls the drainage of the soil column. When the water column becomes saturated, the clay layer controls both the infiltration and drainage of the soil column. During hour 4, the profile reaches a steady-state, controlled by the conductivity of the clay layer.

The response to saturation of the soil column is similar to that of the second scenario with the zero-flux boundary. While the bottom of the soil column is able to freely drain, the rate at

which the soil column is able to infiltrate water is controlled by the clay layer at the bottom of the soil column at later times. The clay acts as a confining layer and limits both the infiltration and drainage of the soil. When the soil column is saturated, the infiltration of water into the soil column is controlled by the permeability of the clay layer.

Observation Nodes: Pressure Heads

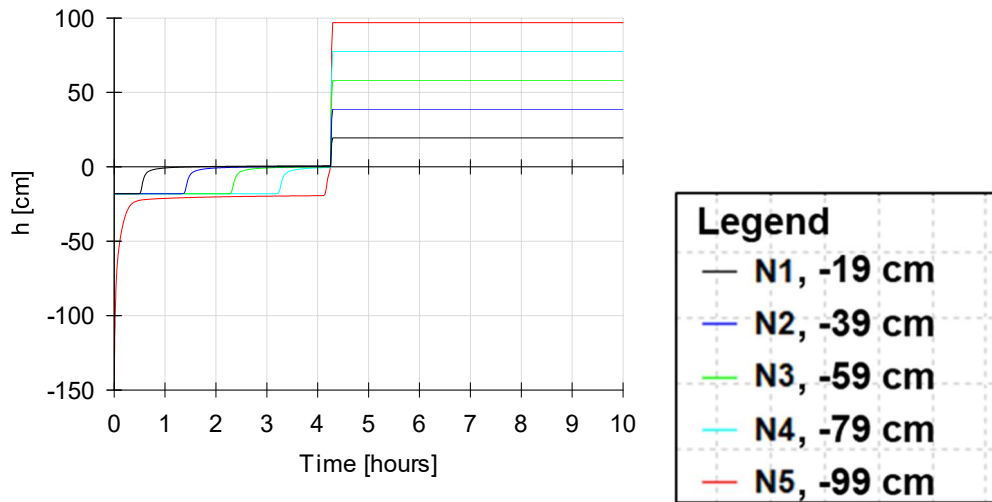


Figure 3-15: Two-Layer Sand-Clay - Pressure Heads

Observation Nodes: Fluxes

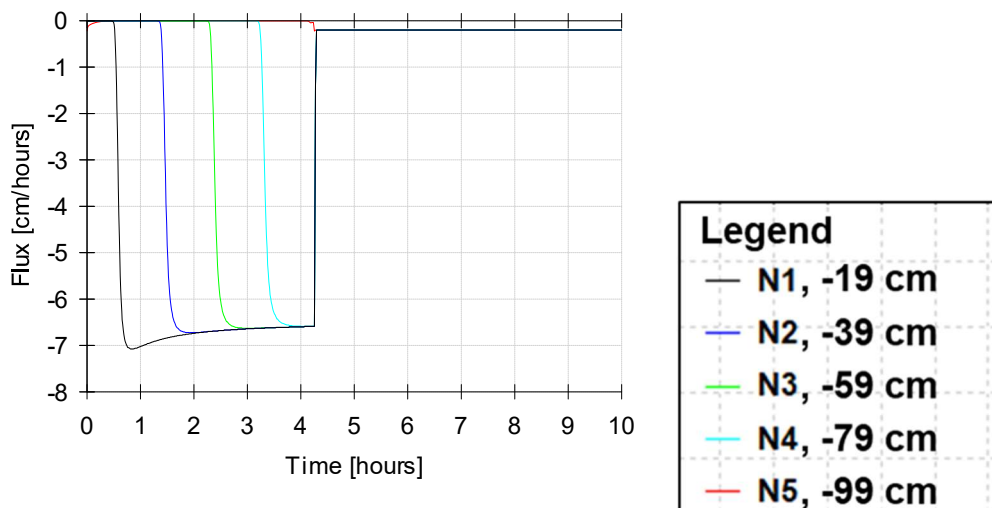


Figure 3-16: Two-Layer Sand-Clay - Fluxes

Discussion

The river alluvium transmits water to underlying layers controlled by the hydraulic conductivity of the riverbed sediments. This transmission of water is dependent on the properties of the sediment and the saturation of the riverbed. When a profile has a confining layer under the alluvium, the properties of that confining layer control the transmission of water when the profile becomes saturated. In western Kansas, the infiltration capacity of the surface of the rivers is high as expected of a sand. The hydraulic conductivities range from 1.4×10^{-5} m/s to 1.4×10^{-3} m/s for the Arkansas River and from 2.0×10^{-6} cm/s to 7.7×10^{-5} cm/s for the Cimarron River. For comparison, the sandy rivers in Nebraska, the Republican and the Platte, have vertical hydraulic conductivity values between 1.7×10^{-4} and 5.4×10^{-4} m/s (Chen, 2004). The expected hydraulic conductivity of a sand is 8.3×10^{-5} m/s with a standard deviation of 4.3×10^{-5} m/s (Carsel and Parrish, 1988). The hydraulic conductivities calculated for the Arkansas River are within the range of expected values. When a wetting front progress down an initially dry riverbed, the infiltration capacity and transmission losses would be high. As the sediments become saturated, the infiltration rate and the transmission losses will continue to be high if there is not confining layer. If the sediments are bounded by a layer with a significantly lower hydraulic conductivity or by an impermeable bedrock, then the transmission losses will be greatly reduced after the riverbed sediments become fully saturated.

The instrumentation used in this study is not able to fully characterize the river system processes that control groundwater-surface water exchanges. Mini-disk tension infiltrometers can capture the surface properties of a soil, and their portability and usability allow for multiple samples in a short amount of time. The mini-disks are limited in their ability to interrogate more than the surface properties of a soil. The volume of water used during the mini-disk

measurements was less than 0.1 liters. The Double-Ring Infiltrometers are able to determine the surface infiltration of the riverbeds at a larger spatial scale than the mini-disk tension infiltrometers. The amount of water added and recorded during the Double-Ring instrumentation was between 1 and 20 liters, and this is after the inner and outer rings had been filled. For the time duration and the amount of water consumed during instrumentation, the Double-Ring Infiltrometers were unable to interrogate a larger in-situ sample of the riverbed and possibly sense the underlying confining layers in the riverbed. Well logs in Appendix B show a bedrock of shale approximately 12 to 15 m (40 to 50 ft) below the riverbed for the western reaches of the Arkansas River. For the eastern reaches of the study area along the Arkansas River, the well logs show alternating layers of sandy gravel and sandy clay. Approaches to further characterize the river system include more focused instrumentation of the confining layer to directly determine its hydraulic properties or larger scale modeling that would be able to indirectly infer the hydraulic properties. In situ measurement methods for hydraulic conductivity are often limiting as only the top layer of the riverbed is typically characterized. From Chen (2011), hydraulic conductivity often decreases with depth. By only measuring the surface of the riverbed, the effective hydraulic conductivity of the entire depth of the riverbed would be overestimated. Other studies have found a pattern of periodicity across the across the channel (Chen, 2005). The results from the mini-disk tension infiltrometers did not produce any discernible patterns at the sites that were instrumented. Appendix B has the results for the six sites that were instrumented with automated mini-disk tension infiltrometers showing the spatial distribution of the $K(h)$ values.

The system is not a simple disconnected losing river where transmission losses are controlled by the surface properties of the riverbed, but instead it is a connected river where the

banks and alluvial sediment store the transmission losses. Assuming the transmission losses of the Arkansas River are controlled by the riverbed infiltration capacity, the transmission losses would be the product of the hydraulic conductivity, the width of the river and the length of the river segment. For the segment between Deerfield, KS and Garden City, KS, the average hydraulic conductivity is 8.4×10^{-5} m/s. The distance along the river between the two cities is 25.6 km or 25,600 m. With an average width of the river of 10 m, the estimated river discharge lost to the riverbed would be $21.5 \text{ m}^3/\text{s}$. Examining the Arkansas River in November 1999, a period when the region did not have measurable precipitation that would contribute surface runoff to the Arkansas River, the average discharge at Deerfield was $8.3 \text{ m}^3/\text{s}$, and the average discharge at Garden City was $6.4 \text{ m}^3/\text{s}$. The actual transmission loss for the month of November 1999 between Deerfield and Garden City was $1.9 \text{ m}^3/\text{s}$. The actual transmission losses are less than $1/10^{\text{th}}$ the modeled transmission losses. Based on the difference between actual and modeled transmission losses, the infiltration capacity of the riverbed is not the primary control mechanism for river transmission losses or potential aquifer recharge.

The one-dimensional flow analysis with Hydrus-1D provides insight on the controlling factors for riverbed infiltration. It is hypothesized that the transmission losses of the river are controlled by a confining layer under the river alluvium that regulates the conveyance of the infiltrated water to the underlying layers. From the available data, the initial infiltration rate when the riverbed is initially unsaturated is controlled by the hydraulic conductivity of the riverbed alluvium at the surface. Once the riverbed becomes fully saturated, then the infiltration rate becomes constrained by an underlying confining layer or bedrock. The water from the river does infiltrate to the underlying aquifer, but not at the rate determined by the surface infiltration measurements. Instead this water is stored in the alluvium and bank of the river. The storage of

water in the riverbed provides opportunities for other hydrologic processes to occur, for example evapotranspiration.

The relationship between the unsaturated and saturated hydraulic conductivities is not what is expected for all sites that were instrumented. From the Gardner model, the saturated hydraulic conductivity is expected to be greater than the unsaturated hydraulic conductivity. The exponential factor in the Gardner model converts between unsaturated and saturated so that the saturated is always greater than the unsaturated. In addition, the unsaturated conductivity at higher magnitude tensions is expected to be less than the unsaturated hydraulic conductivity at lower magnitude tensions. The data from Table 3-4 does not follow this expectation for all measured sites. For example, at Garden City (site 5), the hydraulic conductivity for $K(h = -2 \text{ cm})$ is less than $K(h = -6 \text{ cm})$ which contradicts the expectation. One explanation is that the variability in the measurements is greater than the expected difference of the two unsaturated hydraulic conductivity values. The number of replications was insufficient to determine the true mean of the unsaturated hydraulic conductivities or the true difference between the unsaturated hydraulic conductivities at the two tensions.

The saturated hydraulic conductivity is less than the unsaturated hydraulic conductivity for multiple sites, which also contradicts what is expected. The explanation is the limitations of the measurement methods. The Double-Ring Infiltrimeters were used to measure the saturated hydraulic conductivity, and the mini-disk tension infiltrimeters measured the unsaturated hydraulic conductivity. The Double-Ring Infiltrimeters sample a much larger area and depth than the mini-disks. If there is a confining layer under the surface of the river or the hydraulic conductivity declines with depth, then the Double-Ring Infiltrimeters would be detecting the effects of that layer or other stratification of the riverbed alluvium that the mini-disks cannot

sense due to their small size. The properties of the top 10 centimeters of the riverbed as measured with the mini-disks are different than the properties of the top 100 centimeters of the riverbed as measured with the Double-Ring Infiltrometers. Based on the analysis of the transmission losses between Deerfield and Garden City, it is possible that the effective hydraulic conductivity of the top 10 meters of the riverbed would be different than what was measured with the Double-Ring Infiltrometers.

Notable deviations in the expected relationship between unsaturated and saturated hydraulic conductivities are further examined based on field observations. The Cimarron River at Ulysses (Site 10) had a high unsaturated hydraulic conductivity and a very low saturated hydraulic conductivity. The fine soils and the low conductivity materials below the surface of the riverbed were captured with the Double-Ring Infiltrometer, but the smaller mini-disk tension infiltrometers did not sense that. The site of the Arkansas River near the South Ditch Head Gate (Site 2) had a notable difference between the saturated and the unsaturated measurements. That site had the highest hydraulic conductivity from the Double-Ring Infiltrometers, but moderate values for the mini-disks. This site had a very coarse sand that does not provide the capillary forces to pull the water from the tension infiltrometer. The relationship between the unsaturated hydraulic conductivity and the saturated hydraulic conductivity for Site 2 near the South Ditch Head Gate is not the same as other sites that have a sandy riverbed sediment. Additional characterization of hydraulic properties of the coarse sand is needed to resolve this irregularity.

The variability of the riverbeds was characterized based on the instrumentation results. On the Arkansas River, the hydraulic conductivity of the riverbed is high. It is a sandy soil that is capable of high rates of infiltration. The capacity to infiltrate into the riverbed along the Arkansas River is consistently high. On the Cimarron River, the hydraulic conductivity is

generally lower than on the Arkansas River. The segment in Morton County in the far southwest corner of the state has the greatest infiltration capacity. The sandy soil in the southwestern segment in Morton County transitions to a finer loam as the river progresses downgradient to Haskell and Seward Counties. The infiltration capacity decreases as the river progresses down gradient as expected with the change in riverbed composition. The finer sediments in the eastern counties of the study area allow the soils to retain water better than the sandy soils. This leads to available water to support vegetation and to greater rates of evapotranspiration from the river corridor.

The riverbed of the Arkansas River was primarily sandy due to several factors. As the river experiences cessation of flow, the expectation is that the suspended sediments would settle and deposit on the riverbed either in a layer of fine sediments on the surface or clogging the voids in the sandy riverbed. One of the factors is the John Martin Reservoir upstream of the study area along the Arkansas River in Colorado. The reservoir acts as a sediment trap with a greater suspended sediment load entering the reservoir than exiting the reservoir. The limited overland flow contribution to the Arkansas River is another factor. Between the Colorado State line and Garden City, no major tributaries flow into the river. Also, the management of the landscape prevents runoff and conserves soils resulting in a limited volume of overland flow that would carry the suspended fine sediments to the river. The last factor is the sandy alluvial plain that surrounds the Arkansas River. Unlike the Cimarron River, the Arkansas River has a surficial geology separate from the surrounding watershed. The sediments of the Cimarron River are more heavily influence by the local soils as seen in the lower hydraulic conductivities near Hydrologic Soil Group (HSG) B as it transitions away from the sandier HSG A in Grant County, Kansas. Another consideration is that the hydraulic properties below the surface where not

characterized by the instrumentation methods. From Chen (2011), hydraulic conductivity tends to decrease with depth. While the surface is sandy with high hydraulic conductivity, the composition of the sediments below the surface may be finer with a lower hydraulic conductivity.

Conclusions

The capacity of the riverbed sediment to provide a conduit for groundwater recharge was studied in western Kansas. The Arkansas River and the Cimarron River were instrumented with both Double-Ring Infiltrometers and mini-disk tension infiltrometers to collect the saturated and unsaturated hydraulic conductivities of the riverbed. This provides the infiltration capacity within the channel and along the lengths of the Arkansas River and Cimarron River in southwest Kansas. It was found that the sandy sediment of the Arkansas River had hydraulic conductivities between 1.4×10^{-5} m/s to 1.4×10^{-3} m/s. The Cimarron River transitioned from a sandy riverbed in the western reaches of the state to a loamy sand further east with hydraulic conductivities between 7.7×10^{-5} m/s to 2.0×10^{-6} m/s. The results indicate that the riverbed has a high capacity to infiltrate water.

The computer model Hydrus-1D was used with parameters ascertained from instrumenting the riverbed to simulate the gravity driven infiltration into the riverbed. The interpretation of the in-situ measurements with the one-dimensional analysis and the larger scale transmission loss analysis indicates that when the river is saturated, a confining layer under the riverbed limits the potential groundwater recharge to about $1/10^{\text{th}}$ of the surface infiltration capacity. The next chapter will apply a simple transmission loss model to refine the relationship between the infiltration capacity and potential groundwater recharge.

Chapter 4 - Transmission Loss Model

Introduction

Transmission losses from a river are a potential source of focused recharge to refill depleted groundwater stores at a greater rate than areal recharge. The areal recharge is limited by the annual precipitation, the soil permeability, and annual evapotranspiration. Although covering a smaller area, the groundwater recharge rates from a river have the potential to infiltrate at a much higher rate than areal recharge. As water tables decline in response to unsustainable groundwater extraction (Konikow and Kendy, 2005), the hydrologic regime of a river changes. Brunner et al. (2009) stated that if the area between a river and a groundwater system is fully saturated, then that flow regime is connected. The connected regime may be losing where the primary flow direction is from the river to the groundwater, or it may be gaining where the groundwater discharges into the river. If the area between the river and groundwater system is unsaturated, then that flow regime is disconnected. A clogging layer is a necessary criterion for river-aquifer disconnection (Brunner et al., 2009a). The infiltration rate of a connected, losing river-aquifer system is proportional to the head difference between the river and aquifer. In a fully disconnected river-aquifer system, the infiltration rate is at a maximum value and is not dependent on the depth to water table. The riverbed hydraulic conductivity is the primary factor that controls groundwater recharge, and that riverbed property can be highly variable (Calver, 2001; Bruen and Osman, 2004). Other factors that control transmission losses are the quantity of available water in the river (Jordan, 1977), the properties of the underlying layers (Kalbus et al., 2009), the state of connection between the river and aquifer, and the available storage in the soil and groundwater. Transmission losses and infiltration do not equate to groundwater recharge. Recharge will always be less than infiltration because some fraction of

the infiltration will be lost to evapotranspiration (Shanafield and Cook, 2014). The ability of an infiltration event to contribute to recharge is dependent on the duration of flow and initial moisture condition of the stream banks (Batlle-Aguilar and Cook, 2012) as well as the fraction of transmission losses consumed by evapotranspiration.

The transmission losses vary over time and position in the channel. Infiltration is highest at the onset of flow and at each stage increase resulting in an infiltration rate higher than under a steady-state condition (Batlle-Aguilar and Cook, 2012). When the water level of a ditch is held constant, infiltration into a ditch was at a near constant rate. . Transmission losses from a ditch produce groundwater mounds, and the propagation of the infiltrated water and potential contaminants would be limited to the banks of the ditch (Dages et al., 2008). Induced infiltration is the process of water infiltrating from a surface source to the groundwater water as the result of lowering the water. Groundwater pumping near a stream induces infiltration from the stream and reduces stream baseflow. Areal recharge and its contribution to baseflow is a factor in reducing the impact of stream depletion due to pumping (Chen and Shu, 2002). The impact of induced river infiltration to the total discharge is less than the reduction due to the reduced baseflow. The impact of induced infiltration becomes negligible after pumping, while the impacts of baseflow persist. A high conductance streambed responds to pumping with greater stream depletion. For a low conductance stream, the reduction in baseflow is a significant percent (90%) of the total stream depletion and can have lasting impacts even after pumping concludes (Chen and Shu, 2002).

Transmission loss models are used to quantify and predict the streamflow lost to the aquifer. Quantifying transmission losses are simple when a river is well gaged. Over a large scale, flow gaging can be used to estimate transmission losses if there are no significant

tributaries or surface water extractions (Cook, 2015). The difference between the upstream gage and the downstream gage is the amount gained or lost. Transmission loss estimation is challenging when a river is not well gaged or when the cessation of flow occurs between gages. Several transmission loss models have been developed, and they generally are a function of the upstream discharge plus a mechanism for losses along a length of a river. Niswonger et al. (2008) provides a method to estimate streambed hydraulic conductivity by using the changes in the streamflow front velocity as streamflow progresses down an initially dry channel. Costa et al. (2013) takes an event-based approach to determine a transmission loss rate for a Brazilian river system with channel transmission losses correlating to input river flow. Jordan (1977) applies an exponential decay function that uses the upstream and downstream volume to determine the rate of transmission loss per mile. The transmission loss per mile could be applied to less well gaged streams to determine transmission losses on similar types of streams. The United States Department of Agriculture (USDA) Natural Resources Conservation Service (NRCS) National Engineering Handbook (NEH) model for transmission losses is an approach that estimates the volume of runoff and peak discharge for ephemeral streams following storm event (Woodward, 2007). The NEH model can be used with observed stream flow data or model parameters can be predicted. The Lewis-Milne model is used for border irrigation systems and has been improved upon by Singh et al. (1990). The Lewis-Milne model is based on mass conservation and assumes a constant water depth and has been used to estimate recharge from overbank flooding from rivers (Doble et al, 2012). Abdulrazzak and Morel-Seytoux (1983) developed an approximate analytical solution for recharge over a water table and identified the transient parameters of stream-aquifer interactions affected by the development of a groundwater mound. Others have attempted to simplify the infiltration and transmission loss models that

approximate results of computationally intensive numerical modeling (Crosbie et al., 2014; Reid and Dreiss, 1990). Few models use the material properties of the riverbed as the primary driver for transmission losses from a river, but instead rely on measurements of the upstream and downstream discharges. The rivers in western Kansas are losing systems under a connected or disconnected flow regime. The lowering of the groundwater table has resulted in the decreasing extent of perennial streams in western Kansas (Angelo, 1994) and a decreasing stream flow (Juracek and Eng, 2017). Pathways from the Arkansas River to the Ogallala Aquifer are indicated by the mound formation under the rivers and the sulfate plume in the Ogallala Aquifer near the Arkansas River (Whittemore, 2000). The rivers in western Kansas have the potential to be conduits for natural groundwater recharge.

A simple transmission loss model was developed to understand the relationship between the riverbed infiltration and the declines in the river discharge using the hydraulic conductivity of the riverbed. The study approach is to develop a simple model for the infiltration into the riverbed using known or derived parameters for the Arkansas River in western Kansas, and then to optimize the model to match measured discharge in the river using a transmission loss factor. In the previous chapter, the conductivity of the riverbed was characterized. The Arkansas River is well gaged with gaging stations collecting and recording daily discharge rates. The results are examined along the western reaches of the Arkansas River in Kansas to determine the spatial dependencies and how those dependencies change over time. The results show how the surface properties of the river control the transmission losses and provides an estimate for the quantity of focused recharge entering the groundwater system via the riverbed. The objectives of this chapter are to (1) develop a simple transmission loss model (2) apply the model to the Arkansas River in western Kansas, (3) determine the model parameters to allow the modeled discharges to

match the measured discharges, and (4) analyze the spatial and temporal dependencies of the transmission losses.

Methods

Infiltration is the process of water entering the soil and is one of the key processes for transmission loss. Many approaches are available to model infiltration. Infiltration discharge per unit length of the river, q , is modeled using the Green-Ampt equation for infiltration:

$$q = KW \left[\frac{H+D}{D} \right] \quad [6]$$

where D is the depth of soil between the bottom of the river and the water table, H is the depth of water in the channel, W is the width of the river, and K is the hydraulic conductivity of the soil. If the depth of the water table is considerably greater than the depth of water in the channel, the above equation is simplified to

$$q = KW \quad [7]$$

Applying this relationship to a river, the infiltration discharge per unit length of a river is a factor of the hydraulic conductivity of the riverbed sediments and the width of the riverbed.

A transmission loss model determines the amount of river discharge that is lost due to infiltration into the riverbed along the length of the river or along a segment of river. Building from the simplified Green-Ampt equation [7], the simple transmission loss model is an infiltration model applied across river segments and starts with the assumption that steady-state infiltration is equal to the hydraulic conductivity of the riverbed. The discharge lost to the riverbed, $T_{i,i+1}$ (m^3/s) is modeled for each segment of the river identified by stations along the river, i

$$T_{i,i+1} = K_i(x_{i+1} - x_i) \frac{(W_{i+1} + W_i)}{2} C \quad [8]$$

Where K , hydraulic conductivity of the riverbed (m/s),

x , position along the length of the river (m),

W , width of the channel (m) at the upstream, W_i , and downstream, W_{i+1}

C , dimensionless transmission loss factor, and for a losing river, it varies between 0 and 1

with

$C = 1$, transmission losses controlled by the hydraulic conductivity

$C = 0$, no transmission losses

The simple transmission loss model is applied at the daily time scale. The width, the transmission losses per segment, and the transmission loss factor would vary for each subject day. The transmission loss factor is a fitting coefficient used to adjust the earlier assumption that the steady-state infiltration rate is equal the hydraulic conductivity. From the previous chapter, it was determined that the hydraulic conductivity at the surface is not necessarily the effective hydraulic conductivity of the entire depth of the riverbed. The transmission loss factor is used to fit the transmission loss model to the observed discharges in the river. With transmission losses occurring at each segment of the river, the discharge along the length of the river decreases as represented in the following equation:

$$Q_{i+1} = Q_i - T_{i,i+1} \quad [9]$$

Where Q_i is the inflow discharge (m^3/s) for the river segment, and Q_{i+1} is the outflow discharge (m^3/s) for the river segment.

The width of the river is dependent on the shape of the river cross-section and the discharge in the channel. The river width-discharge relationship from Leopold and Maddock (1953) is a power function with parameters a and b .

$$W = aQ^b \quad [10]$$

Where W is the width of the river (m), Q is the discharge (m^3/s), and a and b are dimensionless parameters. The parameters are determined using assumptions on the river channel cross-section, Manning's equation. The relationship is validated using aerial imagery collected on days with known river discharges. Manning's equation is a function of the river velocity and the cross-sectional area of the river.

$$Q = VA = \left(\frac{1.00}{n}\right) AR^{\frac{2}{3}}S^{\frac{1}{2}} \quad [11]$$

The velocity, V (m/s), is computed using the longitudinal slope of the river, S (%), the hydraulic radius, R (m), and Manning's roughness coefficient, n . Gaging station provide river discharge, Q (m^3/s). The slope of the river is determined from topographic maps. The cross-sectional area and hydraulic radius are dependent on the shape of the river channel. The roughness coefficient is selected based on field observations from Chow (1959).

Case Study

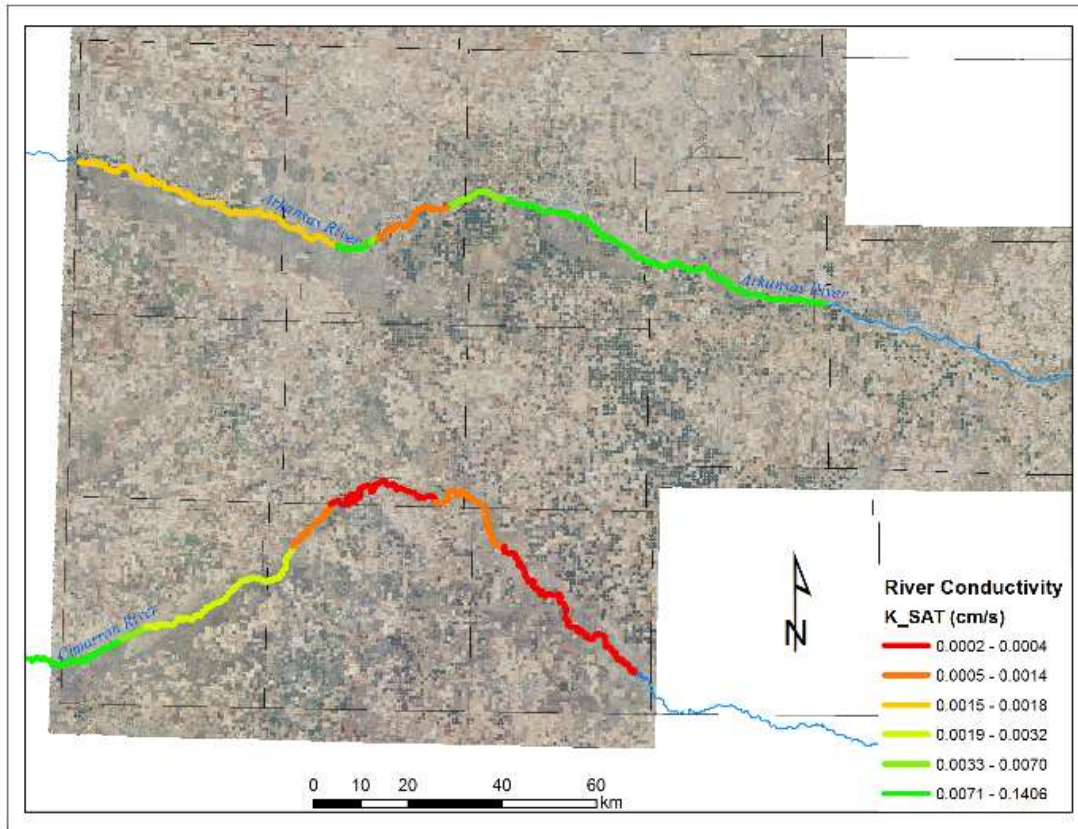


Figure 4-1: Riverbed Conductivity of the Arkansas River and the Cimarron River in Western Kansas.

The riverbed conductivity of the Arkansas River developed in the previous chapter and shown in Figure 4-1 was used as the hydraulic conductivity in the transmission loss model for the Arkansas River. River discharge values were downloaded from the United States Geological Survey (USGS) National Water Information System (NWIS) database. The stations along the Arkansas River where data is available are listed in Table 4-1. Irrigation ditch diversions and return flows were provided by Groundwater Management District 3 (GMD 3). The discharge values were adjusted based on known diversions from irrigation ditches along the river segment.

The simple transmission loss model was applied to the Arkansas River in western Kansas between Coolidge, KS and Garden City, KS over multiple days within the study period of 1985 to 2011. The discharges and the transmission loss factors vary for each analyzed day. The transmission loss model was applied at 100-meter increments, $(x_{i+1} - x_i) = 100 \text{ meters}$. The transmission loss factor varies for each day that the model was applied and along two reaches of the Arkansas River delineated by the Bear Creek Fault. The upper reach of the Arkansas River is west of the Bear Creek Fault and contains gaging stations at Coolidge, Syracuse and Kendall. The lower reach of the Arkansas river is east of the Bear Creek Fault and has gaging stations at Deerfield and Garden City. The Bear Creek Fault is the western extent of the Ogallala aquifer along the Arkansas River. West of the Bear Creek Fault, the Arkansas River is bounded by the alluvial aquifer and bedrock. East of the Bear Creek Fault, the Ogallala Aquifer is under the alluvial aquifer.

Table 4-1: USGS Daily Discharge Data Availability for Arkansas River and Ditches

USGS Site Name	USGS Station ID	Available Years
Frontier Ditch	USGS 07137000	1950 to 2018
Coolidge	USGS 07137500	1950 to 2018
Frontier Ditch Return	USGS 07137010	2015 to 2018
Syracuse	USGS 07138000	1902 to 2018
Kendall	USGS 07138020	1979 to 1982, 2000 to 2018
Amazon Great Eastern Ditch	USGS 07138050	2004 to 2018
Southside Ditch	USGS 07138063	2004 to 2018
Deerfield	USGS 07138070	1998 to 2018
Southside Ditch Return	USGS 07138064	2012 to 2018
Farmer's Ditch	USGS 07138075	2004 to 2018
Garden City	USGS 07139000	1922 to 2018

The river width-discharge relationship was developed for the Arkansas River in western Kansas. Manning's roughness coefficient was determined to be 0.35 based on the observation that the river is a main channel that is generally clean and straight with some stones and weeds. The roughness coefficient was assumed to be a constant value over the length of the study area along the Arkansas River segment and constant over the various levels of discharge.

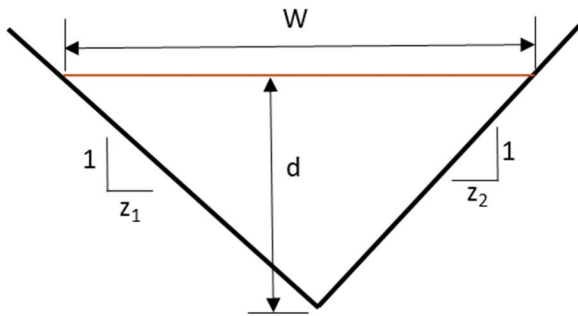


Figure 4-2: V-shaped Channel

The channel was modeled as a V-shaped channel as shown in Figure 4-2 based on field observations. For a V-shaped channel, the area, A , and the hydraulic radius, R are computed with the following:

$$A = \frac{1}{2} W d \quad [12]$$

$$R = \frac{A}{P} = \frac{W d}{2d \left(\sqrt{1+z_1^2} + \sqrt{1+z_2^2} \right)} \quad [13]$$

The wetted perimeter, P (m), is the length of the cross section that is wet. The side slopes of the channel were assumed to be equal. The slope of the channel and the assumed Manning's roughness coefficient were validated using aerial images. The National Agriculture Imagery Program (NAIP) is one source of aerial imagery available to check the assumptions of the model. The discharge of the river is found for the date on which the aerial image was taken, and from the aerial image, the width of the river is measured along a straight segment of river near each of

the gaging stations along the Arkansas River identified in Table 4-1. The measured river widths were converted into discharge using Manning's equation [11]. The parameters of equation [11], including inputs from equations [12] and [13], were adjusted to best fit the discharges reported by the river gaging stations for the subject day and station. The side slopes were set at 5:1 ($z_1 = z_2 = 5$), Manning's n was set to 0.035, and the slope was set at 0.12%. Manning's equation [11] was simplified to the form in equation [10]. The resulting river width-discharge relationship has $a = 6.56$ and $b = 0.375$ in equation [10] for the following:

$$W = 6.56Q^{0.375} \quad [14]$$

The river width-discharge relationship in equation [14] was used for the entire length of the Arkansas River under study from the Colorado-Kansas state line to Garden City.

The transmission loss factor, C , was varied to match the discharges at the downstream extent of the model. The segment of the Arkansas River upstream of the Bear Creek Fault was varied to match primarily the discharges at the Syracuse site and, when available, the discharges at the Kendall site. For the eastern segment of the Arkansas River between the Bear Creek Fault and Garden City, an independent transmission loss factor was applied to the transmission loss model to match the discharges at the Garden City site and, when available, the discharges at the Deerfield site. The location of each site along the Arkansas River is identified by station, which indicates its distance from the Colorado state line, as shown in Table 4-2. The dividing point between the two segments is at station 782, or approximately 78.2 km from the state line measured along the river, and this is the approximate location of the Bear Creek Fault. To account for routing of the Arkansas River discharge, an estimate of the travel time between each station is presented in Table 4-2 and used in the simple transmission loss model. The estimates of the travel time between the stations was obtained by analyzing the daily discharges at the stations. The hydraulic conductivity values along the Arkansas River are presented in Table 4-3.

The eastern and western transmission loss factors were recorded for each day the model was applied. The transmission loss model was applied to the Arkansas River, and the transmission losses and transmission loss factor was assessed for every 16th day.

Table 4-2. USGS Site Locations Downstream from State Line

USGS Site Name	Station, i	Distance from State Line (km)	Transit Time (days)
Frontier Ditch	1	0.1	0
Coolidge	34	3.4	0
Frontier Ditch Return	131	13.1	0
Syracuse	364	36.4	1
Kendall	610	61	2
Amazon Great Eastern Ditch	727	72.7	2
Southside Ditch	793	79.3	2
Deerfield	1151	115.1	3
Southside Ditch Return	1163	116.3	3
Farmers Ditch	1176	117.6	4
Garden City Ditch	1195	119.5	4
Garden City	1407	140.7	4

Table 4-3. Hydraulic Conductivity at the Model Stations.

Station, i	Hydraulic Conductivity, K (m/s)
0 to 782	1.8E-05
782 to 792	1.4E-03
792 to 1278	7.0E-5
1278 to 1407	9.8E-5

An example of results from the transmission loss model is presented in Figure 4-3 with values in Table 4-4. The value at the State Line (17.05 m³/s) is the initial discharge Q₀. The

discharge is translated into a channel width, using the river width-discharge relationship developed for the Arkansas River. The effective channel width is 29.2 m. For the first step, the initial width is assumed to be the final river width for the first 100 m segment of river. For the second step, the hydraulic conductivity from Table 4-3 ($K_{i=0} = 1.8 \times 10^{-5} \text{ m/s}$) was multiplied by the average river width (29.2 m), the length of the segment (100 m), and the transmission loss factor to determine the amount of water lost to the riverbed. Assuming a transmission loss factor of 0.90, the transmission loss for the segment is $5.3 \times 10^{-3} \text{ m}^3/\text{s}$. For the next segment, the Frontier Ditch diverts $0.88 \text{ m}^3/\text{s}$ of water for irrigation. For the third step, the ditch diversion and the transmission loss of $5.3 \times 10^{-3} \text{ m}^3/\text{s}$ are subtracted from the initial discharge of $17.05 \text{ m}^3/\text{s}$, resulting in $16.16 \text{ m}^3/\text{s}$ for the next segment, Q_1 . These steps are repeated for the entire segment from the Stateline to Garden City. The transmission loss factors for each of the two reaches are adjusted to match the measured discharges. The discharge values of the downstream sites are adjusted by the number of days to account for transit time as identified in Table 4-2.

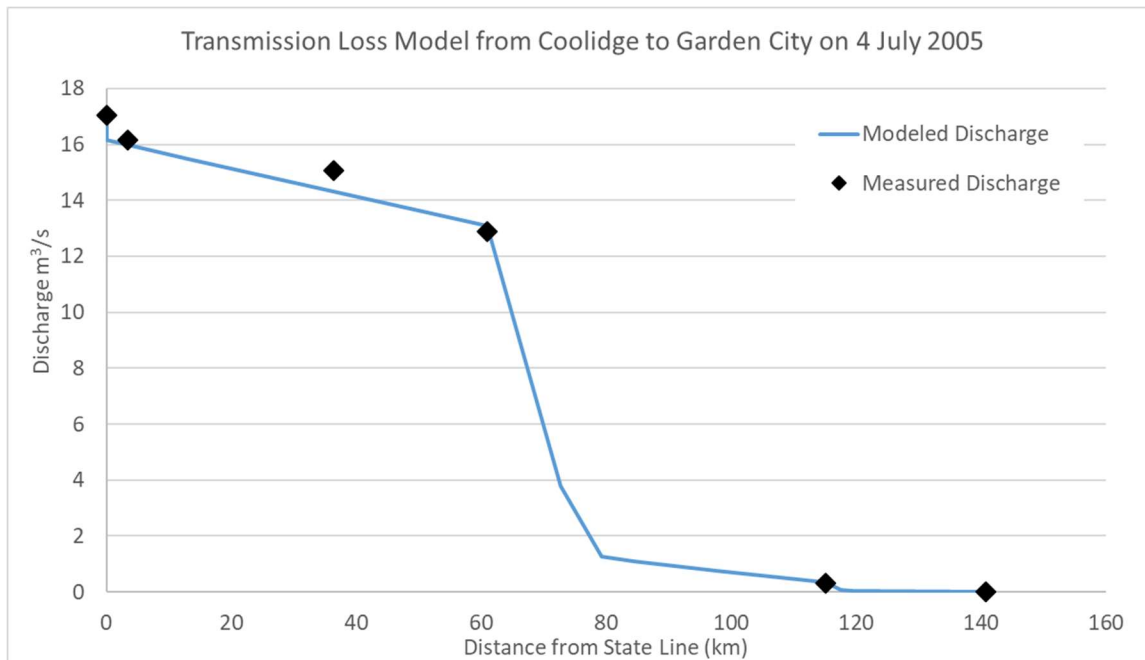


Figure 4-3. Transmission Loss Model Applied to the Arkansas River on July 4, 2005

Table 4-4. Discharge Values from July 4, 2005

USGS Site Name	Diversion (m³/s)	Measured Discharge (m³/s)	Modeled Discharge (m³/s)
State Line	-	17.05	17.05
Frontier Ditch	0.88		
Coolidge	-	16.17	15.99
Frontier Ditch Return	0.00		
Syracuse	-	15.06	14.31
Kendall	-	12.88	13.10
Amazon Great Eastern Ditch	8.75		
Southside Ditch	1.47		
Deerfield	-	0.31	0.36
Southside Ditch Return	-		
Farmers Ditch	0.25		
Garden City Ditch	-		
Garden City	-	0.0	0.0

Results and Discussion

The resulting transmission loss coefficients average 0.015 for the western, upstream segment and 0.027 for the eastern, downstream segment of the Arkansas River. The results of the transmission loss factors are summarized in Table 4-5. The transmission loss factors show that the infiltration capacity of the riverbed is much greater than the observed transmission losses in the river reaches. The variability in the transmission loss factor is greater in the western segment above the Bear Creek Fault than in the eastern segment as seen with the greater range between the minimum and maximum value and the larger standard deviation in Table 4-5. Both reaches experienced negative transmission loss factors for some sampled days, which indicate a

net gain of river discharge instead of a loss of river discharge. A gaining river is the result of contributions from watershed runoff within the study area, unaccounted returns from irrigation ditches, or from discharges of bank stored flood waters. For the eastern reach and for some sample days, the amount of river water diverted to the irrigation ditches exceeded the available water resulting in an unknown transmission loss value. For these days, no transmission loss factor was computed.

Table 4-5. Transmission Loss Factors and Summary Statistics

Transmission Loss Factors, C	Western Reach	Eastern Reach
Minimum	-0.56	-0.06
Maximum	0.45	0.16
Mean	0.015	0.027
Standard Deviation	0.069	0.026
Number	616	552

The comparison of the measured and the modeled discharges for the five USGS gaging sites show a high level of correlation as shown in the following graphs, Figure 4-4. The high correlation is expected due to the transmission loss factor being varied for each day analyzed to meet the values at Syracuse, KS and Garden City, KS. While all comparisons between measured discharge and modeled discharge have high r-squared values, the lines are also expected to be unity with a slope of 1 and intercept of 0. The regression for the Deerfield site is not ideal as the model underestimates the discharge at Deerfield. This indicates that the rate of transmission loss would not be a constant factor for the segment east of the Bear Creek Fault. The reach of the Arkansas River west of Deerfield has lower transmission losses than the reach of the river east of Deerfield indicating a differing geology within the eastern reach or a difference in available storage in the river banks and underlying aquifer. The reach of the Arkansas River east of the Bear Creek Fault has a regular occurrence of cessation of the river resulting in no flow reaching

Garden City. For many sample days at Garden City, both the measured and modeled discharges are zero.

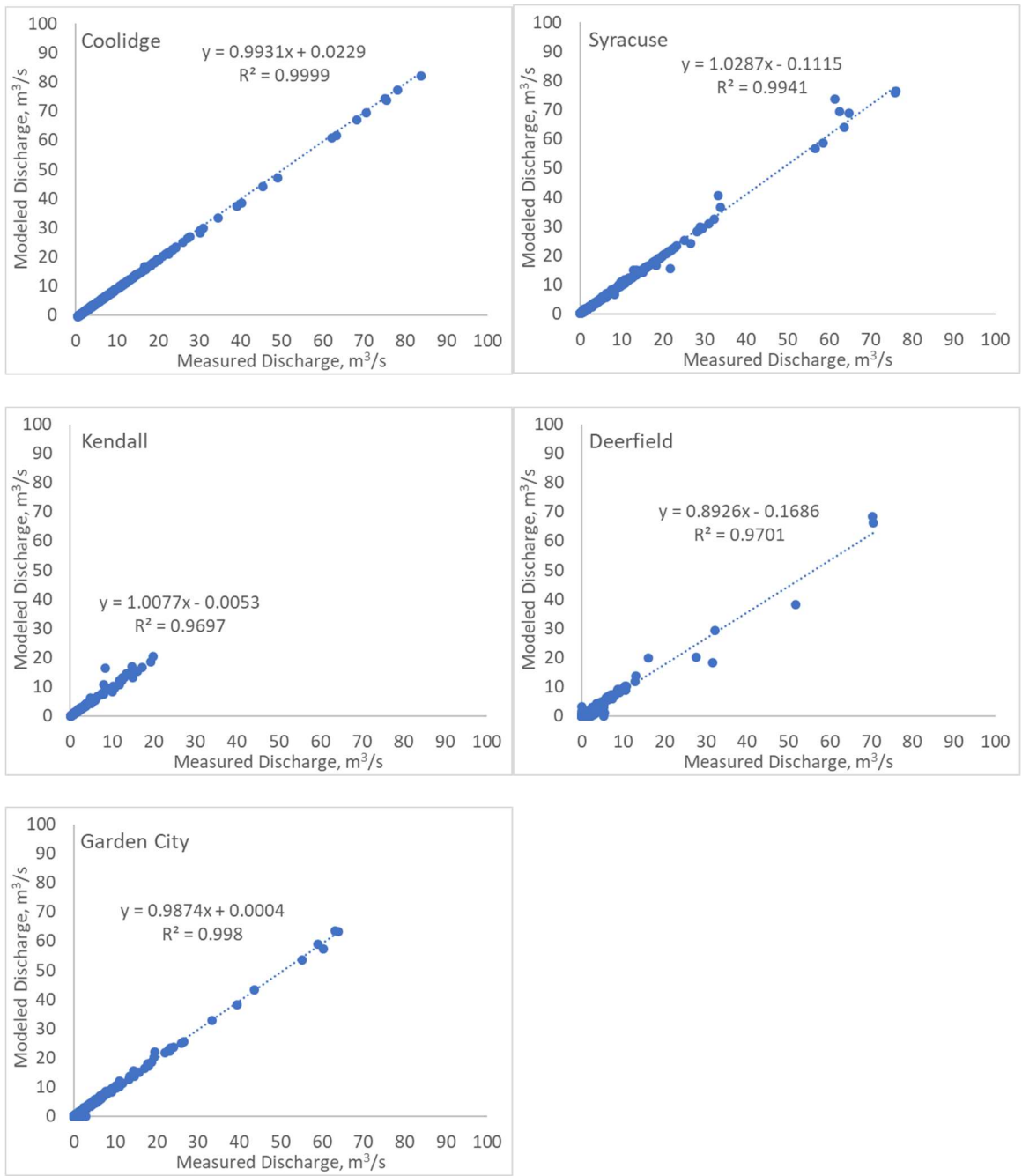


Figure 4-4. Comparisons between Measured and Modeled Discharge in the Arkansas River.

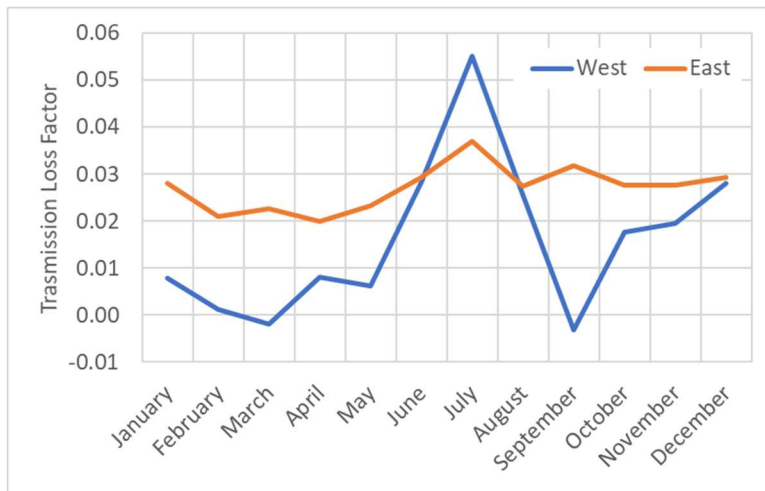


Figure 4-5. Average Transmission Loss Factor by Month

One source of the high variability in the transmission loss factor in the western segment is the seasonal variability as shown in Figure 4-5. The high transmission losses for the summer months is due to the availability of water and the terrestrial demand for water. The Arkansas River discharge is at the peak over the summer months due to the control of the river by the John Martin Reservoir to support irrigation. The demand for water is also the highest in the summer months. The increase in transmission losses over the summer growing period is due to the consumption of groundwater from the riparian vegetation which induces infiltration through the riverbed. The transmission loss factor for the eastern reach between the Bear Creek Fault and Garden City is comparatively constant throughout the year indicating the source of seasonal variability on the western segment does not apply to the eastern segment. While the riparian vegetation along the eastern reach has a similar groundwater demand, that groundwater demand does not impact the transmission losses to the same extent as the western reach. This indicates that there is ample storage in the alluvial sediments throughout the year. For the eastern reach, the infiltrated water is partitioned into evapotranspiration and deep recharge. The drainage of the alluvial aquifer to the Ogallala Aquifer does not experience seasonal variability and is expected to operate on a longer time scale than a single season.

The actual transmission losses of the Arkansas River are only a fraction of the capacity of the riverbed infiltration. The river transmission loss averages 1.5% and 2.7% of capacity of the western and eastern reaches of the Arkansas River, respectively, assuming the hydraulic conductivity of the riverbed is the controlling factor. The hydraulic conductivity of the riverbed was measured to be between 0.0018 cm/s and 0.14 cm/s. For the example above from July 4, 2005, if the transmission losses were controlled by the riverbed sediments, the Arkansas River would have a cessation of flow at station 494 (49.4 km from the State Line) instead of station 1278 (117.6 km from the State Line) as the model predicts based on observed discharges with transmission loss factors of 0.10 and 0.04 for the western and eastern segments, respectively. The difference in the infiltration capacity and the actual transmission losses can be explained by the storage of the river bank and a low permeability layer or bedrock under the river. Results from the Platte River in Nebraska show an order of magnitude decline over a 10-m depth of streambed (Chen, 2011). A layer of low permeability sediments between the alluvial aquifer and the underlying Ogallala aquifer would be the controlling factor for the transmission losses to the lower layers as modeled with Hydrus-1D in the previous chapter. For the eastern reach of the Arkansas River, the bedrock is an impermeable layer under the alluvial aquifer, preventing draining.

The simple transmission loss model captures the variability with the transmission loss factor, C , and the results of this study provides guidance on the selection of the transmission loss factor based on month of the year. The exponential decay model used by Jordan (1977) has a similar fitting factor in the loss per unit length value, R . The exponential decay model from Jordan (1977) is

$$V_{down} = V_{up}R^x \quad [15]$$

Where V_{down} is the downstream volume or discharge (m^3/s), V_{up} is the upstream volume or discharge (m^3/s), x is the distance between the upstream and downstream locations (km), and R is the loss per unit length (m^3/s per km). For the example day of July 4, 2004, the discharge at Coolidge is $16.17 m^3/s$ and at Syracuse is $15.06 m^3/s$. The two stations are 33 km apart along the river. Solving for R results in a value of 0.998. Applying this factor to the next station at Kendall which is 24.6 km downstream, the computation is

$$V_{down} = 15.06 * 0.998^{24.6} = 14.28$$

The Jordan model would predict a discharge of $14.28 m^3/s$ at Kendall, but the actual discharge is $12.88 m^3/s$. The simple transmission loss model predicts a discharge of $13.1 m^3/s$. For this date, the Jordan model would over predict the downstream station discharge at Kendall if R is calculated using the values from the Coolidge and Syracuse gaging stations. Using the information from Table 4-2 and Table 4-4, and continuing the calculations further down gradient, the results are shown in Table 4-6. Based on this comparison for this one sample day, the exponential decay model from Jordan (1977) does not perform well at low flows and is not able to predict the cessation of flow. It would be expected that R would vary based on the season as the transmission loss factor does in the simple transmission loss model, but that was not seen in the results from Jordan (1977). The exponential decay model would be better suited to rivers that are losing and connected. It is not well suited for a river system disconnected from the aquifer or with varying geology under the river.

Table 4-6. Comparison of Transmission Loss Models

			Exponential decay model from Jordan (1977)		Simple transmission loss model	
USGS Site Name	Diversion (m³/s)	Measured Discharge (m³/s)	Modeled Discharge (m³/s)	% error	Modeled Discharge (m³/s)	% error
Coolidge	-	16.17	16.17	0.0%	15.99	-1.1%
Syracuse	-	15.06	15.06	0.0%	14.31	-5.0%
Kendall	-	12.88	14.28	10.9%	13.1	1.7%
Amazon Great Eastern Ditch	8.75		5.18			
Southside Ditch	1.47		3.63			
Deerfield	-	0.31	3.36	985.1%	0.36	16.1%
Farmers Ditch	0.25		3.10			
Garden City	-	0	2.95	-	0	-

The western segment of the Arkansas River can be assumed to be a losing-connected river. From the Arkansas River gaging stations at Coolidge, KS, Syracuse, KS, and Kendall, KS, the discharge in the Arkansas River is non-zero for the period of record and does not experience a cessation of flow. The eastern segment of the Arkansas River can be assumed to be a losing river that transitions from a connected system to a disconnected system because the river does experience a regular cessation of flow. Disconnected rivers have a layer of unsaturated sediment separating the river from the groundwater system. Depending on the magnitude of discharge, bank storage, and aquifer storage, the Arkansas River may lose all of its water to the alluvial sediment by Garden City.

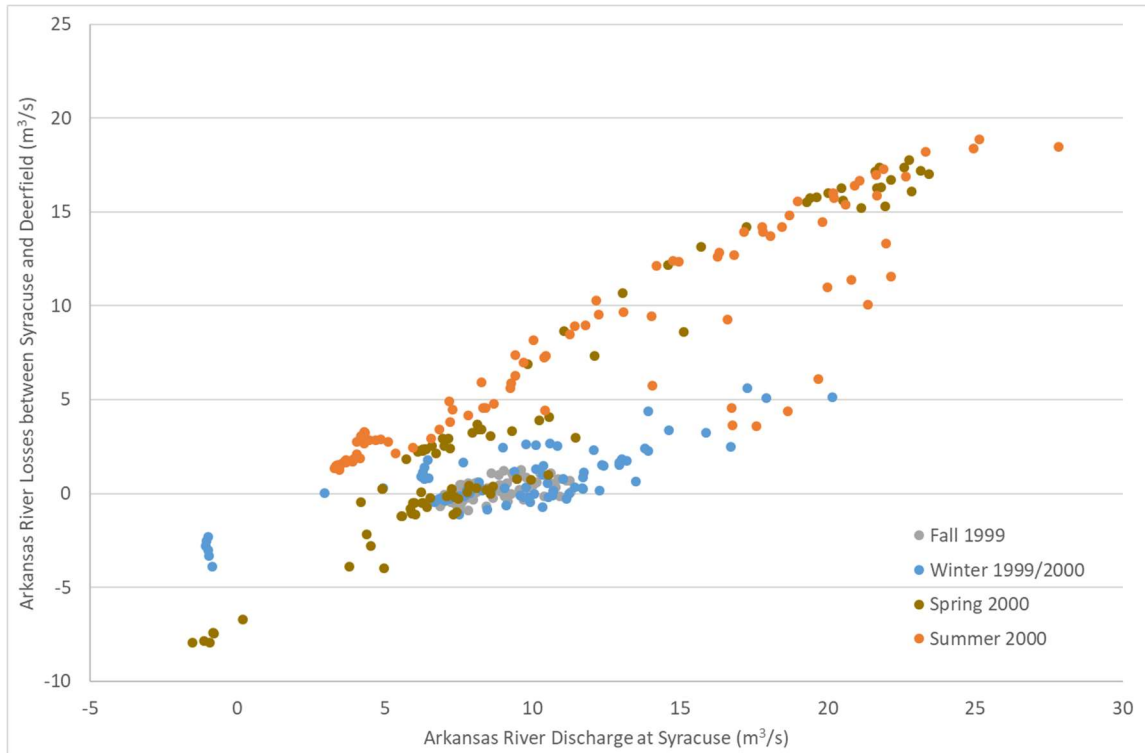


Figure 4-6. Transmission Losses between Syracuse and Deerfield, 2000

A seasonal factor for transmission losses is further examined and shown in Figure 4-6 for the water year 2000. The Arkansas River discharge at Syracuse (x-axis) is adjusted based on the known irrigation ditch diversion. The negative values along the x-axis indicate more water was allocated to the ditches than was available in the channel at Syracuse indicating that there is some surface or bank storage available. The y-axis is the difference in measured discharge between Syracuse and Deerfield. This would be the flow lost to the riverbed, river bank or to other processes like evapotranspiration. A negative value would indicate that the river is gaining water from bank storage or surface water runoff. The water year 2000 was binned into seasons as shown in the legend. For the summer and part of the spring, the losses are approximately equal to the total available water in the river channel. For much of the fall, winter and spring, the river is near an equilibrium discharge where the losses are near zero. The losses are independent of the discharge for the fall, winter and spring, but for the summer the losses are near the unity

line indicating that the riverbed will infiltrate most of the available water independent of the quantity of available water in the channel. From Figure 4-6, the seasonal influence of plant development and the consumption of water to support transpiration processes are the primary factors influencing transmission losses.

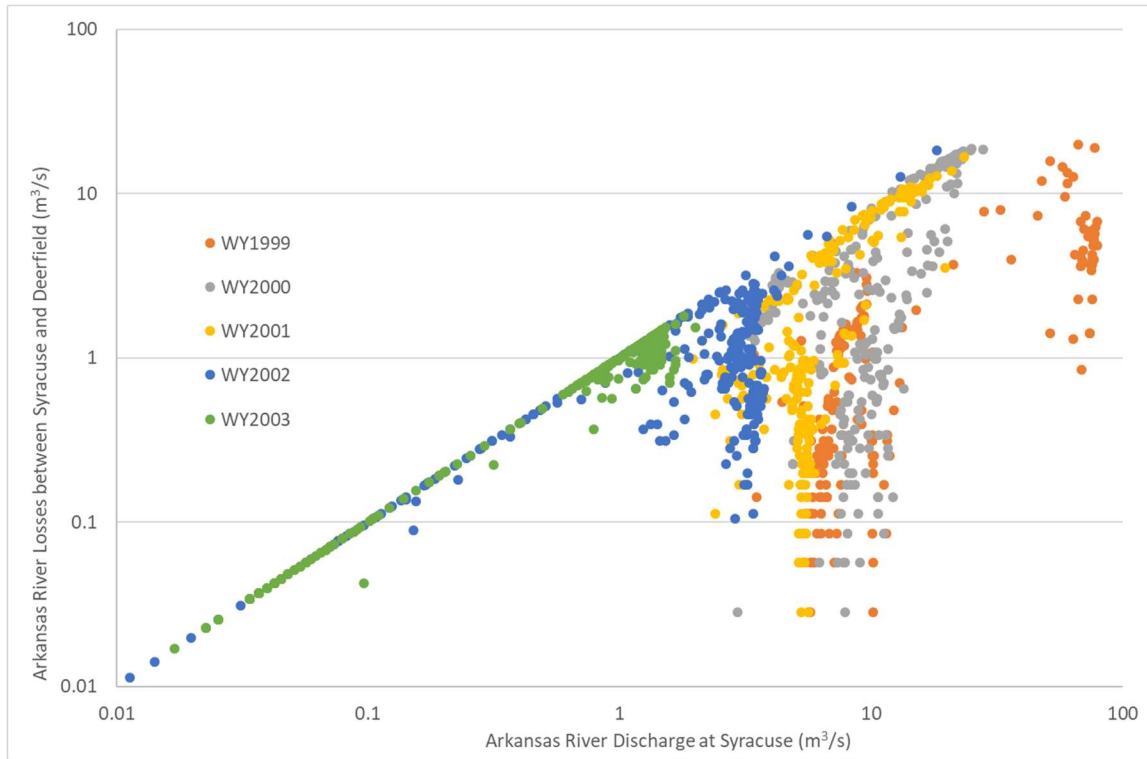


Figure 4-7. Transmission Losses between Syracuse and Deerfield, 1999 to 2003

Figure 4-7 displays the same type of information as Figure 4-6 but on a log-log scale over multiple years (1999 to 2003). Similar to Figure 4-6, transmission losses are shown to be independent of upstream discharge. For a given year, the discharge at Syracuse has a low variance compared to the variance in the transmission losses. This is due to the control of the discharge at the John Martin reservoir on the Colorado side of the border with Kansas and the managed irrigation diversions along the river. Although the river discharge is controlled, the amount of water that is lost to the riverbed sediments varies greatly. With the exception of low

flows where the entire river discharge is lost, the transmission losses between Syracuse and Deerfield are independent of the discharge at Syracuse.

Conclusions

The actual transmission losses in the Arkansas River are a fraction of the infiltration capacity of the riverbed. The transmission losses are not controlled by the surface infiltration of the river. Instead, the transmission losses are controlled by a combination of the underlying geology and the available storage in the alluvial aquifer. The underlying geology is either bedrock for the western segment of the subject reach or a confining layer of low permeability between the river alluvium and the Ogallala Aquifer. The evapotranspiration demand from the riparian vegetation induces infiltration in the Arkansas River by drawing water from the riverbed sediments.

The simple transmission loss model and its use of the transmission loss factor allowed flexibility in fitting the model to match the observations. The transmission loss factor can be interpreted as the percent of infiltration capacity being used to transmit water from the surface to the sediments. For a connected river system, the transmission loss factor can also be interpreted to be a factor of the hydraulic gradient. It was assumed previously that the hydraulic gradient was equal to one, and that the infiltration rate was equal to the hydraulic conductivity. When the water levels of the alluvial aquifer are equal to the water level in the river channel, the hydraulic gradient would be zero. The temporal variability of the transmission loss factor is explained by the seasonal demand for water. The transmission loss factor is not a constant value, but varies based on the season, the location or segment, and available bank storage. The evapotranspiration from the river corridor is a main factor for the seasonal variation. The trees and other riparian vegetation tap into the alluvial aquifer, transport the water to the atmosphere, and induce

infiltration from the river into the streambed. The quantity of water consumed by the trees and riparian vegetation is dependent on the extent and health of the vegetation in addition to the time of year. In the next chapter, the role of evapotranspiration will be examined using satellite remote sensed images.

Chapter 5 - Decoupling Evapotranspiration from River Discharge

Introduction

Evapotranspiration (ET) is the hydrologic flux from the surface to the atmosphere via evaporation from surface water or soil moisture or via transpiration from vegetation. ET is an important component of earth's surface energy balance and an important component to the water balance and hydrologic processes especially in semi-arid and arid environments with limited water resources. ET quantities and rates are used in calculations of soil water storage, runoff to streams and recharge to aquifers, and informs the management of water. Water can be conserved by limiting evapotranspiration (Evans and Sadler, 2008). Efforts to measure ET often focus on a water balance approach or an energy balance approach (Evetts et al., 2012).

In a losing river system, the transmission losses from a river provide a source of available water for plant development. In an arid or semi-arid region, evapotranspiration from riparian vegetation is significant. If transmission losses from a river are cycled into the atmosphere via evapotranspiration, then less water is available. Less water is available for groundwater recharge, less water is conveyed downstream in the river channel, and less water is available for beneficial use in agriculture or industry. In water-constrained environments, water resources are managed to minimize the losses of unproductive ET allowing rivers and aquifers to be maintained as reliable sources of fresh water for domestic and agricultural use. Knowing the stores and fluxes of water in a river system provides insight into the impact the river flows have on the rates of evapotranspiration and groundwater recharge.

Phreatophytes and other riparian vegetation draw from the available water in the groundwater and alluvial deposits. Phreatophytes are plants with deep roots that tap into the groundwater and are a pathway for evapotranspiration. The change in the location and density of

phreatophytes provides insight into changes in the available water (Ahring and Steward, 2012). Diurnal water table fluctuations are a method to determine groundwater consumption by phreatophytes (Loheide et al., 2005). Groundwater fluctuations caused by water demands of phreatophytes are controlled by meteorological drivers, characteristics of the vegetation, and the specific yield of the sediments (Butler et al., 2007). Groundwater ET in riparian zones can draw up water from deep in the aquifer to the water table resulting in a seasonal mixing of shallow and deep aquifer waters (Chen, 2007). ET rates from vegetation and the land surface are high when the system has available water and when there are driving factors to move the water from the ground to the atmosphere; those factors include temperature, humidity, and wind speed.

Quantifying ET rates is challenging due to its spatial dependencies and the costs associated with direct measurements. Multiple methods to estimate evapotranspiration exist that have their own assumptions, strengths and weaknesses (Gowda et al., 2008). Generally, the methods fall into one of four categories: water balance, water vapor fluxes, component estimation, and large-scale estimations. Water balance measurement methods include lysimeters or soil evaporation pan that measure the stores and fluxes of water in a defined system. Large scale lysimeters that directly measure ET are limited to research stations such as USDA ARS-Bushland and are typically used to validate other ET estimation methods (Evetts et al., 2012; Gowda et al., 2012). Water vapor flux measurements include Bowen Ratio or Eddy covariance. Component estimation includes sap-flow measurements or soil evaporation. Large-scale estimation includes scintillometer measurements and remote sensing.

The large-scale estimation methods typically combine remotely sensed imagery from satellite or aerial platforms with ground truth measurements to provide a map of ET over a region. Two large-scale methods are the Surface Energy Balance Algorithm for Land (SEBAL)

(Bastiaanssen et al., 2005) and the Mapping Evapotranspiration at High Resolution using Internalized Calibration (METRIC) (Allen et al., 2007) . These two methods share the assumption that the near-surface temperature difference between the land surface and the air varies linearly with land surface temperature. That assumption is used to estimate the sensible heat flux. The relationship between the near-surface temperature difference and the land surface is derived based on hot and cold anchor pixels for remotely sensed thermal imagery. For these anchor pixels, the hot pixel represents dry and bare agricultural fields, and the cold pixel represents wet and well-vegetated fields. With these anchor pixels and the assumption of the linear relationship, the hot pixel is assumed to experience no latent heat ($ET = 0$) and the cold pixel has the maximum ET. The Surface Energy Balance System (SEBS) (Su, 2002) and the Simplified Surface Energy Balance (SSEB) (Senay et al., 2007) take a similar approach. For the SSEB, these assumptions are further simplified to state that the latent heat flux varies linearly between the hot and cold pixels. Application of the SSEB model against large monolith lysimeters showed that the model accounted for 84% of the measured ET values (Gowda et al., 2009).

The rivers in western Kansas have a riparian zone with trees and shrubs, where riparian vegetation draws water from the river alluvium and the groundwater aquifer. The Arkansas River in Kansas has a phreatophyte population composed of cottonwood, salt cedar, mulberry and willow (Butler et al., 2007; Yang and Steward, 2012). The evapotranspiration rate from salt cedar is comparable to that of cottonwood (Owens and Moore, 2007). A cottonwood tree is expected to draw 98 cm/year to 123 cm/year of water from the soil, and salt cedars can draw between 74 cm/year to 122 cm/year (Dahm et al., 2002). In 2009 and 2010, the seasonal average daily evapotranspiration from a common reed-dominated riparian system in Nebraska was 3.7

mm/day and 5.5 mm/day, and annual evapotranspiration was 67.9 cm/year and 98.2 cm/year (Kabenge et al., 2013). Approaches to determine phreatophyte water consumption include a component estimation approach of the individual water use per phreatophyte and a water balance approach accounting for the stores and fluxes of the components of the system.

The Arkansas River in western Kansas was modeled using the water balance method that includes the surface inflow and outflow, the groundwater-surface water exchanges in the river, and ET rates. From the water balance model, the transmission losses from the river are partitioned between the groundwater recharge and evapotranspiration within the river corridor for the recorded years. The rates of ET were determined based on reference ET calculated using ASCE Reference ET equation (Walter et al., 2000) from the local Garden City, Kansas weather station and remotely sensed data of the thermal emittance of the land surface. Satellite imagery of the study area and the reference ET were processed using the Simple Surface Energy Balance (SSEB) method to provide a map of daily ET rates for all days with available data. The daily ET rates for the river corridor were extracted at 100 m spacing along the Arkansas River. The effective width of the river corridor was determined based on a logistic function of the pre- and post-development tree population. The daily ET rates were aggregated for the river reaches delineated by the active gaging stations along the Arkansas River. The spatially aggregated daily ET rates were interpolated between the available scene dates using the daily reference ET from the Garden City, Kansas weather station. Finally, the ET data was temporally aggregated to develop annual ET rates. The results provide annual estimates of the components of the water balance for the study area.

Methods

Simplified Surface Energy Balance (SSEB)

The Simplified Surface Energy Balance (SSEB) is a model developed to estimate ET from irrigated agriculture and is useful in comparing year-to-year changes in production and water consumption (Senay et al., 2007). The main assumption for the SSEB model is that the variation in the sensible heat flux over the land surface is due to the variation in the latent heat flux. The energy from solar radiation is partitioned into the sensible heat flux, the energy that increases the temperature of the ground surface, and latent heat flux, the energy used in evapotranspiration. Thermal imaging of the land surface captures the spatial variation in the sensible heat flux. SSEB uses the thermal image to develop a map of evaporative fraction (EF) by scaling the brightness values (BVs) based on the anchor pixels representing hot and cold areas in the thermal image. An example of a thermal image from Landsat 5 Thematic Mapper (TM) is shown in Figure 5-1, and the selection of the BVs representing the hot and cold pixels is shown in Figure 5-2. For the hot pixel, the assumption is that the net solar radiation is converted to sensible heat flux, and the latent energy is zero. The cold pixel is assumed to have the maximum rate of ET, and the latent energy is equal to the reference ET. The assumption that the latent energy varies linearly between the hot and cold pixels is presented in the EF equation [16]:

$$EF = \frac{Hot-x}{Hot-Cold} \quad [16]$$

The ET_{actual} in equation [17] is the product of the EF and the reference ET, ET_0 :

$$ET_{actual} = EF \cdot ET_0 \quad [17]$$

The ASCE's Standard Reference ET is used to compute Reference ET, ET_0 . It uses a simplified form of the Penman-Monteith equation. The parameters to compute ET_0 can be estimated or

selected based on the type of vegetation being modeled and from data collected by a weather station within the scene coverage.

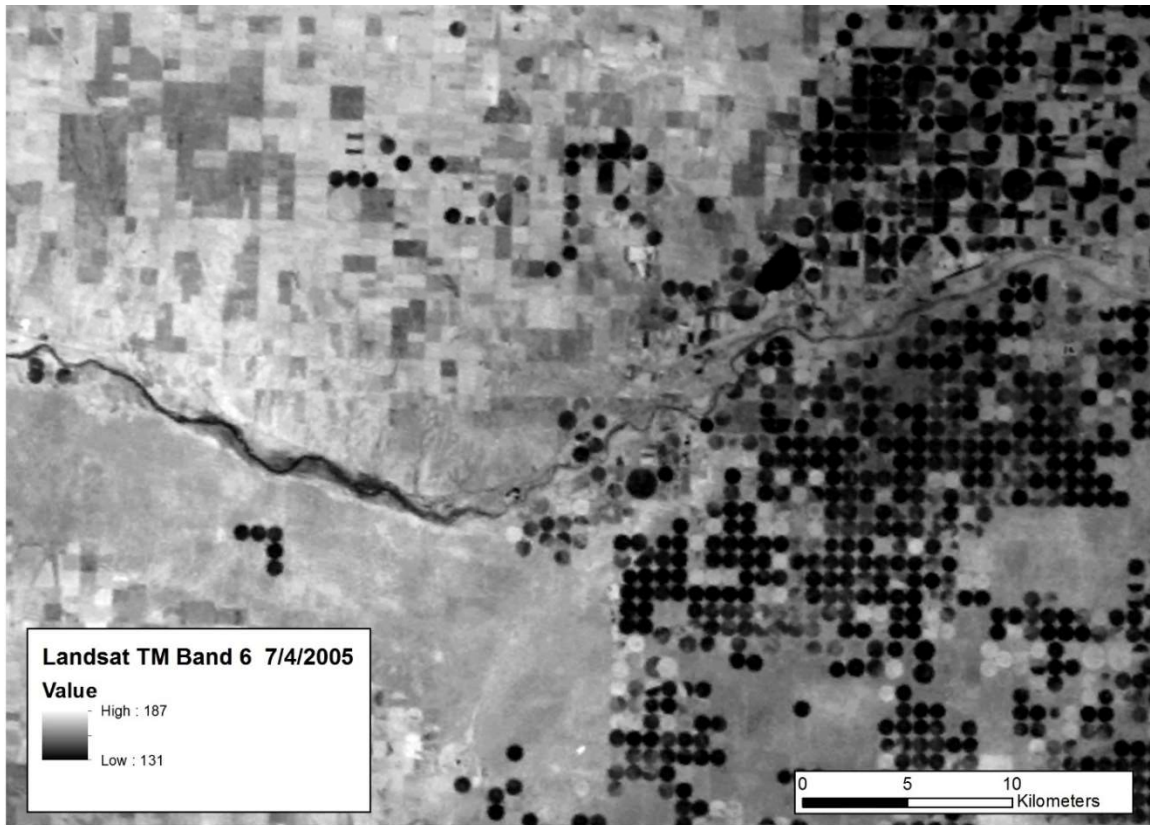


Figure 5-1. Thermal Band of Western Kansas on 4 July 2005.

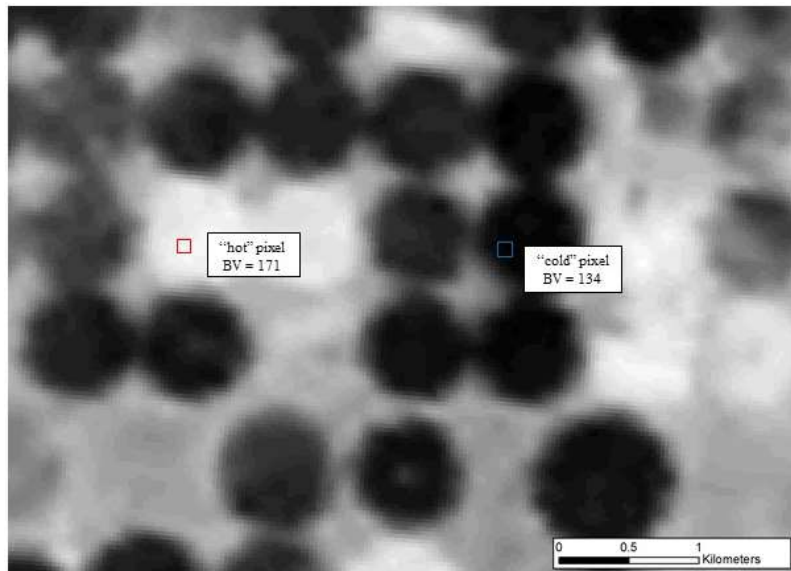


Figure 5-2. Selection of Hot and Cold pixels for 4 July 2005

The determination of the anchor pixels is aided by the Normalized Difference Vegetation Index (NDVI). NDVI aids in selecting the hot and cold BVs in the thermal band by providing an indicator of the live vegetation in a remotely sensed image. The NDVI calculation typically uses the Red and the Near Infrared (NIR) spectral reflectance measurements that are provided in the Landsat 5 TM bands 3 and 4, respectively. NDVI is the ratio of the difference of the brightness values of NIR and Red to the sum of the NIR and Red, and it ranges from -1.0 to +1.0. The equation for NDVI is shown in equation [18]. Larger positive values of NDVI indicate live vegetation, and smaller positive values indicate bare soil. The selection of a cold pixel is cross-checked to have a corresponding large positive value for NDVI, and conversely a hot pixel would be verified to have a small positive value for NDVI.

$$NDVI = \frac{(NIR-Red)}{(NIR+Red)} \quad [18]$$

Data Processing

Extraction to the River

The focus of the study is the evapotranspiration along a river corridor and not the entire coverage of the satellite image, resulting in most of the data processed with SSEB being unused in the following analysis. By extracting the evapotranspiration rates along the subject river, the size of the database is significantly reduced. Using ArcGIS, a shapefile of the river is developed using the National Hydrography Dataset (NHD) from the USGS. The lines representing the river within the study area are copied to a new shapefile and combined into a single line segment. Another shapefile is created with points generated at 100-meter increments along the length of the line segment representing the river. The 100-meter spacing is used based on the 120-meter spatial resolution of thermal infrared band (Band 6) of the Landsat 5 TM. Values from the SSEB

raster of daily ET rates are extracted to populate the data table of the river point file. The data tables are exported and manipulated in Excel.

The daily ET rates at 100 m increments along the river are processed in Excel as follows. The first operation is to combine all daily ET data tables for each available day. The daily ET data is organized by setting up the tabs by year and copying the daily data into the corresponding tab. Next, a series of filters are applied to the values in the table to eliminate the effects of clouds or to correct errors in the processing of daily ET rates. Images with significant cloud cover over the river are typically not processed, but images with scattered or isolated clouds may be included depending on the percent of cloud cover over the area of interest. Clouds have a very low brightness value in a thermal image, and when processed with SSEB, the cloud cover would translate into a very high value of the daily ET rate. ET rates that are higher than the reference ET are corrected to the reference ET value for that day. The other correction is applied to negative values of ET. If a pixel value in the thermal image was less than the selected hot pixel, then the resulting daily ET rate would be negative. Because a negative value is not practical, those values are corrected to be zero. To further reduce the size of the data set, the river is segmented by gaging station or other delineating features. The data points at 100 m spacings are summed along the river segments, producing an aggregate daily ET value for that segment.

Mean Tree Distance

The effective width of the river corridor is determined by a time-dependent logistic function of the mean tree distances. The resolution of the thermal band of Landsat 5 TM does not provide the fidelity to determine the effective width of the river corridor. As the water table declines with the development of the aquifer, the trees redistribute closer to the river (Ahring and

Steward, 2012). The logistic function, shown in equation [19] is based on the initial and final mean tree distances within the river corridor over the period of development.

$$W(t) = W_{post} + \frac{W_{pre} - W_{post}}{1 + e^{a_0 + a_1 t}} \quad [19]$$

The tree width, $W(t)$ is dependent on the pre- and post- tree widths (W_{pre} , W_{post}), the year, t , and T , the dimensionless time represented by equation [20]:

$$T = a_0 + a_1 t \quad [20]$$

The logistic function of the weighted mean tree distance to the river is combined with the daily ET along the river calculated from the SSEB model to provide the volumetric loss of water due to evapotranspiration from the river corridor for the day.

Temporal Interpolation of ET data

A process of interpolating the ET data fills the gaps in coverage due to the limited availability of thermal imagery from the satellite. The Landsat 5 TM satellite passes over and collects data on the same area every 16 days which provides no more than 29 coverages for any year. The availability of the data is further limited if the study area is covered in clouds during the repeat cycle day when the satellite is collecting data. With the information available from both the available satellite scenes and the daily data from the weather stations, the ET data can be interpolated to estimate a daily ET from the river system for each day of the year. The temporal interpolation takes the daily data from the weather station and scales the daily ET rate from the SSEB model. This interpolation method determines the aggregate evaporative fraction, EF_{agg} , for the river corridor by dividing the daily ET rate from the available scene by the reference ET for the subject day. The aggregate evaporative fraction is then multiplied by the daily reference ET for all days without satellite coverage. This combines the spatial variation of the ET coverage from the SSEB model and the temporal variation of the reference ET determined from the weather station.

The Water Balance

The water balance is one method for determining the stores and fluxes in a system. The stores and fluxes are modeled by first defining the system and boundary conditions along the rivers. For the river system, the boundaries are defined by the length of the river with the upstream and downstream stations as the boundaries and by the width of the river corridor. The width of the corridor is the effective tree width determined by the logistic function. The components of the river system are the river or surface water, the groundwater, the water in the alluvial sediments, and the atmospheric water. The pathways and fluxes of the system include the discharge of the river into and out of the system, the surface water and groundwater exchanges including recharge, and the evapotranspiration from the surface or groundwater into the atmosphere. The water balance is developed for the annual time scale. The annual fluxes of the known components that have been directly measured or estimated for the system over the study period are inputted in to the water balance model, and the unknown components are determined based on the conservation of flow. For the river system, the discharges into and out of the river are measured by the gaging stations, the ET is modeled using the SSEB. Other values can be assumed based on knowledge of the system. For example, groundwater discharge to the river can be set to zero with the assumption that the river is a losing system. An example of a water balance model is shown in Figure 5-3.

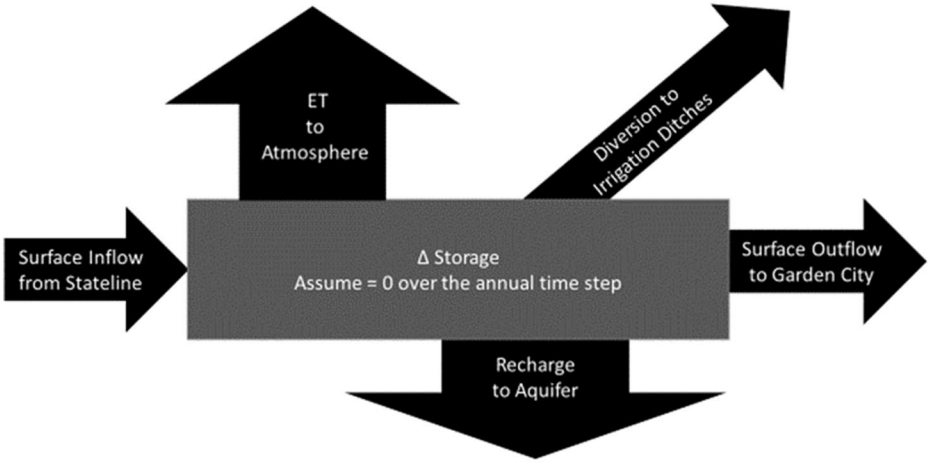


Figure 5-3. Water Balance Model of the Arkansas River

Case Study

The Arkansas River corridor between Coolidge, KS near the Colorado state line and Garden City was examined. Thermal imagery from Landsat 5 TM was converted into ET estimates for the river corridor. The period of effective operation for Landsat 5 TM was between 1985 and 2011, and those years are set as the study period. The study area is captured with Landsat 5 TM in Path 31, Row 34. All available satellite scenes were downloaded from the USGS database. For this study, 249 satellite scenes were used. The thermal scenes for each were converted into daily ET coverages using the SSEB method. The coverages were further processed using the methods described in the above section.

The Garden City weather station, as shown in Figure 5-4, is operated by Kansas State University and provides the source of the reference ET. Weather data measured at the Garden City station includes temperature, solar radiation, wind speed and direction, precipitation, pressure, 10-meter wind speed and direction, 2-inch soil temperature, 4-inch soil temperature, and soil moisture at multiple depths.



Figure 5-4: Garden City Weather Station

The Arkansas River has multiple gaging stations between the Coolidge, KS and Garden City, KS providing daily discharge and gage height. The stations along the Arkansas River and stations at the diversions to the irrigation ditches are operated by the USGS. The availability of data for each station varies. Daily discharge data at the Coolidge, Syracuse, and Garden City stations are available for the entire period of operation of Landsat 5 TM, but the data for the Deerfield site is only available after 1998. The flow of the Arkansas River is controlled by the John Martin Reservoir across the state line in Colorado. The reservoir is managed to contain the high volume of runoff from the spring season and release it over the length of the growing season. The flow in the Arkansas river is diverted to the irrigation ditches in eastern Colorado

and western Kansas. Flood pulses in the Arkansas River are due to a release of surplus storage of the John Martin Reservoir or from regional rainfall runoff.

The parameters for the logistic function were informed by Ahring (2009). From the logistic function, the parameters a_0 and a_1 are determined using the predevelopment and post-development effective tree width dimensions. The predevelopment width for the Arkansas River in 1965 is 210 m, and the post-development width in 2005 is 190 m. Setting the range of T from -6 to 6, the data points for (t,T) are (1965, -6) and (2005, 6) which results in $a_0 = -595.5$ and $a_1 = 0.3$ in equation [21].

$$T = -595.5 + 0.3t \quad [21]$$

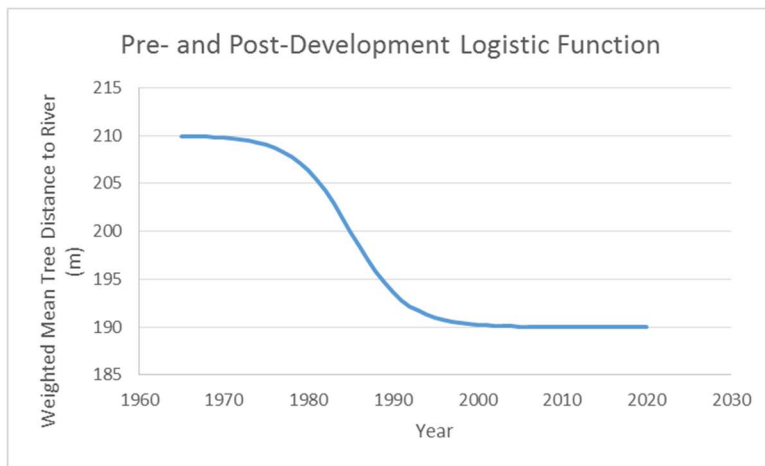


Figure 5-5. Logistic Function for the Mean Tree Distance to the Arkansas River

Next, the fluxes into and out of the system are defined and simplified with assumptions. For the water balance model, the system is defined as the Arkansas River between the Colorado Stateline and Garden City, Kansas. The fluxes into the system include the river discharge recorded at the Colorado Stateline plus any contributions from tributaries, surface runoff and groundwater inflow. The fluxes out of the system are the combination of the discharge of the Arkansas River at Garden City, KS, the diversions to irrigation ditches, losses to the groundwater system, and ET within the river corridor. To simplify the water balance of the Arkansas River

system, three assumptions are made. First, the runoff contributions due to precipitation events are negligible because of the flat terrain and lack of significant tributaries to the Arkansas River within the study area. From Wetter (1990), the average annual runoff in the study area varies between 0 and 0.5 inches. Second, because the river is a losing system, net inflow from the groundwater is assumed to be negligible. Third, over a period of a year, the change in storage of the river or the river alluvium is assumed to be zero.

The water balance model was applied to the dates with ET coverage (1985 to 2011). The discharges along the Arkansas River are measured and recorded at river gaging stations operated by the USGS. The ET from the river corridor is computed using the SSEB modeled ET along the length of the Arkansas River multiplied by the effective tree width. The remaining value is the water lost to the groundwater, which would be the river contribution to groundwater recharge. The groundwater recharge is assumed to be deep groundwater recharge that would contribute to the storage of the Ogallala Aquifer. The daily ET rates were summed annually for the period of record for each segment.

Results and Discussion

The satellite coverages and the resulting daily ET rates show a spatial variability of the available water on the land surface. In Figure 5-6, the daily ET map from September 8, 2000 shows the Arkansas River as a bright path meandering through the study area of Hamilton, Kearny, and Finney Counties of southwest Kansas. The daily ET map shows contrasting areas from the dry rangeland on the western half of the study area to the wet areas on the eastern half of the map where irrigation systems are extracting groundwater from the Ogallala Aquifer.

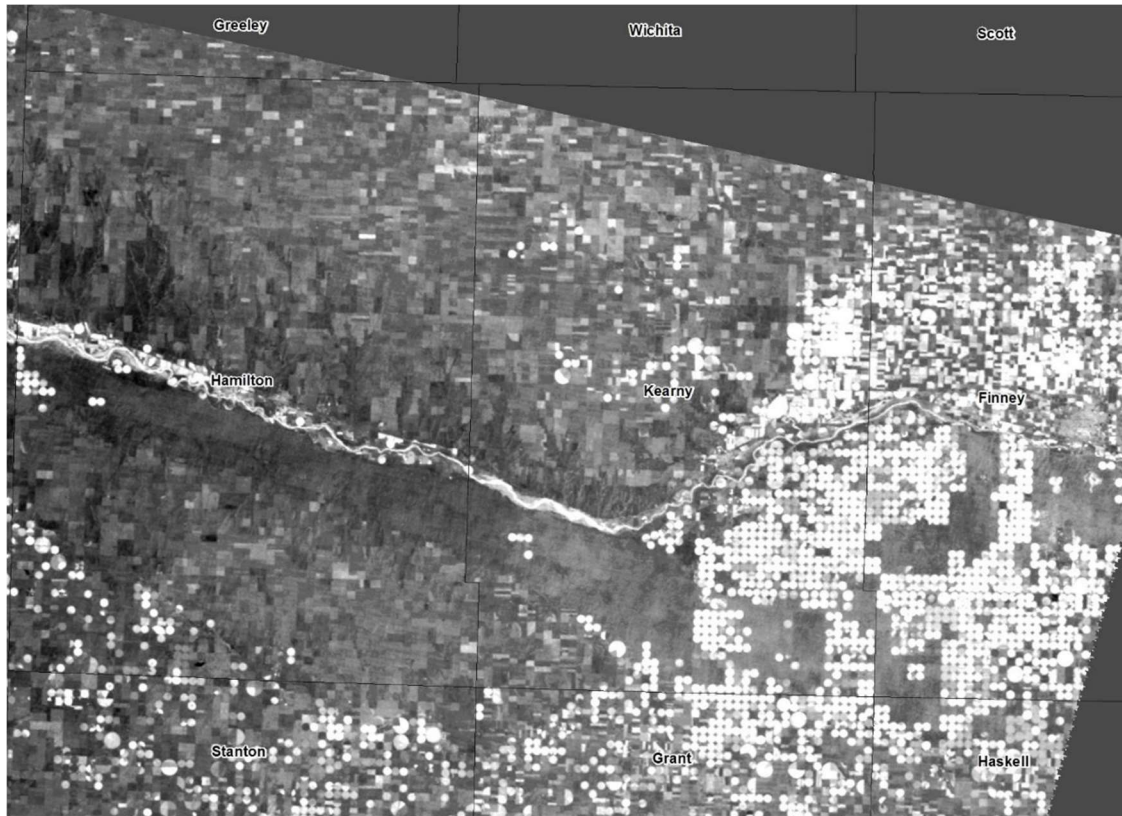


Figure 5-6: SSEB Daily ET in SW Kansas: 08 September 2000, Reference ET is 8.17 mm

The variability of daily ET is shown along the Arkansas River in Figure 5-7. The river discharge for the available stations are shown in cubic feet per second (cfs) at their locations along the river. The river discharge declines from a maximum of 182 cfs at Kendall to 0 cfs at Garden City due to transmission losses along the river. The points graphed are the extracted daily ET values along the centerline of the Arkansas River at 100-meter spacing. The reference ET for that day is 8.17 mm/day. From Figure 5-7, the daily ET rate is highest east of Kendall, Kansas near the Bear Creek Fault. The daily ET rates do not appear to be correlated to the river discharge for that day. The gaging stations at Deerfield and Garden City have less discharge in the Arkansas River than at Coolidge or Syracuse on the subject day, but the ET rates are comparable. If the ET would be dependent on river discharge, then it is expected that the ET at Garden City would approach zero as the discharge approaches zero. The sustained rate of ET

along the study area indicates that there is available water in the alluvial sediments at Garden City despite a lack of surface water.

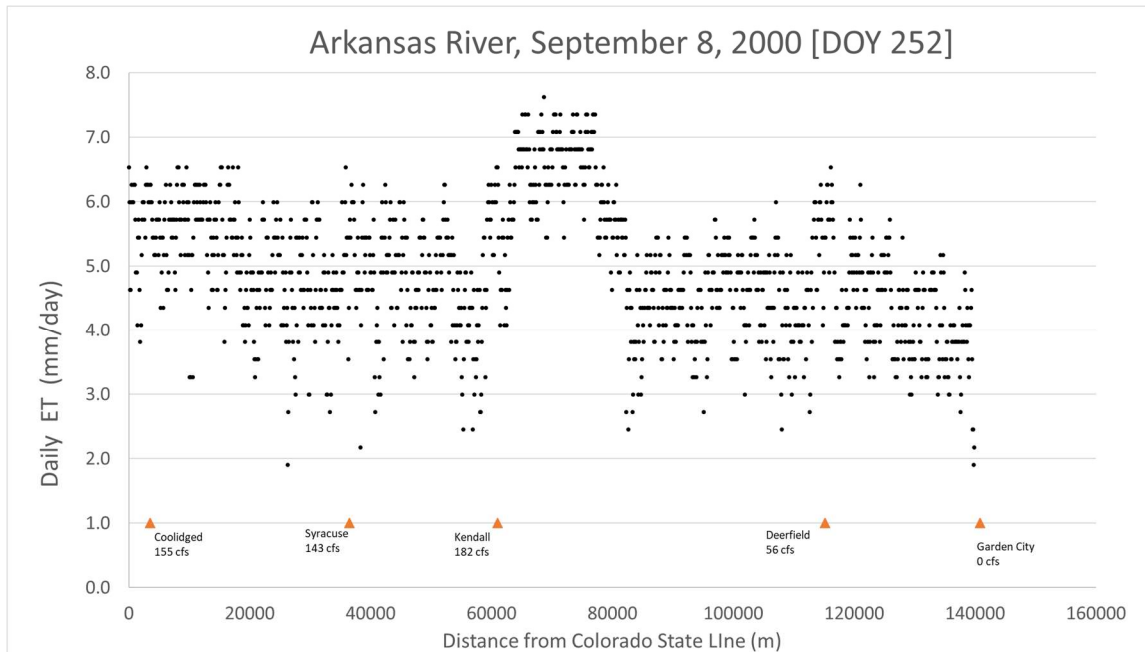


Figure 5-7: Evapotranspiration along the Arkansas River on September 8, 2000

A comparison of four dates in 2000 shows the temporal variability of ET in Figure 5-8 with discharge values in Table 5-1. For visual clarity, the extracted point data for the four dates are represented as lines, smoothed using a moving average of the previous 20 points. The segment of the Arkansas River west of the Bear Creek Fault has consistent daily ET rates across the four dates. The daily ET rates from the segment near the Bear Creek Fault is dependent on the day of year and daily reference ET rates, indicating that water is available at this location. Comparing the Garden City discharge from Table 5-1 with the daily ET graphs in Figure 5-8, the available surface water in the Arkansas River changes between the earlier and later dates, and the daily ET rates also decline. This indicates that the alluvial sediments are a source of available water when the river is dry, but that source is susceptible to depletion over prolonged dry periods

resulting in a water stressed environment for the vegetation in this area. As Figure 5-8 shows for the two no-flow days at Garden City, water stress will be experienced first on the eastern edge of the study area if the river or subsurface flow does not transport water to the segment of alluvial aquifer at Garden City. The rate of ET near Garden City in the fall of 2000 has declined compared to the spring and summer of that year, while the western segments of the Arkansas River appear unchanged. This decline in ET near Garden City indicates that the alluvial aquifer is being exhausted. The water stored in the alluvial aquifer is being consumed by phreatophytes, is being extracted for irrigation or other beneficial use, or is leaking to the Ogallala Aquifer.

Table 5-1. Evapotranspiration and Discharge along the Arkansas River of 4 days in 2000.

Day of Year	Date	Reference ET (mm/day)	Discharge at Syracuse (m ³ /s)	Discharge at Deerfield (m ³ /s)	Discharge at Garden City (m ³ /s)
124	May 3	6.47	14.1	7.67	8.63
204	Jul 22	6.62	18.66	13.99	9.66
252	Sep 8	8.17	4.05	1.33	0
284	Oct 10	7.20	11.84	2.94	0

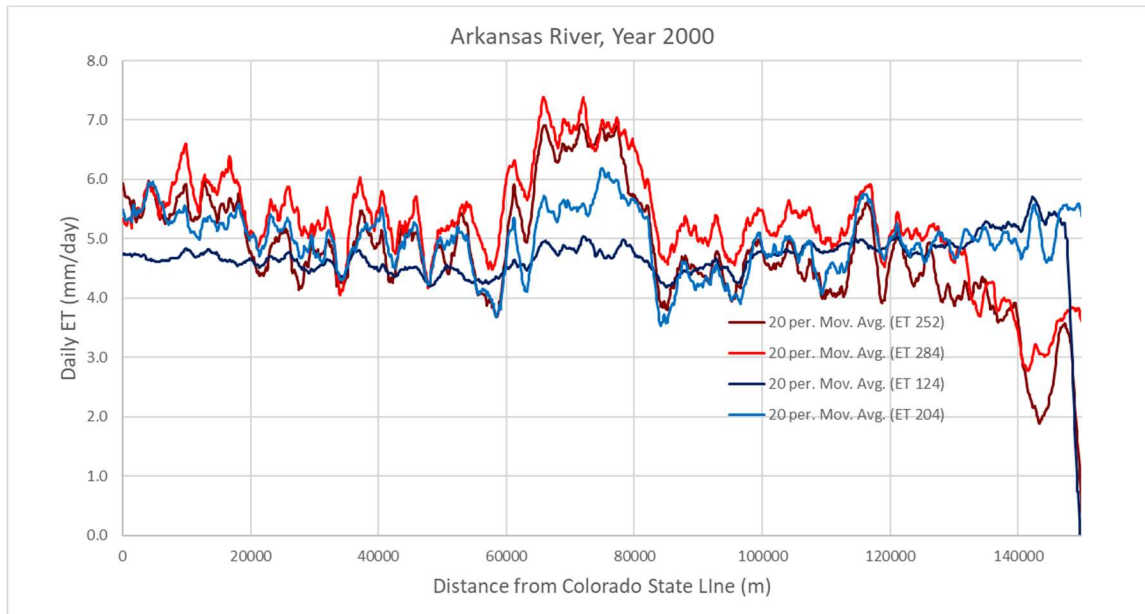


Figure 5-8: Evapotranspiration along the Arkansas River, Moving Average of 4 days in 2000

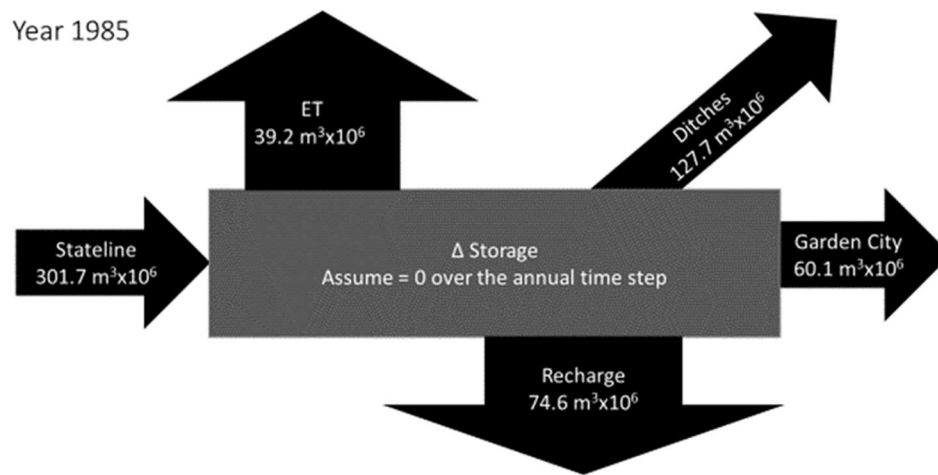
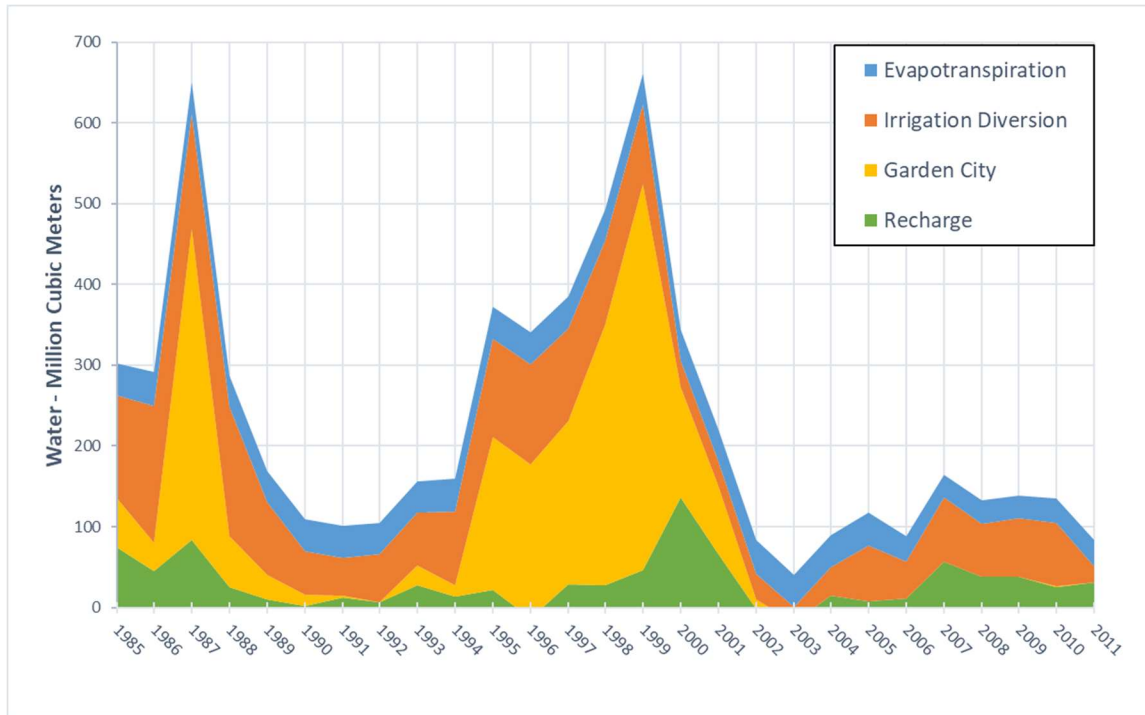


Figure 5-9. Water Balance of the Arkansas River in 1985

The results of the water balance model show that the annual rates of ET are less variable than the other components of the system. The water balance model of the Arkansas River for the first year of the study in 1985, Figure 5-9, shows that the annual recharge to the groundwater aquifer is about twice the annual ET. Figure 5-10 and Table 5-2 show the annual components to the water balance model for the system over the entire period of the study. The river discharge inflow from the Stateline and outflow at Garden City, KS are the two components of the system with the highest degree of variability. Descriptive statistics for the annual water balance are shown in Table 5-3. The standard deviation and variance for the annual evapotranspiration is low compared to the other components of the water balance indicating that the evapotranspiration of the river corridor is a consistent value compared with river discharge or groundwater recharge. Table 5-4 shows the correlation coefficients between the components of the water balance model. The amount of water the system loses to the atmosphere is not dependent on river discharge, as the source of the evapotranspiration is from the alluvial sediments. While periods of drought would reduce the available water in the river and alluvium, the impact to the evapotranspiration rates is minimal for this period of study.

Table 5-2: Annual Water Balance Model of the Arkansas River

Year	Annual Volume, Million Cubic Meters				
	State Line Discharge	Irrigation Diversion	Garden City Discharge	Evapotranspiration	Groundwater Recharge
1985	301.7	127.7	60.1	39.2	74.6
1986	291.9	170.3	34.9	41.9	44.8
1987	650.8	140.5	386.3	40.5	83.5
1988	286.7	159.8	63.0	38.3	25.6
1989	168.9	89.9	30.5	38.0	10.5
1990	109.9	54.8	13.2	39.7	2.2
1991	100.9	47.2	1.9	39.0	12.7
1992	104.3	60.2	0.0	37.7	6.5
1993	156.5	65.2	24.4	39.1	27.8
1994	159.9	91.4	13.7	41.1	13.7
1995	372.8	121.4	189.8	39.8	21.8
1996	340.8	123.0	191.3	40.0	-13.6
1997	385.2	115.3	201.7	39.5	28.7
1998	492.7	103.5	323.3	38.8	27.0
1999	661.7	97.5	478.4	39.3	46.5
2000	344.6	32.3	137.2	38.9	136.3
2001	220.9	31.1	84.0	40.1	65.7
2002	83.4	31.9	11.8	41.7	-2.0
2003	40.6	18.0	0.0	40.2	-17.6
2004	89.6	34.9	0.0	39.5	15.1
2005	117.3	68.8	0.0	40.4	8.1
2006	87.9	45.3	0.0	31.7	10.9
2007	164.8	78.7	0.1	29.1	57.0
2008	132.4	65.4	0.1	29.1	37.8
2009	138.7	73.1	0.1	27.9	37.5
2010	134.5	78.2	1.2	30.4	24.7
2011	84.0	19.1	0.0	33.5	31.5



Note: The sum of all four components is the inflow volume to the state via the Arkansas River. “Garden City” is the surface outflow volume via the Arkansas River.

Figure 5-10. Annual Water Balance of the Arkansas River

Table 5-3. Descriptive Statistics for Annual Water Balance

<i>in million cubic meters per year</i>	<i>State Line Discharge</i>	<i>Irrigation Diversion</i>	<i>Garden City Discharge</i>	<i>Evapo-transpiration</i>	<i>Groundwater Recharge</i>
Mean	230.50	79.43	83.22	37.57	30.27
Standard Error	32.42	8.17	25.20	0.81	6.25
Median	159.90	73.13	13.74	39.20	25.61
Mode	#N/A	#N/A	0.00	#N/A	#N/A
Standard Deviation	168.48	42.43	130.92	4.19	32.47
Sample Variance	28384.77	1800.60	17139.96	17.55	1054.10
Kurtosis	1.20	-0.57	2.76	0.47	3.25
Skewness	1.32	0.47	1.85	-1.37	1.45
Range	621.04	152.23	478.36	14.00	153.81
Minimum	40.63	18.02	0.00	27.92	-17.56
Maximum	661.68	170.25	478.36	41.91	136.25
Sum	6223.38	2144.61	2247.00	1014.45	817.32
Count	27	27	27	27	27

Table 5-4. Correlation Coefficients between Annual Water Balance Components

	<i>State Line Discharge</i>	<i>Irrigation Diversion</i>	<i>Garden City Discharge</i>	<i>Evapotranspiration</i>	<i>Groundwater Recharge</i>
<i>State Line Discharge</i>	1.00	-	-	-	-
<i>Irrigation Diversion</i>	0.62	1.00	-	-	-
<i>Garden City Discharge</i>	0.96	0.44	1.00	-	-
<i>Evapotranspiration</i>	0.30	0.19	0.31	1.00	-
<i>Groundwater Recharge</i>	0.48	0.13	0.32	-0.09	1.00

The quantity of river discharge is important because it is the primary inflow component of the water balance model for the study area. The quantity of water from the upstream end of the river is partitioned to evapotranspiration, recharge, irrigation ditch diversions, and surface discharge downstream. Evapotranspiration from the river corridor was determined to be near constant at an annual time scale despite periods of severe drought and floods. The average annual evapotranspiration for the study area is about 16% of the available surface water. During drought years, the trees pull water from the sediments and alluvial aquifer. During floods and years with above average river discharge, the capacity of the trees and other riparian vegetation to consume water has an upper limit. Increasing the availability of water does not increase the evapotranspiration rates from the river. The recharge from the river was not directly determined, but it was calculated as the residual of the water balance model. On average, annual recharge is about 13% of the available surface water, which is slightly lower than the annual evapotranspiration. The diversions to irrigation ditches are a managed water resource, similar to the outflow of the John Martin Reservoir that controls the Arkansas River entering Kansas. The diversions to the irrigation ditches make up about 34% of available surface water. The

downstream discharge of the Arkansas River at Garden City accounts for about 36% of the inflow to the state of Kansas. Over the period of study, about 36% of the Arkansas River discharge that enters the state is still present in the channel when it progresses past Garden City. For the last ten years of the study, the discharge downstream of Garden City has been at or near zero.

The annual ET from the river corridor is a lagging indicator of the health of the system. The years 2002 and 2004 have the lowest discharge of the Arkansas River at the state line, but the annual rates of evapotranspiration do not indicate a reduction in available water. Examining the years 2007 to 2009, the annual rates of evapotranspiration are the lowest on record indicating that the storage in the alluvial sediment had depleted to the point where the trees in the river corridor experience water stress. This indicates that the change in storage of the of the river system is not negligible. From Ahring (2009), the decline of the water levels and stream flow has affected the riparian ecology with declining numbers of trees and a shift from cottonwood trees to salt cedar. Between the years of 2003 to the end of the study period in 2011, the discharge at Garden City was at or near zero, which indicates that there is a water deficit in the system where the demand for water is greater than the supply. The evapotranspiration from the river indicates that the alluvial aquifer is a significant source of water for the region, but the volume stored in that source of water can be depleted if it is not periodically replenished. The declining water table in the Ogallala Aquifer and Arkansas River alluvial aquifer has resulted in the change of tree communities that favor the drought resistant salt cedar. Further reductions in the water table and the elimination of the reliable source of water to the riparian ecosystem could result in irreparable damage to the tree community.

Declining groundwater tables and the depletion of the water stores in the alluvial sediments results in less available water to support vegetation. While this study shows the resilience of the vegetation within the river corridor to draw from the stores in the alluvial sediments even during periods when the river is dry, the long-term survival of the river ecosystem is not guaranteed. The decline of the water levels in the Ogallala aquifer is resulting in the shift from a connected river to a disconnected river with regular occurrence of cessation of flow in the river. If the river discharge experiences periods of low flows either due to drought or upstream irrigation diversions, the stores of water in the alluvial sediment will be depleted. Without water, the trees and the ecosystem of the Arkansas River will experience a local extinction or extirpation.

An increase in river discharge into Kansas would result in more water in the system, with part of those gains partitioned between recharge to the aquifer from transmission losses and increased discharge at Garden City, Kansas. Based on the results of the water balance model between 1985 to 2011, an increase in river discharge would not have a proportional or significant increase in ET. The additional water in the channel of the Arkansas River would replenish lost storage in the alluvial aquifer and reduce the risk of extirpation of the trees and riparian community along the river. When the storage of the alluvial aquifer is full, then it is expected that increases in the Arkansas River discharge into the state of Kansas would result in a proportional increase in discharge at Garden City. Returning to a pre-development river regime would benefit the river ecosystem. A return to a normal flood regime has been shown to regenerate native trees and reduce the percentage of invasive salt cedars (Nagler et al., 2005).

Conclusions

The rate of evapotranspiration from the river corridor was analyzed from remotely sensed data and a regional weather station across a study period of growing seasons and years, and it was shown unequivocally that ET values depend upon the yearly stage of plant development and is completely independent of the river discharge. Evapotranspiration is not dependent on the discharge of the river. The average annual evapotranspiration for the study area is about 16% of the available surface water in the river, and the average annual recharge is about 13% of the available surface water. The river flows are managed by seasonal dam releases and irrigation water needs, and for much of the time does not flow at all on the eastern reaches of the Arkansas River. Reaches of the river with little to no surface water have been able to support vegetation as evidenced by the consistent evapotranspiration rates from the river corridor. The trees within the river corridor are consuming water from the groundwater including water stored in the alluvial sediments across hydrologic flow regimes. The infiltration from the river is stored in the alluvial sediments due to an underlying confining layer that inhibits groundwater recharge. While the water stored in the alluvial sediments are currently being lost from the system through evapotranspiration, they provide a potential store to be tapped in future water management decisions.

The ramifications of a depleted alluvial aquifer include the potential for extirpation of native plant and animal communities. Without replenishment water within the alluvial sediment will be depleted as the trees along the river corridor continue to consume water and the alluvial aquifer leaks into the Ogallala Aquifer. The loss of available water in the river has already had negative impacts on the native ecosystem of western Kansas. The tree communities have become less diverse with the replacement of native cottonwood trees with salt cedar. The

absence of available water in the alluvial sediments would result in further extirpation in the native plant and animal species of western Kansas.

Chapter 6 - Synthesis

The broader impacts and ramifications of the findings in the previous three chapters are discussed. One of the significant points of discovery is that the evapotranspiration from the river corridor was shown to be independent of the river discharge. By using remotely sensed imagery, atmospheric fluxes are included in the groundwater-surface water interactions to better understand the river system. The high infiltration capacity of the riverbed and how the transmission losses occur along the length of the river contribute to the characterization of the river and to the understanding of the hydrology of the river-aquifer system.

The examination of the river discharge and the atmospheric fluxes from the river were determined to be independent of each other at an annual scale. The atmospheric fluxes are driven by the riparian vegetation and the seasonal demand for water. The seasonal demand for water was identified in Chapter 4, and evapotranspiration was further investigated in Chapter 5. In Chapter 4, the transmission loss factor for the western reach of the Arkansas River fluctuates by season, with the summer months experiencing higher transmission losses as shown in Figure 4-5. Figure 4-6 and Figure 4-7 show how the transmission losses are independent of the river discharge. Based on the SSEB estimations of evapotranspiration within the river corridor, the evapotranspiration does not correlate to the river discharge. The coefficient of determination, r^2 , of the annual discharge at Syracuse, KS and the annual evapotranspiration over the study period is 0.095, indicating a low degree of correlation. The river discharge and the evapotranspiration are independent because the source water for evapotranspiration is the alluvial sediments. The trees and other riparian vegetation will consume water as long as there is available water in the alluvial sediments.

Transmission losses were determined to vary by location. From the water balance model in the previous chapter, the average annual transmission losses are the combination of ET and recharge at 68 million cubic meters. Upstream of the Bear Creek Fault, the transmission losses are driven by the seasonal vegetation growth. Transmission losses are partitioned into ET or recharge. The bedrock layer under the alluvial aquifer prevents further downward progression of the infiltrated river water. All transmission losses can be assumed to be consumed by evapotranspiration for the western reach of the Arkansas River. If the annual quantity of ET is assumed to be equal for the eastern segment and the western segment of the Arkansas River, then both segments will lose approximately 19 million cubic meters of water annually to ET. For the eastern segment of the Arkansas River, where the Ogallala Aquifer is present, the transmission losses are also partitioned into ET and recharge, and with the combined annual transmission losses being 49 million cubic meters. From the above assumption on ET losses, the transmission losses that contribute to recharging the aquifer would be 30 million cubic meters annually. From the simple transmission loss model, and the gaging stations along the Arkansas River, the transmission losses are greater upgradient than downgradient. The regular cessation of flow before Garden City does not provide many opportunities to recharge the area of the Ogallala Aquifer in the vicinity of Garden City. It can be assumed that the recharge rate is greatest at the western extent of the Ogallala Aquifer because of the regular presence of water in the river channel. The rate of recharge from the Arkansas River to the Ogallala Aquifer may be increased by building low-head dams in the river over the western extent of the Ogallala, creating a hydraulic gradient greater than one, resulting in an infiltration rate greater than hydraulic conductivity. Other strategies to increase the recharge rate are predicated on the availability of water. Given the consistent annual ET losses and the geology of the two reaches of the Arkansas

River, maximizing transmission losses on the eastern segment of the river would result in maximizing the recharge from the river to the Ogallala Aquifer.

Evapotranspiration is a significant component of the water balance of the Arkansas River. The average annual evapotranspiration for the study area is about 16% of the available surface water. The evapotranspiration from the river corridor is expected to fluctuate seasonally with plant development and to change year-to-year based on the quantity of water available. The results of this study show the seasonal fluctuation, but the annual variations in ET are minimal. The long-term storage capacity of the alluvial aquifer permits the riparian ecosystem to survive drought years. The annual evapotranspiration from the river corridor is near constant even when there is low or no flow in sections of the Arkansas River. This supports the conclusion that the evapotranspiration from the river corridor is independent of the flow in the Arkansas River. The results of the water balance model show that the annual evapotranspiration is less variable than the other components of the system, including river inflow, outflow, and recharge. The phreatophytes and other riparian vegetation are able to tap into the reliable source of water in the alluvial deposits.

The annual evapotranspiration from the river corridor is a lagging indicator of the health of the riparian ecosystem. The drought conditions resulting in low stream flows in 2002-2006 were followed by below average annual ET starting in 2006 through the end of the study period in 2011. This decline in ET is an indicator that, while the alluvial aquifer has been a consistent source of water for the riparian ecosystem, the supply of water is limited. When there is zero water in the riparian ecosystem, then there will be zero ET from the river. Declining groundwater tables and the depletion of water stores in the alluvial aquifer result in less available water to support vegetation. With less water, the trees experience water stress. The result of

water stressed phreatophytes has been a change in tree population from cottonwoods to salt cedars. While both trees have equivalent rates of ET, the salt cedars are able to withstand drought and declining water tables better than native tree species. Salt cedar has a different, more resilient response than cottonwood when water tables decline resulting in a lower mortality rate (Shafroth et al., 2000). Cottonwoods are dependent on alluvial groundwater and sensitive to short-term groundwater pumping. The cottonwood trees are vulnerable to declining water tables (Scott et al., 1999). If the water table drops rapidly or drops below a threshold (e.g. below the annual minimum), then cottonwood trees die off (Cooper et al., 2003). During a drought period, cottonwoods experienced a 90% mortality when the groundwater depth was between 12 and 13 feet compared to a 30% mortality when groundwater depth was less than 10 ft (Braun et al., 2004). A rising water table may have similar effects in tree mortality and the establishment of a new community if the root systems are unable to adjust to the change (Naumburg et al., 2005).

The ramifications of a decoupled river discharge and evapotranspiration are that the river can be managed independently from the ET losses. Surface water resources can be allocated to ET losses from the river because the annual ET from the river is fairly consistent. The recommended allocation is the annual mean of 38 million cubic meters per year. Because the available storage in the alluvial sediments is able to withstand periods of drought, the surface water allocation for ET can be reduced in favor of more economically beneficial uses. Flood pulses in the Arkansas River are not expected to result in higher rates of ET. The flood pulse would be partitioned into the other components of the water balance equation – diversions to irrigation ditches, recharge of the aquifer, and conveyance of the flood pulse downstream. Unless the river is diverted to the irrigation ditches, annual river volumes greater than 38 million cubic meters will either become groundwater recharge or surface water discharge.

The water in the alluvial sediments is dependent upon recharge from the river. The riverbed of the Arkansas River has a great capacity to infiltrate river flow as discussed in Chapter 3. The riverbed sediments have high hydraulic conductivity and transmit the infiltrated water to lower levels in the alluvial aquifer. The continued downward infiltration is restricted by either bedrock or confining layers of lower permeable deposits. The actual transmission losses are a small percent of the expected transmission losses under the assumption that the surface hydraulic conductivity controls the process. While, a confining layer under the riverbed sediments would inhibit downward transmission of the infiltrated river water, it does allow near-surface storage of water in the alluvial deposits. This storage provides the reliable source of freshwater to the riparian vegetation. The bank storage for the western reach of the Arkansas River is at or near capacity. This claim is supported by the low transmission losses during the winter and the higher transmission losses in the summer due to the induced infiltration from evapotranspiration shown in Figure 4-5. For the eastern reach, the river often experiences a cessation of flow prior to Garden City that is independent of the season. This indicates that there is ample storage in the alluvial sediments for this reach to store and transmit river water to the lower layers. The available storage is the result of the declining water table of the Ogallala Aquifer. The water in the alluvial aquifer leaks to the Ogallala Aquifer. This claim is supported by the high sulfate levels in the Ogallala Aquifer dispersing from the Arkansas River (Whittemore, 2000). The Arkansas River is recharging the alluvial aquifer, which, in turn, leaks and recharges the Ogallala Aquifer. From the well logs in Appendix B, the delineation between the Arkansas River alluvial aquifer and the Ogallala Aquifer is not clear.

The flow of the Arkansas River has changed significantly since pre-development. The Arkansas River derived approximately 50% of its streamflow from groundwater during low flow

periods and approximately 14% during high flow periods. Approximately 8.5 m³/s (300 cfs) of groundwater contributed to the Arkansas River baseflow during the predevelopment period (Allen 2012). The groundwater baseflow has since disappeared due to the declining water levels of the Ogallala Aquifer. The transition to a losing river has resulted in further reductions in the river flow as the water conveyed from upstream is lost to the riverbed. Elimination of the baseflow combined with transmission losses has resulted in many low flow or no flow days on the Arkansas River near Garden City, Kansas. While the groundwater extraction has reduced the amount of water in the Arkansas River, the timing of flows has also been altered. The high flow periods during the summer months have been restricted by impoundment of the river. Before the construction of the John Martin Reservoir, the predevelopment flows were unregulated, and flood pulses and larger summer flows progressed down the channel. The lack of flood pulses has had a negative impact on the Cottonwood trees. The Cottonwoods favor perennial rivers with natural flow regimes, while salt cedars are invasive species and are better able to adapt to water stress (Stromberg et al., 2007). The lack of flood pulses has also altered the evolution of the riverbed. The hydraulic conductivity of the riverbed is not only variable spatially, but it can change over time as well. From a tracer experiment from Lange et al. (1997), an artificial flood pulse disturbed a compacted upper layer and enhanced infiltration. Flood pulses have the energy to mobilize, convey, and deposit riverbed sediments. Suspended sediment concentrations are highest at the flow front in response to a storm event (Dunkerley and Brown, 1999). The quantity of water in the channel has a non-linear response to transmission losses and groundwater recharge. Transmission losses from high flow events are more important for providing recharge than medium or low flow events (Lange, 2005). An unregulated river with

natural flood pulses alters the conditions that impact groundwater-surface water interactions and may result in higher transmission losses and higher rates of groundwater recharge.

The regulation and dewatering of the Arkansas River has provided many benefits to the region. The John Martin Reservoir has controlled flooding in the Arkansas River valley and has limited the damaging effects to land and property along the river. The reservoir stores and releases the spring snowmelt to support irrigated agriculture along the river, providing an economic benefit to both Colorado and Kansas. The reservoir also serves as a source of recreation and conservation for the region. The John Martin Reservoir State Park provides amenities including boating, fishing, camping, and hiking. The reservoir offers a habitat for wildlife including threatened and endangered birds. While the impacts to the river from groundwater extraction are not desirable, the dewatering of the Arkansas River is an unintended consequence of the unsustainable groundwater extraction. The economic benefit of irrigated agriculture to western Kansas has shown to outweigh the negative consequences of the dewatered river by the continuation of groundwater extraction after the impacts to the rivers were known.

The declining streamflow resulting from the extraction of groundwater has had negative impacts on the ecosystem. Salt cedar are dominant in intermittent rivers with dam regulated flows because of their ability to adapt to water stress and their opportunistic reproductive traits, while cottonwoods favor perennial rivers with natural flow regimes (Stromberg et al., 2007). A drawdown of a water table resulted in a change in plant community from wetland grasses to shrubby phreatophytes and reduced annual ET by 32% (Cooper et al., 2006). The decrease in available water has not had significant impacts to the annual ET rates from the Arkansas River corridor, but the riparian ecosystem is changing in response to the limited availability of water.

The dewatering of rivers and streams in Kansas has already lead to the extirpation of aquatic life in the river and is partially responsible for half of Kansas' original native fish fauna to be recommended for listing on a special conservation list (Campbell et al., 2016). The disappearance of the habitat to support aquatic ecosystems is an indication of what may happen to the trees and riparian ecosystem adjacent to the river if the alluvial aquifer is depleted. Even if the river flows were to be restored to minimum desired stream flow standards set by the Kansas legislature, it is unlikely that the river ecosystem of western Kansas will return to its predevelopment state (Ferrington, 1993). Land use changes and water use has altered the prairie streams of the Great Plains resulting in large scale loss of native grassland streams (Dodds et al., 2004). Fragmentation and drying of the rivers in Kansas has resulted in a decline in fish diversity (Perkin et al., 2015). Dewatering of the Arkansas River has resulted in extirpation or near extirpation of aquatic insect communities (Ferrington, 1993). Restoration of natural communities may not be possible even if the river returns to a perennial pre-development flow regime. Because of the river-aquifer connection, the restoration of the Arkansas River is predicated on the management and regulation of the groundwater withdrawals. In Cimarron River Basin in southwest Kansas, the rivers have had a statistically significant decrease in annual mean discharge between 1951 and 2013 as a result of the groundwater withdrawals, which adversely affects the habitat of the Arkansas darter (Juracek, 2015). The indirect benefit of the dewatering of the rivers is the groundwater capture of the river discharge which has lessened the aquifer storage loss by approximately 12% (Liu et al., 2010).

The negative environmental impacts of overdrawn groundwater are limited in Kansas. Zekster et al. (2005) identified four negative impacts including a decline in surface water, reduction in vegetation, land subsidence, and sea water or groundwater intrusion. Kansas has

experience the surface water decline as evidenced by the decline in extent of perennial streams. Kansas has also seen changes in vegetation and a reduction of the diversity of vegetation. As water tables in riparian ecosystems have declined, the cottonwoods have died and have been replaced by salt cedars. The tree distribution has altered between pre-development and post-development (Ahring and Steward, 2012). The land subsidence has not been in issue with respect to groundwater withdrawals in Kansas because of the granular composition of the Ogallala Aquifer. The water quality issues from sea water or groundwater intrusion are also not observed, but the declining water table has induced river infiltration. The Arkansas River water has high concentrations of sulfate that is entering the Ogallala Aquifer (Whittemore, 2000). The river water high in sulfates would have been diluted by the baseflow of the Arkansas River and conveyed downstream, but instead the sulfates are infiltrating the Ogallala Aquifer. The sulfate plume is an indication that the Ogallala Aquifer is vulnerable to contamination from the river.

The transmission losses are controlled, in part, by seasonal vegetation growth, available storage in the river alluvium, and a confining layer under the river alluvium. The seasonal variability in the transmission losses is the result of phreatophyte induced streambed infiltration. The seasonal factor is identified in the transmission loss model and in the analysis of the gaging data over seasonal and annual time scales. From Figure 4-4, the transmission loss model is overestimating the transmission losses at Deerfield; there is more water flowing through Deerfield than what the simple transmission loss model predicts. This indicates that the segment of river between the Bear Creek Fault and Deerfield has less available storage than the segment of river between Deerfield and Garden City. The relationship of the river to the aquifer and the geology of the river valley influences the river transmission losses and can be characterized in one of three ways – connected gaining, connected losing, or disconnected. The river regime of

the Arkansas River is not a simple disconnected river, but instead it varies over time and segment of the river. Sections of the eastern reaches of the Arkansas River are likely to be disconnected or transitioning to a disconnected state. The western reach where the river and alluvial aquifer is bounded by bedrock. Depending on the stage of the river and the water level of the alluvial aquifer, the river may be gaining or losing. The river-aquifer relationship determines the flow paths between the two systems. If the river is a connected-losing or connected-gaining, then the river exchanges would occur at the banks (Genereux and Bandopadhyay, 2001). If the river is in a disconnected losing state, then the flux from the surface water in the river to the groundwater would occur along the bottom width of the river (Brunner et al., 2009).

The reach of the Arkansas River that is over the Ogallala does experience regular cessations of flow. The reach of the Arkansas River that is bounded by bedrock does not experience a cessation of flow because the regulated supply of surface water from upstream and the lower boundary layer that prevents leakage of the alluvial aquifer. The terrestrial demand for water is comparable for the eastern reach and the western reach. The explanation for the cessation of flow on the eastern reach is the difference in the lower boundary conditions of the alluvial aquifer. When the alluvial aquifer is bounded by bedrock, the river is perennial, and the riparian vegetation induces infiltration and experiences transmission losses under that mechanism. When the alluvial aquifer is bounded by a permeable confining layer over a large aquifer, the alluvial aquifer will leak to the underlying aquifer, if the water level of the alluvial aquifer is higher than the underlying aquifer. The leakage mechanism combined with the terrestrial ET demand for water will result in a cessation of flow if the rate of leakage and ET are greater than the supply of river water.

The alluvial aquifer of the Arkansas River is a source of fresh water that the riparian vegetation tap into. The available of water from the river bank is a potential source of freshwater that is regularly recharged by the Arkansas River, but tapping into the alluvial deposits or regulating the surface flow below the recommended volume would result an expanded dewatering of the Arkansas River. Management of the water in Arkansas river, the river alluvium, and the Ogallala Aquifer should be coordinated due to their coupled relationship. The assessment of the role of ET in the river system has allowed the decoupling of the river discharge and ET at the annual scale. By allocating sufficient water to the root water uptake of the phreatophytes, the remaining water can be budgeted for surface irrigation, river discharge, and focused recharge from the river.

Chapter 7 - Summary and Conclusions

This dissertation studied the water balance in western Kansas including groundwater-surface water interactions and the role of evapotranspiration in the rivers. An examination of the major rivers in western Kansas assessed the ability of the riverbed to act as a conduit to recharge the groundwater system. The riverbeds were instrumented to determine the conductivity of the riverbeds, the transmission losses of the river were modeled using the measured hydraulic conductivity of the riverbeds to determine the interactions between the surface water and groundwater, and the evapotranspiration of the river corridor was estimated using satellite remote sensing to quantify of water lost to the atmosphere. The interactions between the surface, groundwater and atmosphere were assessed over time revealing that the flux to the atmosphere can be decoupled from the groundwater recharge. While the declining discharge in the river can be attributed to the extraction of groundwater resources and the management of surface water resource, the atmospheric fluxes are shown to be independent of the surface water and groundwater at an annual scale.

Chapter 3 was a study on the hydraulic conductivity of the riverbed. The Arkansas River and the Cimarron River were instrumented to measure the infiltration rates under saturated and unsaturated conditions. The rivers were found to have riverbed sediments that range from a coarse sand to a sandy loam. The composition of the riverbed provides for a high conductivity of the riverbed as confirmed by the results of the infiltration instrumentation. In a disconnected system where a layer of unsaturated material separates the riverbed from the groundwater table, the transmission losses from the river would be controlled by the hydraulic conductivity of the riverbed sediments. An initial examination of the transmission losses as compared to the measured discharges along the Arkansas River indicates that the hydraulic conductivity of the

riverbed is not the controlling factor of transmission losses. Characterizing the hydraulic conductivity of the riverbed sediments is only one measure of hydraulic properties of the river. Other considerations are the storage state of the riverbed and underlying aquifer and the hydraulic properties of the sediments under the river.

Chapter 4 expanded the transmission loss analysis by developing a simple transmission loss model that uses the hydraulic conductivity measured in the previous chapter. The transmission loss model was applied to the Arkansas River between the Colorado state line near Coolidge, KS and Garden City, KS. In the previous chapter, hydraulic conductivity for the Cimarron River was also collected, but the lack of discharge measurements and the limited number of flow days prevented an analysis of the Cimarron River. The results of the transmission loss model along the Arkansas River confirm the initial findings from Chapter 3 that the hydraulic conductivity of the riverbed is not the primary controlling factor for transmission losses. The transmission loss factor, which is the variable in the simple transmission loss model used to match the modeled river discharge to the measured river discharge, indicates that there is a difference in groundwater-surface water connection between the reaches upgradient and downgradient of the Bear Creek Fault line. The average transmission loss factor in the upgradient, western reach of the Arkansas River is 0.015 and is 0.027 in the downgradient, eastern reach. The Bear Creek Fault line is the western edge of the Ogallala Aquifer along the Arkansas River. While the hydraulic conductivity of the surface of the river bed may be high, the subsurface properties impact the transmission of the river discharge to lower layers. The Arkansas River has a high capacity to infiltrate river discharge, but it is limited in its ability to transmit the water to effectively refill the Ogallala Aquifer because of the confining layer under the alluvial aquifer. The transmission loss factor indicates a strong

seasonal influence indicated by higher transmission losses from the river in the spring and summer months which is noticeable in the western reach of the Arkansas River above the Bear Creek Faultline. The role of evapotranspiration plays a role in the transmission losses. When assessing the river's contribution to groundwater recharge, the role of evapotranspiration and the riparian demand for water should be factored into the water balance of the river system.

Chapter 5 examined the role of evapotranspiration (ET) in the river system. The ET from the river corridor was estimated using the Simple Surface Energy Balance (SSEB) model with data collected by the Landsat 5 Thematic Mapper (TM) Satellite. The ET was aggregated across the river system and the season to determine the quantity of water consumed by the ET process. The estimates for ET were combined with the measured river discharges to get a water balance of the river system. From the water balance model, the water entering the system is partitioned into the ET, the surface water and the groundwater. The results indicate that the annual inflow from the river is highly variable while the annual ET from the river corridor is near constant. The average annual evapotranspiration for the study area is about 16% of the available surface water in the river, and the average annual recharge is about 13% of the available surface water. The ET from the river corridor fluctuates based on the season. The trees and other riparian vegetation draw water from the surface and alluvial aquifer to maintain the river ecosystem. Although the consistency of the ET over the period of the study indicates that the river discharge does not control ET, the lack of surface water to recharge the alluvial aquifer will eventually cause negative and possibly permanent extirpation of the riverine community. ET of the river system was able to be decoupled from the river discharge because the trees are a constant presence in the river corridor that sources its water from the aquifer. The trees and vegetation within the river corridor have a source of water that is persistent and less variable than river

discharge. The confining layer under the alluvial aquifer allows it to be a reliable store of infiltrated water from the river.

Chapter 6 discussed the major findings of this study. The river discharge and the atmospheric fluxes are independent at the annual time scale. The ramifications of the decoupling of river discharge and ET are that the river can be managed independently as long as sufficient water is allocated to ET. Without the proper management and planning of the water resources, the alluvial aquifer will be depleted. The alluvial aquifer is dependent on the recharge from the Kansas River and is the source water for the phreatophytes and riparian vegetation. The rivers in western Kansas have been degraded by the reduction in stream flow and the reduction in extent of perennial flows. Eliminating the source of water for the riparian vegetation will further degrade the ecosystem, and that degradation may be beyond recovery.

This research provides new insight into riverbed hydrologic fluxes between surface water, groundwater, and the atmosphere. While riverbed sediments have relatively high hydraulic conductivity, their capacity to conduct river water to lower deposits is limited to a small fraction of their potential recharge capacity. Analysis of the evapotranspiration rates of phreatophytes within the river corridor indicate that a significant fraction of total discharge is being released to the environment through root water uptake. The timing of these releases is consistent across changes in streamflow, indicating that bank storage in the alluvial deposits is being tapped. While these waters are currently being lost from the system through evapotranspiration, they provide a potential store to be tapped in future water management decisions.

References

- Abdulrazzak, M.J and H.J. Morel-Seytoux. 1983. Recharge from an Ephemeral Stream Following Wetting Front Arrival to Water Table. *Water Resources Research*. 19: 194-200.
- Ahring, T.S 2009. Phreatophytes in Southwest Kansas Used as a Tool for Predicting Hydrologic Properties (Master's Thesis). Retrieved from K-Rex - <http://krex.k-state.edu/dspace/handle/2097/4>.
- Ahring, T.S. and D.R. Steward. 2012. Groundwater surface water interactions and the role of phreatophytes in identifying recharge zones. *Hydrology and Earth System Sciences*. 16:4133-4142.
- Allen, R.G., M Tasumi, and R. Trezza. 2007. Satellite Based Energy Balance for Mapping Evapotranspiration with Internalized Calibration (METRIC) – Model. *Journal of Irrigation and Drainage Engineering*. 133: 380-394.
- Allen, A. 2012. Analytic Element Modeling of The High Plains Aquifer: Non-Linear Model Optimization Using Levenberg-Marquardt And Particle Swarm Algorithms (Master's Thesis). Retrieved from K-Rex - <http://krex.k-state.edu/dspace/handle/2097/14103>
- Alyamani, M.S., and Z. Sen. 1993. Determination of hydraulic conductivity from complete grain-size distribution curves. *Ground Water* 31, no. 4: 551-555.
- Angelo, R.T. 1994. Impacts of Declining Stream Flow on Surface Water Quality. Pages 1–2 in: *Proceedings of the Eleventh Annual Conference on Water and the Future of Kansas*, Kansas State University, Manhattan.
- Bastiaanssen, W.G.M, E.J.M Noordman, H. Pelgrum, G. Davids, B.P. Threnson, and R.G. Allen. 2005. SEBAL Model with Remotely Sensed Data to Improve Water-Resource Management under Actual Field Conditions. *Journal of Irrigation and Drainage Engineering*. 131:89-93.
- Battle-Aguilar, J., and P. G. Cook. 2012., Transient infiltration from ephemeral streams: A field experiment at the reach scale, *Water Resources Research* 48. doi:10.1029/2012WR012009.
- Bloschl, G. and M. Sivapalan. 1995. Scale Issues in Hydrological Modelling: a review. *Hydrologic Processes* 9: 251-290.
- Braun, C.L., S.M. Eberts, S.A. Jones, and G.J. Harvey. 2004. Water-Level Variations and Their Effects on Tree Growth and Mortality and on the Biogeochemical System at the Phytoremediation Demonstration Site in Fort Worth, Texas, 1996–2003. U.S. Geological Survey Scientific Investigations Report 2004-5107.

- Bruen, M.P. and Y.Z. Osman. 2004. Sensitivity of stream-aquifer seepage to spatial variability of the saturated hydraulic conductivity of the aquifer. *Journal of Hydrology* 293: 289-302.
- Brunner, P., C.T. Simmons, and P.G. Cook. 2009. Spatial and temporal aspects of the transition from connection to disconnection between rivers, lakes and groundwater. *Journal of Hydrology* 376: 159–169.
- Brunner, P., P.G. Cook and C.T. Simmons. 2009a. Hydrogeologic controls on disconnection between surface water and groundwater. *Water Resources Research* 45.
- Brunner, P., R. Therrien, P. Renard, C. T. Simmons, and H.-J. H. Franssen. 2017. Advances in understanding river-groundwater interactions, *Rev. Geophys.*, 55: 818–854. doi:10.1002/2017RG000556.
- Buchanan, R.C., B.B. Wilson, R.R. Buddemeier, and J.J. Butler, Jr. 2015. The High Plains Aquifer. Public Information Circular 18.
- Butler, J.J. Jr., G.J. Kluitenberg, D.O. Whittemore, S.P. Loheide II, W. Jin, M.A. Billinger, and X. Zhan. 2007. A field investigation of phreatophyte-induced fluctuations in the water table. *Water Resources Research*. 43.
- Calver, A. 2001. Riverbed Permeabilities: Information from Pooled Data. *Ground Water*. 39: 546-553.
- Campbell, S.W., C.S. Szuwalski, V.M. Tabor, and F deNoyelles. 2016. Challenges to Reintroduction of a Captive Population of Topeka Shiner (*Notropis topeka*) into Former Habitats in Kansas. *Transactions of the Kansas Academy of Science*, 119(1):83-92.
- Carsel, R.F. and R.S. Parrish. 1988. Developing Joint Probability Distributions of Soil Water Retention Characteristics. *Water Resources Research*. 24: 755-769.
- Chen, X. 2000. Measurement of streambed hydraulic conductivity and its anisotropy. *Environmental Geology* 39: 1317-1324.
- Chen, X. and L Shu. 2002. Stream-Aquifer Interactions: Evaluation of Depletion Volume and Residual Effects from Ground Water Pumping. *Groundwater* 40: 284-290.
- Chen, X. 2004. Streambed Hydraulic Conductivity for Rivers in South-Central Nebraska. *Journal of the American Water Resources Association*: 561-573.
- Chen, X. 2005. Statistical and geostatistical features of streambed hydraulic conductivities in the Platte River, Nebraska. *Environmental Geology* 48: 693-701.
- Chen, X. 2007. Hydrologic connections of a stream-aquifer-vegetation zone in south-central Platte River valley, Nebraska. *Journal of Hydrology* 333: 554-568.

- Chen, X. 2011. Depth-dependent hydraulic conductivity distribution patterns of a streambed. *Hydrological Processes* 25: 278-287.
- Chow, V.T. 1959 *Open-Channel Hydraulics*. McGraw-Hill, New York.
- Cook, P.G. 2015. Quantifying river gain and loss at regional scales. *Journal of Hydrology*. 531: 749-758.
- Cooper, D. J., D.R. D'Amico, and M.L. Scott. 2003. Physiological and Morphological Response Patterns of *Populus deltoids* to Alluvial Groundwater Pumping. *Environmental Management* 31(2): 215-226.
- Cooper, D. J., J. S. Sanderson, D. I. Stannard, and D. P. Groeneveld. 2006. Effects of long-term water table drawdown on evapotranspiration and vegetation in an arid region phreatophyte community, *J. Hydrol.*,325(1– 4), 21– 34.
- Conrad, L.P. and M.S. Beljin. 1996. Evaluation of an induced infiltration model as applied to glacial aquifer systems. *Water Resources Bulletin* 32, no.6: 1209-1220.
- Constantz, J. 1998. Interaction between stream temperature, streamflow, and groundwater exchanges in alpine streams. *Water Resources Research* 34: 1609-1615.
- Constantz, J. 2008. Heat as a tracer to determine streambed water exchanges. *Water Resources Research* 44.
- Costa. A.C., S. Foerster, J.C. de Araujo, and A. Bronstert. 2013. Analysis of channel transmission losses in a dryland river reach in north-eastern Brazil using streamflow series, groundwater level series, and multi-temporal satellite data. *Hydrological Processes* 27: 1046-1060.
- Crosbie, R.S., A.R. Taylor, A.C. Davis, S. Lamontagne, and T. Munday. 2014. Evaluation of infiltration from losing-disconnected rivers using a geophysical characterization of the riverbed and a simplified infiltration model. *Journal of Hydrology* 508: 102-113.
- Dages, C., M. Voltz, J.G. Lacas, O. Huttel, S. Negro, and X. Louchart. 2008. An experimental study of water table recharge by seepage losses from a ditch with intermittent flow. *Hydrological Processes* 22: 3555-3563.
- Dahm, C.N, J.R. Cleverly, J.E Allred Coonrod, J.R. Thibault, D.E. McDonnell, and D.J. Gilroy. 2002. Evapotranspiration at the land/water interface in a semi-arid drainage basin. *Freshwater Biology* 47.
- Doble, R. C., R. S. Crosbie, B. D. Smerdon, L. Peeters, and F. J. Cook (2012), Groundwater recharge from overbank floods, *Water Resour. Res.*, 48.
- Dodds, W.K., K. Gido, M.R. Whiles, K.M. Fritz, and W.J. Matthews. 2004. Life on the Edge: The Ecology of Great Plains Prairie Streams. *BioScience*, 54(3):205-216.

- Dunkerley, D. and K. Brown. 1999. Flow behavior, suspended sediment transport and transmission losses in a small (sub-bank-full) flow event in an Australian desert stream. *Hydrological Processes* 13: 1577-1588.
- Evans, R.G. and E.J. Sadler. 2008. Methods and technology to improve efficiency of water use. *Water Resources Research* 44.
- Evett, S.R., W.P. Kustas, P.H. Gowda, M.A. Anderson, J.H. Prueger, and T.A. Howell. 2012. Overview of the Bushland Evapotranspiration and Agricultural Remote sensing EXperiment 2008 (BEAREX08): A field experiment evaluating methods for quantifying ET at multiple scales. *Advances in Water Research* 50: 4-19.
- Ferrington, Jr., L.C. 1993. Endangered river: a case history of the Arkansas River in the Central Plains. *Aquatic Conservation: Marine and Freshwater Ecosystems* 3: 305-316.
- Fleckenstein, J.H., S. Krause, D.M. Hanna, and F. Boano. 2010. Groundwater-surface water interactions: New methods and models to improve understanding of processes and dynamics. *Advances in Water Resources* 33: 1291-1295.
- Gardner, W.R. 1958. Some steady-state solutions of the unsaturated moisture flow equation with application to evaporation from a water table. *Soil Sci.* 85:467-470.
- Genereux, D.P., Bandopadhyay, I., 2001. Numerical investigation of lake bed seepage patterns: effects of porous medium and lake properties. *J. Hydrol.* 241, 286–303
- Genereux, D.P. S. Leahy, H. Mitasova, C.D. Kennedy, and D.R. Corbett. 2008 Spatial and temporal variability of streambed hydraulic conductivity in West Bear Creek, North Carolina, USA. *Journal of Hydrology* 358: 332-352.
- Gribb, M.M., R. Kodesova, and S.E. Ordway. 2004. Comparison of Soil Hydraulic Property Measurement Methods. *Journal of Geotechnical and Geoenvironmental Engineering.* 1084-1095.
- Gowda, P.H., J.L. Chavez, P.D. Colaizzi, S.R. Evett, T.A. Howell, and J.A. Tolk. 2008. ET mapping for agricultural water management: present status and challenges. *Irrigation Science* 26: 223-237.
- Gowda, P.H., G.B. Senay, T.A. Howell, and T.H. Marek. 2009. Lysimetric Evaluation of Simplified Surface Energy Balance Approach in the Texas High Plains. *Applied Engineering in Agriculture* 25(5): 665-669.
- Gowda, P.H., T.A. Howell, G. Paul, P.D. Colaizzi, T.H. Marek, B. Su, and K.S. Copeland. 2012. Deriving Hourly Evapotranspiration Rates with SEBS: A Lysimetric Evaluation. *Vadose Zone.*
- Hansen, C. V., 1991, Estimates of freshwater storage and potential natural recharge for principal aquifers in Kansas: U.S. Geological Survey, Water Resources Investigations Report 87-4230.

- Haverkamp, R., P.J. Ross, K.R.J. Smettem, and J.-Y. Parlange. 1994. Three-dimensional analysis of infiltration from the disc infiltrometer. 2. Physically based infiltration equation. *Water Resour. Res* 30:2931–2935.
- Jordan, P.R. 1977. Streamflow Transmission Losses in Western Kansas. *Journal of Hydraulics Division* 103:905-919.
- Juracek, K.E. 2015. Streamflow Characteristics and Trends at Selected Streamgages in Southwest and South-Central Kansas. U.S. Geological Survey Scientific Investigations Report 2015-5167.
- Juracek, K.E. and K. Eng. 2017. Streamflow Alteration at Selected Sites in Kansas. U.S. Geological Survey Scientific Investigations Report 2017-5046.
- Kalbus, E., F. Reinstorf, and M. Schirmer. 2006. Measuring methods for groundwater – surface water interactions: a review. *Hydrology and Earth System Sciences* 10: 873-887.
- Kalbus, E., C. Schmidt, J.W. Molson, F. Reinstorf, and M Schirmer. 2009. Influence of aquifer and streambed heterogeneity of the distribution of groundwater discharge. *Hydrology and Earth System Sciences* 13: 69-77.
- Kennedy, C.D., D.P. Genereux, H. Mitsova, D.R. Corbet, and S. Leahy. 2008. Effect of sampling density and design on estimation of streambed attributes. *Journal of Hydrology* 355: 164-180.
- Kennedy, C.D., D.P Genereux, D.R. Corbett, and H. Mitsova. 2009. Spatial and temporal dynamics of coupled groundwater and nitrogen fluxes through a streambed in an agricultural watershed. *Water Resources Research* 45
- Klemes V. 1983. Conceptualization and scale in hydrology, *Journal of Hydrology* 65: 1-23.
- Konikow, L.F. and Kendy, E., 2005. Groundwater depletion: a global problem. *Hydrogeology Journal* 13: 317-320.
- Landon, M.K., D.L. Rus, and F.E. Harvey. 2001. Comparison of Instream Methods for Measuring Hydraulic Conductivity in Sandy Streambeds. *Ground Water* 39:870-885.
- Lange, J., C. Leibundgut, T. Grodek, J. Lekach, and A. Schick. 1997. Using artificial tracers to study water losses of ephemeral floods in small arid streams. *Karst Hydrology*. IAHS Publ no 247.
- Lange, J. 2005. Dynamics of transmission losses in a large arid stream channel. *Journal of Hydrology* 306: 112-126.
- Leopold L.B. and T. Maddock, Jr. 1953. The Hydraulic Geometry of Stream Channels and Some Physiographic Implications. *Geologic Survey Professional Paper* 252.

- Lopez, O.M. K.Z. Jadoon, and T.M. Missimer. 2015. Method of Relating Grain Size Distribution to Hydraulic Conductivity in Dune Sands to Assist in Assessing Managed Aquifer Recharge Projects: Wadi Khulays Dune Field, Western Saudi Arabia. *Water* 7: 6411-6426.
- Liu, G., B. Wilson, D. Whittemore, W. Jin, and J. Butler Jr. 2010. Ground-Water Model for Southwest Kansas Groundwater Management District No. 3. Kansas Geological Survey Open File Report 2010-18.
- Loheide, S.P. II, J.J. Butler Jr., S.M. Gorelick. 2005. Estimation of groundwater consumption by phreatophytes using diurnal water table fluctuations: A saturated-unsaturated flow assessment. *Water Resources Research* 41.
- Madsen, M.D and D.G. Chandler. 2007. Automation and use of Mini Disk Infiltrimeters. *Soil Science Society of America* 71: 1469-1472.
- McGuire, V.L. 2017. Water-Level and Recoverable Water in Storage Changes, High Plains Aquifer, Predevelopment to 2015 and 2013–15. USGS Scientific Investigations Report 2017–5040.
- Nagler, P.L, O. Hinojosa-Huerta, E.P. Glenn, J. Garcia-Hernandez, R. Romo, C. Curtis, A.R. Huete, and S.G. Nelson. 2005. Regeneration of Native Trees in the Presence of Invasive Saltcedar in the Colorado River Delta, Mexico. *Conservation Biology*: 1842-1852.
- Naumburg, E., R. Mata-Gonzalez, R. G. Hunter, T. McLendon, and D. W. Martin. 2005. Phreatophytic vegetation and groundwater fluctuations: A review of current research and application of ecosystem response modeling with an emphasis on Great Basin vegetation, *Environ. Manage.*, 35(6), 726– 740.
- Niswonger, R.G., D.E. Prudic, G.E. Fogg, D.A. Stonestrom, and E.M. Buckland. 2008. Method for estimating spatially variable seepage loss and hydraulic conductivity in intermittent and ephemeral streams, *Water Resour. Res.*, 44, W05418, doi:10.1029/2007WR006626.
- Nowinski, J.D., M.B. Cardenas, and A.F. Lightbody. 2011. Evolution of hydraulic conductivity in the floodplain of a meandering river due to hyporheic transport of fine materials. *Geophysical Research Letters* 38.
- Owens, M.K and G.W. Moore. 2007. Saltcedar Water Use: Realistic and Unrealistic Expectations. *Society for Range Management* 60: 553-557.
- Peel, M. C., Finlayson, B. L., and McMahon, T. A. 2007. Updated world map of the Köppen-Geiger climate classification, *Hydrol. Earth Syst. Sci.*, 11, 1633-1644, <https://doi.org/10.5194/hess-11-1633-2007>.
- Perkin, J.S., K.B. Gido, K.H. Costigan, M.D. Daniels, and E.R. Johnson. 2015. Fragmentation and drying ratchet down Great Plains stream fish diversity. *Aquatic Conservation: Marine and Freshwater Ecosystems* 25: 639-655.

- Philip, J.R. 1957. The theory of infiltration: 4. Sorptivity and algebraic infiltration equations. *Soil Sci.* 84:257–264.
- Postel, S. L. 2000. Entering and era of water scarcity: the challenges ahead. *Ecological Applications* 10: 941-948.
- Reid, M.E., and S.J. Dreiss. 1990. Modeling the effects of unsaturated, stratified sediments on groundwater recharge from intermittent streams. *Journal of Hydrology* 114: 149-174.
- Reitz, M., W.E. Sanford, G.B. Senay, and J. Cazenias. 2017. Annual estimates of recharge, quick-flow runoff, and ET for the contiguous US using empirical regression equations, 2000-2013: U.S. Geological Survey data release, <https://doi.org/10.5066/F7PN93P0>
- Reynolds, W.D. D.E. Elrick, and E.G. Young. 2002. Single-Ring and Double- or Concentric-Ring Infiltrimeters in *Methods of Soil Analysis Part 4 – Physical Methods*. p. 821-826.
- Rogers, D.H. and F.R. Lamm. 2012. Kansas Irrigation Trends. Proceedings of the 24th Annual Central Plains Irrigation Conference, Colby, Kansas, February 21-22, 2012.
- Rosas, J., O. Lopez, T.M. Missimer, K.M. Coulibaly, A.H. Dehwah, K. Sesler, L.R. Lujan, and D. Mantilla. 2014. Determination of hydraulic conductivity from grain-size distribution for different depositional environments. *Ground Water* 52(3): 399-413.
- Rus, D.L., V.L. McGuire, B.R. Zurbuchen, and V.A. Zlotnik. 2001. Vertical Profiles of Streambed Hydraulic Conductivity Determined Using Slug Tests in Central and Western Nebraska. U.S. Geological Survey Water-Resources Investigation Report 01-4212.
- Schmidt, C., M. Bayer-Raich, and M. Schirmer. 2006. Characterization of spatial heterogeneity of groundwater-stream water interactions using multiple depth streambed temperature measurements at the reach scale. *Hydrology and Earth System Sciences*, 10: 849-859.
- Scott, M.L., P.B. Shafroth, and G.T. Auble. 1999. Responses of Riparian Cottonwoods to Alluvial Water Table Declines. *Environmental Management* 23(3): 347-358.
- Senay, G.B., M. Budde, J.P. Verdin, and A.M Melesse. 2007. A Coupled Remote Sensing and Simplified Surface Energy Balance Approach to Estimate Actual Evapotranspiration from Irrigated Fields. *Sensors* 7: 979-1000.
- Shafroth, P.B., J.C. Stromberg, and D.C. Patten. 2000. Woody Riparian Vegetation Response to Different Alluvial Water table regimes. *Western North American Naturalist* 60(1): 66-76.
- Shanafield, M. and P.G. Cook. 2014. Transmission losses, infiltration and groundwater recharge through ephemeral and intermittent streambeds: A review of applied methods. *Journal of Hydrology* 511: 518-529.
- Singh, V.P., P.D. Scarlatos, and S.N. Prasad. 1990. An improved Lewis-Milne equation for the advance phase of boarder irrigation. *Irrigation Science* 11: 1-6.

- Sophocleous, M., M.A. Townsend, L.D. Vogler, T.J. McClain, E.T. Marks, and G.R. Coble. 1988. Experimental studies in stream-aquifer interaction along the Arkansas River in central Kansas—Field testing and analysis. *Journal of Hydrology* 98: 249-273.
- Sophocleous, M. 2002. Interactions between groundwater and surface water: the state of the science. *Hydrogeology Journal* 10: 52-67.
- Stromberg, J.C., S.J. Lite, R. Marler, C. Paradzick, P.B. Shafroth, D. Shorrock, J.M. White, and M.S. White. 2007. Altered stream-flow regimes and invasive plant species: the Tamarix case. *Global Ecology and Biogeography* 16(3): 381-393.
- Su, Z. 2002. The Surface Energy Balance System (SEBS) for estimation of turbulent fluxes. *Hydrol. Earth Syst. Sci.* 6:85–99.
- Woodward, D.E. 2007. Part 630 National Engineering Handbook. Chapter 19: Transmission Losses, 210–VI–NEH. Ed. H.F. Moody. USDA NRCS.
- van Genuchten, M.Th. 1980. A closed-form equation for predicting the hydraulic conductivity of unsaturated soils. *Soil Sci. Soc. Am. J.* 44: 892-898.
- Vandervaere, J-P., M. Vauclin, and D.E. Elrick. 2000. Transient Flow from Tension Infiltrimeters: II. Four Methods to Determine Sorptivity and Conductivity. *Soil Science Society of America.* 64:1272-1284.
- Vukovic, M., and A. Soro. 1992. Determination of Hydraulic Conductivity of Porous Media from Grain-Size Composition. Littleton, Colorado: Water Resources Publications.
- Walter, I.A., R.G. Allen, R. Elliott, M.E. Jensen, D. Itenfisu, B. Mecham, T.A. Howell, R. Snyder, P. Brown, S. Echings, T. Spofford, M. Hattendorf, R.H. Cuenca, J.L. Wright, and D. Martin. 2000. ASCE's Standardized Reference Evapotranspiration Equation. Watershed Management.
- Walter, G.R., M. Necsoiu, and R. McGinnis. 2012. Estimating Aquifer Channel Recharge Using Optical Data Interpretation. *Ground Water* 50: 68-76.
- Wetter, L.H. 1990. "Chapter 3: Water Conservation for More Crop Production in the Great Plains" in *Ground Water Quality and Agricultural Practices*. Ed. D.M. Fairchild. Chelsea, MI: Lewis Publishers. 13-33.
- Whittemore, D.O. 2000. Ground-water Quality of the Arkansas River Corridor in Southwest Kansas. Kansas Geological Survey, Open-file Report 2000-73.
- Whittemore, D.O, E.R. Grieve, D.P. Young, and B.B. Wilson. 2005. Water Quality in the High Plains Aquifer and the Cimarron River in Seward and Meade Counties, Kansas. Kansas Geological Survey, Open-file Report 2005-27.
- Winter, T.C., J.W. Harvey, O.L. Franke, and W.M. Alley. 1998. Ground Water and Surface Water A Single Resource. U.S. Geological Survey Circular 1139.

- Yang, X. and D.R. Steward. 2012. Explore the Interactions between Human-induced Groundwater Salt Intrusion and Salt Cedar Invasion in the Upper Arkansas River Corridor in Kansas, U.S. *Procedia Environmental Sciences* 12: 744 – 750.
- Yang, X. 2012. Application of the Conceptualized Groundwater Data Model to study the Upper Arkansas River Corridor, Western Kansas. *Journal of Earth Science* 23(1): 77-78.
- Zekster, S., Loaiciga, H.A., Wolf, J.T., 2005. Environmental impacts of groundwater overdraft: selected case studies in the southwestern United States. *Environ. Geol.* 47, 396–404.
- Zellweger, G.W. 1994. Tests and comparison of four ionic tracers to measure stream flow loss by multiple tracer injection. *Hydrological Processes* 8: 155-165.
- Zhang, R. 1997. Determination of Soil Sorptivity and Hydraulic Conductivity from the Disk Infiltrimeter. *Soil Science Society of America.* 61:1024-1030.
- Zlotnik, V.A, and H. Huang. 1999 Effect of Shallow Penetration and Streambed Sediments on Aquifer Response to Stream Stage Fluctuations (Analytical Model). *Ground Water* 37: 599-605.

Appendix A - Instructions for Processing Satellite Imagery

Instruction on How to Select and Download Landsat Scenes

Remote sensing data including imagery from LANDSAT can be found on the USGS website: <http://earthexplorer.usgs.gov/>. A login ID and password are required to download material. .

Step 1. Register and Log In to <http://earthexplorer.usgs.gov/>

The webpage is divided into three sections: (1) top menu bar, (2) left search menu, and (3) the map view. Use the search menu and the map to identify and select the data you want to download. The minimum criteria are the location and data set.

There are various ways to define the location, but I find that it is easiest to define the location graphically by defining coordinate boundaries in the map view.

Step 2. Identify the location by defining points in the map view.

To do this, zoom in on the area of interest and left-click on the map to define a polygon.

As an example, I have I selected an area in southwestern Kansas.

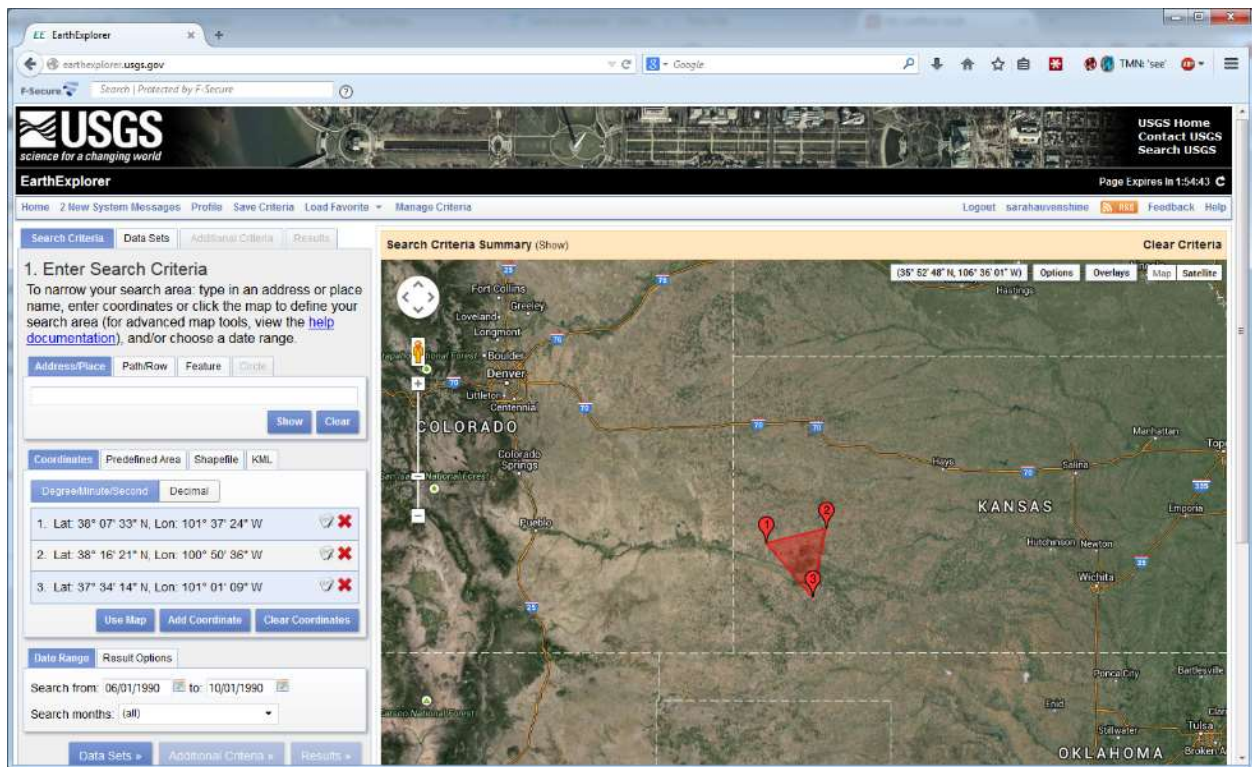


Figure A-1. USGS EarthExplorer

Step 3. In the search criteria menu, define the desired date range.

To limit the number of results, the time frame should be identified. Unless a specific date is needed, have the date range be at least a month long to account for the 16 between scenes of the same area. For this example, let's select dates for the summer of 1990.

Next define the data source. EarthExplorer has many options for satellite, aerial, elevations, digital maps and digital line graphs. We want to use the Landsat Archive, and the L4-5 TM.

Step 4. Under the Data Sets tab in the search criteria menu, select L4-5 TM under Landsat Archive.

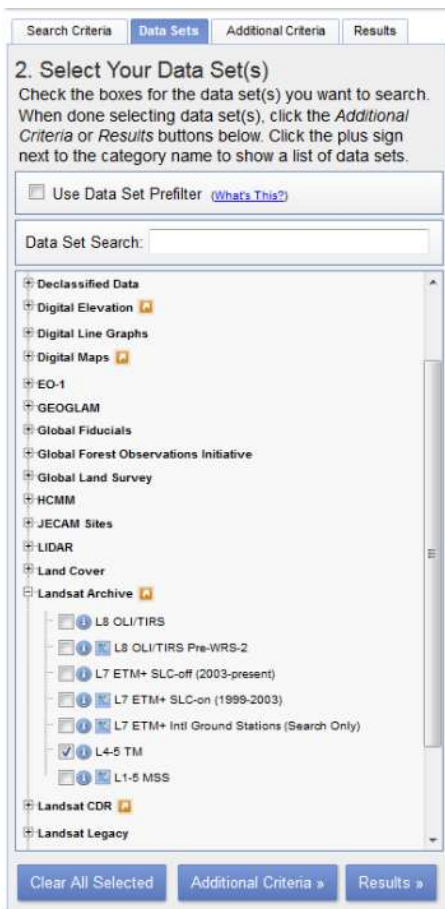


Figure A-2. Data Set Options from USGS EarthExplorer

You can further refine your search in the Additional Criteria tab. For example, we want to avoid images with excessive cloud cover.

Step 5. Under the Additional Criteria tab, select “Less than 30%” under the Cloud Cover option.

Step 6. Click on the results tab to see the results.

The results show the scenes matching the search criteria defined.

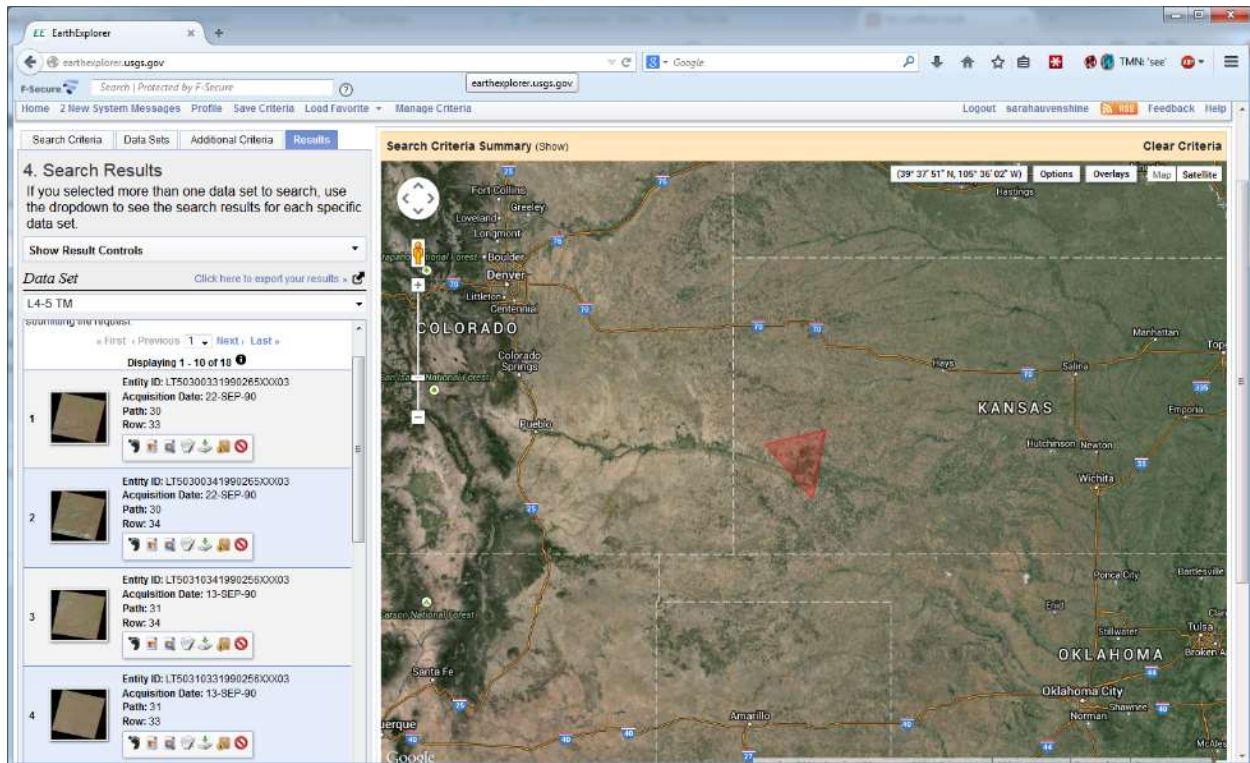


Figure A-3. Search Results from USGS EarthExplorer

The entity ID shows some key information about the scenes in the results. The first scene is LT50300331990265XXX03. The first three characters (LT5) define the satellite source – Landsat thematic mapper 5. The next six are the path (030) and row (033) – this defines the geographic area of the scene. Next is year (1990) and day of year (265). Day 265 is September 22 for 1990.

There are several options available for each scene to help evaluate its usefulness. You can display the footprint with the first icon shown as a footprint. The footprint shown below covers only a fraction of our area of interest.

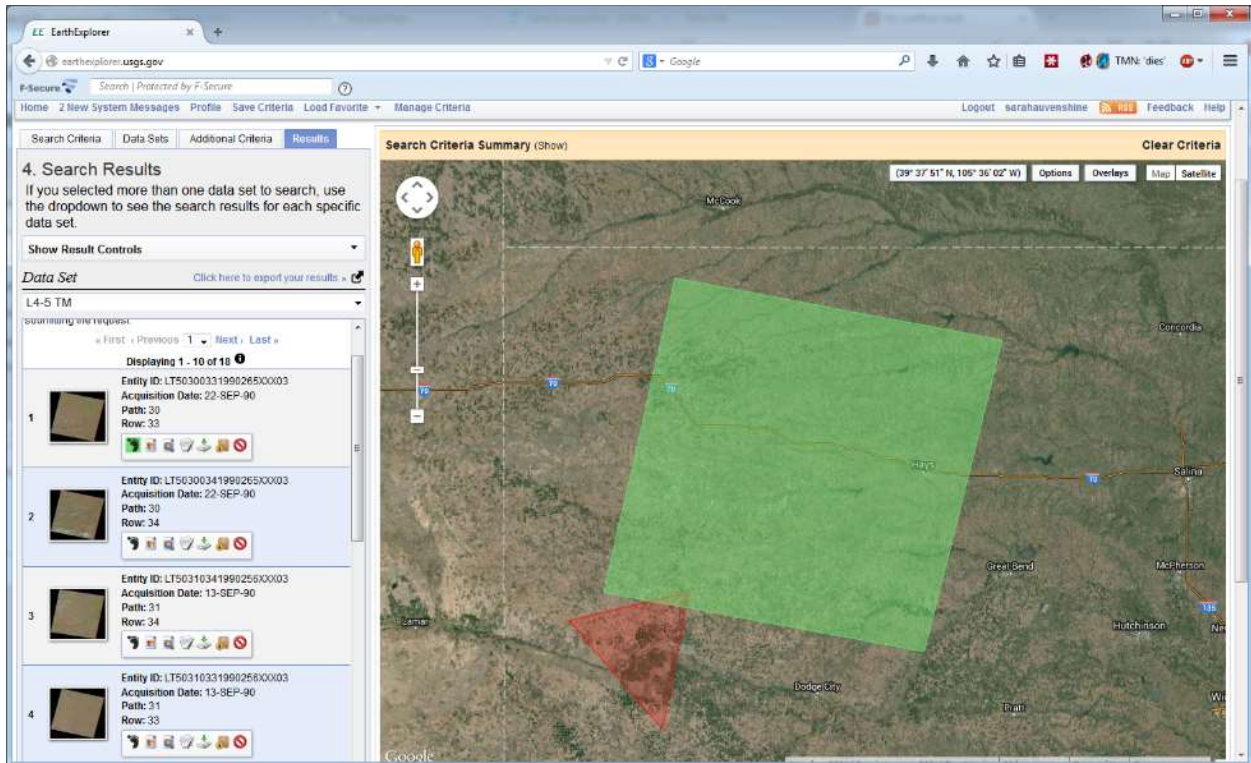


Figure A-4. Footprint of Result from USGS EarthExplorer

The second icon shows the true color preview. Displaying this shows some scattered clouds in the southern portion of the scene and some lighter clouds in the center.

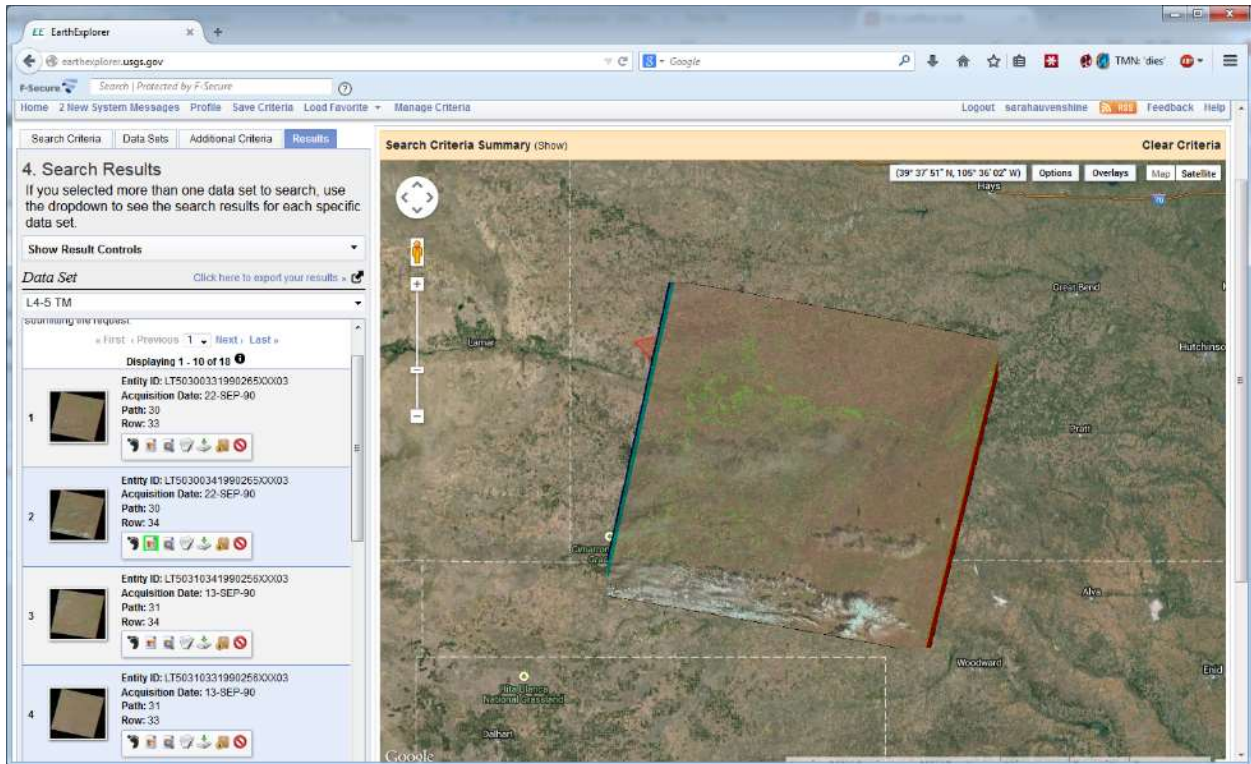


Figure A-5. Image of Results from USGS EarthExplorer

After reviewing the footprints and the previews, decide on which scene to download. There are two options for downloading – individual and bulk. The individual download allows for one scene at a time to be downloaded immediately. The bulk download requires a separate USGS program to be installed. Multiple scenes can be selected for download at once, but an order to create the bulk download needs to be submitted. The order is typically processed within two days.

See “USGS Bulk Download tutorial.pdf” for instructions on how to use the Bulk Download Application.

The scene on 13-sept-90 for path 31/row 34 covers most of the area of interest and appears free of clouds.

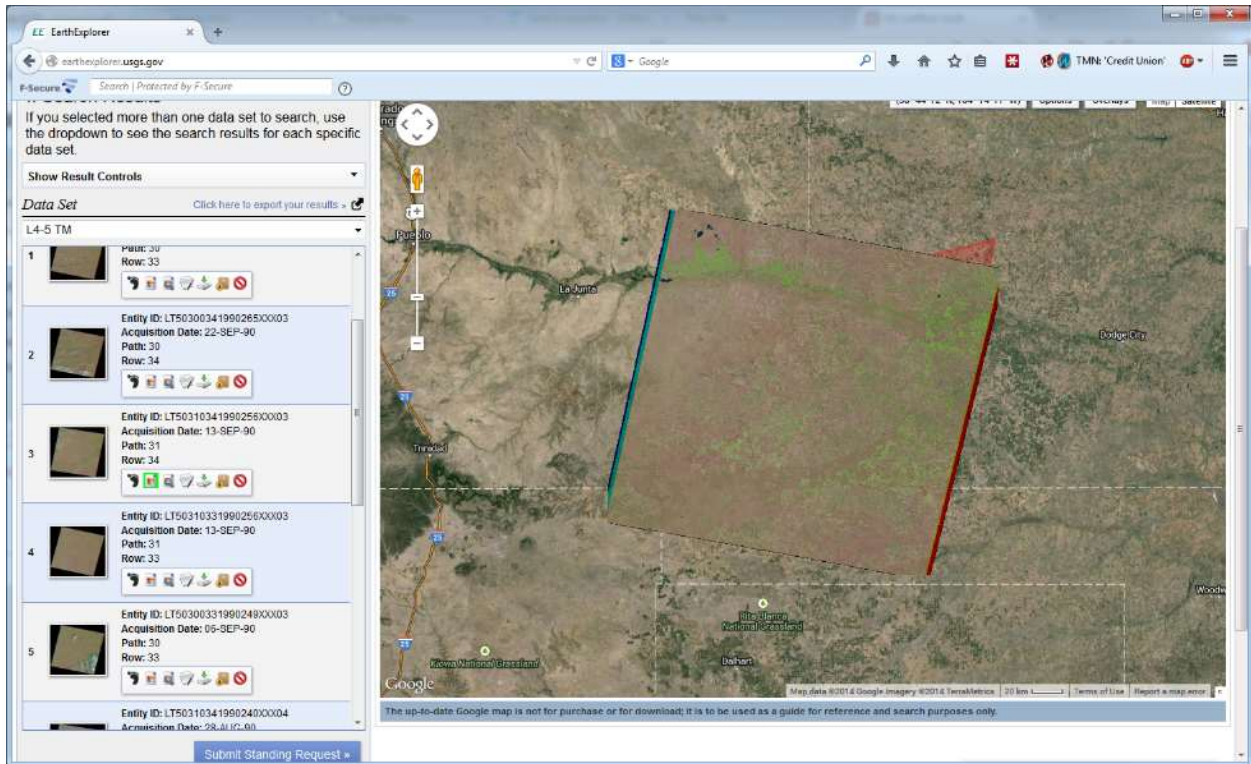


Figure A-6. Additional Result from USGS EarthExplorer

Step 7. Download individual scenes

To download this individual scene, click the download icon which is the fifth option for the scene. (The sixth option is for the bulk download.)

Step 8. Select the Level 1 Product

When presented with the following options:



Figure A-7. Options for Download

If the Level 1 Product is not available, it can be requested. The request may take a few days to process.

Step 9. Save the zip file (.tar.gz) to an appropriate location.

Step 10. Unzip the file

The file is double-zipped. The first time, the extracted file is a .tar. The second time, the 8 image files are extracted.

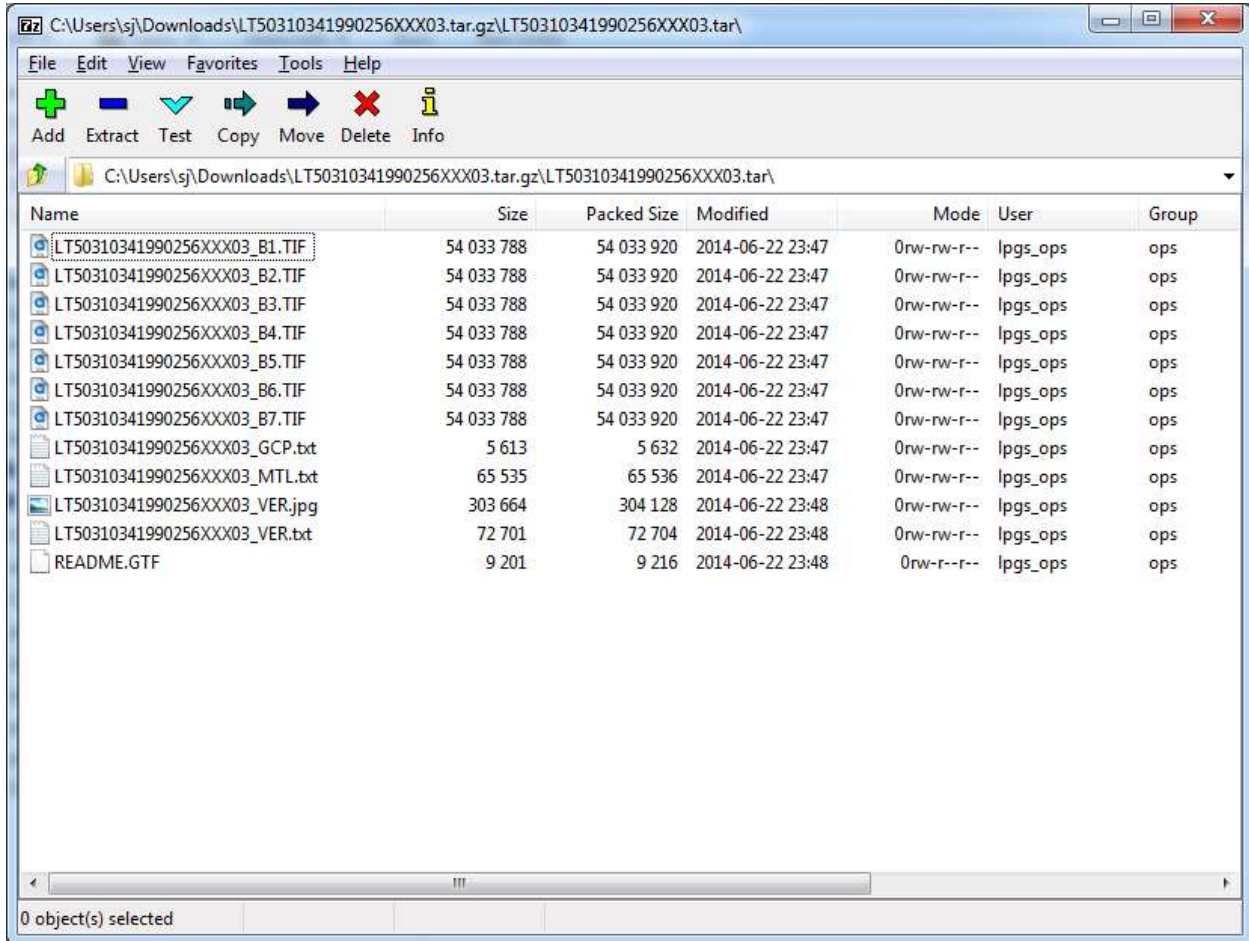


Figure A-8. Files in typical LANDSAT 5 TM package

The file size of the download is 146.2 MB. The extracted files are around 800 MB.

Downloading and extracted multiple scenes can quickly use up space. Ensure that adequate storage resources are available or extract the files when preparing to process the files to manage storage space.

Now the scene can be viewed using ArcGIS, BEAM VISAT, or other image viewing software, and the scene can be processed using one of the Evapotranspiration programs created by USDA-ARS Bushland.

Evapotranspiration from Weather Data

The Simple Surface Energy Balance Application requires several inputs – the thermal coverage of the study area, the selection of hot and cold pixels and a reference Evapotranspiration (ET) from within the study area. The reference ET may be provided with the other weather data at a weather station. Kansas State Research and Extension maintains the database in the Weather Data Library for several weather stations in Kansas at <http://mesonet.k-state.edu/>. Daily and hourly weather data is available at over 50 stations across Kansas. The available data is maximum air temperature, minimum air temperature, total precipitation, average relative humidity, average wind velocity, solar radiation, and ET for grass and alfalfa. The format and availability of the weather data has changed since the start of this study. Daily weather data was available since 1985, and hourly data was available beginning in 2006. Additional data requests can also be submitted through kansas-wdl@k-state.edu.

The reference ET can be calculated using the Bushland Reference ET calculator as shown in Figure A-9. This calculator has been developed by USDA-ARS Conservation and Production Research Laboratory in Bushland, Texas. The calculator uses the ASCE Reference ET formula to translate weather data into daily or hourly ET.

To start, open the application. To calculate the daily ET, select the “Single Calculation > Daily” from the top menu bar. The latitude is 37.933 degrees north and the elevation is 882.0912 meters for the Garden City weather station used for this study. The year and day of year correspond to the Landsat scene that will be processed in the SSEB application. The year and day of year are found on the file name of the Landsat scene. The next six items are found in the weather data. The barometric pressure is estimated based on the elevation, which the application computes. After all data has been entered or estimated, click the “Calculate” button on the bottom.

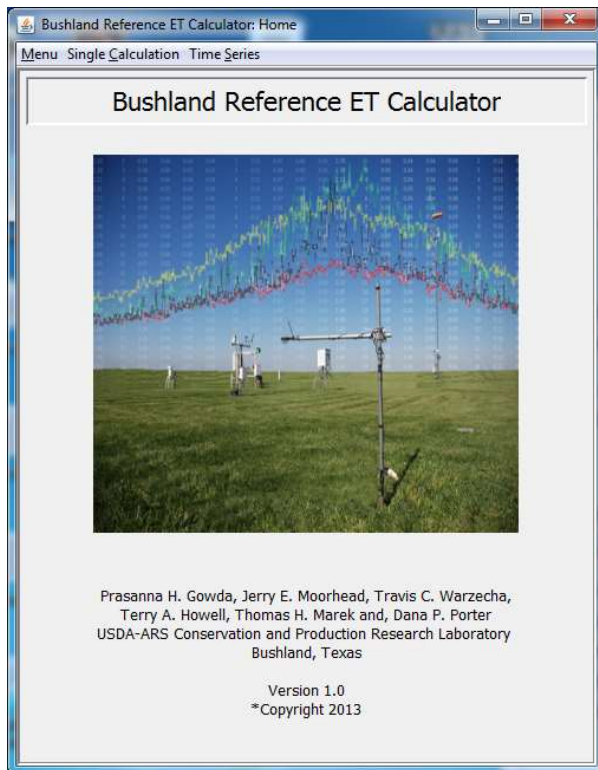


Figure A-9. Bushland Reference ET Calculator

Latitude:	<input type="text" value="37.933"/>				
Elevation (m):	<input type="text" value="882.0912"/>				
Year:	<input type="text" value="1988"/> <input type="button" value="Calendar"/>				
Day Of the Year:	<input type="text" value="340"/>				
Max Air Temperature (Deg. C):	<input type="text" value="17.8"/>				
Min Air Temperature (Deg. C):	<input type="text" value="-5.9"/>				
Average Dew Temperature (Deg. C):	<input type="text" value="-6.95"/> <input type="button" value="Estimate"/>				
Average Relative Humidity (%):	<input type="text" value="39.4"/> <input type="button" value="Estimate"/>				
Average Solar Radiation (MJ/sq.m./d):	<input type="text" value="12.2"/> <input type="button" value="Estimate"/>				
Average Wind Speed (m/s):	<input type="text" value="1.03"/>				
Barometric Pressure (kPa):	<input type="text" value="91.29858260732902"/> <input type="button" value="Estimate"/>				
<table border="1"> <tr> <td>Grass Reference ET (mm):</td> <td><input type="text" value="1.1685"/></td> </tr> <tr> <td>Alfalfa Reference ET (mm):</td> <td><input type="text" value="1.9444"/></td> </tr> </table>		Grass Reference ET (mm):	<input type="text" value="1.1685"/>	Alfalfa Reference ET (mm):	<input type="text" value="1.9444"/>
Grass Reference ET (mm):	<input type="text" value="1.1685"/>				
Alfalfa Reference ET (mm):	<input type="text" value="1.9444"/>				
<input type="button" value="Calculate"/> <input type="button" value="Exit"/>					

Figure A-10. Inputs for Computation of Daily Referenc ET

Record the Grass and Alfalfa Reference ET in a separate file. The weather station data was downloaded from the Kansas Weather Data Library, and the calculated reference ET is recorded as shown in Figure A-11 under columns J and K for the subject day.

	A	B	C	D	E	F	G	H	I	J	K	
4	YEAR	DOY	MAXAIRT	MINAIRT	DEWPT	RH	SOLRAD	WINDSP	BP	G ET	A ET	hot
1436	1988	337.00	19.7	-3.7	-5.54	38.1	12.4	1.96	91.29858			
1437	1988	338.00	14.3	-4.5	-7.57	40.4	12.4	4.49	91.29858			
1438	1988	339.00	10.5	-7.4	-5.85	58.3	12.1	1.66	91.29858			
1439	1988	340.00	17.8	-5.9	-6.95	39.4	12.2	1.03	91.29858	1.1685	1.9444	
1440	1988	341.00	14.7	-5.9	-8.31	39.5	12	3.33	91.29858			
1441	1988	342.00	3.5	-5.3	-4.86	74.8	4.9	5.28	91.29858			
1442	1988	343.00	1.5	-10	-14.28	45.9	7.4	2.25	91.29858			
1443	1988	344.00	12.9	-10.8	-8.40	49.7	11.7	1.5	91.29858			
1444	1988	345.00	6.7	-5.7	-4.69	68.5	9.8	2.82	91.29858			
1445	1988	346.00	8.3	-6.9	-5.29	64.6	6.5	4.01	91.29858			
1446	1988	347.00	16.6	-8.3	-5.11	51.3	8.2	1.45	91.29858			
1447	1988	348.00	22.7	-4.9	-6.43	33.5	11.1	2.81	91.29858			
1448	1988	349.00	12.7	-0.1	-6.63	39.4	11.4	5.15	91.29858			
1449	1988	350.00	-0.1	-10.6	-9.79	71.3	3.7	3.04	91.29858			
1450	1988	351.00	9.4	-3.7	-6.02	52.5	11.3	2.88	91.29858			
1451	1988	352.00	13.5	-6.8	-9.03	40.2	10.3	1.33	91.29858			
1452	1988	353.00	18	-4.1	-6.91	36.9	10.4	1.44	91.29858			
1453	1988	354.00	16.6	-0.4	-0.51	54.9	3	5.48	91.29858			
1454	1988	355.00	12.7	-3.9	-4.00	54.8	8.5	1.4	91.29858			
1455	1988	356.00	13.5	-5.7	-5.37	51.2	9.8	6.42	91.29858			
1456	1988	357.00	10.9	-5.9	-15.02	26.4	10.5	4.58	91.29858			
1457	1988	358.00	13.7	-6.9	-13.44	28.2	9.5	2.67	91.29858			
1458	1988	359.00	5.9	-9.3	-11.36	48.1	8.7	1.5	91.29858			

Figure A-11. Excerpt of Data Sheet with Weather Data

BEAM VISAT

BEAM VISAT is an open source program developed by the European Space Agency to analyze and process Earth observation data. In this study, BEAM VISAT is used to select the “hot” and “cold” anchor pixels used in the Simple Surface Energy Balance application.

To start, run the BEAM installation program. Have a Landsat scene unzipped and stored in a working directory. Open BEAM VISAT. From the top menu bar, select File>Open Product. Find and select the location of the unzipped Landsat scene. Load the image file ending in _B6 – this is the thermal image. From the Products View menu on the left, expand the “Bands” folder and double-click on “band_1”. This displays the band 6 image in the viewing window. At the bottom of the Products View window, there is the active tab for “Products” and Pixel Info. Click the Pixel Info tab. The Pixel Info View has five options to view pixel information and they can be turned on or off with the buttons on the bottom of the window. The information we want to collect is in “Bands”.

Explore the scene by moving the mouse around the band 6 image and see how the values of band_1 change. The darker pixels are lower values and the lighter pixels are higher values. The interpretation is that the darker pixels have a lower temperature and thermal emittance than the lighter pixels. The pixels outside the extent of the valid data are zero-value, and the pixels outside the extents of the scene are “Invalid pos.”

The information used in the SSEB application are the “hot” and “cold” pixels. The values for the “hot” pixel is assumed to have zero evapotranspiration. The “hot” pixel has a large value because the area in the scene is adsorbing the solar radiation and converting the solar energy into thermal energy. The “cold” pixel is cooler because evapotranspiration converts the solar energy into latent energy. The “cold” pixel should be active vegetation and not open water which will have equivalent values. The Simple Surface Energy Balance (SSEB) method uses the assumption that the “cold” pixel has ET equal to the reference ET for grass. The SSEB program translates the 8-bit Landsat data into evapotranspiration estimates across the Landsat scene. Using as the subject scene LT50300341987209XXX05_B6, the cold pixel has a brightness value (BV) of 140, and the hot pixel has a BV of 174. Since the weather station is near Garden City,

recommend looking for the hot and cold pixels in the vicinity of Garden City. In addition to viewing the pixel information in the “pixel info view”, create a histogram for band_1 by selecting from the top menu Analysis > Histogram. This opens a window to compute and view the histogram for this band. Click the “Refresh View” button in the top left of the Histogram window to compute statistics.

Notice that the histogram has many values at 0. These are the null, zero-value pixels within the extents of the scene but outside of the collected data. Zoom into the bell curved portion of the histogram. From this we can validate that the hot and cold pixels are at the upper and lower extents of the values without being outliers.

Record the Hot and Cold pixel values for this scene in a data sheet. The weather data sheet developed in the previous set of instructions is the recommended file.

Multiple views can be opened and combined to create color images. For example, a true color image can be created by combining the blue, green, and red bands, or a false color infrared image can be created by combining the green, red, and infrared bands. These operations can also be done using ArcGIS, and instructions for that are in the section for “Creating Composite Bands in ArcGIS”

Open bands 1, 2, 3, and 4 from the unzipped Landsat images. Combine the images

Right click on the product and select “open RGB image”

In the window the red, green and blue colors can be assigned to the bands.

For true color, set red to red (band 3), green to green (band 2), and blue to blue (band 1).

For false color, set red to infrared (band 4), green to red (band 3), and blue to green (band 2).

Simple Surface Energy Balance (SSEB) application

The Simple Surface Energy Balance (SSEB) application was developed by USDA ARS Bushland to develop Evapotranspiration (ET) coverages from remotely sensed thermal images. Copy the Programs Folder Open SSEBtest program from the “Programs” folder. If the Java runtime environments message appears, run the “JRE 6 32 bit” application from the “32-bit Installers” folder. The SSEB application has 5 steps.

The screenshot shows the SSEB application window with five distinct steps for data processing:

- Step 1: Select Working Directory**: A text box for 'Working Directory:' with a 'Browse' button and a 'Save' button.
- Step 2: Calculate NDVI**: Three text boxes for 'Red Band Image:', 'Near Infrared Band:', and 'NDVI Output:', each with a 'Browse' button. A 'Calculate NDVI' button is centered below.
- Step 3: Create Hot and Cold Pixel Table**: Text boxes for 'NDVI Image:', 'Thermal Band Image:', 'Number of Pairs:', 'Maximum Threshold', and 'Minimum Threshold'. 'NDVI Image:' and 'Thermal Band Image:' have 'Browse' buttons. 'Create Table' and 'Create Histogram' buttons are below.
- Step 4: Calculate Evaporative Fraction**: Text boxes for 'Hot Pixel Value:', 'Cold Pixel Value:', 'Thermal Image:', and 'EF Output:'. 'Thermal Image:' and 'EF Output:' have 'Browse' buttons. A 'Calculate EF' button is centered below.
- Step 5: Calculate ET**: Text boxes for 'EF Image:', 'Ref. ET (mm/hr or mm/d):', 'Coefficient:', and 'ET Map Output:'. 'EF Image:', 'Ref. ET (mm/hr or mm/d):', and 'ET Map Output:' have 'Browse' buttons. A 'Calculate ET' button is centered below.

Figure A-12. Simple Surface Energy Balance (SSEB) Application

Step 1. Select Working Directory

This is the location where the subsequent steps will look for the bands to load and save the created files. Recommend selecting an internal hard drive space rather than an external storage. Click “Save”. This sets the folder location as default for the next steps.

Step 2. Calculate NDVI

NDVI is the Normalized Difference Vegetation Index. It is computed by taking the difference in the near-infrared band (band 4) and the red band (band 3) and dividing by the sum of the near-infrared band and the red band.

$$NDVI = \frac{NIR - Red}{NIR + Red}$$

The purpose of the NDVI is to identify active photosynthesis. Live green plants adsorb red light and reflect near infrared. A large difference between NIR and Red would result in a high NDVI value, indicating healthy plants or active photosynthesis. Conversely, bare earth would have a low NDVI because the difference between NIR and Red is not as great as active healthy vegetation.

Step 3. Create Hot and Cold Pixel Table

This step in the application can be skipped in place of viewing the thermal (band 6) and near infrared (band 4) together in ArcGIS or VISAT or viewing the thermal and NDVI together. When selecting the cold pixel in the following step, it is desired that the pixels have a large NDVI value (or large value in near infrared) indicating very active photosynthesis. This prevents selecting a cold pixel that is open water with a negative NDVI. Using VISAT in the study area of western Kansas, I recommend selecting an active, irrigated crop circle south of Garden City for the Cold pixel. For the Hot I typically select a dry area near the river corridor or in fallow, non-irrigated land, whichever has the higher thermal emittance value. The brightness values for the Hot and Cold pixels are used in the next step.

Step 4. Calculate Evaporative Fraction

Input the Hot and Cold pixel values determined in the prior step, and select the corresponding Thermal image to process. The “EF Output” is a temporary file that converts the thermal image to an evaporative fraction based on the brightness values inputs for the Hot and Cold pixels. I recommend the file to be named “EF” or similar, and it is used in the next step.

Step 5. Calculate ET

The “EF” image is the file created in the previous step. The “Ref. ET” is the value computed using the “ETCalculator” (see “Instructions for gathering weather data for ET maps”)

Use the value for Grass in mm/d. The “Coefficient” is set to 1. The “ET Map Output” should be named “SSEB_[YEAR][DOY]” or “SSEB_1985043” for the scene taken on the 43rd day of 1985.

Creating Composite Bands in ArcGIS

Landsat 5 Thematic Mapper has seven spectral bands of data. When the data is downloaded from the USGS data source, the files need to be unzipped and stored in a working directory. The bands can be combined in a composite image by combining the seven bands. With a composite image, three of the bands can be displayed as red, green, and blue to aid in the interpretation of the land surface.

To start, open ArcMap 10 or equivalent to a new empty map. Add the subject Landsat coverage to the map as shown in Figure A-13. In the toolbox, select the tool “Composite Bands”

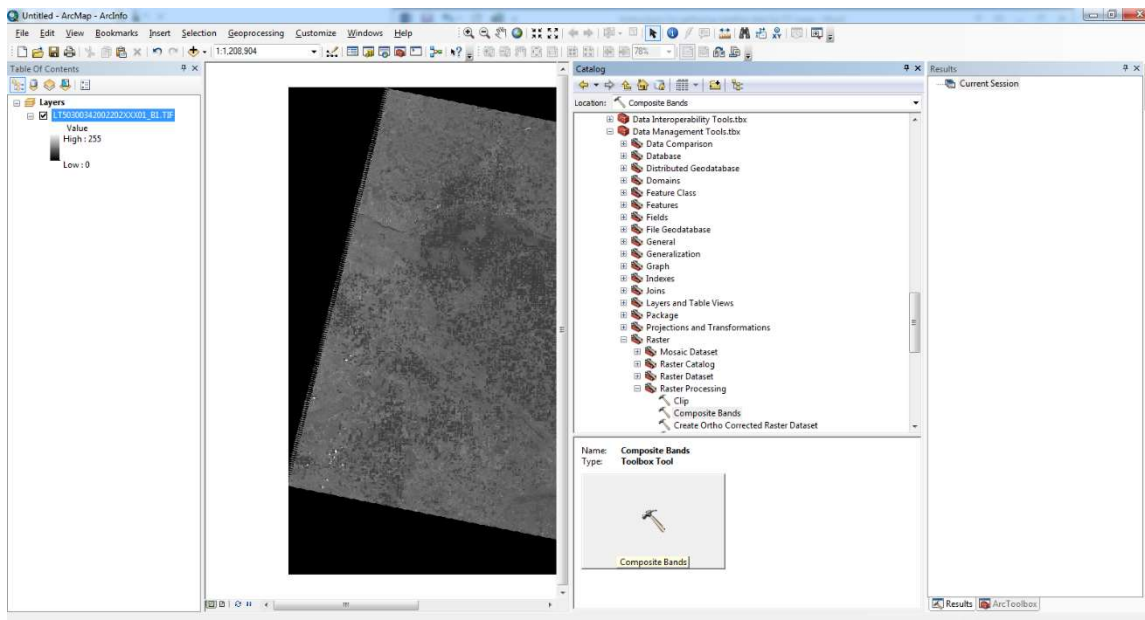


Figure A-13. ArcMap 10 with Landsat Scene

In the Composite Band dialog box, select the bands in the subject Landsat scene, and select an output raster as shown in Figure A-14.

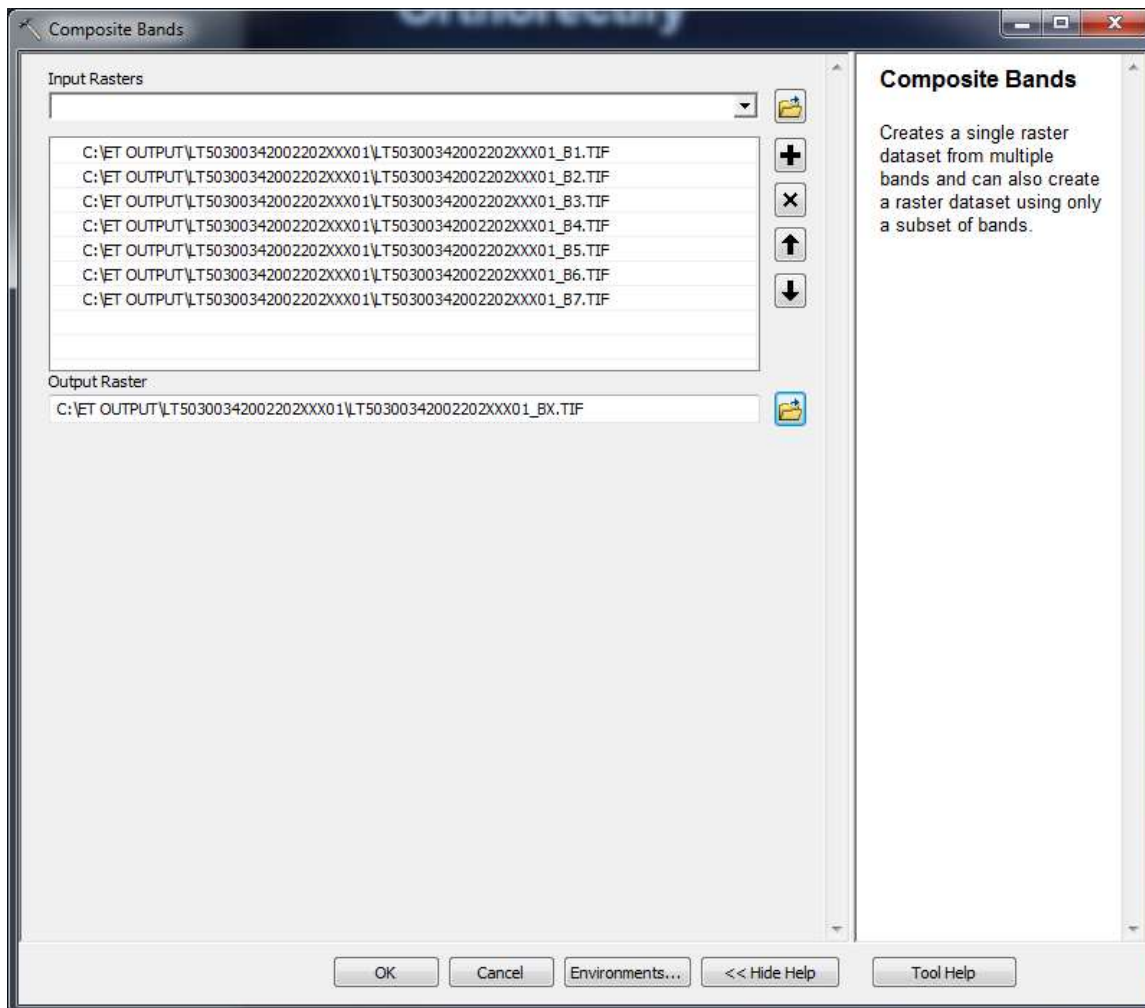


Figure A-14. Selection of Images to Include in Composite Bands

By default, the display is set to band 1 is red, band 2 is green, and band 3 is blue as shown in Figure A-15, but band 3 is the red band and band 1 is the blue band. To get a Natural Color image, the assignment of colors is adjusted using the layer properties as shown in Figure A-16 with the resulting Natural Color displayed in Figure A-17. Several other color combinations are available to help in the land surface interpretation. The Color Infrared display is useful in identifying active vegetation by displaying the near infrared band 4 with the red band 3. The Color Infrared sets red to band 4, green to band 3, and blue to band 2 as shown in Figure A-18 for the resulting image in Figure A-19.

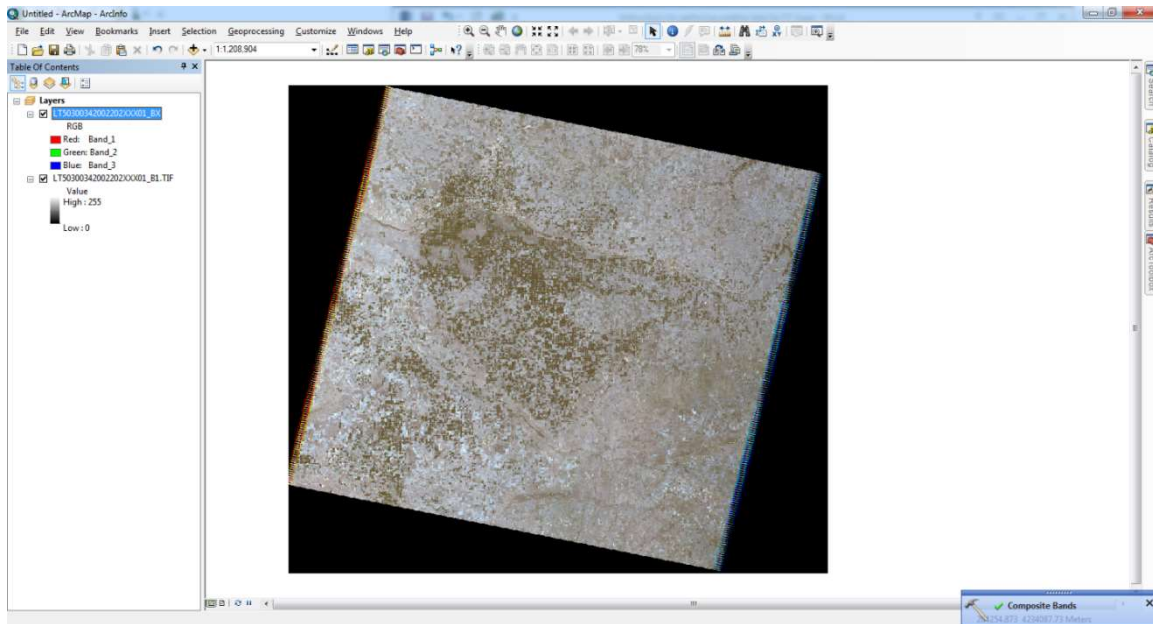


Figure A-15. Resultant Composite Band with Default Settings

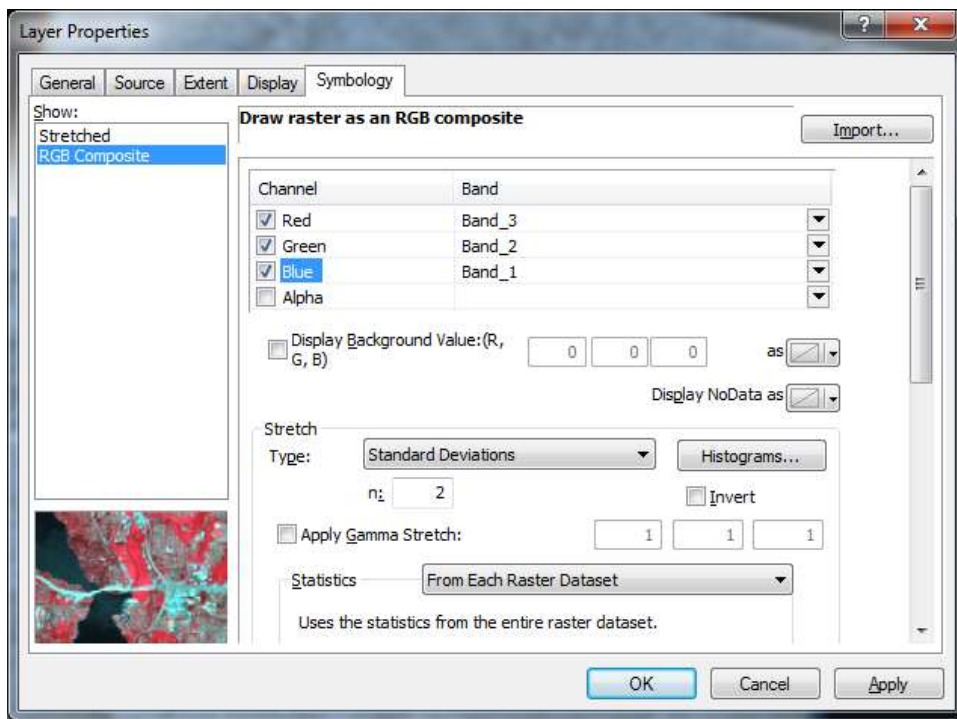


Figure A-16. Assignment of Colors for the Bands for Natural Color in Layer Properties

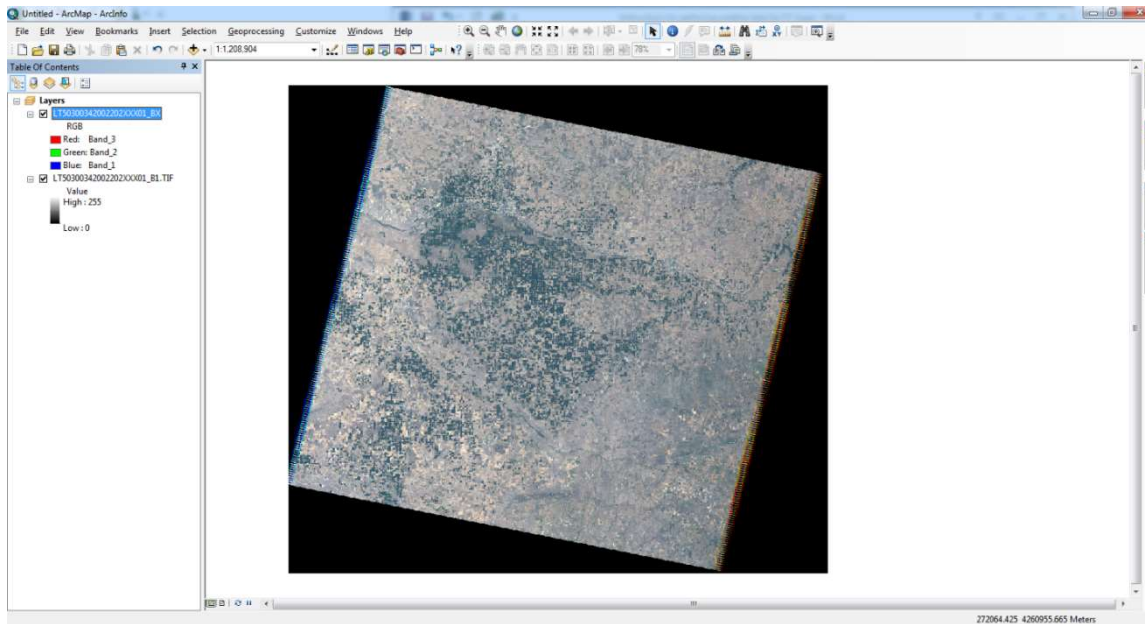


Figure A-17. Composite Band with Natural Color Displayed

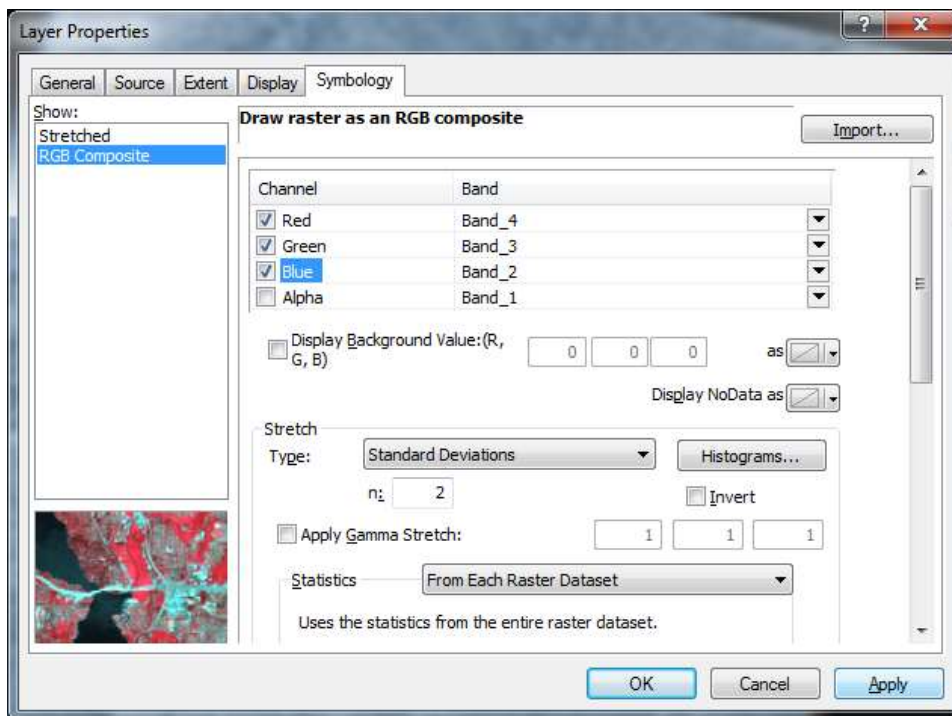


Figure A-18. Assignment of Colors for the Bands for Color Infrared in Layer Properties

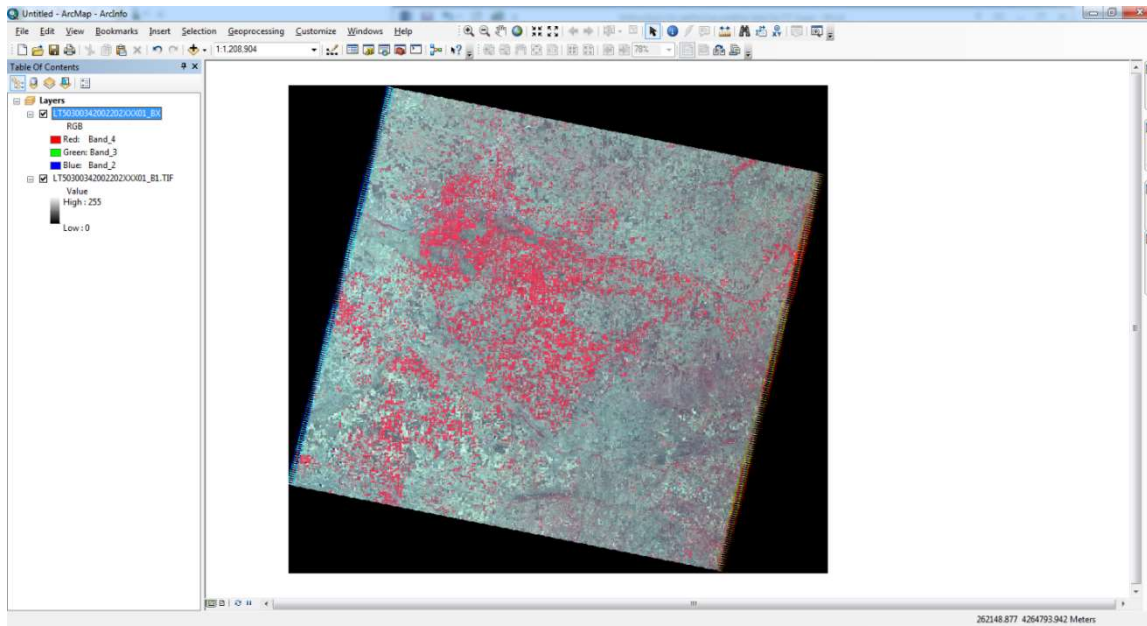


Figure A-19. Composite Band with Color Infrared Displayed

Appendix B - Site Information and Instrumentation Results

Table B-1. Soil parameters by texture from Carsel and Parish (1988)

Soil Texture	α (cm ⁻¹)	n
sand	0.145	2.68
loamysand	0.124	2.28
loam	0.036	1.56
sandy loam	0.075	1.89
silt loam	0.02	1.41
sandy cl.loam	0.059	1.48
silty cl loam	0.01	1.23
clay loam	0.019	1.31
silt	0.016	1.37
clay	0.008	1.09
sandy clay	0.027	1.23
silty clay	0.005	1.09

Site 1: Arkansas River at Syracuse, Kansas

Vicinity Map of Arkansas River near Syracuse, KS



Figure B-1. Site 1: Arkansas River at Syracuse, Kansas

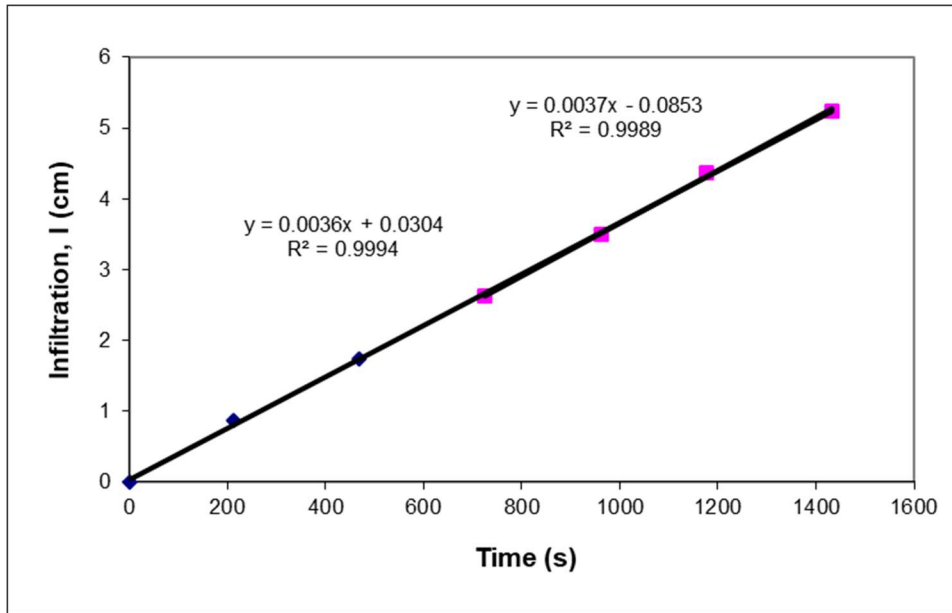


Figure B-2. Single-Ring Infiltrometer results for Site 1

Table B-2. Calculation of Hydraulic Conductivity for Site 1

Description	Symbol	Value
Diameter of Outer Ring	d_o	Water in channel
Diameter of Inner Ring	d_i	27 cm
Ring Radius	a	13.5 cm
Ponded Height	H	15 cm
Depth of Insertion	d	9.5 cm
Soil Macroscopic Length	α^*	0.36 cm^{-1}
dimensionless quasi-empirical constants	C_1	0.992743
	C_2	0.578053
Infiltration rate	q	0.0037 cm/s
Hydraulic Conductivity	K	0.001824 cm/s

Table B-3. Constant Head Permeability Test for Site 1

Sample Name	Syracuse First Sample			Syracuse Second Sample		
Weight	736g			780g		
Test No.	1	2	3	1	2	3
Average Flow, Q(cm ³)	100	200	300	100	200	300
Time of Collection, t(s)	10.37	21.7	32.63	10.46	19.6	30.85
Head Difference, h(cm)	66.7	66.7	66.7	66.7	66.7	66.7
Diameter of Specimen, D(cm)	6.35	6.35	6.35	6.35	6.35	6.35
Length of Specimen, L(cm)	14	14	14	14	14	14
Area of Specimen, A=($\pi/4$)D ² (cm ²)	31.65	31.65	31.65	31.65	31.65	31.65
k=QL/Aht (cm/s)	0.064	0.061	0.061	0.063	0.068	0.064
Average k (cm/s)	0.062			0.065		

Table B-4. Well log near Site 1

County: Hamilton	
Location: T24S, R41W, Sec. 11, SE NW	
Directions: From Syracuse, 1 mile West and 0.75 mile South	
Longitude: -101.7917352	
Latitude: 37.9811038	
Datum NAD 83	
Lithologic Log	
(Log data entered by KGS.)	
From: 0 ft. to 9 ft.	top soil & clay
From: 9 ft. to 54 ft.	sand & gravel
From: 54 ft. to 56 ft.	shale

Source: http://chasm.kgs.ku.edu/ords/wwc5.wwc5d2.well_details?well_id=25503

Site 2: Arkansas River near the South Ditch Head Gate

Vicinity Map of Arkansas River at the Head Gate to the South Ditch

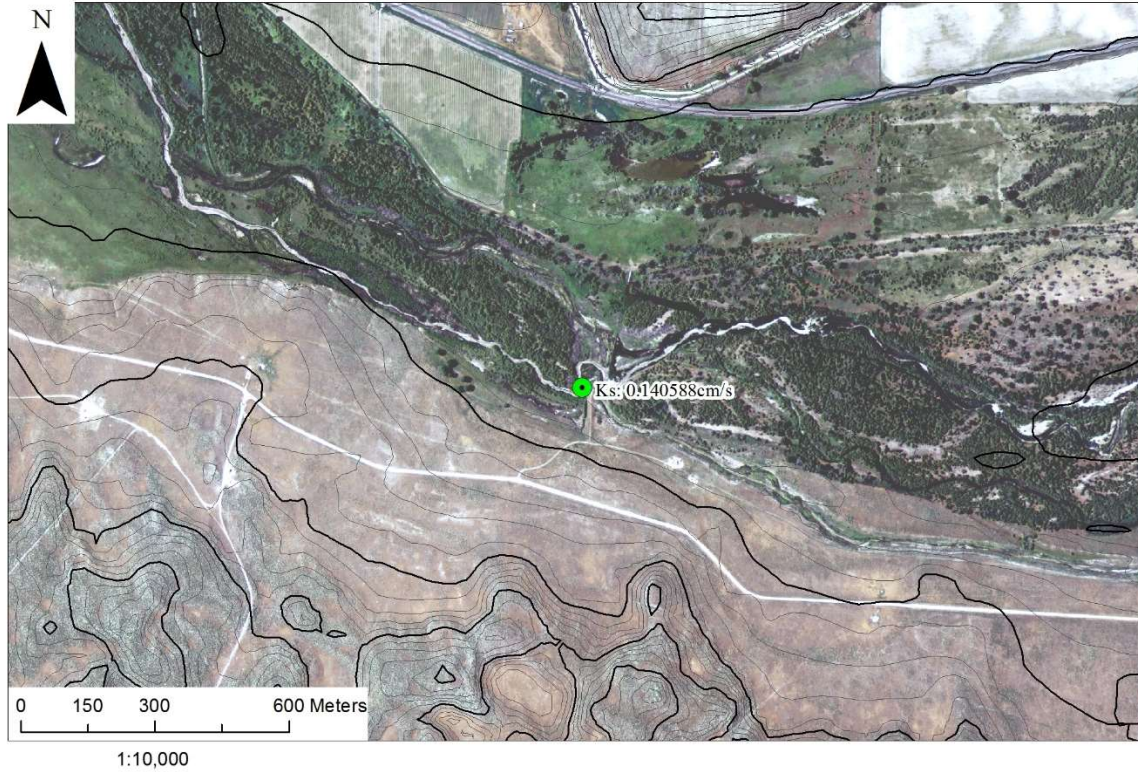


Figure B-3: Site 2: Arkansas River near the South Ditch Head Gate

Infiltration in the Arkansas River near the Head Gate of the South Ditch

using automated mini-disk tension infiltrometers

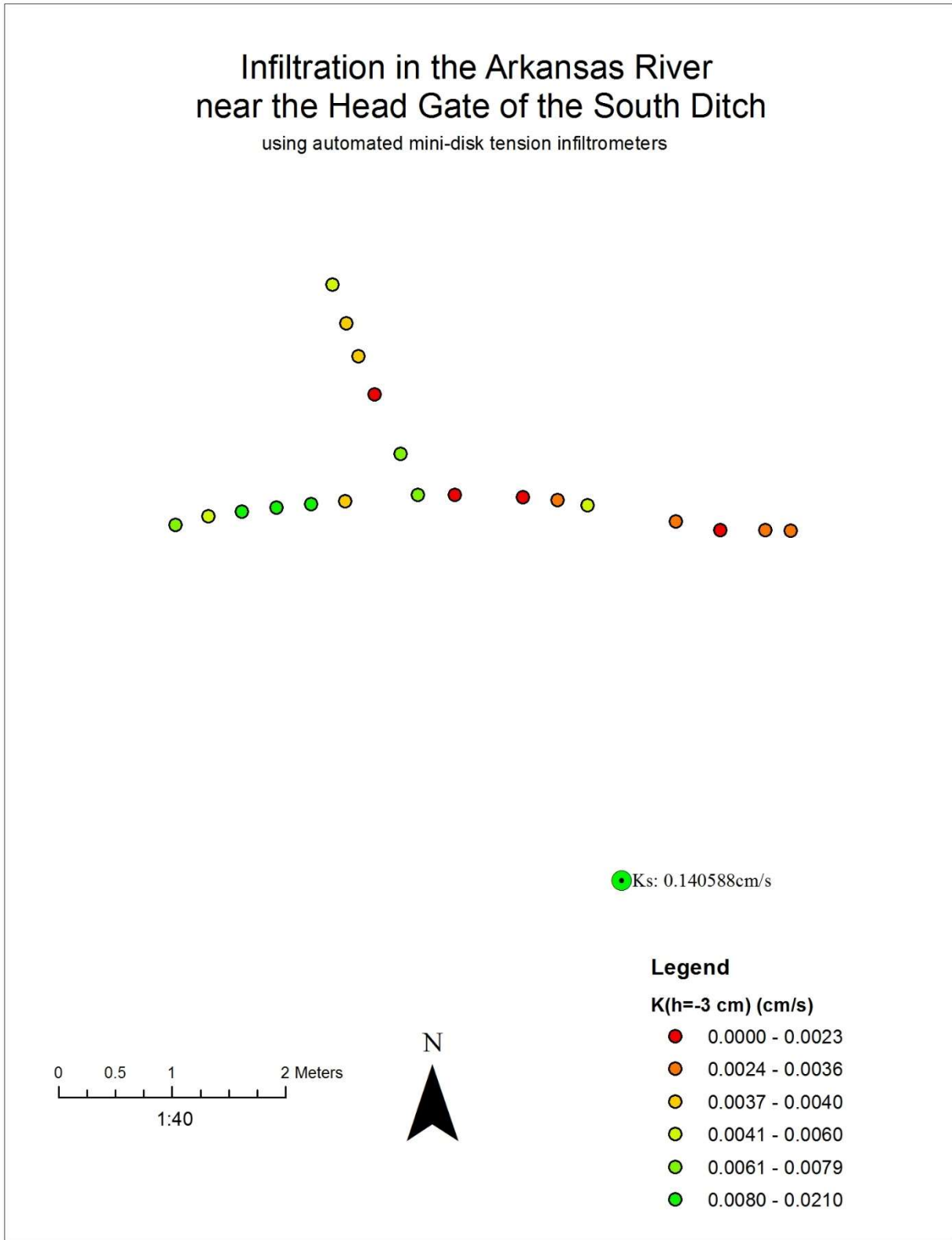


Figure B-4. Site 2: Results from Mini-Disk Infiltrometer in Arkansas River near the South Ditch Head Gate

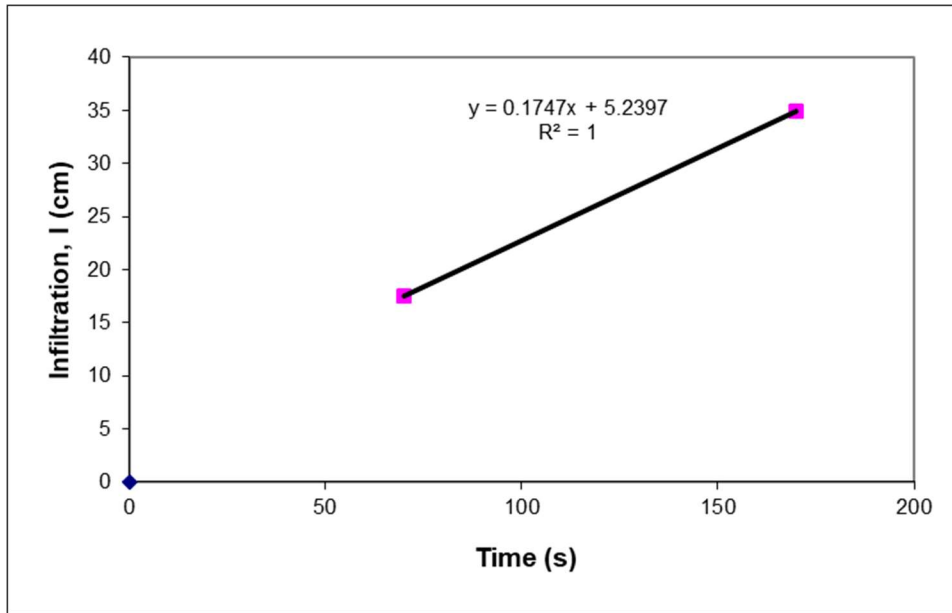


Figure B-5. Double-Ring Infiltrometer results for Site 2

Table B-5. Calculation of Hydraulic Conductivity, K, for Site 2

Description	Symbol	Value
Diameter of Outer Ring	d_o	51 cm
Diameter of Inner Ring	d_i	27 cm
Ring Radius	a	13.5 cm
Ponded Height	H	2 cm
Depth of Insertion	d	12 cm
Soil Macroscopic Length	α^*	0.12 cm^{-1}
dimensionless quasi-empirical constants	C_1	0.992743
	C_2	0.578053
Infiltration rate	q	0.175 cm/s
Hydraulic Conductivity	K	0.14 cm/s

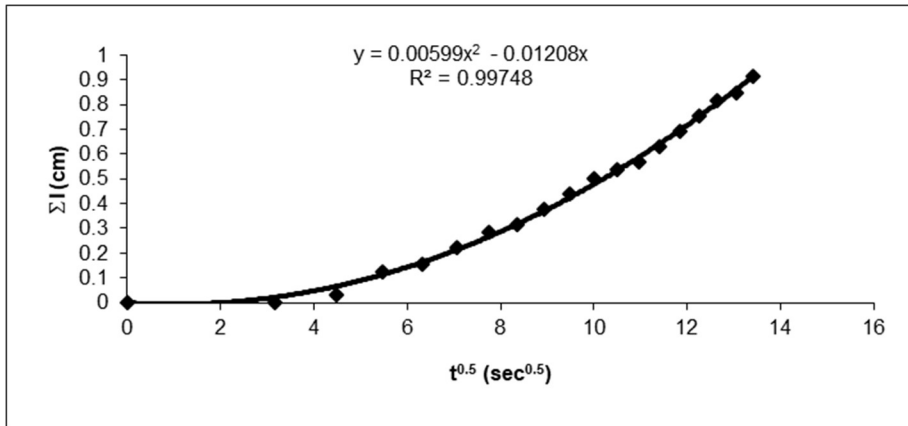


Figure B-6. Mini-Disk Infiltrometer (h = -6 cm) results for Site 2

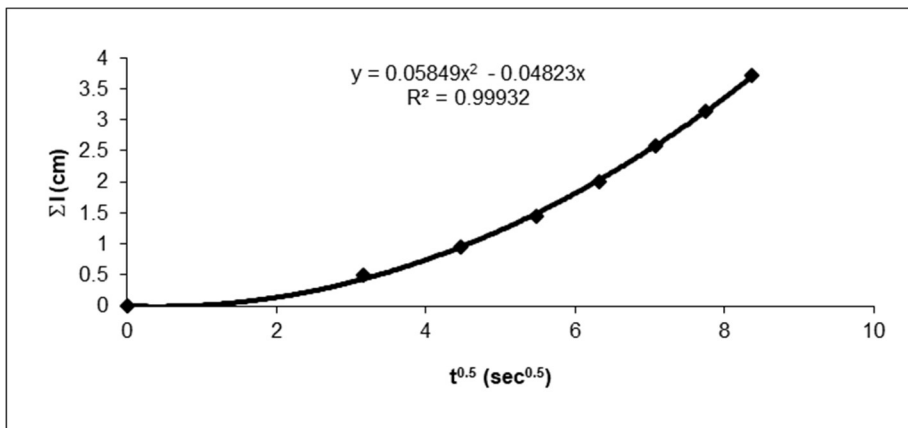


Figure B-7. Mini-Disk Infiltrometer (h = -2 cm) results for Site 2

Table B-6. Calculation of K(h) for Site 2

Description	Run 1	Run 2
n	2.680	2.680
α	0.145	0.145
β	0.55	0.55
h	-6 cm	-2 cm
r	2.25 cm	2.25 cm
A	0.461	1.728
V	14.5 mL	59 mL
C_2	0.0599	0.0585
K(h)	0.013 cm/s	0.034 cm/s
K_s	0.031 cm/s	0.045cm/s

Table B-7. Results from automated mini-disk tension infiltrometer for Site 2

Mote ID	Channel ID	Tension, h (cm)	Water remaining (cm)	C₂	K(h) (cm/s)	K_s (cm/s)
7	1	3	15	0.0012	7.2E-04	1.1E-03
7	2	3	0	0.0147	8.6E-03	1.3E-02
7	4	3	17	0.0080	4.7E-03	7.2E-03
7	6	3	0	0.0197	1.1E-02	1.8E-02
10	1	3	0	0.0315	1.8E-02	2.8E-02
10	2	3	0	0.0144	8.4E-03	1.3E-02
10	3	3	0	0.0098	5.7E-03	8.8E-03
10	5	3	0	0.0101	5.9E-03	9.1E-03
10	6	3	0	0.0423	2.5E-02	3.8E-02
12	1	3	0	0.0249	1.5E-02	2.2E-02
12	2	3	0	0.0439	2.6E-02	4.0E-02
12	3	3	0	0.1090	6.4E-02	9.8E-02
12	4	3	0	0.0885	5.2E-02	8.0E-02
12	5	3	0	0.0319	1.9E-02	2.9E-02
12	6	3	0	0.0384	2.2E-02	3.5E-02
13	1	3	0	0.0309	1.8E-02	2.8E-02
13	3	3	0	0.0134	7.8E-03	1.2E-02
13	4	3	0	0.0242	1.4E-02	2.2E-02
13	5	3	0	0.0226	1.3E-02	2.0E-02
13	6	3	0	0.0232	1.4E-02	2.1E-02

Table B-8. Well log near Site 2

County: Kearny	
Location: T25S, R37W, Sec. 17, NW SE NE	
Directions: from NW corner of Lakin: 6 mi W, 4 mi S, 1 mi W, 1330' S, 810' W	
Longitude: -101.3989402	
Latitude: 37.8813634	
Datum NAD 83	
Lithologic Log	
(log data not edited or checked by the KGS.)	
From: 0 ft. to 2 ft.	Type: CLAY
From: 2 ft. to 6 ft.	Type: FINE SAND
From: 6 ft. to 9 ft.	Type: SAND & GRAVEL
From: 9 ft. to 34 ft.	Type: COARSE GRAVEL
From: 34 ft. to 41 ft.	Type: MEDIUM GRAVEL
From: 41 ft. to 50 ft.	Type: SHALE

Source: http://chasm.kgs.ku.edu/ords/wwc5.wwc5d2.well_details?well_id=31750

Site 3: Arkansas River at Lakin, Kansas

Vicinity Map of Arkansas River near Lakin, KS

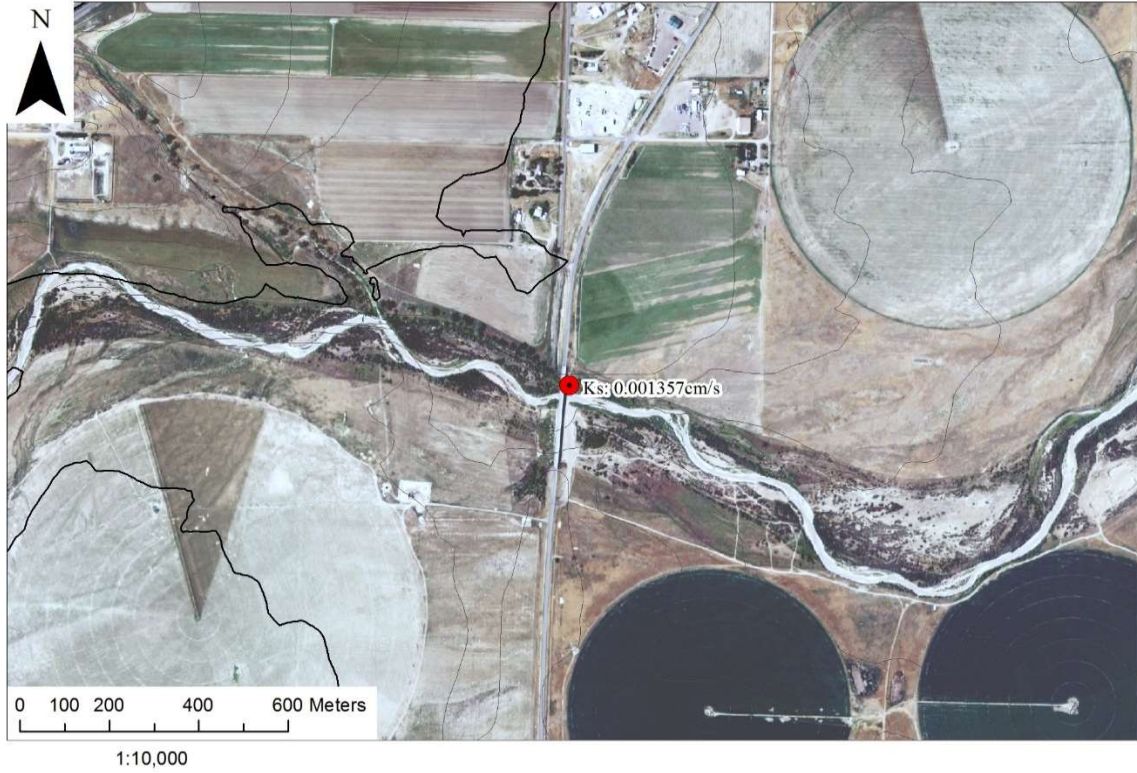


Figure B-8. Site 3: Arkansas River at Lakin, Kansas

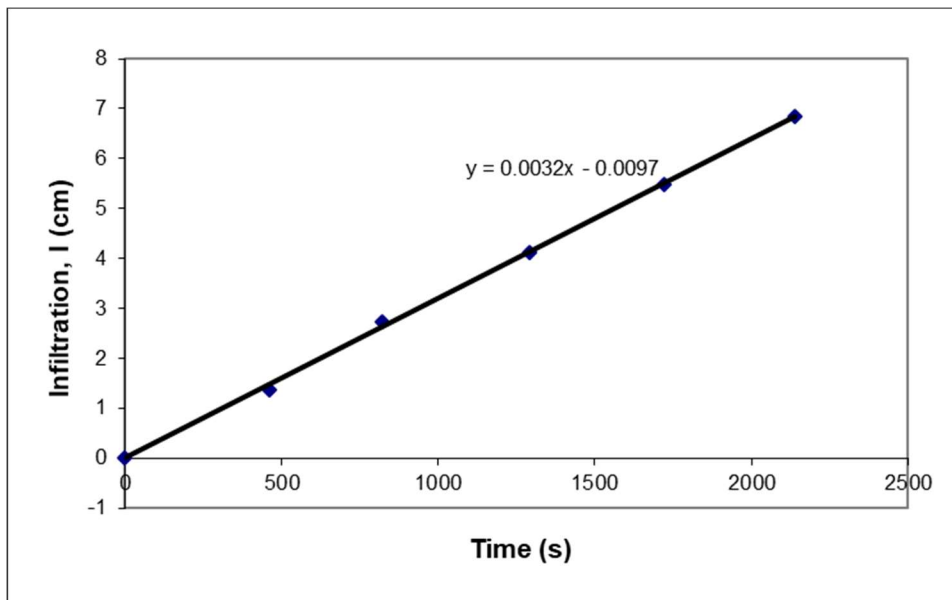


Figure B-9. Double-Ring Infiltrometer results for Site 3

Table B-9. Calculation of Hydraulic Conductivity for Site 3

Description	Symbol	Value
Diameter of Outer Ring	do	59 cm
Diameter of Inner Ring	di	30 cm
Ring Radius	a	15 cm
Ponded Height	H	18 cm
Depth of Insertion	d	10 cm
Soil Macroscopic Length	α^*	0.36 cm ⁻¹
dimensionless quasi-empirical constants	C ₁	0.992743
	C ₂	0.578053
Infiltration rate	q	0.0032 cm/s
Hydraulic Conductivity	K	0.0014 cm/s

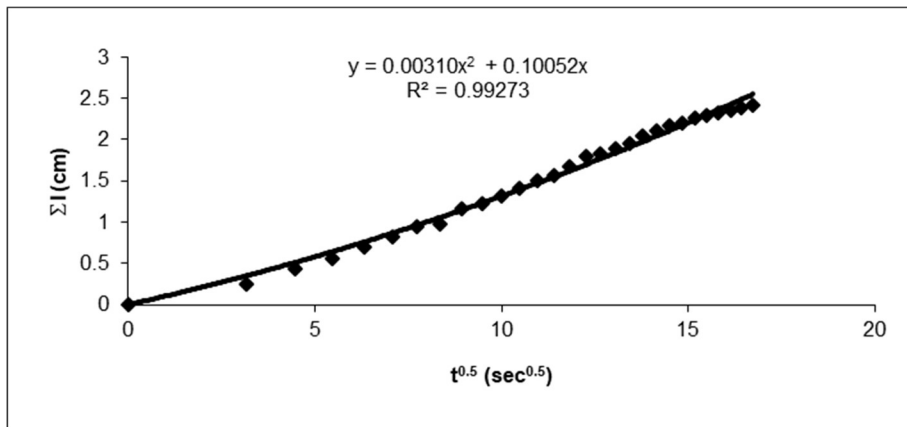


Figure B-10. Mini-Disk Infiltrometer (h = -6 cm) results 1 of 4 for Site 3

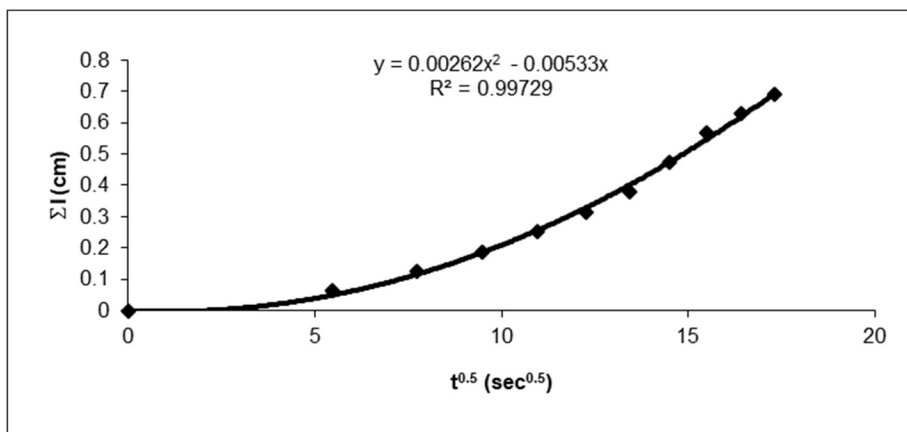


Figure B-11. Mini-Disk Infiltrometer (h = -6 cm) results 2 of 4 for Site 3

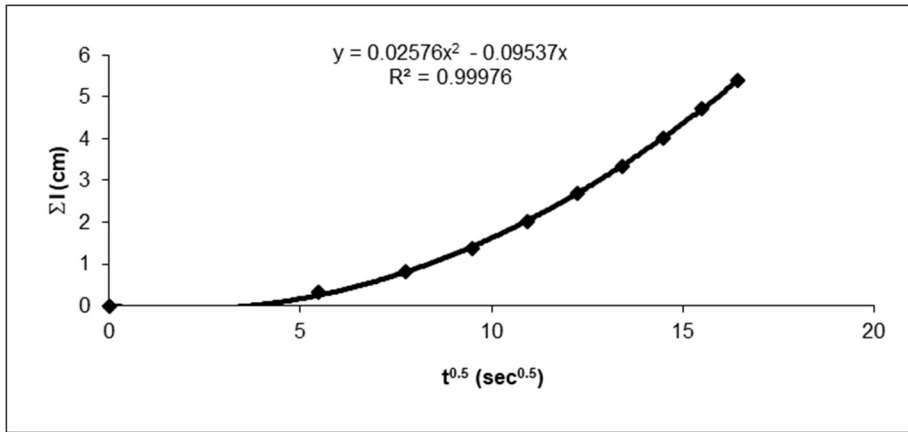


Figure B-12. Mini-Disk Infiltrometer (h = -6 cm) results 3 of 4 for Site 3

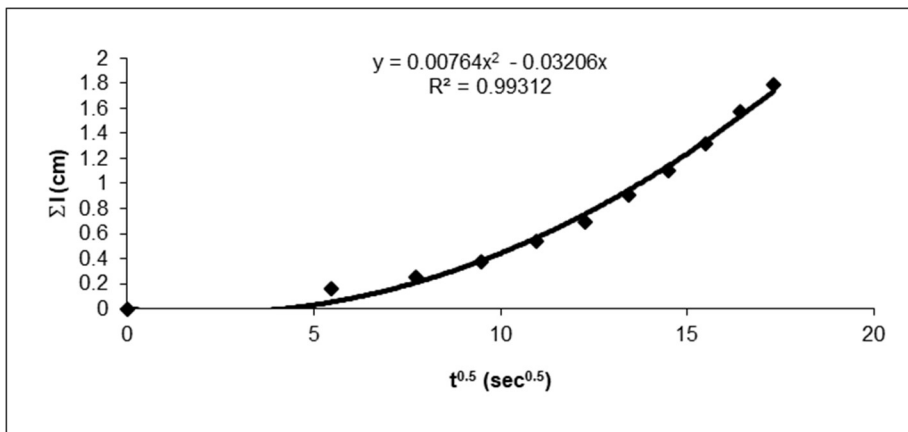


Figure B-13. Mini-Disk Infiltrometer (h = -6 cm) results 4 of 4 for Site 3

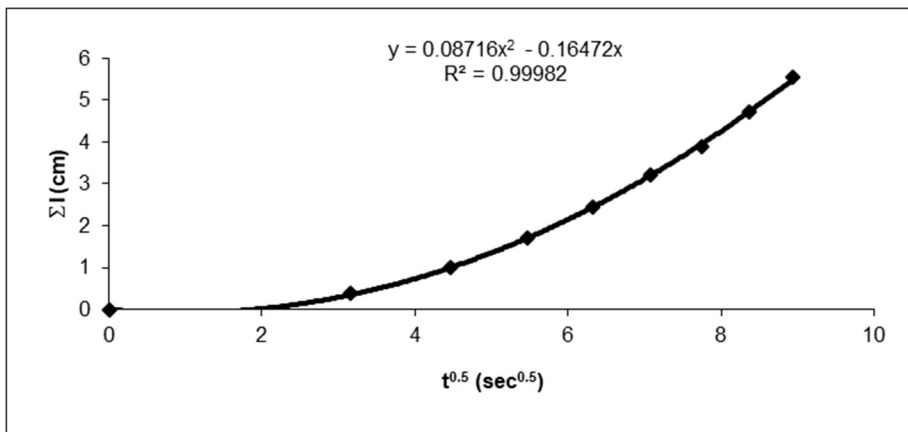


Figure B-14. Mini-Disk Infiltrometer (h = -2 cm) results 1 of 4 for Site 3

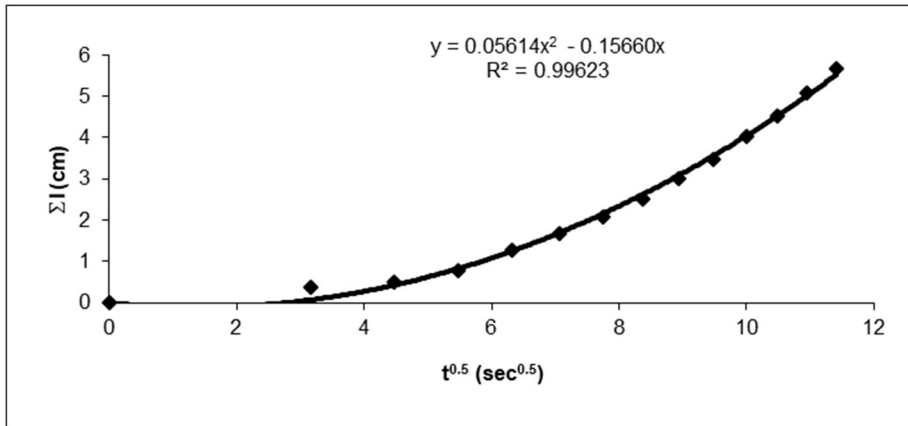


Figure B-15. Mini-Disk Infiltrometer (h = -2 cm) results 2 of 4 for Site 3

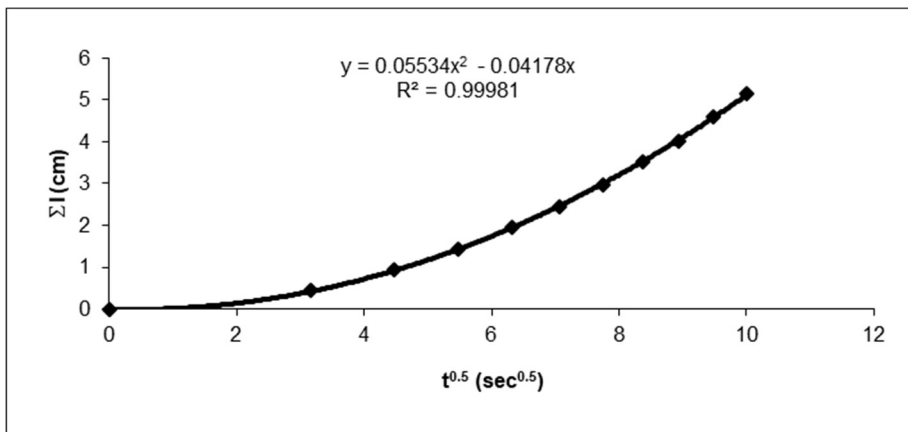


Figure B-16. Mini-Disk Infiltrometer (h = -2 cm) results 3 of 4 for Site 3

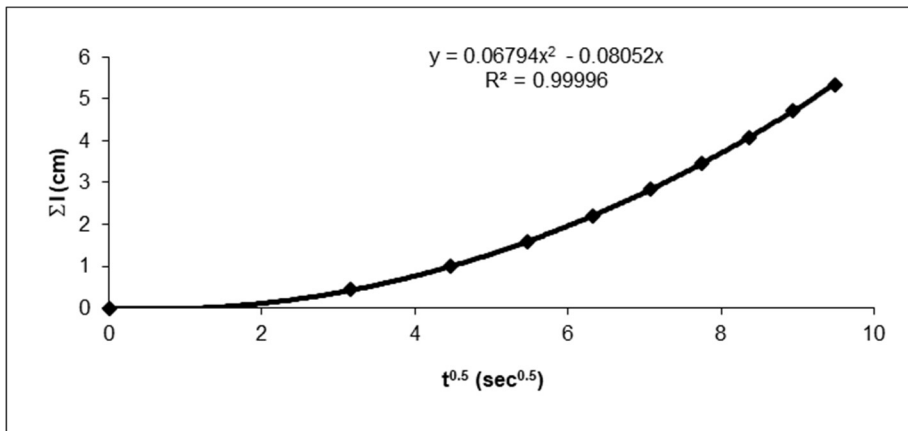


Figure B-17. Mini-Disk Infiltrometer (h = -2 cm) results 4 of 4 for Site 3

Table B-10. Calculation of K(h) for Site 3

Symbol	Run 1	Run 2	Run 3	Run 4	Run 5	Run 6	Run 7	Run 8
n	2.680	2.680	2.680	2.680	2.680	2.680	2.680	2.680
α	0.145	0.145	0.145	0.145	0.145	0.145	0.145	0.145
β	0.55	0.55	0.55	0.55	0.55	0.55	0.55	0.55
h	-6 cm	-6 cm	-6 cm	-6 cm	-2 cm	-2 cm	-2 cm	-2 cm
r	2.25 cm	2.25 cm	2.25 cm	2.25 cm	2.25 cm	2.25 cm	2.25 cm	2.25 cm
A	0.461	0.461	0.461	0.461	1.728	1.728	1.728	1.728
V	31 mL	11 mL	86 mL	29 mL	88 mL	90 mL	82 mL	85 mL
C_2	0.0031	0.0026	0.026	0.0076	0.087	0.056	0.055	0.068
K(h)	0.0067 cm/s	0.0057 cm/s	0.056 cm/s	0.017 cm/s	0.050 cm/s	0.032 cm/s	0.032 cm/s	0.039 cm/s
K_s	0.016 cm/s	0.014 cm/s	0.134 cm/s	0.041 cm/s	0.067 cm/s	0.043 cm/s	0.043 cm/s	0.052 cm/s

Table B-11. Constant Head Permeability Test for Site 3

Sample Name	Lakin Main Channel			Lakin Side Channel		
Weight	713.9g			747g		
Test No.	1	2	3	1	2	3
Average Flow, Q(cm ³)	100	200	300	100	200	300
Time of Collection, t(s)	11.6	20.69	33.81	13.6	25.69	40.13
Head Difference, h(cm)	66.7	66.7	66.7	66.7	66.7	66.7
Diameter of Specimen, D(cm)	6.35	6.35	6.35	6.35	6.35	6.35
Length of Specimen, L(cm)	14	14	14	14	14	14
Area of Specimen, A=($\pi/4$)D ² (cm ²)	31.65	31.65	31.65	31.65	31.65	31.65
k=QL/Aht (cm/s)	0.057	0.064	0.059	0.049	0.052	0.050
Average k (cm/s)	0.060			0.050		

Table B-12. Well log near Site 3

County: Kearny	
Location: T24S, R36W, Sec. 34, NW SE NW	
Directions: from Lakin: 1 mi S	
Longitude: -101.2620916	
Latitude: 37.925176	
Datum NAD 83	
Lithologic Log	
(Log data entered by KGS.)	
From: 0 ft. to 6 ft.	top soil
From: 6 ft. to 10 ft.	caliche
From: 10 ft. to 50 ft.	sand and gravel
From: 50 ft. to 75 ft.	sand, gravel, and clay streaks
From: 75 ft. to 167 ft.	gravel and blue clay

Source: http://chasm.kgs.ku.edu/ords/wwc5.wwc5d2.well_details?well_id=470892

Site 4: Arkansas River at Deerfield, Kansas

Vicinity Map of Arkansas River near Deerfield, KS



Figure B-18. Site 4: Arkansas River at Deerfield, Kansas

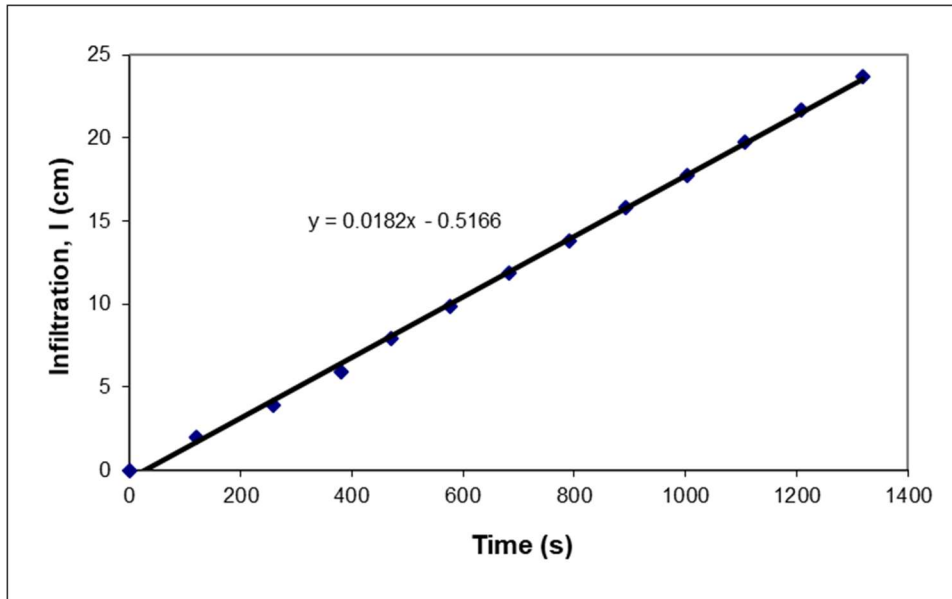


Figure B-19. Double-Ring Infiltrometer results for Site 4

Table B-13. Calculation of Hydraulic Conductivity for Site 4

Description	Symbol	Value
Diameter of Outer Ring	d_o	53 cm
Diameter of Inner Ring	d_i	25.4 cm
Ring Radius	a	12.7 cm
Ponded Height	H	20.3 cm
Depth of Insertion	d	10.2 cm
Soil Macroscopic Length	α^*	0.12 cm^{-1}
dimensionless quasi-empirical constants	C_1	0.992743
	C_2	0.578053
Infiltration rate	q	0.0182 cm/s
Hydraulic Conductivity	K	0.0070 cm/s

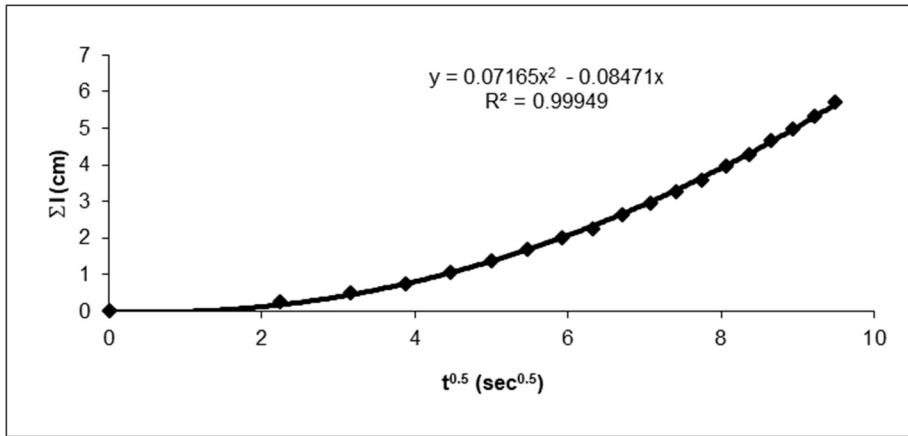


Figure B-20. Mini-Disk Infiltrometer (h = -2 cm) results 1 of 3 for Site 4

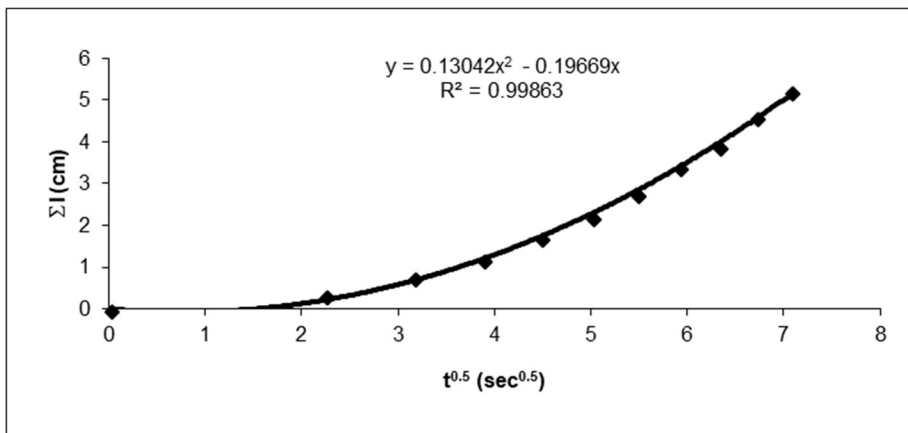


Figure B-21. Mini-Disk Infiltrometer (h = -2 cm) results 2 of 3 for Site 4

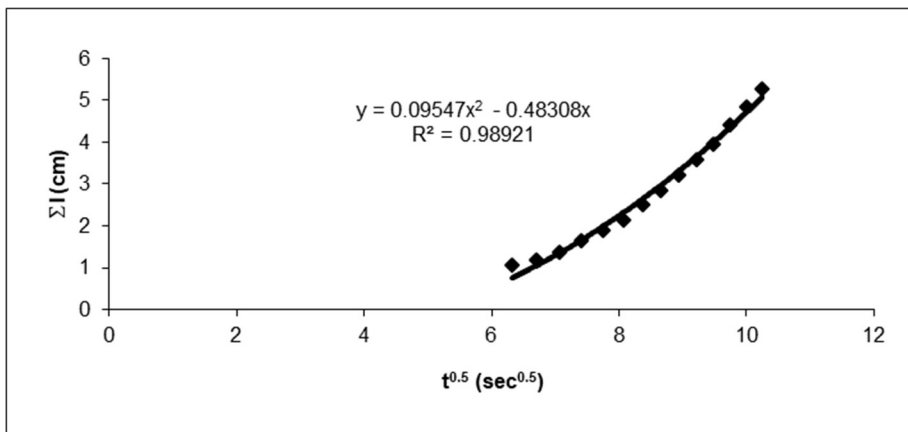


Figure B-22. Mini-Disk Infiltrometer (h = -2 cm) results 3 of 3 for Site 4

Table B-14. Calculation of K(h) for Site 4

Description	Run 1	Run 2	Run 3
n	2.680	2.680	2.680
α	0.145	0.145	0.145
β	0.55	0.55	0.55
h	-2 cm	-2 cm	-2 cm
r	2.25 cm	2.25 cm	2.25 cm
A	1.728	1.728	1.728
V	91 mL	83 mL	84 mL
C_2	0.072	0.13	0.095
K(h)	0.041 cm/s	0.075 cm/s	0.055 cm/s
K_s	0.055 cm/s	0.100 cm/s	0.074 cm/s

Table B-15. Constant Head Permeability Test for Site 4

Sample Name	Deerfield Main Channel			Deerfield Side Channel		
Weight	767g			786g		
Test No.	1	2	3	1	2	3
Average Flow, Q(cm ³)	100	200	300	100	200	300
Time of Collection, t(s)	13.26	26.82	43.17	44.08	90.92	141.74
Head Difference, h(cm)	66.7	66.7	66.7	66.7	66.7	66.7
Diameter of Specimen, D(cm)	6.35	6.35	6.35	6.35	6.35	6.35
Length of Specimen, L(cm)	14	14	14	14	14	14
Area of Specimen, $A=(\pi/4)D^2$ (cm ²)	31.65	31.65	31.65	31.65	31.65	31.65
$k=QL/Aht$ (cm/s)	0.050	0.049	0.046	0.015	0.015	0.014
Average k (cm/s)	0.049			0.015		

Table B-16. Well log near site 4

County: Kearny	
Location: T24S, R35W, Sec. 14, SE NW	
Directions: from Deerfield: 1 mi S	
Longitude: -101.1325628	
Latitude: 37.9685158	
Datum NAD 83	
Lithologic Log	
(Log data entered by KGS.)	
From: 0 ft. to 6 ft.	topsoil
From: 6 ft. to 10 ft.	brown clay
From: 10 ft. to 26 ft.	coarse gravel (mix of clay)
From: 26 ft. to 32 ft.	brown sandy clay
From: 32 ft. to 40 ft.	fine to medium sand and gravel (loose)
From: 40 ft. to 70 ft.	brown sandy clay
From: 70 ft. to 75 ft.	fine to medium sand and gravel (loose)
From: 75 ft. to 80 ft.	brown sandy clay
From: 80 ft. to 93 ft.	fine to medium sand and gravel (loose)
From: 93 ft. to 100 ft.	brown sandy and small sand and gravel
From: 100 ft. to 105 ft.	fine to medium sand and gravel (loose)
From: 105 ft. to 110 ft.	brown sandy clay
From: 110 ft. to 136 ft.	fine to medium sand and gravel (loose)
From: 136 ft. to 137 ft.	hard rock
From: 137 ft. to 140 ft.	fine to medium sand and gravel (small)
From: 140 ft. to 145 ft.	fine to medium sand and gravel (loose)
From: 145 ft. to 156 ft.	brown sandy clay
From: 156 ft. to 160 ft.	hard rock
From: 160 ft. to 167 ft.	fine to medium sand and gravel (loose)
From: 167 ft. to 173 ft.	brown sandy clay
From: 173 ft. to 185 ft.	fine to medium sand and gravel (loose)

From: 185 ft. to 206 ft.	brown sandy clay
From: 206 ft. to 215 ft.	fine to medium sand and gravel (loose)
From: 215 ft. to 230 ft.	brown sandy clay
From: 230 ft. to 235 ft.	fine sand (loose)
From: 235 ft. to 240 ft.	white rock (hard)
From: 240 ft. to 248 ft.	brown sandy clay (hard rock)
From: 248 ft. to 250 ft.	hard rock
From: 250 ft. to 255 ft.	brown sandy clay
From: 255 ft. to 260 ft.	fine sand (loose)
From: 260 ft. to 277 ft.	brown clay (streak)
From: 277 ft. to 295 ft.	fine to medium sand and gravel (loose)

Source: http://chasm.kgs.ku.edu/ords/wwc5.wwc5d2.well_details?well_id=455490

Site 5: Arkansas River at Garden City, Kansas

Vicinity Map of Arkansas River South of Garden City, KS



Figure B-23. Site 5: Arkansas River at Garden City, Kansas

Infiltration in the Arkansas River near US 83

using automated mini-disk tension infiltrometers

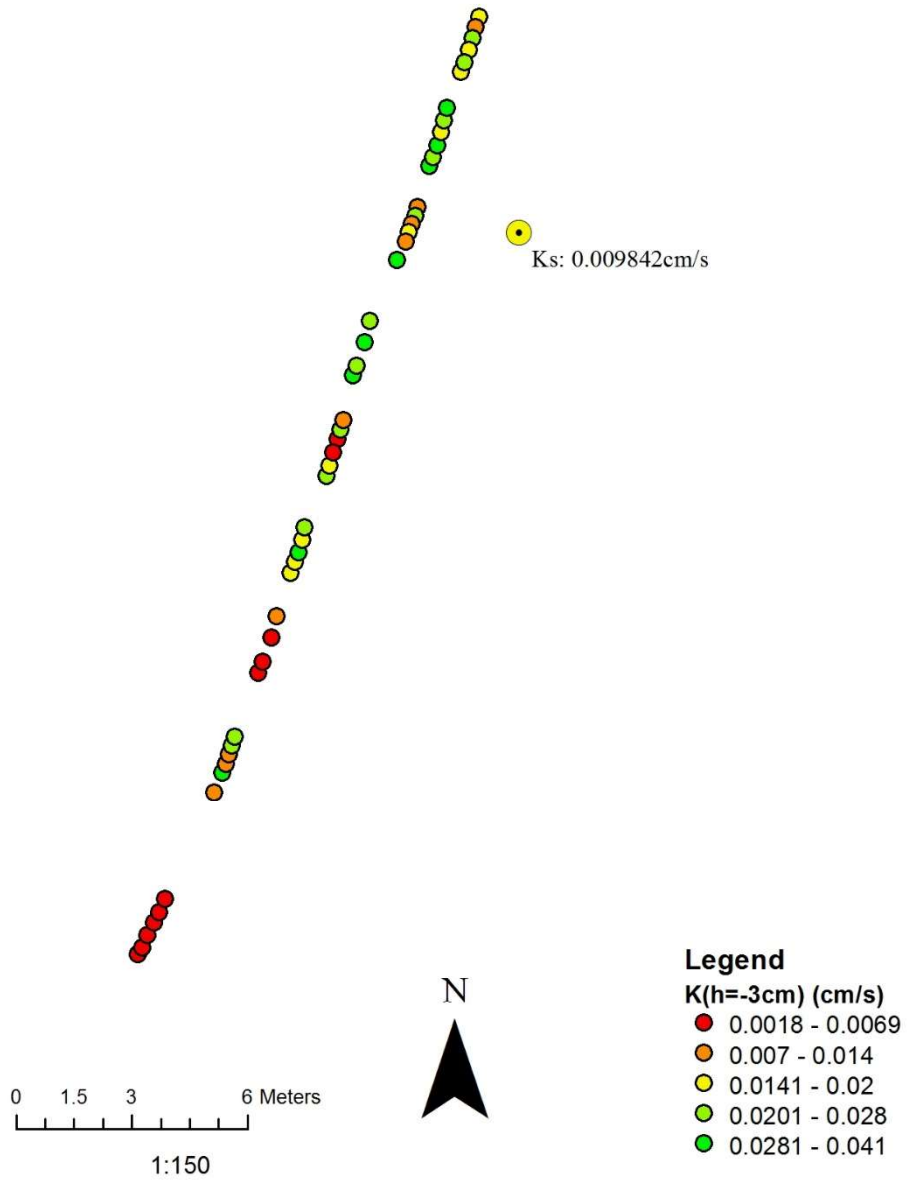


Figure B-24. Site 5: Results from Mini-Disk Infiltrometer in Arkansas River at Garden City, Kansas

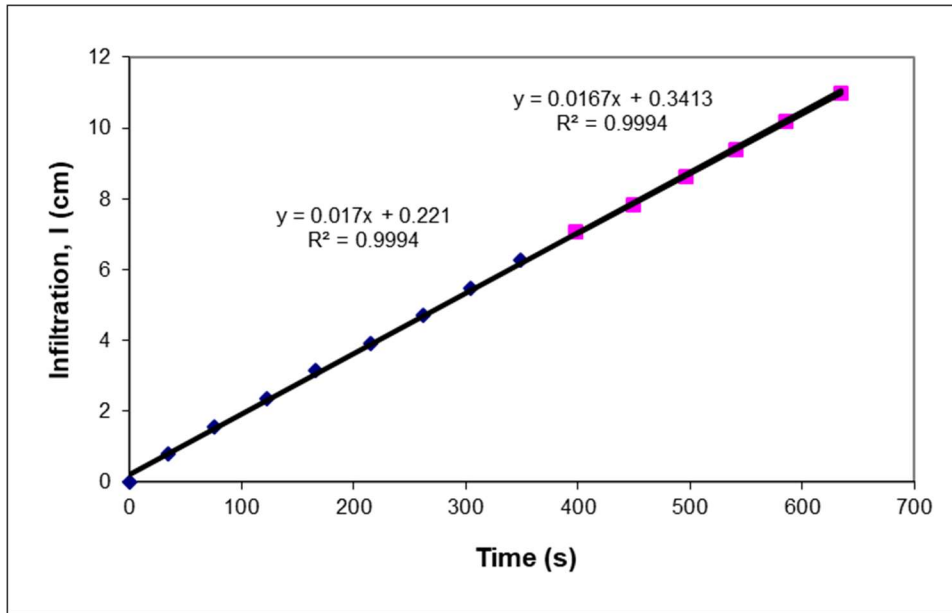


Figure B-25. Double-Ring Infiltrometer results for Site 5

Table B-17. Calculation of Hydraulic Conductivity for Site 5

Description	Symbol	Value
Diameter of Outer Ring	d_o	51.5 cm
Diameter of Inner Ring	d_i	28.5 cm
Ring Radius	a	14.25 cm
Ponded Height	H	10 cm
Depth of Insertion	d	10 cm
Soil Macroscopic Length	α^*	0.36 cm^{-1}
dimensionless quasi-empirical constants	C_1	0.992743
	C_2	0.578053
Infiltration rate	q	0.0167 cm/s
Hydraulic Conductivity	K	0.00984 cm/s

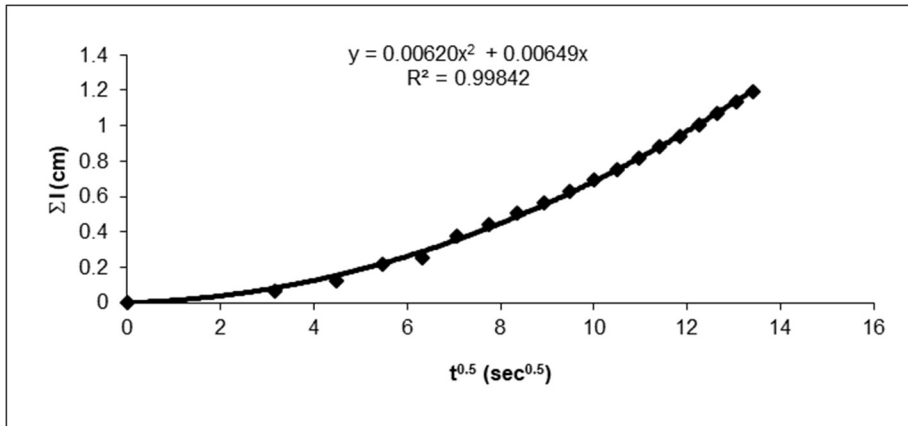


Figure B-26. Mini-Disk Infiltrometer ($h = -6$ cm) results for Site 5

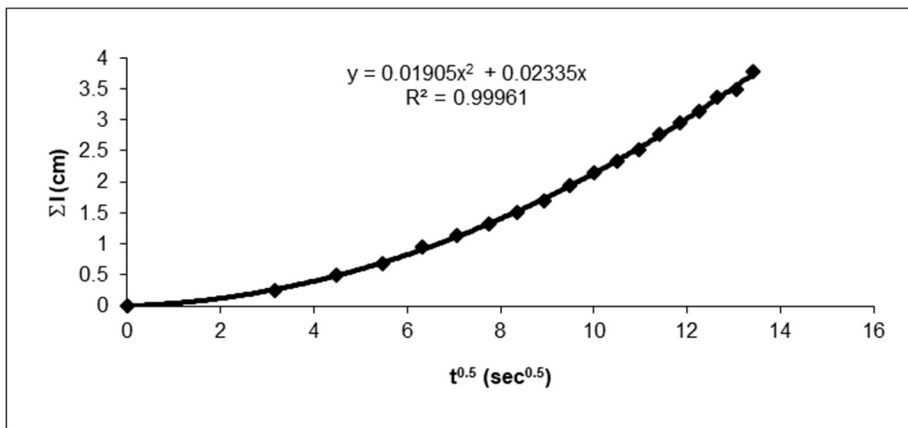


Figure B-27. Mini-Disk Infiltrometer ($h = -2$ cm) results for Site 5

Table B-18. Calculation of $K(h)$ for Site 5

Description	Run 1	Run 2
n	2.680	2.680
α	0.145	0.145
β	0.55	0.55
h	-6 cm	-2 cm
r	2.25 cm	2.25 cm
A	0.461	1.728
V	19 mL	60 mL
C_2	0.0062	0.019
$K(h)$	0.013 cm/s	0.011 cm/s
K_s	0.031 cm/s	0.147 cm/s

Table B-19. Results from automated mini-disk tension infiltrometer for Site 5

Mote ID	Run	Channel ID	Tension, h (cm)	Water remaining (cm)	C₂	K(h) (cm/s)	Ks (cm/s)
7	1	1	3	0	0.0580	3.4E-02	5.2E-02
7	1	2	3	0	0.0360	2.1E-02	3.2E-02
7	1	4	3	0	0.0597	3.5E-02	5.4E-02
7	1	6	3	0	0.0484	2.8E-02	4.4E-02
7	2	1	3	0	0.0044	2.6E-03	4.0E-03
7	2	2	3	0	0.0092	5.4E-03	8.3E-03
7	2	4	3	0	0.0050	2.9E-03	4.5E-03
7	2	6	3	0	0.0200	1.2E-02	1.8E-02
10	1	1	3	0	0.0325	1.9E-02	2.9E-02
10	1	2	3	0	0.0381	2.2E-02	3.4E-02
10	1	3	3	0	0.0320	1.9E-02	2.9E-02
10	1	4	3	0	0.0449	2.6E-02	4.0E-02
10	1	5	3	0	0.0194	1.1E-02	1.8E-02
10	1	6	3	0	0.0293	1.7E-02	2.6E-02
10	2	1	3	0	0.0449	2.6E-02	4.1E-02
10	2	2	3	0	0.0264	1.5E-02	2.4E-02
10	2	3	3	0	0.0119	6.9E-03	1.1E-02
10	2	4	3	0	0.0071	4.1E-03	6.4E-03
10	2	5	3	0	0.0411	2.4E-02	3.7E-02
10	2	6	3	0	0.0143	8.4E-03	1.3E-02
12	1	1	3	0	0.0493	2.9E-02	4.4E-02
12	1	2	3	0	0.0428	2.5E-02	3.9E-02
12	1	3	3	0	0.0615	3.6E-02	5.5E-02
12	1	4	3	0	0.0337	2.0E-02	3.0E-02
12	1	5	3	0	0.0382	2.2E-02	3.4E-02
12	1	6	3	0	0.0541	3.2E-02	4.9E-02
12	2	1	3	0	0.0250	1.5E-02	2.3E-02
12	2	2	3	0	0.0285	1.7E-02	2.6E-02

Mote ID	Run	Channel ID	Tension, h (cm)	Water remaining (cm)	C₂	K(h) (cm/s)	Ks (cm/s)
12	2	3	3	0	0.0547	3.2E-02	4.9E-02
12	2	4	3	0	0.0270	1.6E-02	2.4E-02
12	2	5	3	0	0.0398	2.3E-02	3.6E-02
12	3	1	3	8	0.0031	1.8E-03	2.8E-03
12	3	2	3	8	0.0034	2.0E-03	3.1E-03
12	3	3	3	7	0.0039	2.3E-03	3.5E-03
12	3	4	3	0	0.0063	3.7E-03	5.7E-03
12	3	5	3	7	0.0032	1.9E-03	2.9E-03
12	3	6	3	2	0.0051	2.9E-03	4.6E-03
13	1	1	3	0	0.0707	4.1E-02	6.4E-02
13	1	3	3	0	0.0199	1.2E-02	1.8E-02
13	1	4	3	0	0.0334	1.9E-02	3.0E-02
13	1	5	3	0	0.0209	1.2E-02	1.9E-02
13	1	6	3	3	0.0371	2.2E-02	3.3E-02
13	1	7	3	0	0.0194	1.1E-02	1.7E-02
13	2	1	3	0	0.0232	1.4E-02	2.1E-02
13	2	3	3	0	0.0525	3.1E-02	4.7E-02
13	2	4	3	0	0.0223	1.3E-02	2.0E-02
13	2	5	3	0	0.0132	7.7E-03	1.2E-02
13	2	6	3	0	0.0371	2.2E-02	3.3E-02
13	2	7	3	0	0.0405	2.4E-02	3.7E-02

Table B-20. Well log near Site 5

County: Finney	
Location: T24S, R33W, Sec. 23, SE NE NE	
Directions: 6000 Cowgill Dr	
Longitude: -100.9025735	
Latitude: 37.9573663	
Datum NAD 83	
Lithologic Log	
(Log data entered by KGS.)	
From: 0 ft. to 31 ft.	fine sand
From: 31 ft. to 40 ft.	brown sandy clay
From: 40 ft. to 55 ft.	fine sand
From: 55 ft. to 60 ft.	rock and gravel
From: 60 ft. to 117 ft.	brown sandy clay
From: 117 ft. to 135 ft.	fine to medium sand and gravel
From: 135 ft. to 163 ft.	brown sandy clay and brown clay
From: 163 ft. to 170 ft.	fine to medium sand and gravel
From: 170 ft. to 200 ft.	brown sandy clay
From: 200 ft. to 229 ft.	fine to medium sand and gravel
From: 229 ft. to 246 ft.	brown sandy clay
From: 246 ft. to 252 ft.	fine to medium sand and gravel
From: 252 ft. to 255 ft.	brown sandy clay
From: 255 ft. to 300 ft.	fine to medium sand and gravel

Source: http://chasm.kgs.ku.edu/ords/wwc5.wwc5d2.well_details?well_id=18610

Site 6: Arkansas River at Cimarron, Kansas

Vicinity Map of Arkansas River South of Cimarron, KS



Figure B-28. Site 6: Arkansas River at Cimarron, Kansas

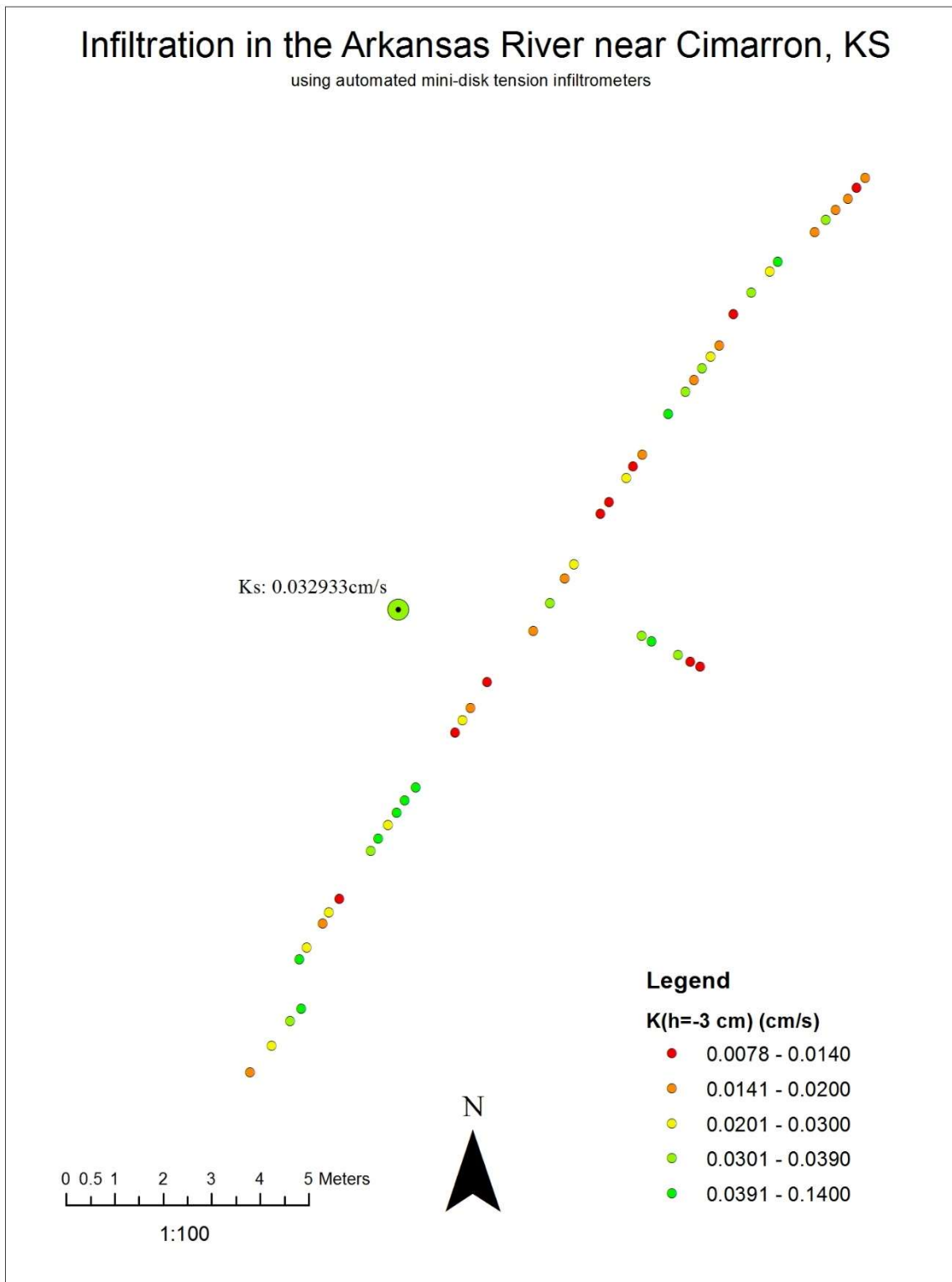


Figure B-29. Site 6: Results from Mini-Disk Infiltrometer in Arkansas River at Cimarron, Kansas

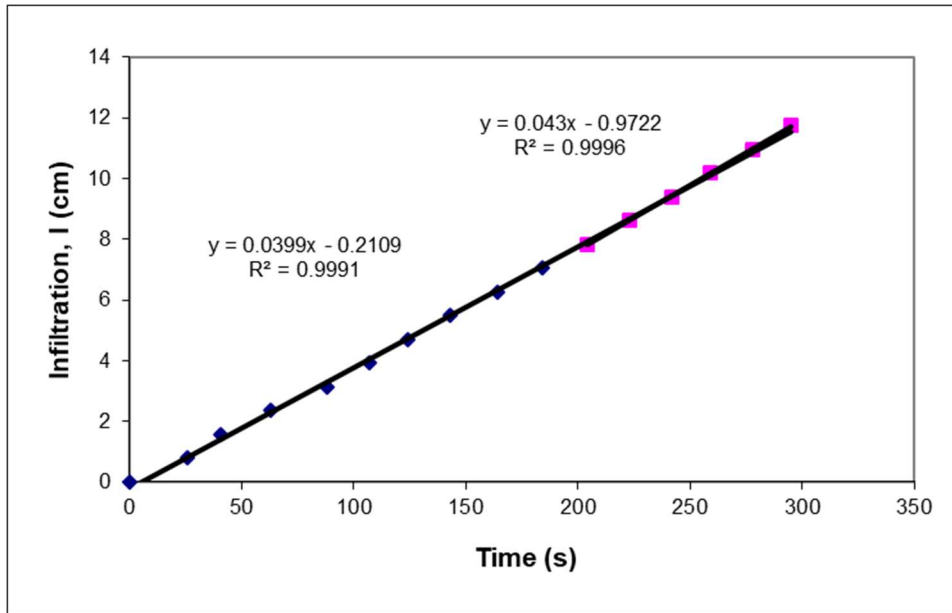


Figure B-30. Double-Ring Infiltrometer results Site 6

Table B-21. Calculation of Hydraulic Conductivity for Site 6

Description	Symbol	Value
Diameter of Outer Ring	d_o	60 cm
Diameter of Inner Ring	d_i	20 cm
Ring Radius	a	15 cm
Ponded Height	H	6 cm
Depth of Insertion	d	4 cm
Soil Macroscopic Length	α^*	0.12 cm^{-1}
dimensionless quasi-empirical constants	C_1	0.992743
	C_2	0.578053
Infiltration rate	q	0.043 cm/s
Hydraulic Conductivity	K	0.033 cm/s

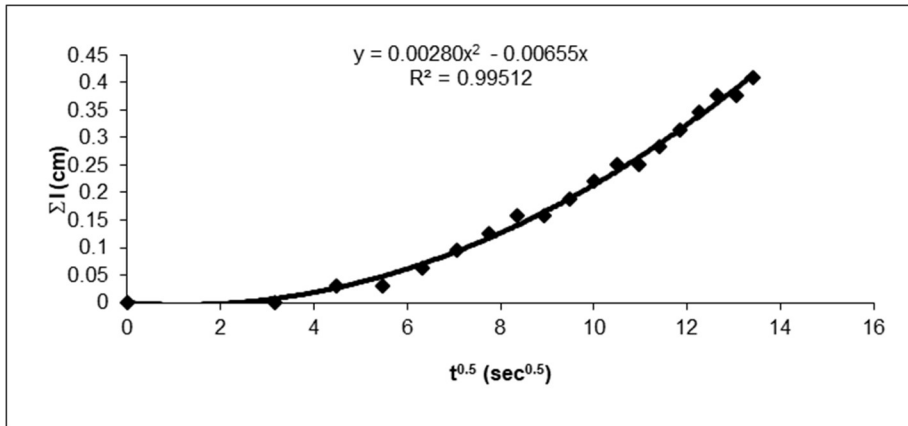


Figure B-31. Mini-Disk Infiltrometer (h = -6 cm) results for Site 6

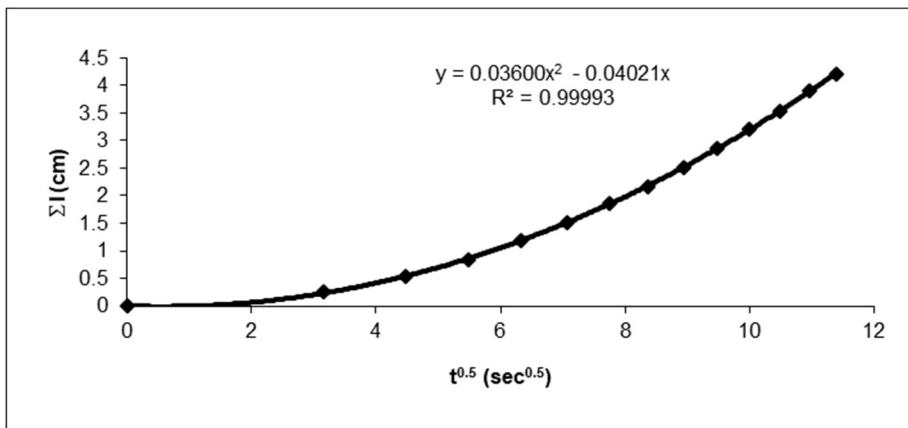


Figure B-32. Mini-Disk Infiltrometer (h = -2 cm) results for Site 6

Table B-22. Calculation of K(h) for Site 6

Description	Run 1	Run 2
n	2.680	2.680
α	0.145	0.145
β	0.55	0.55
h	-6 cm	-2 cm
r	2.25 cm	2.25 cm
A	0.461	1.728
V	19 mL	60 mL
C_2	0.0028	0.036
K(h)	0.0061 cm/s	0.021 cm/s

Table B-23. Well log for Site 6

County: Gray	
Location: T26S, R28W, Sec. 11, NW SE SE	
Directions: 401 S Second St., Cimarron	
Longitude: -100.3457773	
Latitude: 37.7982184	
Datum NAD 83	
Lithologic Log	
(Log data entered by KGS.)	
From: 0 ft. to 2 ft.	Topsoil
From: 2 ft. to 35 ft.	very course sand
From: 35 ft. to 37 ft.	Yellow clay
From: 37 ft. to 48 ft.	white rock
From: 48 ft. to 85 ft.	Brown sandy clay
From: 85 ft. to 95 ft.	Course sand
From: 95 ft. to 102 ft.	Brown sandy clay
From: 102 ft. to 110 ft.	Course sand
From: 110 ft. to 140 ft.	Medium Sand and Brown Sandy clay

Source: http://chasm.kgs.ku.edu/ords/wwc5.wwc5d2.well_details?well_id=333839

Site 7: South Ditch at Deerfield, Kansas

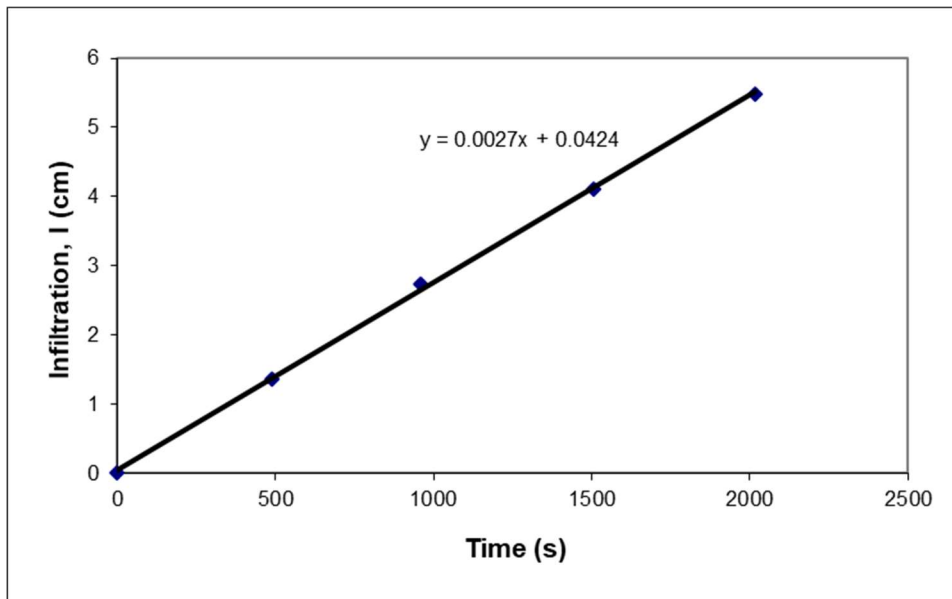


Figure B-33. Double-Ring Infiltrometer results for Site 7

Table B-24. Calculation of Hydraulic Conductivity for Site 7

Description	Symbol	Value
Diameter of Outer Ring	d_o	59 cm
Diameter of Inner Ring	d_i	30.5 cm
Ring Radius	a	15.2 cm
Ponded Height	H	23.5 cm
Depth of Insertion	d	10 cm
Soil Macroscopic Length	α^*	0.36 cm^{-1}
dimensionless quasi-empirical constants	C_1	0.992743
	C_2	0.578053
Infiltration rate	q	0.0027 cm/s
Hydraulic Conductivity	K	0.0010 cm/s

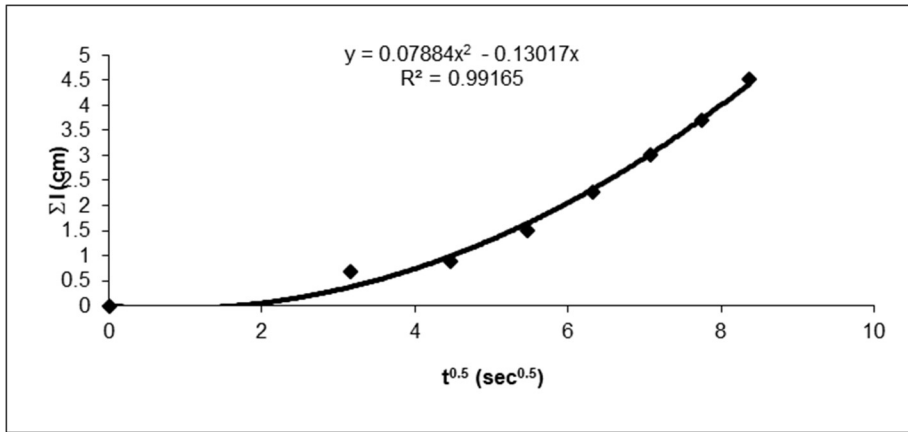


Figure B-34. Mini-Disk Infiltrometer ($h = -6$ cm) results 1 of 3 for Site 7

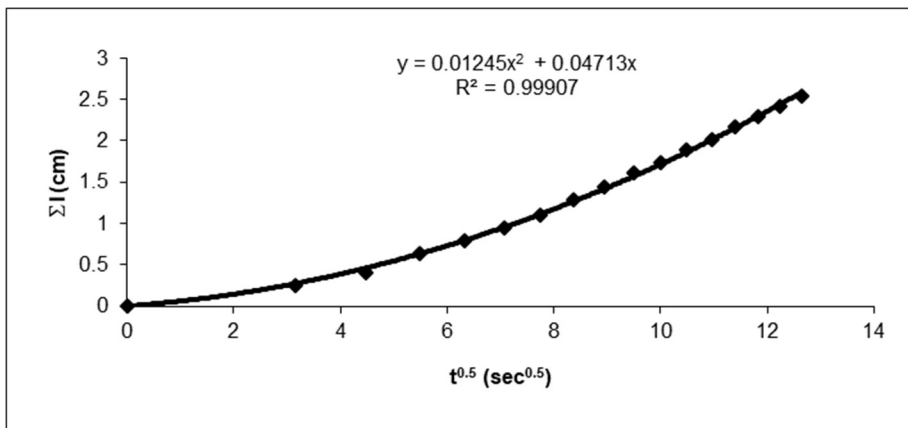


Figure B-35. Mini-Disk Infiltrometer ($h = -6$ cm) results 2 of 3 for Site 7

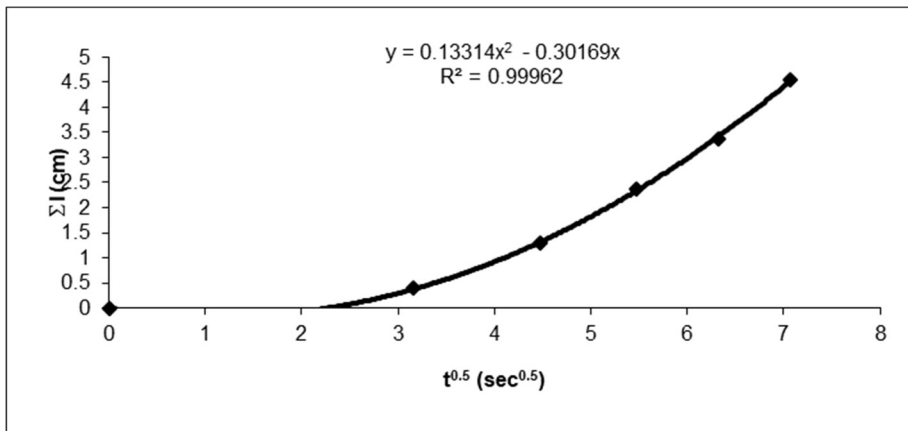


Figure B-36. Mini-Disk Infiltrometer ($h = -6$ cm) results 3 of 3 for Site 7

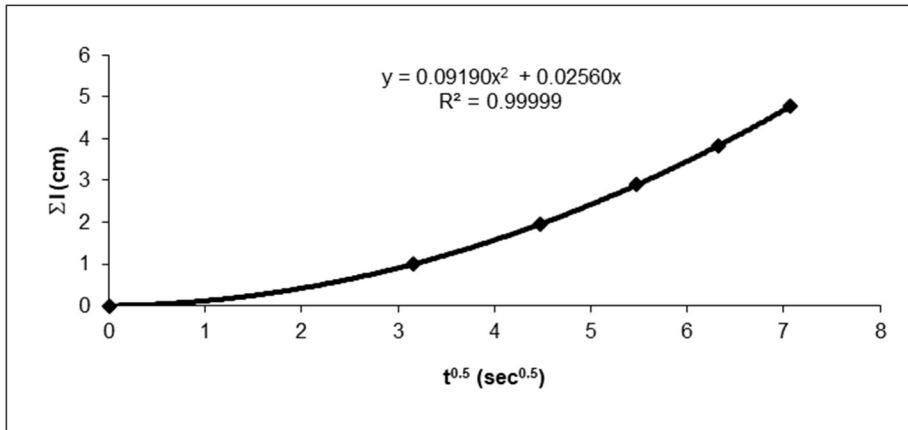


Figure B-37. Mini-Disk Infiltrometer (h = -2 cm) results 1 of 3 for Site 7

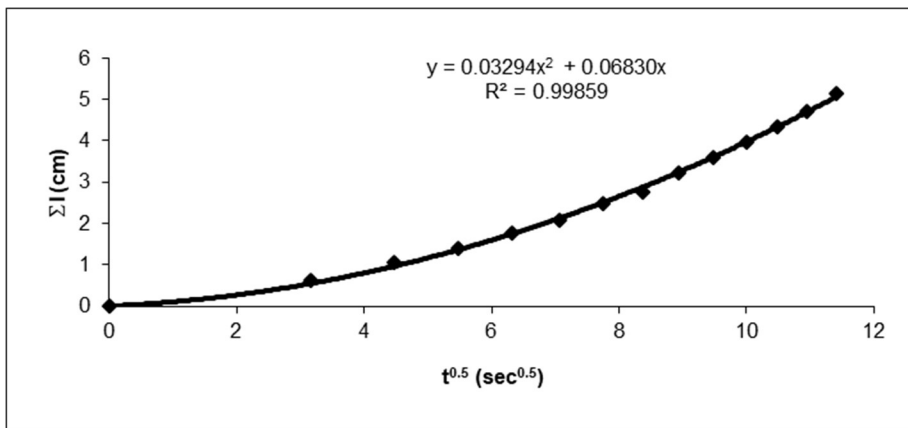


Figure B-38. Mini-Disk Infiltrometer (h = -2 cm) results 2 of 3 for Site 7

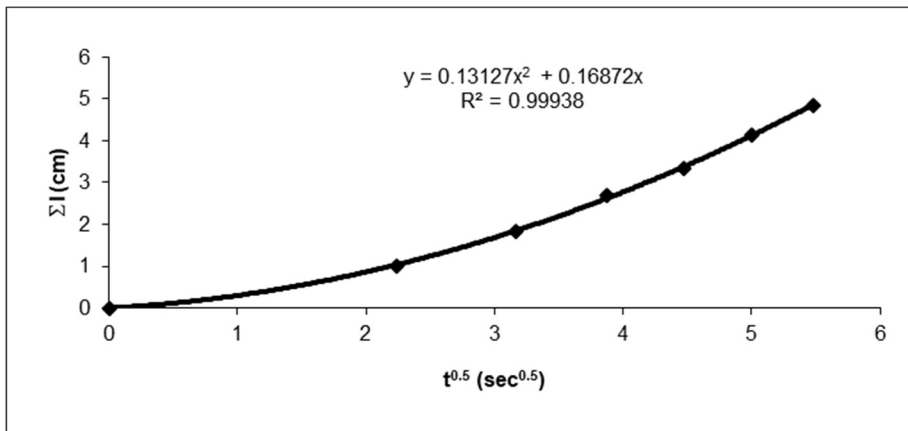


Figure B-39. Mini-Disk Infiltrometer (h = -2 cm) results 3 of 3 for Site 7

Table B-25. Calculation of K(h) for Site 7

Symbol	Run 1	Run 2	Run 3	Run 4	Run 5	Run 6
n	2.680	2.680	2.680	2.680	2.680	2.680
α	0.145	0.145	0.145	0.145	0.145	0.145
β	0.55	0.55	0.55	0.55	0.55	0.55
h	-6 cm	-6 cm	-6 cm	-2 cm	-2 cm	-2 cm
r	2.25 cm					
A	0.461	0.461	0.461	1.728	1.728	1.728
V	72 mL	41 mL	73 mL	76 mL	82 mL	77 mL
C_2	0.079	0.012	0.13	0.092	0.033	0.13
K(h)	0.171	0.027	0.29	0.053	0.019	0.076
	cm/s	cm/s	cm/s	cm/s	cm/s	cm/s

Site 8: Cimarron River at Elkhart, Kansas

Vicinity Map of Cimarron River near Elkhart, KS



Figure B-40. Site 8: Cimarron River at Elkhart, Kansas

Infiltration in the Cimarron River
near Elkhart, KS in Morton County
using mini-disk tension infiltrometers and double-ring infiltrometer

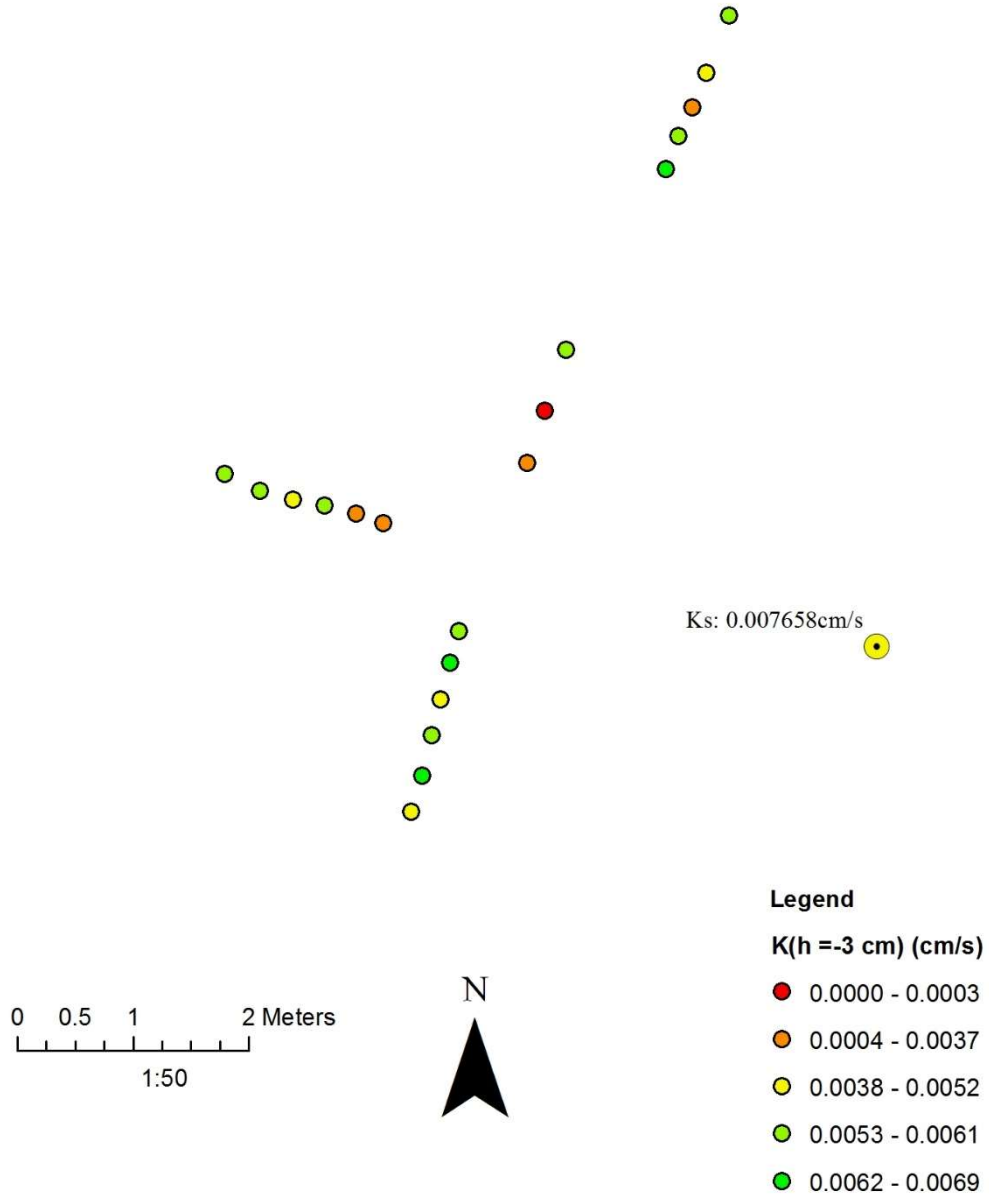


Figure B-41. Site 8: Results from Mini-Disk Infiltrometer in Cimarron River at Elkhart, Kansas

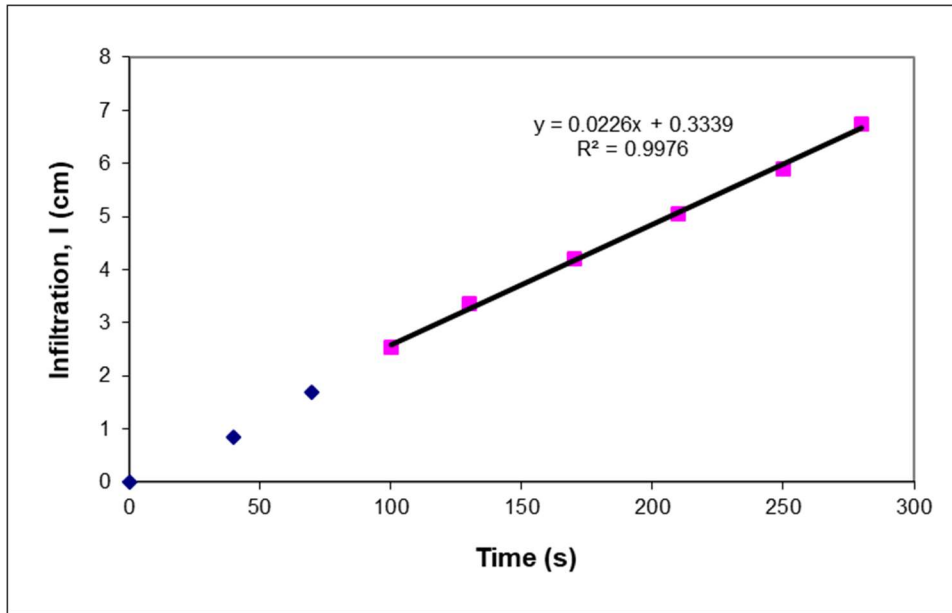


Figure B-42. Double-Ring Infiltrometer results for Site 8

Table B-26. Calculation of Hydraulic Conductivity for Site 8

Description	Symbol	Value
Diameter of Outer Ring	d_o	51.5 cm
Diameter of Inner Ring	d_i	27.5 cm
Ring Radius	a	13.75 cm
Ponded Height	H	10 cm
Depth of Insertion	d	10 cm
Soil Macroscopic Length	α^*	0.12 cm^{-1}
dimensionless quasi-empirical constants	C_1	0.992743
	C_2	0.578053
Infiltration rate	q	0.0226 cm/s
Hydraulic Conductivity	K	0.0112 cm/s

Table B-27. Results from automated mini-disk tension infiltrometer for Site 8

Mote ID	Channel ID	Tension, h (cm)	Water remaining (cm)	C₂	K(h) (cm/s)	K_s (cm/s)
7	2	3	0	0.0061	3.5E-03	5.5E-03
7	4	3	0	0.0005	2.9E-04	4.4E-04
7	6	3	0	0.0094	5.5E-03	8.4E-03
10	1	3	0	0.0100	5.8E-03	9.0E-03
10	2	3	0	0.0114	6.7E-03	1.0E-02
10	3	3	0	0.0089	5.2E-03	8.0E-03
10	4	3	0	0.0105	6.1E-03	9.4E-03
10	5	3	0	0.0118	6.9E-03	1.1E-02
10	6	3	0	0.0080	4.7E-03	7.2E-03
12	1	3	0	0.0061	3.6E-03	5.5E-03
12	2	3	0	0.0063	3.7E-03	5.7E-03
12	3	3	0	0.0094	5.5E-03	8.5E-03
12	4	3	8	0.0087	5.1E-03	7.8E-03
12	5	3	9	0.0102	5.9E-03	9.2E-03
12	6	3	7	0.0094	5.5E-03	8.5E-03
13	1	3	0	0.0102	6.0E-03	9.2E-03
13	3	3	0	0.0087	5.0E-03	7.8E-03
13	4	3	4	0.0051	3.0E-03	4.6E-03
13	5	3	0	0.0094	5.5E-03	8.5E-03
13	6	3	0	0.0111	6.5E-03	1.0E-02

Site 9: Cimarron River in Morton County, Kansas



Figure B-43. Site 12: Cimarron River in Morton County, Kansas

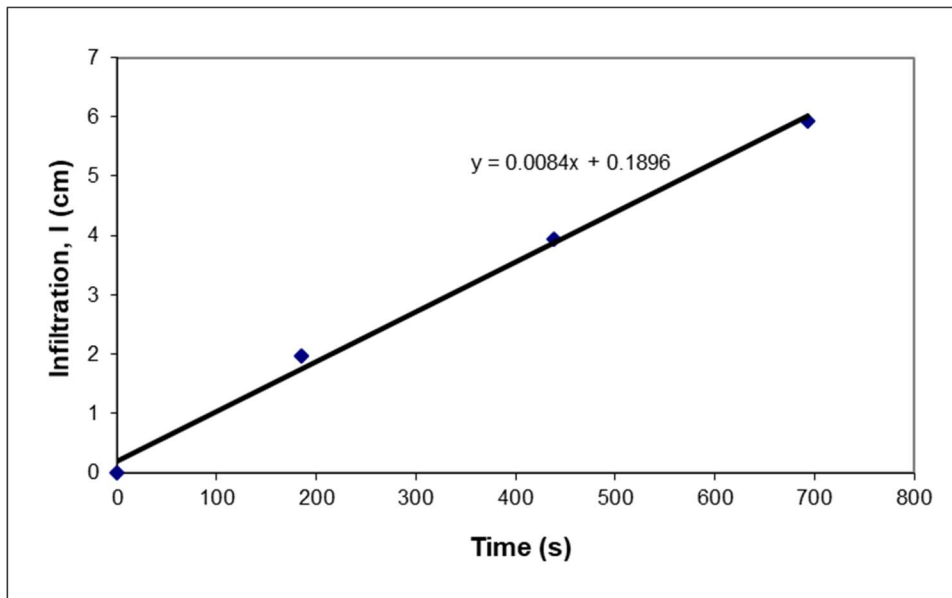


Figure B-44. Double-Ring Infiltrometer results for Site 9

Table B-28. Calculation of Hydraulic Conductivity for Site 9

Description	Symbol	Value
Diameter of Outer Ring	do	53.3 cm
Diameter of Inner Ring	di	25.4 cm
Ring Radius	a	12.7 cm
Ponded Height	H	20.3 cm
Depth of Insertion	d	10.2 cm
Soil Macroscopic Length	α^*	0.12 cm^{-1}
dimensionless quasi-empirical constants	C_1	0.992743
	C_2	0.578053
Infiltration rate	q	0.0084 cm/s
Hydraulic Conductivity	K	0.0032 cm/s

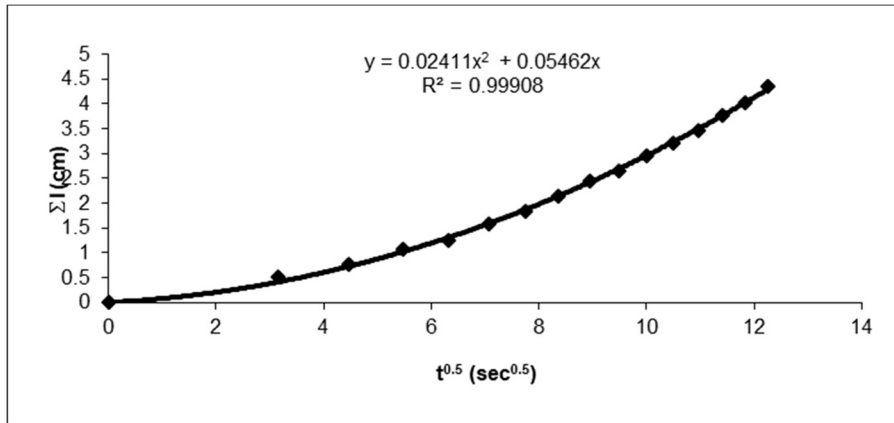


Figure B-45. Mini-Disk Infiltrometer (h = -2 cm) results 1 of 3 for Site 9

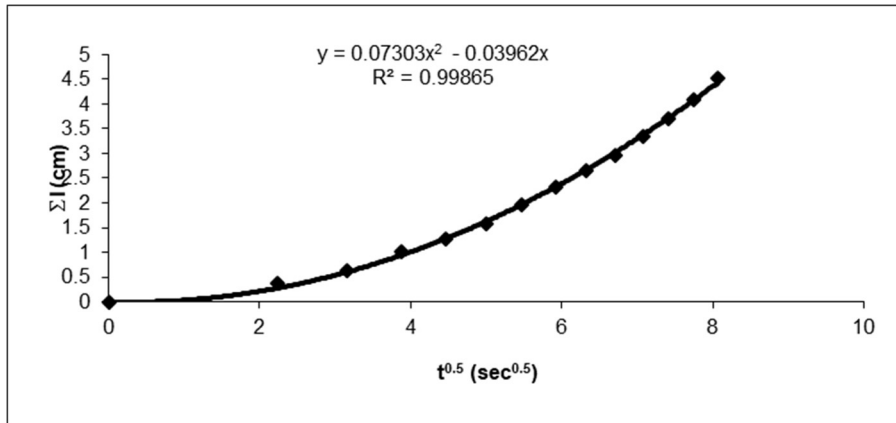


Figure B-46. Mini-Disk Infiltrometer (h = -2 cm) results 2 of 3 for Site 9

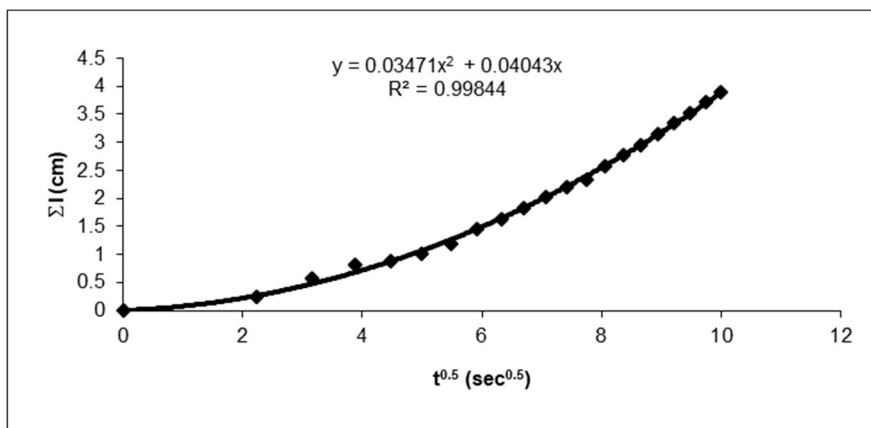


Figure B-47. Mini-Disk Infiltrometer (h = -2 cm) results 3 of 3 for Site 9

Table B-29. Calculation of K(h) for Site 9

Description	Run 1	Run 2	Run 3
n	2.680	2.680	2.680
α	0.145	0.145	0.145
β	0.55	0.55	0.55
h	-2 cm	-2 cm	-2 cm
r	2.25 cm	2.25 cm	2.25 cm
A	1.728	1.728	1.728
V	69 mL	72 mL	62 mL
C_2	0.024	0.042	0.035
K(h)	0.014 cm/s	0.073 cm/s	0.020 cm/s
K_s	0.019 cm/s	0.098 cm/s	0.027 cm/s

Site 10: Cimarron River at Ulysses, Kansas

Vicinity Map of Cimarron River in Grant County, KS

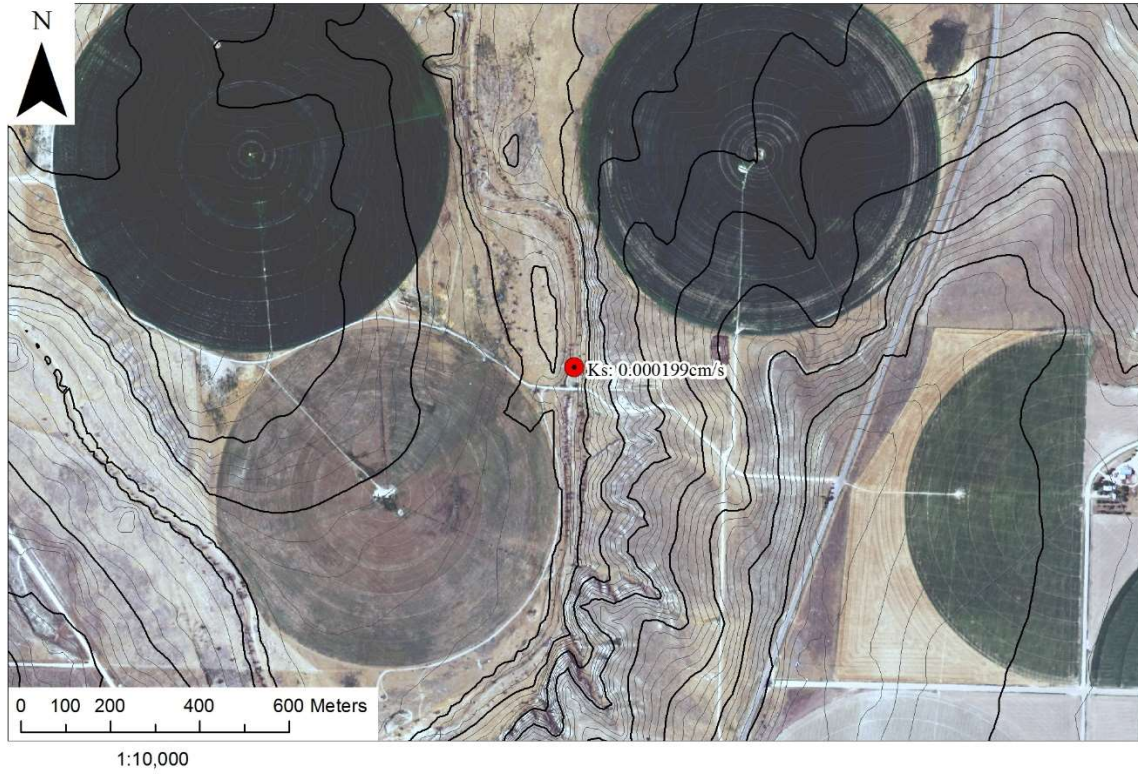


Figure B-48. Site 10: Cimarron River at Ulysses, Kansas

Infiltration in the Cimarron River near Ulysses, KS in Grant County

using automated mini-disk tension infiltrometers

Ks: 0.000199cm/s | K(h): 0.00777cm/s

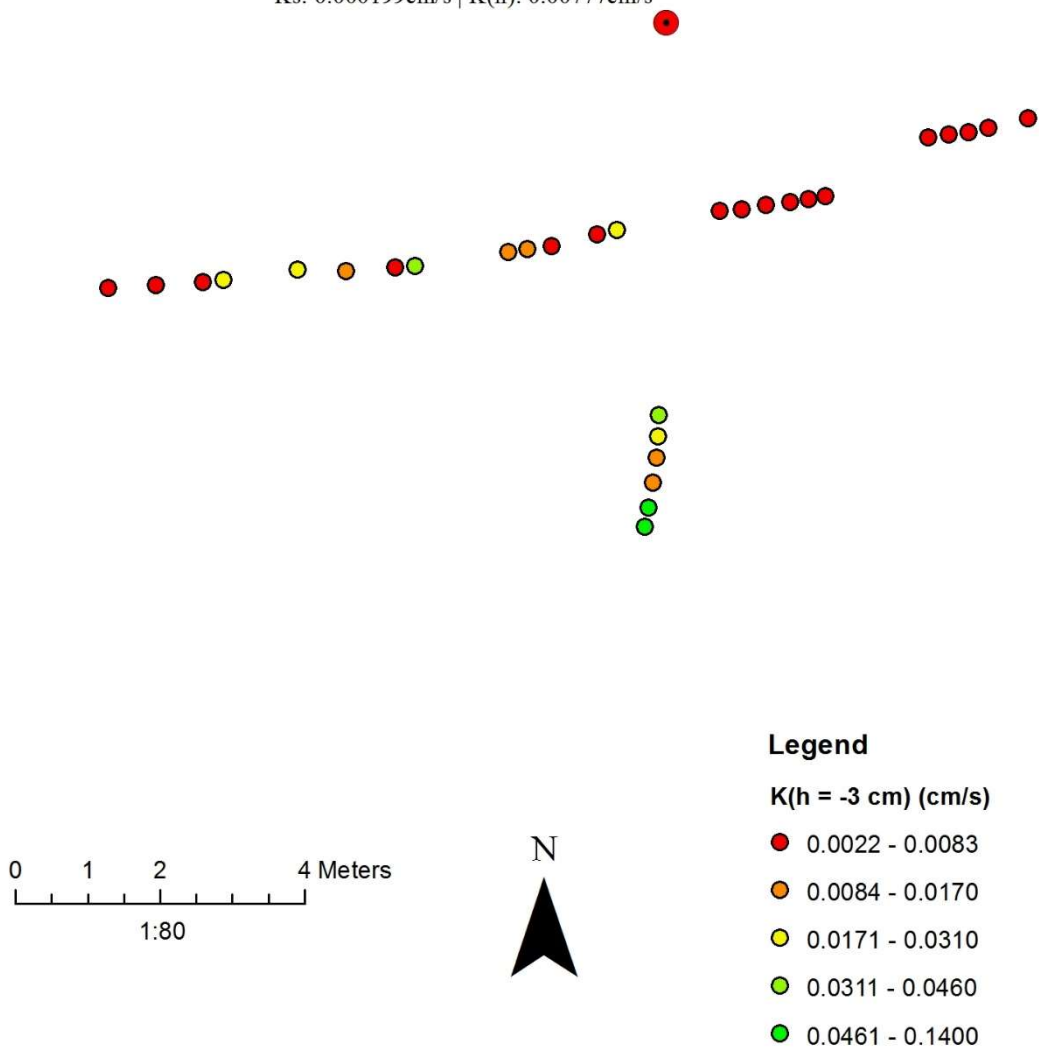


Figure B-49. Site 10: Results from Mini-Disk Infiltrometer in Cimarron River at Ulysses, Kansas

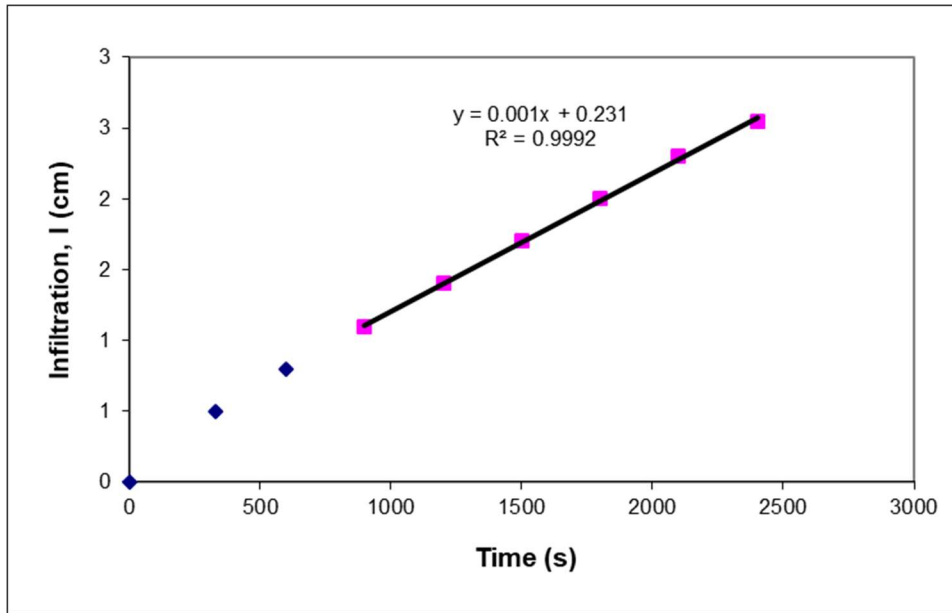


Figure B-50. Double-Ring Infiltrometer results for Site 10

Table B-30. Calculation of Hydraulic Conductivity for Site 10

Description	Symbol	Value
Diameter of Outer Ring	d_o	51 cm
Diameter of Inner Ring	d_i	27.5 cm
Ring Radius	a	13.75 cm
Ponded Height	H	35 cm
Depth of Insertion	d	8 cm
Soil Macroscopic Length	α^*	0.04 cm^{-1}
dimensionless quasi-empirical constants	C_1	0.992743
	C_2	0.578053
Infiltration rate	q	0.001 cm/s
Hydraulic Conductivity	K	0.00020 cm/s

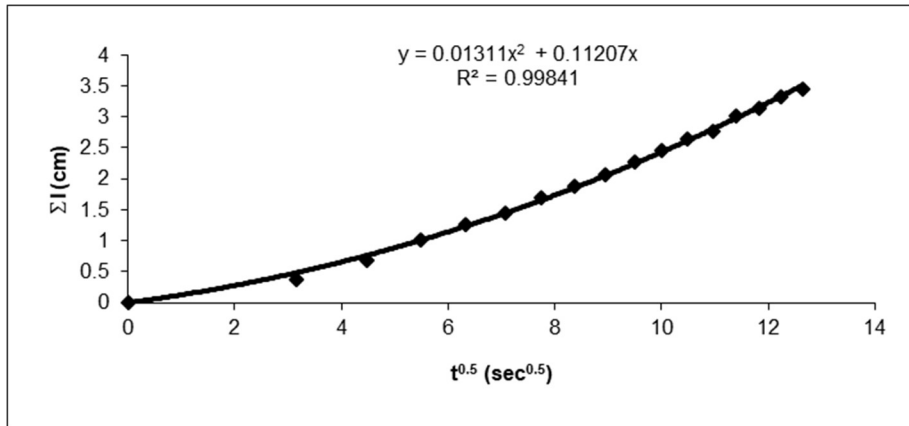


Figure B-51. Mini-Disk Infiltrometer ($h = -6$ cm) results for Site 10

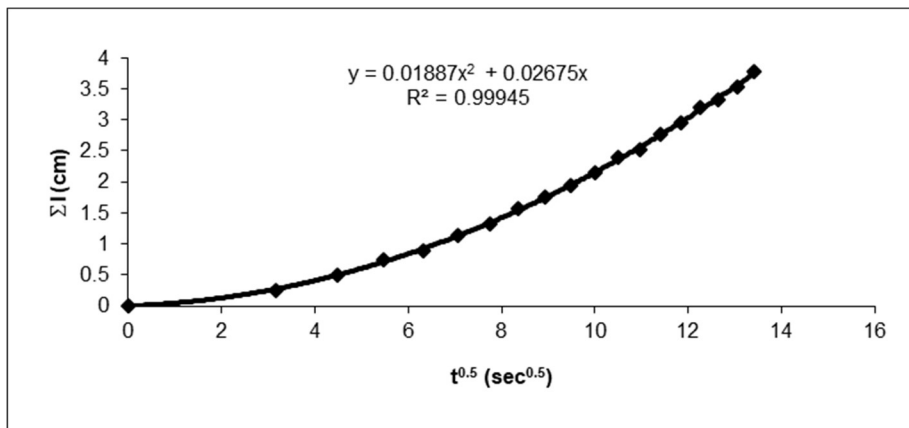


Figure B-52. Mini-Disk Infiltrometer ($h = -2$ cm) results for Site 10

Table B-31. Calculation of $K(h)$ for Site 10

Description	Run 1	Run 2
n	2.280	2.280
α	0.124	0.124
β	0.55	0.55
h	-6 cm	-2 cm
r	2.25 cm	2.25 cm
A	1.401	2.429
V	55 mL	59 mL
C_2	0.013	0.019
$K(h)$	0.0094 cm/s	0.0078 cm/s
K_s	0.020 cm/s	0.010 cm/s

Table B-32. Results from automated mini-disk tension infiltrometer for Site 10

Mote ID	Run	Channel ID	Tension, h (cm)	Water remaining (cm)	C₂	K(h) (cm/s)	K_s (cm/s)
7	1	1	3	0	0.1331	4.6E-02	6.6E-02
7	1	2	3	0	0.0241	8.3E-03	1.2E-02
7	1	4	3	0	0.0340	1.2E-02	1.7E-02
7	1	6	3	0	0.0620	2.1E-02	3.1E-02
7	2	1	3	0	0.0796	2.7E-02	4.0E-02
7	2	2	3	0	0.0198	6.8E-03	9.8E-03
7	2	4	3	0	0.0149	5.1E-03	7.4E-03
7	2	6	3	0	0.0213	7.3E-03	1.1E-02
10	1	1	3	0	0.0443	1.5E-02	2.2E-02
10	1	2	3	0	0.0680	2.3E-02	3.4E-02
10	1	3	3	0	0.0277	9.5E-03	1.4E-02
10	1	4	3	0	0.0321	1.1E-02	1.6E-02
10	1	5	3	0	0.0487	1.7E-02	2.4E-02
10	1	6	3	0	0.0408	1.4E-02	2.0E-02
10	2	1	3	0	0.4125	1.4E-01	2.0E-01
10	2	2	3	0	0.2781	9.5E-02	1.4E-01
10	2	3	3	0	0.0476	1.6E-02	2.4E-02
10	2	4	3	0	0.0448	1.5E-02	2.2E-02
10	2	5	3	0	0.0919	3.1E-02	4.6E-02
10	2	6	3	0	0.1306	4.5E-02	6.5E-02
12	1	1	3	0	0.0166	5.7E-03	8.2E-03
12	1	2	3	0	0.0109	3.7E-03	5.4E-03
12	1	3	3	0	0.0173	5.9E-03	8.6E-03
12	1	4	3	0	0.0105	3.6E-03	5.2E-03
12	1	5	3	0	0.0141	4.8E-03	7.0E-03
12	1	6	3	0	0.0207	7.1E-03	1.0E-02

Mote ID	Run	Channel ID	Tension, h (cm)	Water remaining (cm)	C₂	K(h) (cm/s)	Ks (cm/s)
13	1	1	3	0	0.0233	8.0E-03	1.2E-02
13	1	3	3	0	0.0281	9.6E-03	1.4E-02
13	1	4	3	0	0.0103	3.5E-03	5.1E-03
13	1	5	3	0	0.0123	4.2E-03	6.1E-03
13	1	6	3	0	0.0064	2.2E-03	3.2E-03

Site 11: Cimarron River in Haskell County, Kansas



Figure B-53. Site 11: Cimarron River near Haskell, Kansas

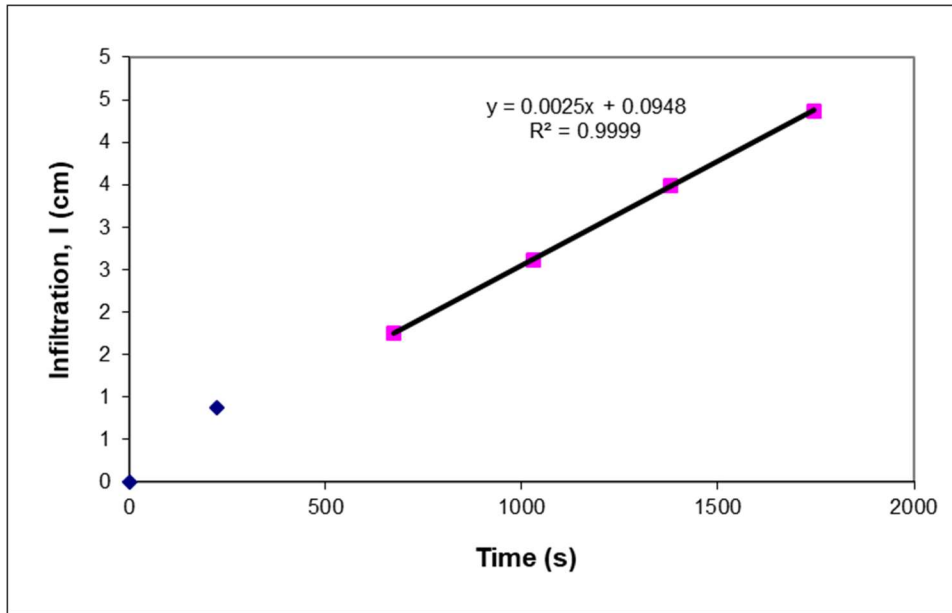


Figure B-54. Double-Ring Infiltrometer results for Site 11

Table B-33. Calculation of Hydraulic Conductivity for Site 11

Description	Symbol	Value
Diameter of Outer Ring	d_o	51 cm
Diameter of Inner Ring	d_i	27 cm
Ring Radius	a	13.5 cm
Ponded Height	H	16 cm
Depth of Insertion	d	10 cm
Soil Macroscopic Length	α^*	0.04 cm^{-1}
dimensionless quasi-empirical constants	C_1	0.992743
	C_2	0.578053
Infiltration rate	q	0.0025 cm/s
Hydraulic Conductivity	K	0.000737 cm/s

Site 12: Cimarron River in Seward County, Kansas

Vicinity Map of Cimarron River in Seward County, KS

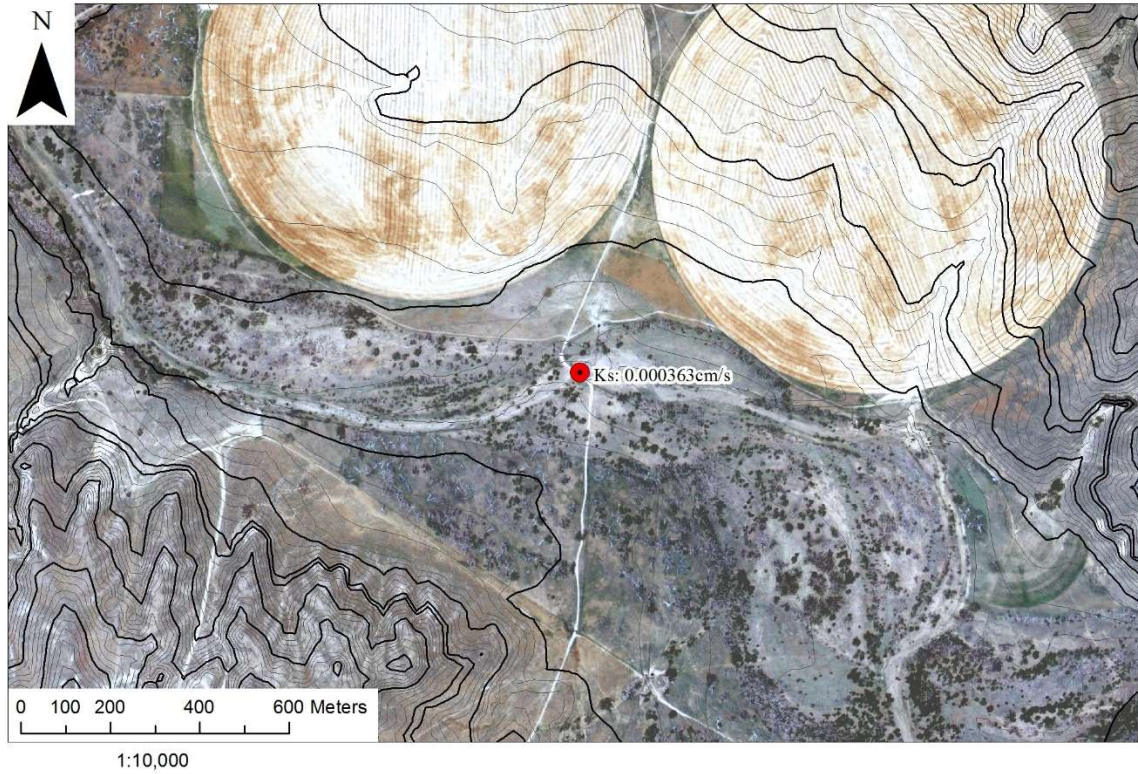


Figure B-55. Site 12: Cimarron River in Seward County, Kansas

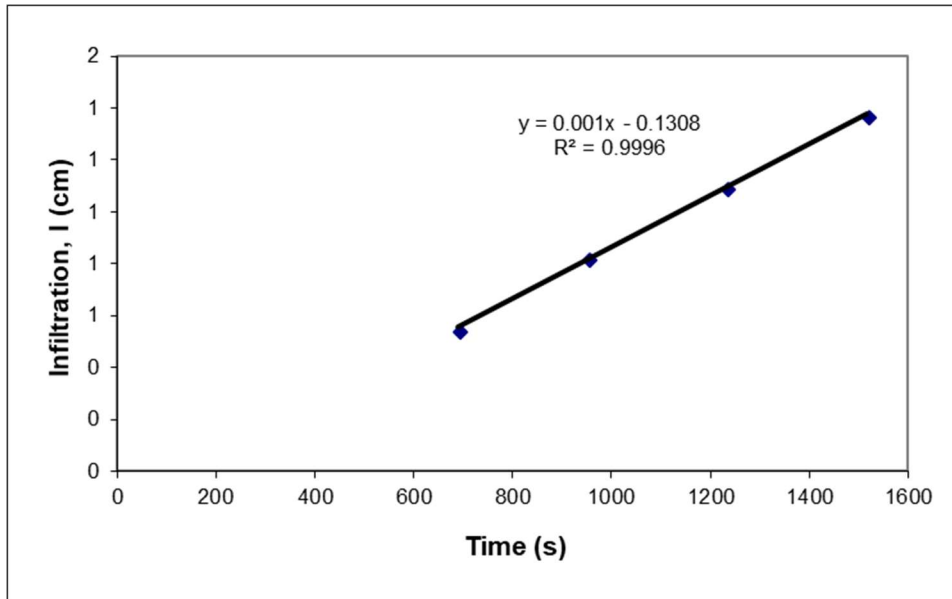


Figure B-56. Double-Ring Infiltrometer results for Site 12

Table B-34. Calculation of Hydraulic Conductivity for Site 12

Description	Symbol	Value
Diameter of Outer Ring	d_o	59 cm
Diameter of Inner Ring	d_i	30.48 cm
Ring Radius	a	15.24 cm
Ponded Height	H	23.5 cm
Depth of Insertion	d	10 cm
Soil Macroscopic Length	α^*	0.12 cm^{-1}
dimensionless quasi-empirical constants	C_1	0.992743
	C_2	0.578053
Infiltration rate	q	0.0010 cm/s
Hydraulic Conductivity	K	0.00036 cm/s

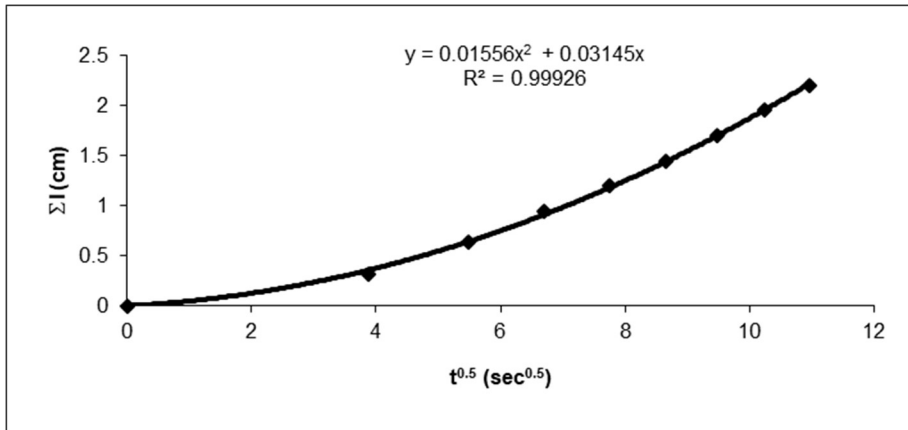


Figure B-57. Mini-Disk Infiltrometer (h = -6 cm) results 1 of 3 for Site 12

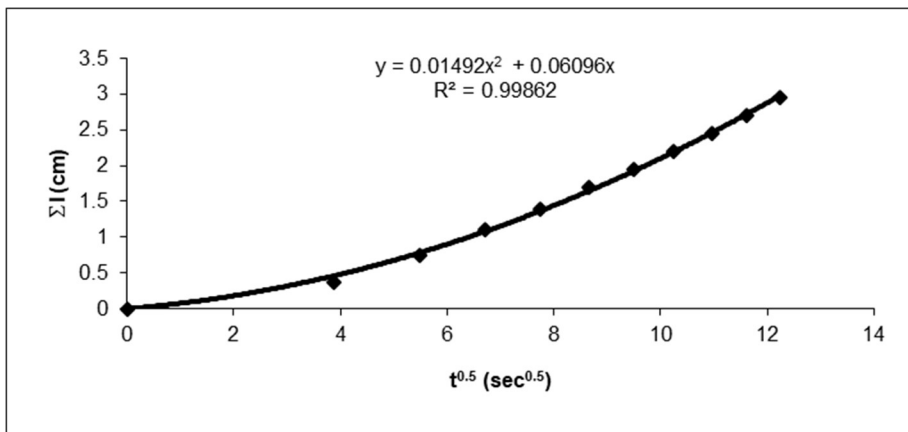


Figure B-58. Mini-Disk Infiltrometer (h = -6 cm) results 2 of 3 for Site 12

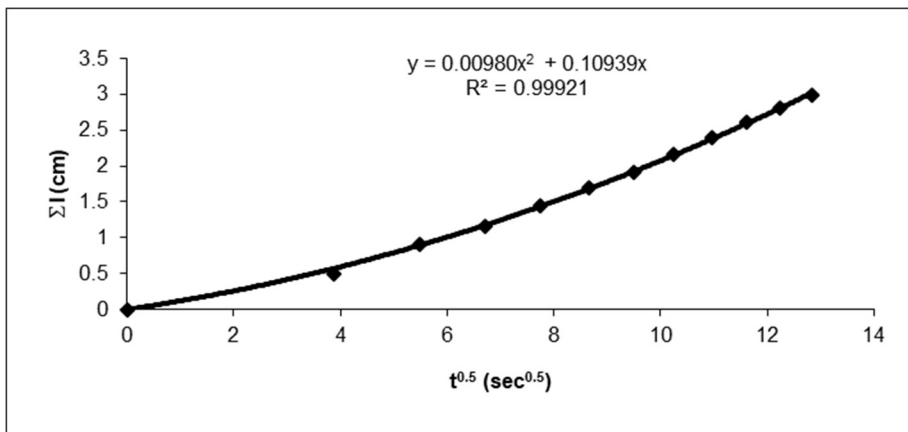


Figure B-59. Mini-Disk Infiltrometer (h = -6 cm) results 3 of 3 for Site 12

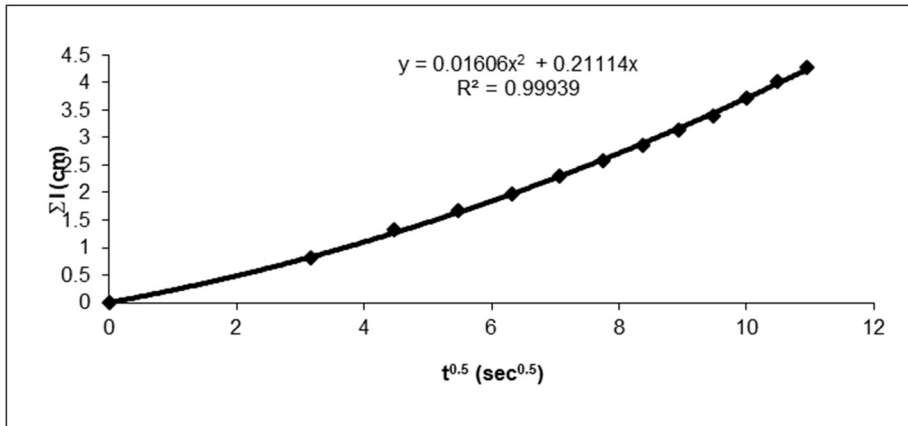


Figure B-60. Mini-Disk Infiltrometer (h = -2 cm) results 1 of 3 for Site 12

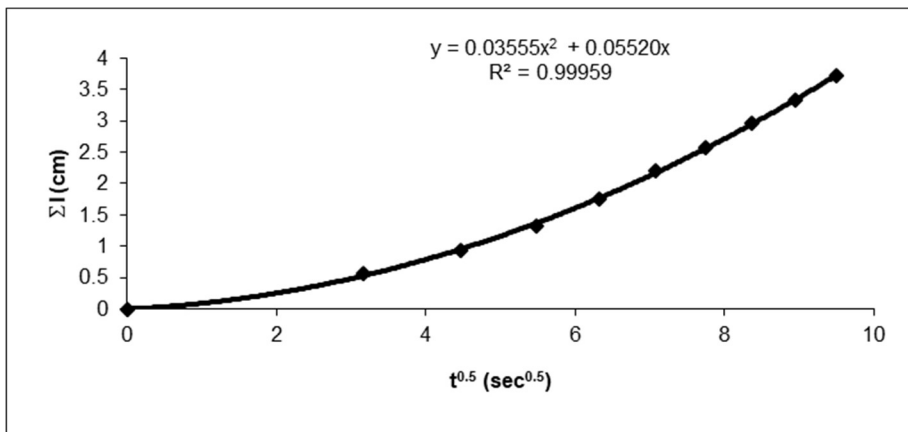


Figure B-61. Mini-Disk Infiltrometer (h = -2 cm) results 2 of 3 for Site 12

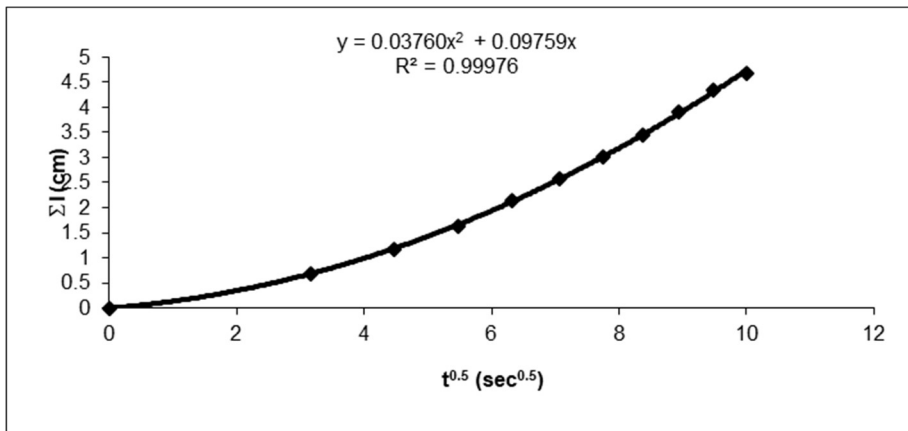


Figure B-62. Mini-Disk Infiltrometer (h = -2 cm) results 3 of 3 for Site 12

Table B-35. Calculation of K(h) for Site 12

Symbol	Run 1	Run 2	Run 3	Run 4	Run 5	Run 6
n	1.090	1.090	1.090	1.090	1.090	1.090
α	0.005	0.005	0.005	0.005	0.005	0.005
β	0.55	0.55	0.55	0.55	0.55	0.55
h	-6 cm	-6 cm	-6 cm	-2 cm	-2 cm	-2 cm
r	2.25 cm					
A	7.181	7.181	7.181	6.360	6.360	6.360
V	35 mL	47 mL	48 mL	68 mL	59 mL	75 mL
C_2	0.016	0.015	0.010	0.016	0.036	0.038
K(h)	0.0022 cm/s	0.021 cm/s	0.0014 cm/s	0.0025 cm/s	0.0056 cm/s	0.0059 cm/s
K_s	0.0023 cm/s	0.0216 cm/s	0.0014 cm/s	0.0025 cm/s	0.0057 cm/s	0.0060 cm/s

Site 13: North Cimarron River near Ulysses, Kansas

Vicinity Map of North Cimarron River near Ulysses, KS

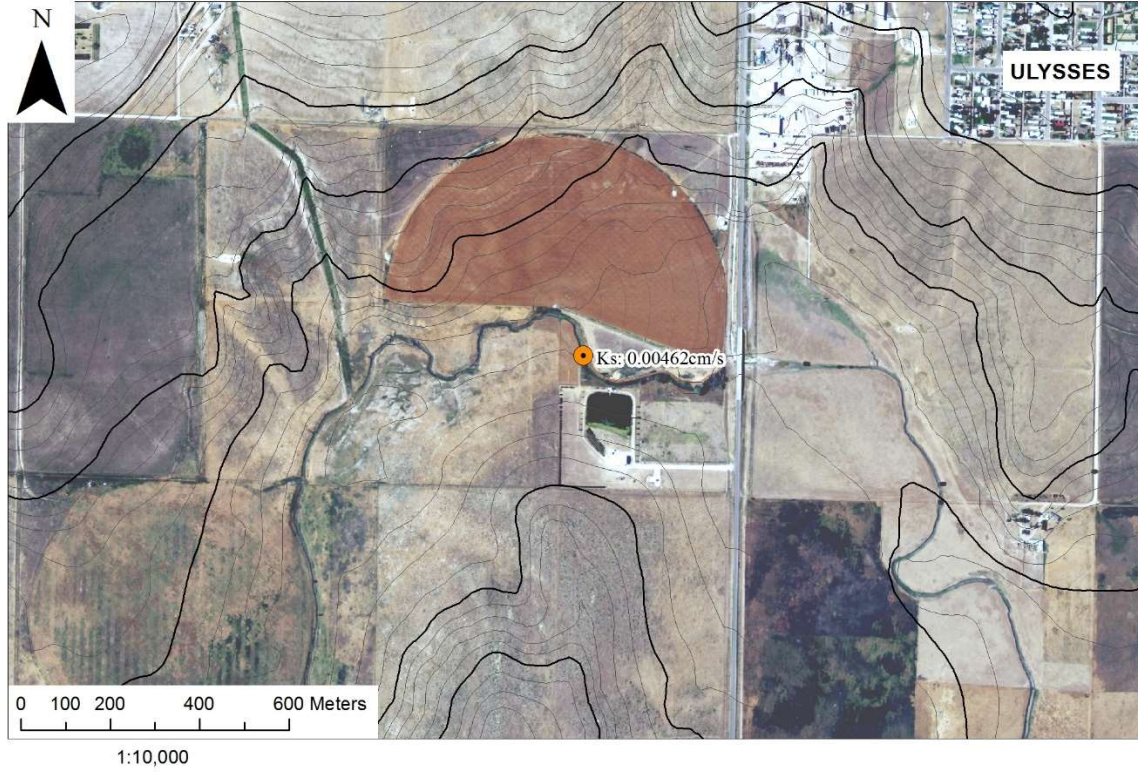


Figure B-63. Site 13: North Cimarron River near Ulysses, Kansas

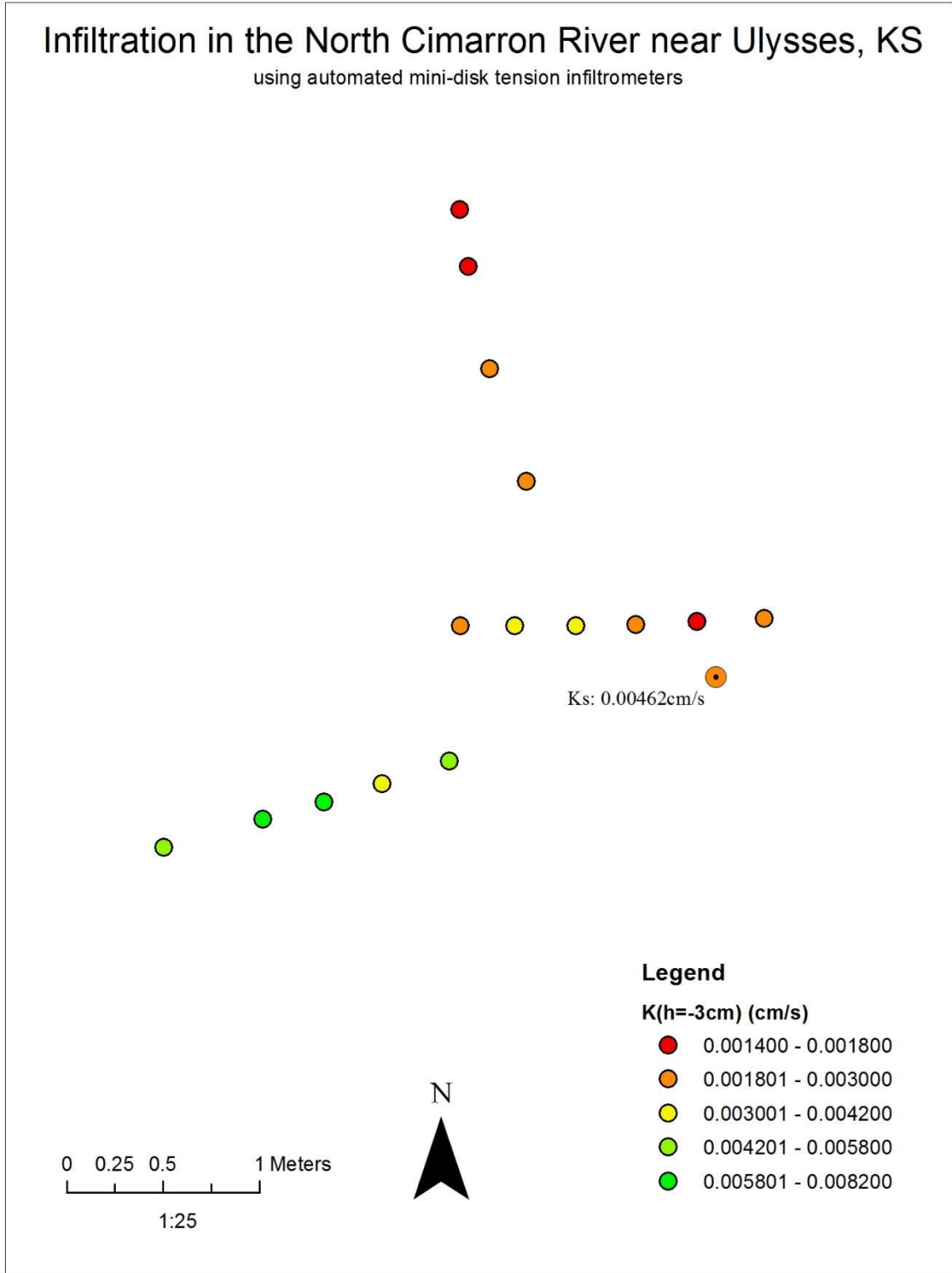


Figure B-64. Site 13: Results from Mini-Disk Infiltrometer in North Cimarron River near Ulysses, Kansas

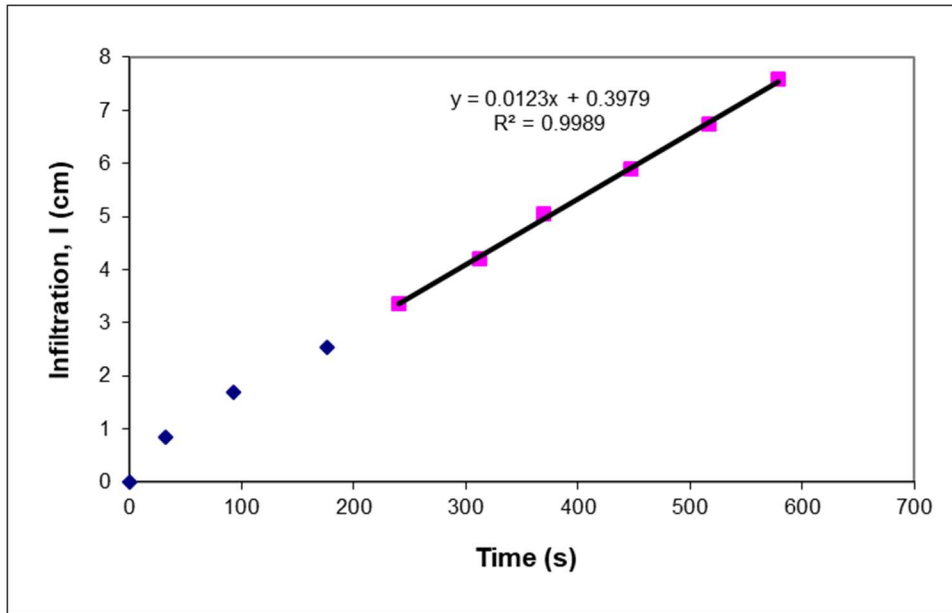


Figure B-65. Double-Ring Infiltrometer results for Site 13

Table B-36. Calculation of Hydraulic Conductivity for Site 13

Description	Symbol	Value
Diameter of Outer Ring	d_o	51 cm
Diameter of Inner Ring	d_i	27.5 cm
Ring Radius	a	13.75 cm
Ponded Height	H	10 cm
Depth of Insertion	d	13 cm
Soil Macroscopic Length	α^*	0.04 cm^{-1}
dimensionless quasi-empirical constants	C_1	0.992743
	C_2	0.578053
Infiltration rate	q	0.0123 cm/s
Hydraulic Conductivity	K	0.00462 cm/s

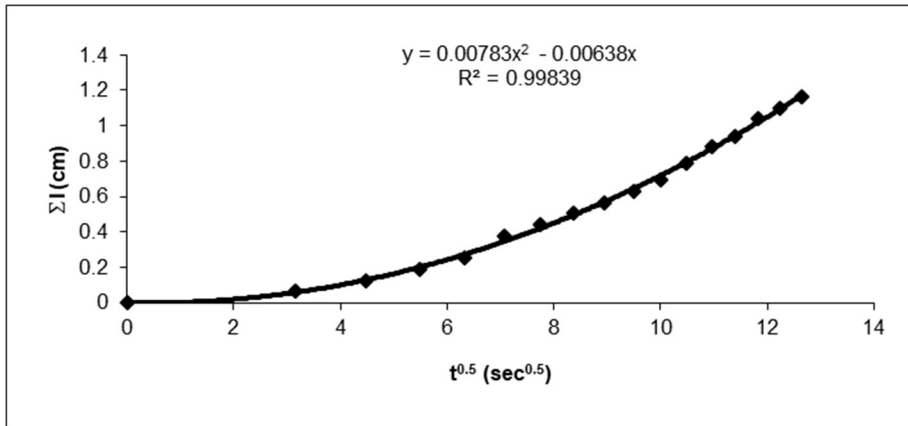


Figure B-66. Mini-Disk Infiltrometer ($h = -6$ cm) results for Site 13

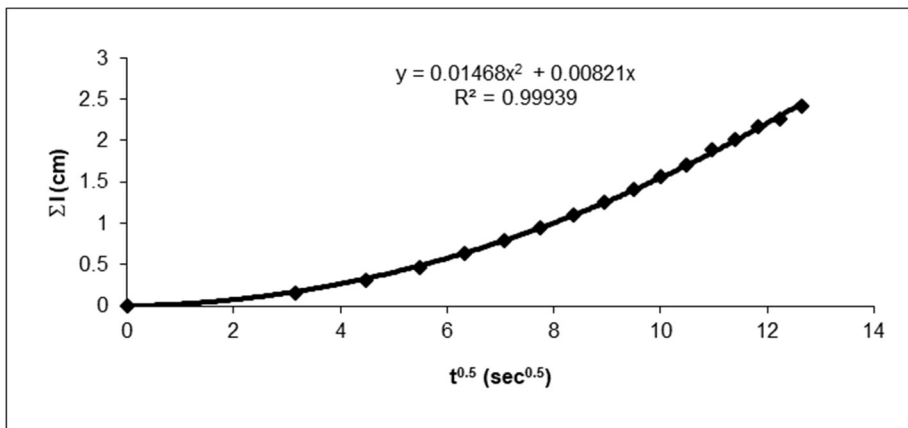


Figure B-67. Mini-Disk Infiltrometer ($h = -2$ cm) results for Site 13

Table B-37. Calculation of $K(h)$ for Site 13

Description	Run 1	Run 2
n	2.280	2.280
α	0.124	0.124
β	0.55	0.55
h	-6 cm	-2 cm
r	2.25 cm	2.25 cm
A	1.401	2.429
V	19 mL	39 mL
C_2	0.0078	0.0082
$K(h)$	0.0056 cm/s	0.0060 cm/s
K_s	0.012 cm/s	0.0077 cm/s

Table B-38. Results from automated mini-disk tension infiltrometer for Site 13

Mote ID	Channel ID	Tension, h (cm)	Water remaining (cm)	C₂	K(h) (cm/s)	K_s (cm/s)
7	1	3	0	0.00977	1.8E-03	2.3E-03
7	2	3	0	0.00778	1.4E-03	1.8E-03
7	4	3	0	0.01491	2.7E-03	3.4E-03
7	6	3	0	0.01308	2.4E-03	3.0E-03
12	1	3	0	0.01607	3.0E-03	3.7E-03
12	2	3	0	0.01845	3.4E-03	4.3E-03
12	3	3	0	0.02290	4.2E-03	5.3E-03
12	4	3	0	0.01207	2.2E-03	2.8E-03
12	5	3	0	0.00815	1.5E-03	1.9E-03
12	6	3	0	0.01226	2.3E-03	2.8E-03
13	1	3	0	0.03152	5.8E-03	7.3E-03
13	3	3	0	0.04312	7.9E-03	1.0E-02
13	4	3	0	0.04434	8.2E-03	1.0E-02
13	5	3	0	0.01942	3.6E-03	4.5E-03
13	6	3	0	0.02583	4.8E-03	6.0E-03